



**HAL**  
open science

## Molecular characterisation of new bacterial effectors

Arthur Louche

► **To cite this version:**

Arthur Louche. Molecular characterisation of new bacterial effectors. Biochemistry, Molecular Biology. Université de Lyon, 2020. English. NNT : 2020LYSE1337 . tel-04114477

**HAL Id: tel-04114477**

**<https://theses.hal.science/tel-04114477v1>**

Submitted on 2 Jun 2023

**HAL** is a multi-disciplinary open access archive for the deposit and dissemination of scientific research documents, whether they are published or not. The documents may come from teaching and research institutions in France or abroad, or from public or private research centers.

L'archive ouverte pluridisciplinaire **HAL**, est destinée au dépôt et à la diffusion de documents scientifiques de niveau recherche, publiés ou non, émanant des établissements d'enseignement et de recherche français ou étrangers, des laboratoires publics ou privés.



N°d'ordre NNT : 2020LYSE1337

## **THESE de DOCTORAT DE L'UNIVERSITE DE LYON**

opérée au sein de

**l'Université Claude Bernard Lyon 1**

**Ecole Doctorale N° 205**

**Ecole Doctorale Interdisciplinaire Sciences-Santé**

**Spécialité de doctorat** : Infectiologie

Soutenue publiquement le 16/12/2020, par :

**Arthur Louche**

---

# **Caractérisation de protéines effectrices bactériennes**

---

Devant le jury composé de :

GOUET Patrice  
BONAZZI Matteo  
SUBTIL Agathe  
DE BOLLE Xavier  
SALCEDO Suzana

PR Université Claude Bernard Lyon1  
DR CNRS, Université de Montpellier  
DR Institut Pasteur  
PR Université de Namur  
CR INSERM, Université Claude Bernard Lyon1

Président  
Rapporteur  
Rapporteuse  
Examineur  
Directrice de thèse



## **Université Claude Bernard – LYON 1**

Administrateur provisoire de l'Université	M. Frédéric FLEURY
Président du Conseil Académique	M. Hamda BEN HADID
Vice-Président du Conseil d'Administration	M. Didier REVEL
Vice-Président du Conseil des Etudes et de la Vie Universitaire	M. Philippe CHEVALLIER
Vice-Président de la Commission de Recherche	M. Jean-François MORNEX
Directeur Général des Services	M. Pierre ROLLAND

### **COMPOSANTES SANTE**

Département de Formation et Centre de Recherche en Biologie Humaine	Directrice : Mme Anne-Marie SCHOTT
Faculté d'Odontologie	Doyenne : Mme Dominique SEUX
Faculté de Médecine et Maïeutique Lyon Sud - Charles Mérieux	Doyenne : Mme Carole BURILLON
Faculté de Médecine Lyon-Est	Doyen : M. Gilles RODE
Institut des Sciences et Techniques de la Réadaptation (ISTR)	Directeur : M. Xavier PERROT
Institut des Sciences Pharmaceutiques et Biologiques (ISBP)	Directrice : Mme Christine VINCIGUERRA

### **COMPOSANTES & DEPARTEMENTS DE SCIENCES & TECHNOLOGIE**

Département Génie Electrique et des Procédés (GEP)	Directrice : Mme Rosaria FERRIGNO
Département Informatique	Directeur : M. Behzad SHARIAT
Département Mécanique	Directeur M. Marc BUFFAT
Ecole Supérieure de Chimie, Physique, Electronique (CPE Lyon)	Directeur : Gérard PIGNAULT
Institut de Science Financière et d'Assurances (ISFA)	Directeur : M. Nicolas LEBOISNE
Institut National du Professorat et de l'Education	Administrateur Provisoire : M. Pierre CHAREYRON
Institut Universitaire de Technologie de Lyon 1	Directeur : M. Christophe VITON
Observatoire de Lyon	Directrice : Mme Isabelle DANIEL
Polytechnique Lyon	Directeur : Emmanuel PERRIN
UFR Biosciences	Administratrice provisoire : Mme Kathrin GIESELER
UFR des Sciences et Techniques des Activités Physiques et Sportives (STAPS)	Directeur : M. Yannick VANPOULLE
UFR Faculté des Sciences	Directeur : M. Bruno ANDRIOLETTI



## Remerciements :

Je tiens tout d'abord à remercier sincèrement ma directrice de thèse, le Dr Suzana Salcedo. Suzana, ça fait maintenant un petit bout de temps que je travaille dans ton équipe de recherche. En effet j'ai commencé à travailler à ses côtés en Novembre 2013 où à l'époque elle m'avait engagé pour un contrat à durée déterminée de 1 an qui a été reconduit pour deux années supplémentaire en tant qu'assistant ingénieur/ ingénieur d'étude. A la fin de ces CDD, Suzana m'a proposé de réaliser une thèse dans son équipe de recherche, après avoir hésité j'ai finalement accepté de réaliser la thèse. Aujourd'hui je ne regrette absolument pas ce choix. Suzana a été une chef formidable, toujours à l'écoute et de bons conseils. Outre le coté scientifique et les journal club qui m'ont permis de développer un esprit critique, je la remercie également pour les moments partagés en équipe notamment les repas de Noël, les barbecues d'été et les activités que nous avons pu faire en dehors du labo. C'est un tout qui fait que les « plus ou moins » matin j'étais heureux de venir travailler au labo.

Je remercie l'Agence National de la Recherche pour leur financement.

Je remercie la Dr. Agathe Subtil et le Dr. Matteo Bonazzi d'avoir accepté d'être rapporteurs de ma thèse. Je remercie le Dr. Xavier De Bolle d'avoir accepté de juger mon travail en tant qu'examineur. Je remercie également le Pr. Patrice Gouet d'avoir accepté de présider ce jury de thèse.

Je remercie également les membres de mes différents comités de suivi de thèse, la docteure Anne Vianney et le docteur Lionel Ballut pour tous leurs conseils prodigués durant les 3 CST.

Durant ma thèse, j'ai pu utiliser différents équipements de la plateforme *Protein Science Facility* PSF (SFR Biosciences, UMS 3444). Ainsi, je souhaite remercier pour leur accueil chaleureux et leur disponibilité : Frédéric Delolme, Aline Page, Roland Montserret, Eric Diesis et plus particulièrement Virginie Gueguen-Chaignon qui a contribué à l'obtention de la structure cristallographique. Je remercie également la plateforme d'imagerie et microscopie PLATIM (SFR Biosciences, UMS 3444/US8) et plus particulièrement Claire Lionnet.

Je remercie Laurent Terradot, qui m'a accueilli dans son laboratoire pour mon stage de M2. Laurent m'a appris toutes les étapes en partant de l'ADN jusqu'à l'obtention de protéine

purifiée. Ainsi, je le remercie pour tous ses conseils sur les purifs réalisés au cours de ses travaux, et pour avoir pu utiliser ses Aktä. Je le remercie également pour notre collaboration et le travail réalisé pour l'obtention de la structure cristallographique de NyxB.

Je tenais également à remercier Celia Berger, pour les expériences de SAXS qu'elle a réalisées sur NyxB, et pour nos nombreuses discussions scientifiques ou non et nos échanges IBCPien.

Je remercie aussi l'équipe de Victor Cid, nos collaborateurs sur le projet BtpA BtpB. Et surtout Julia qui m'a aidé pour les clonages et les bons moments passés lors de ton passage au labo.

Ces quatre années de thèse n'auraient pas été si agréables et si marquantes sans un environnement de travail plaisant, stimulant et la bonne ambiance qui régnait au labo. Ainsi je tiens à remercier : les membres passés et actuels de l'équipe de biologie cellulaire de la pathogénie bactérienne. Je commence à remercier les anciens thésards du laboratoire : Paul Imbert, Stéphanie Gagné et Jean-Baptiste Luizet. Je remercie les anciens Post-Doc. Guillermo Repizo, Tristan Rubio. Je remercie également Orane Chabiron et Chloé Dias.

Je tenais également à remercier Francine Gérard qui vient tout juste d'arriver au laboratoire et lui souhaite le meilleur pour la suite.

Je souhaite également adresser de sincères remerciements à Amandine Blanco, Morgane Roussin, Julie Raymond. J'ai été très heureux de pouvoir travailler en votre compagnie.

Je tenais à remercier les stagiaires que j'ai pu encadrer au cours de ma thèse et qui m'ont aussi permis d'évoluer, merci Rémi Lagorce et Mariam Taktek.

Merci aux autres collègues de travail de l'IBCP : Celia, Halima, Christelle, Marine R, Margaux, Thomas, Julien, Maty, Sylvain, Maxime, Marine L, Lea, Mathieu, Cecilia, Jorgaq, Arnaud, Alexis, Fred et Guillaume pour les moments de détente et de rires passés au Bureau, au Ninkasi ou ailleurs. Merci à Gina, Cyril et Jean-Baptiste pour nos soirées jeux et les parties de G-Switch.

En fin, je tiens à remercier ma famille et mes proches pour le soutien apporté tout au long de ces années de thèses.

## Abstracts

### Résumé en langue française :

Les agents pathogènes intracellulaires ont la capacité de moduler les réponses cellulaires de l'hôte pour survivre et proliférer. Ceci est réalisé en produisant et en injectant des protéines effectrices dans les cellules hôtes. Ces effecteurs peuvent notamment moduler la réponse immunitaire et le trafic intracellulaire. *Brucella*, l'agent causal de la brucellose, une maladie animale transmissible à l'homme, délivre des effecteurs dans la cellule hôte via son système de sécrétion de type IV. À ce jour, seuls quelques effecteurs ont été identifiés chez *Brucella* et leurs fonctions moléculaires restent floues.

Au cours de ma thèse, nous nous sommes intéressés à deux effecteurs de *Brucella abortus* contenant un domaine TIR, BtpA et BtpB, connues pour moduler la réponse immunitaire innée de l'hôte. Cependant, il a été démontré récemment que les domaines TIR purifiés ont une activité NADase *in vitro*. Nous avons ainsi montré que BtpA et BtpB conservent cette activité et sont capables de réduire la quantité de NAD présente dans la cellule hôte pendant l'infection. Ces résultats suggèrent que la NAD intracellulaire joue un rôle dans les infections à *B. abortus* et pourrait constituer un nouveau mécanisme de pathogénie. Parallèlement à ce projet, j'ai également eu l'occasion de travailler sur la caractérisation des effecteurs contenant un domaine TIR chez d'autres agents pathogènes. J'ai apporté une contribution majeure à la caractérisation de l'effecteur PumA chez *Pseudomonas aeruginosa* et participé à la caractérisation de l'effecteur TirS chez *Staphylococcus aureus*.

Le projet principal de ma thèse était d'initier une caractérisation structurale et fonctionnelle de deux nouveaux effecteurs de *B. abortus*, que nous avons nommés NyxA et NyxB. Après avoir établi qu'ils sont transloqués dans la cellule hôte pendant l'infection, nous avons observés ces effecteurs dans des compartiments nucléaires et cytosoliques. Par des expériences de co-précipitation, nous avons montré que ces deux effecteurs sont capables d'interagir entre eux et nous avons identifié SENP3 comme leur cible eucaryote. SENP3 est une désSUMOylase essentiellement située dans un sous-compartiment nucléaire, le nucléole. Cette protéine est impliquée dans la régulation de nombreuses fonctions cellulaires et joue un rôle majeur dans la biogenèse des ribosomes. Nous avons montré que SENP3 est nécessaire à la réplication de *B. abortus* dans la cellule hôte. L'analyse structurale de NyxB, nous a permis d'identifier une poche acide impliquée dans l'interaction avec SENP3. De façon surprenante, dans les cellules infectées par *B. abortus*, SENP3 est délocalisée et ne s'accumule plus dans les nucléoles. Dans les cellules transfectées par NyxA et NyxB, nous avons observé que ces deux effecteurs recrutent SENP3 dans un autre compartiment nucléaire : les corps nucléaires PML. En outre, ces effecteurs modulent également la distribution de NVL et RPL5, composants clés de la machinerie de biogenèse ribosomique dans les nucléoles, qui dans les cellules infectées forment des structures punctiformes dans le cytosol de manière dépendante de SENP3. Nous avons observé que ces structures cytosoliques correspondent à la localisation cytosolique des effecteurs Nyx et sont également enrichies en NUFIP1, un récepteur de la ribophagie.

En résumé, ce deuxième projet identifie deux nouveaux effecteurs chez *B. abortus*, qui ont un impact sur la localisation nucléolaire de SENP3. Ils sont impliqués dans la formation de structures cytosoliques enrichies en NUFIP1, NVL et RPL5, ce qui suggère un processus similaire à celui de la ribophagie.

## Abstract in english :

Intracellular pathogens have the ability to modulate the hosts' cellular responses to survive and proliferate. This is achieved by producing and injecting effector proteins into host cells. These effectors can modulate various cellular functions, including immune response and intracellular trafficking. *Brucella*, the causative agent of brucellosis, an animal disease transmissible to humans, delivers effector proteins into the host cell through its type IV secretion system. To date, only a few effectors have been identified in *Brucella* and their molecular functions remain unclear.

During my thesis, we were particularly interested in two *Brucella* effector proteins containing a TIR domain, BtpA and BtpB, known to modulate the host innate immune response. However, more recently, purified TIR domains were also shown to have NADase activity *in vitro*. We have thus shown that BtpA and BtpB retain this activity and are able to reduce the amount of NAD present in the cell host during infection. These results suggest that intracellular NAD plays a role in *Brucella* infections and may constitute a new mechanism for *Brucella* pathogenicity. In parallel to this project, I also had the opportunity to work on the characterization of TIR-domain-containing effectors in other pathogens. I have made a major contribution to the characterization of the PumA effector in *Pseudomonas aeruginosa* and participated to the characterization of the TirS effector in *Staphylococcus aureus*.

The major project of my thesis was to initiate a structural and functional characterization of two new *B. abortus* effectors, which we named NyxA and NyxB. After establishing they were translocated into the host cell during infection, we imaged these effectors and found them in nuclear and cytosolic compartments. By pull-down experiments, we showed that these two effectors were able to interact with each other and we identified SENP3 as their eukaryotic target. SENP3 is a deSUMOylase essentially located in a nuclear sub-compartment, the nucleolus. This protein is involved in the regulation of many cellular functions and plays a major role in ribosome biogenesis. We have shown that SENP3 is necessary for the replication of *B. abortus* within the host cell. The structural analysis of NyxB allowed us to identify an acidic pocket involved in the interaction with SENP3. Surprisingly, in cells infected with *B. abortus*, SENP3 is delocalized and no longer accumulating in nucleoli. In NyxA and NyxB transfected cells we could observe these two effectors recruited SENP3 to another nuclear compartment: the PML nuclear bodies. Furthermore, these effectors were also able to modulate the distribution of NVL and RPL5, key components of the ribosomal biogenesis machinery in the nucleoli, which in infected cells form cytosol punctate structures in a manner dependent on SENP3. We have observed that these cytosolic structures correspond to the cytosolic location of Nyx effectors and are also enriched in NUFIP1, a ribophagy receptor.

In summary, this second project identifies two new *Brucella* effectors, which have an impact on the nucleolar localization of SENP3. They are involved in the formation of cytosolic structures enriched in NUFIP1, NVL and RPL5 suggesting a process similar to that of ribophagy.

## Lists of publications

### Articles :

1. Patot S, Imbert PR, Baude J, Martins Simões P, Campergue JB, **Louche A**, Nijland R, Bès M, Tristan A, Laurent F, Fischer A, Schrenzel J, Vandenesch F, Salcedo SP, François P, Lina G.

**The TIR Homologue Lies near Resistance Genes in Staphylococcus aureus, Coupling Modulation of Virulence and Antimicrobial Susceptibility.** PLoS Pathog. 2017 Jan 6 ;13(1) : e1006092.

2. Imbert PR, **Louche A**, Luizet JB, Grandjean T, Bigot S, Wood TE, Gagné S, Blanco A, Wunderley L, Terradot L, Woodman P, Garvis S, Filloux A, Guery B, Salcedo SP.

**A Pseudomonas aeruginosa TIR effector mediates immune evasion by targeting UBAP1 and TLR adaptors.** EMBO J. 2017 Jul 3;36(13):1869-1887.

3. Coronas-Serna JM#, **Louche A**#, Rodríguez-Escudero M, Roussin M, Imbert PRC, Rodríguez-Escudero I, Terradot L, Molina M, Gorvel JP, Cid VJ, Salcedo SP.

# co-first author

**The TIR-domain containing effectors BtpA and BtpB from Brucella abortus impact NAD metabolism.** PLoS Pathog. 2020 Apr 16;16(4):e1007979.

4. **Louche A**, Blanco A, Lacerda TL, Lionnet C, Gueguen-Chaignon V, Bergé C, Rolando M, Lembo F, Borg JP, Buchrieser C, Gorvel JP, Nagahama M, Terradot L, Salcedo SP.

**Brucella effectors target SENP3, inducing subcellular mislocalisation of nucleolar proteins and induction of ribophagy.** (Article in preparation)

### Book chapters :

1. **Louche A**, Salcedo SP, Bigot S.

**Protein-Protein Interactions: Pull-Down Assays.** Methods Mol Biol. 2017;1615:247-255.

## Lists of scientific presentations:

### Posters:

1. 11/2016 Biomolecular interaction analysis 2016: From molecules to cells EMBO  
Practical Course, Porto, Portugal

#### **Modulation of cellular responses by bacterial pathogens**

2. 11/2017 22<sup>th</sup> EDISS Interdisciplinary Doctoral School of Health Sciences Day, Lyon,  
France

#### **Molecular and cellular characterization of two new *Brucella* effectors. Poster price**

3. 09/2019 The new microbiology, Spestes island, Greece

#### **Structural-functional studies of *Brucella* effectors**

### Communications orals:

1. 05/2018 Internal seminar MMSB, IBCP, Lyon, France

#### **Structural-functional studies of *Brucella* effectors**

2. 10/2018 23<sup>th</sup> EDISS Interdisciplinary Doctoral School of Health Sciences Day, Lyon,  
France

#### **Structural and functional study of *Brucella* effector**



## Table of Contents

Remerciements .....	4
Abstracts.....	6
Résumé en langue française.....	6
Abstract in english .....	7
Lists of publications .....	8
Lists of scientific presentations: .....	9
Abbréviations .....	14
<b>Chapter I: introduction .....</b>	<b>16</b>
1. Brucellosis : general information.....	17
1. Brucellosis.....	17
2. Epidemiology .....	17
3. <i>Brucella</i> spp .....	19
4. Transmission.....	21
5. Symptoms.....	22
6. Diagnosis.....	23
7. Treatments, prevention & vaccins .....	24
8. Consequences.....	26
2. Brucella intracellular life.....	27
1. Entry into the cells.....	27
2. Intracellular traffic.....	29
3. The endoplasmic reticulum: the replicating niche .....	30
4. The exit of Brucella : The autophagic BCV.....	31
3. Brucella T4SS and its effectors .....	33
1. Brucella T4SS .....	33
2. Brucella effectors.....	35
3. Effector proteins secreted by <i>Brucella</i> T4SSs .....	36
4. The different research projects of my thesis work.....	40
5. TIR proteins and innate immune system.....	41
1. Immune system .....	41
2. Recognition of microbes and pathogens by the innate immune system .....	42
3. Toll-like receptors (TLRs) .....	45
4. Microbial targeting of the TLR signaling pathway .....	52



5.	Bacterial TIR proteins .....	54
6.	Bacterial TIR domain peptides as therapeutic agents .....	55
7.	Other roles of bacterial TIR domains .....	57
6.	Foreword to the second part of the thesis .....	58
7.	The nucleus.....	59
1.	Architecture of the nucleus .....	59
2.	The different nuclear compartments: nuclear bodies.....	60
3.	The nucleolus: an assembly platform .....	61
4.	The PML nuclear bodies: .....	66
8.	SUMOYLATION .....	67
1.	The enzymatic mechanism of SUMOylation.....	70
2.	The SUMO Interacting Motif (SIM: SUMO Interacting Motif) .....	73
3.	Consequences of SUMOylation .....	74
4.	The pathway of sumoylation targeted by bacteria:.....	74
9.	The SENP family.....	77
10.	SEN3.....	79
1.	SEN3 as a redox-sensor under stress.....	80
2.	SEN3 as a modulator of gene expression .....	82
3.	SEN3 and immune response.....	82
4.	SEN3 as a regulator of macromolecular assemblies in the nucleus : ribosome biogenesis	83
<b>Chapter II: Results.....</b>		<b>85</b>
1.	The TIR-domain containing effectors BtpA and BtpB from <i>Brucella abortus</i> impact NAD metabolism.....	86
2.	<i>Brucella</i> effectors target SENP3, inducing subcellular mislocalisation of nucleolar proteins and induction of ribophagy .....	88
1.	Two newly identified <i>B. abortus</i> effectors, NyxA and NyxB, accumulate in cytosolic and nuclear structures.....	88
2.	NyxA and NyxB interact with each other and target the same cellular compartments .....	92
3.	NyxA and NyxB enriched nuclear structures are in close association with PML-nuclear bodies .....	95
4.	NyxA and NyxB do not interact with SUMO <i>in vitro</i> .....	97
5.	The Nyx effectors interact with SENP3, which is necessary for efficient <i>B. abortus</i> intracellular multiplication .....	98
6.	The NyxB structure defines a novel family of effectors.....	101
7.	Identification of the Nyx-SEN3 interacting groove .....	104
8.	The <i>Brucella</i> Nyx effectors induce delocalisation of SENP3 .....	105
9.	Nyx effectors and SENP3 depletion induce cytosolic accumulation of the nucleolar proteins	

NVL 109	
10. <i>B. abortus</i> induces NVL cytosolic structures enriched in RPL5 and the ribophagy receptor NUFIP1 .....	114
3. Materials and Methods .....	122
1. Cells and culture conditions .....	122
2. <i>Brucella</i> strains, cultures and infections.....	122
3. <i>Brucella</i> expressing vectors .....	123
4. Eukaryotic expression vectors .....	123
5. Bacterial expression vectors.....	124
6. Immunofluorescence microscopy .....	124
7. Transfections and siRNA.....	125
8. <i>Legionella</i> infection .....	125
9. Pulldown assays.....	125
10. Quantification of SENP3 localization .....	126
11. TEM1 translocation assay .....	126
12. Thermophoresis.....	126
13. SUMOylation assay .....	127
14. Protein expression and purification .....	127
15. Crystallization and data collection.....	128
16. Size exclusion Multi-angle light scattering .....	129
17. Small-angle X-ray scattering .....	129
18. Yeast two-hybrid.....	130
19. Stats .....	130
Chapter III: Discussion and conclusion .....	134
ANNEXES.....	148
1. <b>Annexe 1: The TIR Homologue Lies near Resistance Genes in <i>Staphylococcus aureus</i>, Coupling Modulation of Virulence and Antimicrobial Susceptibility .....</b>	<b>149</b>
2. <b>Annexe 2 : A <i>Pseudomonas aeruginosa</i> TIR effector mediates immune evasion by targeting UBAP1 and TLR adaptors .....</b>	<b>151</b>
3. <b>Annexe 3 : Protein-Protein Interactions: Pull-Down Assays.....</b>	<b>153</b>
REFERENCES .....	154

## Abbréviations :

aBCV: autophagic *Brucella*-containing vacuole  
ATG : Autophagy-related gene  
ATP: Adénosine TriPhosphate  
AP1 :Activator protein1  
BCV: Brucella-Containing Vacuole  
BSL3 : BioSafety Level3  
Bsp: Brucella secreted protein  
BMDM: Bone-Marrow Derived Macrophages  
CagA : Cytotoxin-Associated Gene A  
CDC : Centers for Disease control Prevention  
CFU : Colony Forming Unit  
CLR : C-type lectin receptor  
DC: Dendritic Cell  
DNA : deoxyrionucleic acid  
dsDNA/RNA : double stranded DNA/RNA  
eBCV : endosomal *Brucella*-containing vacuole  
EEA1: Early Endosomal Antigen 1  
ER: Endoplasmic Reticulum  
ESCRT : endosomal sorting complex required for transport  
Hsp: Heat-shock protein  
iBMDM: immortalized Bone-Marrow Derived Macrophages  
IL: Interleukin  
IRF : Interferon Regulatory Factor  
IRAK : IL-1R-associated protein kinases  
KD: Knock-Down  
KO: Knock-Out  
LAMP1: Lysosomal-associated membrane protein 1  
LLO: Listeriolysin O  
LRR : Leucine rich repeat  
LPS :Lipopoly  
MyD88: myeloid differentiation factor-88  
MAL : MyD88-adapter-like  
mRNA: messenger RNA  
NLR: Nod-Like Receptor  
PAMP: Pathogen associated molecular pattern  
PBS: Phosphate Buffer Salt  
PCR: Polymerase Chain Reaction  
PI : Phosphatidylinositol  
PDI: Protein Disulfide Isomerase  
Prpc: cellular prion protein  
PRR: Pattern Recognition Receptor  
rBCV : replicative *Brucella*-containing vacuole  
RLRs : RIG-1 like Receptors  
ROS: Reactive Oxygen Species

SR-A : class A scavengers receptors  
SUMO : Small Ubiquitin like modifier  
ssDNA/RNA : single stranded DNA/RNA  
T4SS : Type IV Secretion System  
TLR: Toll-like Receptor  
TIRAP : TIR domain-containing adaptor protein  
TNF: Tumor Necrosis Factors  
TRAF6 : TNF receptor-associated factor 6  
Tcp ; TIR domain-containing protein  
Ub: Ubiquitin  
UPR: Unfolded Protein Response  
WHO: World Health Organization  
WT: Wild Type  
Y2H: Yeast two hybrid

## Chapter I: introduction

## 1. Brucellosis : general information

### 1. Brucellosis

Brucellosis is a worldwide infectious disease caused by intracellular bacteria belonging to the genus *Brucella* [1]. It seems that brucellosis is an old disease, present among humans since a long time. Indeed, macroscopic and microscopic analysis of the lumbar vertebrae of ancient human remains of the Pliocene period (2.8 million years ago) have been suggested as signs of brucellosis [2]. Archaeologists have also found a jar containing fossilized cheese in an Egyptian tomb dating back to the 19th dynasty (-1293-1185 BC), for which proteomic analysis revealed the presence of *Brucella* [3]. Moreover, symptoms reminiscent of brucellosis have been described by Hippocrates in his publication Epidemics (around 410 BC). It wasn't until the late 19<sup>th</sup> century that the causative agent of brucellosis was isolated by a British physician Dr David Bruce from the spleen of a dead soldier on the Malta island, and for this reason the organism bears his name. Over time brucellosis had different names, including undulant fever, Maltese fever, Gibraltar fever, Crimean fever, goat fever and Bang disease.

### 2. Epidemiology

#### **Brucellosis in the world:**

Brucellosis is one of the most prevalent zoonosis. The word zoonosis, from the Greek zoo (animal) and nosos (disease) are defined as diseases that are naturally transmitted from vertebrate animals to humans. Every year more than 500,000 cases of human brucellosis are recorded [4], which is why WHO has classified this disease as an important neglected zoonosis re-emerging in the world. However, the incidence of disease is believed to be under-diagnosed and the true incidence is evaluated to be 10 times higher (5,000,000 cases) [5]. Brucellosis is still endemic in many regions, namely the countries of the Mediterranean basin, Latin America and the Middle East. Throughout the world, the geographical distribution of the disease varies greatly (figure1). While the incidence of the disease is clearly declining in the developed world,

this is not the case in developing countries where it often reaches worrying levels. The prevalence of the disease ranges from 0.3 cases per million in developed countries to more than 1000 cases per million in endemic regions [6].

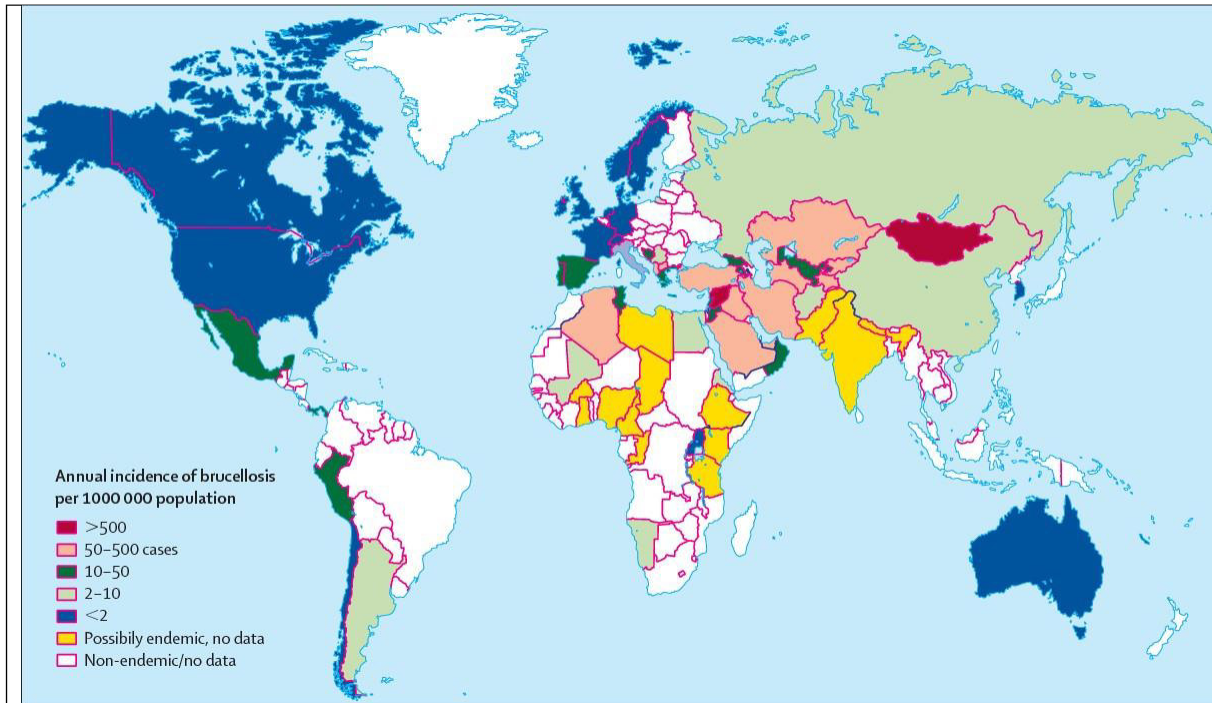


**Figure 1. Global distribution of brucellosis cases in the year 2000.**

The most affected countries are Mongolia and the countries of the Middle East and the Balkans. Some Central and South American countries and the countries of the Mediterranean basin also have numerous cases of human brucellosis. [6]

### **Brucellosis in France:**

As a result of strong prophylactic campaigns in the 1960s on ruminant farms, cases of human brucellosis in France decreased from 800 cases in 1976 to 44 cases in 2000[6]. France has been declared officially free of bovine brucellosis since 2005, and no outbreaks in animals have been identified on the national territory from 2003 to 2012. Every year, cattle, sheep and goat farms are regularly tested for brucellosis. Now, any confirmation of brucellosis on a farm will lead to slaughtering of the entire herd and the destruction of resulting products, as a precautionary measure.

However, two outbreaks of bovine brucellosis were confirmed in 2012 on the French territory, thus calling for vigilance regarding this zoonosis [7] [8]. A first outbreak was due to the importation of an infected bovine animal and was rapidly eradicated. The second outbreak was related to a large wild reservoir discovered in mountain ibexes [8], which resulted in a

massive eradication program of the older ibex members of the herd (infected and non-infected) in the Bargy mountain range to prevent further dissemination. These measures were highly controversial and in fact proven inefficient in the control of brucellosis in the ibex population. Therefore, recent new surveillance measures have been set in place for monitoring all wild-life in the region (ibex, chamoises, deer) as well as local pastures (sheep, goats and cows) [9]. Selective slaughtering programs are in place and a vaccination program being studied.

### 3. *Brucella* spp

*Brucella* are small coccobacilli Gram-negative bacteria, 0.6–1.5  $\mu\text{m}$  long by 0.5–0.7  $\mu\text{m}$  in width. They are non-motile, non-encapsulated, non-spore-forming and do not present pili nor toxins. *Brucella* are strictly aerobic but some strains growth better in an atmosphere containing 5 to 10 %  $\text{CO}_2$ . *Brucella* does not present classical virulence factors known in others pathogenic bacteria such as: lysogenic phages, virulence plasmids, invasive protease, exotoxin and toxic lipopolysaccharide (LPS).

Nevertheless, the LPS plays an important role in the virulence of *Brucella*. The LPS, which found in the outer membrane of all Gram-negative bacteria, is composed of a hydrophobic lipid moiety, called lipid A, normally associated with its toxic properties linked to a polysaccharide, with a hydrophilic core and a repeating O-antigenic oligosaccharide side chain. There are 2 types of LPS depending on the surface morphology: smooth or rough. Smooth correspond to the presence of the O-polysaccharide side chain in the LPS moiety and rough without the O-polysaccharide side chain. Most *Brucella* species are naturally smooth, except for *B. ovis* and *B. canis* but can transition to form rough colonies in the laboratory, usually associated with reduced virulence.

Bases on 16S rRNA sequence homology, *Brucella* spp. belongs to the  $\alpha 2$ -subdivision of the proteobacteria, together with animal pathogens such as *Bartonella* spp., *Rickettsia* spp. and plant pathogens such as *Agrobacterium tumefaciens*, but also plant symbiont such as *Sinorhizobium meliloti* [10].



*Brucella* spp. are facultative intracellular bacteria that can infect many species of animals and can also be associated with disease in humans. Recently, identification of several new *Brucella* species has considerably expanded the genus. To date 12 species form the genus *Brucella*. The classification of these species was based on the difference in host preference (Table 1) and phenotypic characteristics. In 1968, the genus was composed by 6 “classical” or “core” *Brucella* species affecting terrestrial mammals: *Brucella abortus*, *Brucella canis*, *Brucella melitensis*, *Brucella neotomae*, *Brucella ovis* and *Brucella suis* [4]. These species are very close genetically, they share on average more than 94% of identity at the nucleotide level [11]. Biovars were recognized for certain of these species. Since the 1990s, 6 new and “atypical” strains have joined the genus *Brucella*: *Brucella microti*, *Brucella inopinata*, *Brucella ceti*, *Brucella pinnipedialis*, *Brucella papionis* and *Brucella vulpis*.

Each species of *Brucella* has one or more preferential animal reservoirs that maintain their transmission cycle (Table 1). However, they are not totally specific to their reservoir.

Recently, bacteria of the genus but not belonging to any of the known families have been isolated in amphibians as the natural host [12], the first non-mammal host described for *Brucella*. *In vitro* and *in vivo* experiments suggest that this strain is able to invade and proliferate in macrophages but also survive in the murine host model. The mechanisms explaining the apparent *Brucella* host-specificity of the different species remains to this day poorly understood. The majority of brucellosis infections in humans are due to: *Brucella melitensis*, *Brucella abortus*, *Brucella canis* and *Brucella suis* (Table 1). In addition, the new strains of *Brucella ceti* and *Brucella pinnipedialis* associated with cases of brucellosis in marine mammals also appear to be capable of transmitting the disease to humans [13].

**Table 1: Host preference and zoonotic potential of the different *Brucella* species.** Modified from [14].

<b><i>Brucella</i> spp.</b>	<b>Natural Host</b>	<b>Pathogenicity to humans</b>	<b>LPS type</b>	<b>Ref</b>
<b><i>Brucella melitensis</i></b>	Sheep, goats, camels	High	Smooth	Bruce D 1887
<b><i>Brucella abortus</i></b>	Cattle, buffalo, elk, yaks, camels	High	Smooth	Bang B 1897
<b><i>Brucella suis</i> different biovar</b>	Pig (biovar 1-3); wild boar, hare (biovar2); Reindeer, caribou (biovar4); Rodent (biovar5)	High	Smooth	Huddleson 1929
<b><i>Brucella canis</i></b>	Canines	Moderate	Rough	[15]
<b><i>Brucella ovis</i></b>	Sheep	No reported infection	Rough	[16]
<b><i>Brucella neotomae</i></b>	Desert wood rat	No reported infection	Smooth	[17]
<b><i>Brucella pinnipedialis</i></b>	Pinnipeds (Seals, sea lions and walruses)	Low	Smooth	[18]
<b><i>Brucella ceti</i></b>	Cetaceans (Dolphins, whales, porpoises)	Low	Smooth	
<b><i>Brucella microti</i></b>	Wild voles, red foxes	No reported infection	Smooth	[19]
<b><i>Brucella inopinata</i></b>	Unknown Human from a breast implant infection, Amphibians	High	Smooth	[20]
<b><i>Brucella papionis</i></b>	Baboons	No reported infection	(?)	[21]
<b><i>Brucella vulpis</i></b>	Red foxes	No reported infection	(?)	[22]

#### 4. Transmission

In animals, transmission occurs generally at the time of abortion or parturition. High concentrations of *Brucella* are found in fetal waters from infected animals [23]. This pathogen is able to survive outside its host for up to several months depending on the environment, temperature, humidity.

Human brucellosis has always been associated with an animal reservoir of *Brucella* spp. [24]. We can distinguish different transmission routes:

-The most common way is the ingestion of food from animal origin, unpasteurized milk or raw dairy products. Indeed, when animals are infected with *Brucella*, their milk becomes contaminated. Consumers of unpasteurized dairy products are at risk of contracting brucellosis. Nevertheless, veterinary controls and pasteurization have made contamination by dairy products exceptional in France.

-Inhalation of aerosolized infectious material is one of the most common routes for human infection. Persons at risk for this mode of transmission are meat slaughterhouse workers and people in laboratories that work with the bacteria [25]. Brucellosis is the most common laboratory-acquired infection, in the majority of cases aerosols are involved [26] [27]. For example, more than 100 students and staff became infected in two different institutes in China (Lanzhou and Harbin Veterinary research institute) (Nature new 17december2019). That is why in French laboratories, experiments on *Brucella* must be carried out in a biosafety level 3 (BSL3) containment. Its high infectious power (10 to 100 bacteria are sufficient to infect humans) coupled with its possible spread by aerosols make *Brucella* an organism with the potential to be used as a weapon of bioterrorism [28]. For this reason, *Brucella* has been included in the list of possible bioterrorism agents by the Centers for Disease Control and Prevention (CDC)[6].

-Close contact with infected animals. *Brucella* can penetrate into the body through skin wounds or mucous membranes. People most sensitive to this type of transmission are veterinarians, hunters and slaughterhouse workers.

-Human to human transmission is very rare. The disease can be transmitted to the newborn through transplacental route or breastfeeding of the infected mother. Transplantation, sexual or blood transfusions have also been reported as possible routes of human to human transmission [29] [30] [31].

## 5. Symptoms

Symptoms are different between animals and humans.

In animals, *Brucella* has a tropism for the reproductive system. In pregnant female animals, bacteria colonize the placenta leading generally to abortion of the foetus in the second half of gestation. This is due to high colonization of trophoblasts by *Brucella*. Brucellosis in cows and goats also leads to a reduction in milk production, due to bacterial colonization of the mammary glands [32] [33].

In male animals, brucellosis is characterized by orchitis which leads to sterility. In both male and female animals, symptoms can include arthritis [34].

In humans, brucellosis is a serious debilitating disease that can have a fatal outcome if untreated. The incubation period of the pathogen is 1 to 4 weeks but sometimes the incubation period can last several months without any symptoms. The symptoms of brucellosis are not dependent on the mode of transmission by which the patient became infected.

The clinical presentation of brucellosis can be subdivided in three phases: acute, sub-acute and chronic. In the acute phase, clinical manifestations are variable and non-specific. The infected individual may present with flu-like symptoms, fever, chills, sweating, malaise, weight loss or osteoarticular pain, hepatosplenomegaly, lymphadenopathy and hearing loss [35].

Then the bacterium spreads and can reach different organs. In absence of treatment, the disease evolves into a subacute or chronic phase which are much more complicated to treat [36]. The sites of infection are the bones and joints, the liver, and sometimes the heart and the nervous system. The latter two infections cause endocarditis and neuro-brucellosis, which can lead to death in 2% of cases [37].

## 6. Diagnosis

Diagnosis from clinical observation data is difficult due to symptom variability and non-specificity in the acute phase. Nevertheless, it is important to be able to start as early as possible a treatment in order to avoid the establishment of the chronic phase. For this reason, diagnosis is initially based on the patient's history of possible exposures (travels and/or consumption of contaminated milk products imported from endemic areas...). Subsequently, an adequate laboratory diagnostic method is essential to confirm or not brucellosis. There are several diagnoses that can be direct or indirect.

Direct diagnosis includes culture and isolation of the strain from biological samples (blood culture, lymph node, bone marrow, cerebrospinal fluid...), which is the gold standard. However, in the chronic phase of the disease, detection is only very rarely positive in the case of blood cultures. However, this technique is time-consuming and expensive. Another direct detection technique is polymerase chain reaction (PCR) and real-time PCR. These techniques are sensitive and specific. They also have the advantage of being relatively fast and reduce the risk of acquisition of brucellosis by the personnel performing the analysis, because the bacteria are inactivated. On the other hand, false negatives may be observed as a result of the presence of DNA polymerase inhibitors in clinical samples. False positives may also be observed in the case of sample contamination or cross-amplification reactions.

Indirect diagnoses include serological tests, which are the most commonly used diagnoses for brucellosis. They have the advantage of being quick, less expensive and safer. Among these techniques are the Rose Bengal Test, the Wright agglutination (WHO reference reaction), the Coombs antibrucella, immunocapture techniques and serology to detect specific IgG and IgM antibodies. False positives may occur due to an antigenic relationship with other pathogens (*Escherichia coli* O157, *Francisella tularensis*, *Yersinia enterocolitica*, *Vibrio cholerae* and *Salmonella* species) [38].

## 7. Treatments, prevention & vaccins

Unfortunately, there is no safe and effective vaccine for brucellosis in humans. During the acute phase, the treatment of brucellosis is based on the combination of two antibiotics doxycycline and rifampicin (treatment according to WHO) for a period of 6 weeks or streptomycin and doxycycline [39]. However, in some cases relapses are reported, despite the treatment [40]. In the absence of treatment or when treatment is insufficient, the disease progresses and enters a subacute focused phase, leading to the constitution of isolated or multiple infectious foci at the osteoarticular, neurological, genital, hepatic or cardiac level. In this case a treatment based on three antibiotics (doxycycline, rifampicin and gentamicin) is used at least 3 months. In the chronic phase, treatment of the disease is made impossible by the fact that the bacteria have become inaccessible. Only symptoms are treated, sometimes

surgical operations are performed to remove the site of infection in the case of endocarditis or osteoarticular localization.

Prevention of infection relies on reducing people's exposure to infected animals, food hygiene measures (milk sterilization), personal hygiene measures (wearing gloves, masks) for exposed occupations. In order to be able to control the disease in the human population it is important to be able to control and eradicate the disease in domestic and wild animals. Indeed, the decrease in the incidence of the disease in animals is correlated with a decrease in the number of infected individuals. Control and eradication of the disease in animals must be achieved through surveillance tests, slaughter of infected animals but also vaccination. Indeed, vaccination of cattle, sheep and goat herds is one of the best means of prevention to limit the transmission of the disease as much as possible. There are two types of brucellosis vaccines: live attenuated vaccines and inactivated vaccines. Currently the vaccines licensed for use in livestock are live attenuated vaccines. The most commonly used vaccines to protect farm animals are S19 and RB51 for *Brucella abortus*, Rev1 for *Brucella melitensis*.

Vaccine strain S19 is a live *B. abortus*, spontaneously attenuated mutant discovered in 1923 (Graves., 1943). This vaccine has been the reference vaccine and has a high level of protection. It is used for the vaccination of calves and cows with reduced dose. This vaccine provides a good rate of immunization and greatly reduces the number of abortions. However, S19 vaccination has some disadvantages. S19 has a smooth phenotype due to its O-antigen LPS which induces a specific antibody response and leads to interference with serodiagnosis [41]. This serological interference impedes the distinction between immunized and naturally infected animals. It has a residual virulence that can lead to abortion if administered in pregnant cows, and orchitis in male. For this reason, vaccination with S19 is currently only available in female calves between 3 and 8 months of age. In addition, S19 is fully pathogenic to humans, so veterinary personnel should pay particular attention at the time of vaccination to avoid accidental contamination.

Vaccine strain RB51 is a live attenuated *B. abortus* developed in 1982 [42]. Unlike S19, RB51 has a rough phenotype, it does not possess O-antigen LPS chain and therefore does not present serological interference problems. Like S19, RB51 has a good protection against infection and abortion [43]. For this reason, it is used as the reference vaccine in many

countries. However, this vaccine does have some drawbacks. RB51 is still pathogenic for humans and it is resistant to rifampicin which is used in treatment in human brucellosis.

Vaccine strain Rev1 is a live attenuated *B. melitensis* developed in the 1960s. To date Rev1 is the most effective strain against goat and sheep brucellosis [44]. Just like S19, Rev1 has a smooth phenotype and therefore will cause serological interference problems and is still virulent to humans [45]. In pregnant animals, Rev1 can lead to abortion even with reduced doses of vaccine.

Efforts are currently being made to develop new and better livestock vaccines, and generate human vaccines. Live attenuated vaccines against farm animals have been in use for several decades. They are mostly effective in preventing abortion and disease transmission. However, they still have disadvantages as described above and immunization protocols must be chosen carefully (single or multiple dose vaccination, reduced dose, route of administration, age of the animal to be vaccinated, etc). Besides, not all countries have the same vaccination regulations. In France, for example, vaccination of cattle, sheep and goats is prohibited because vaccination is not compatible with serological screening. However, departments that are still infected may have derogations for the vaccination of sheep and goats.

## 8. Consequences

Nowadays, this disease seems to be re-emerging in the world, with the identification of new strains (marine mammals, and amphibian) and the appearance of wild foci (bison, deer, hare, caribou, wild boar, chamois, ibex, etc.). Indeed, animal brucellosis in wild animals constitutes a *Brucella* reservoir with possibility of accidental transmission to farm animals and therefore also to humans [46] [47]. This is the case in the Greater Yellowstone in USA where bison and elk remain a major reservoir for the disease [48] or in France with ibex and wild boar [49]. Brucellosis is still a highly infectious disease with a worldwide distribution. It is a threat to public health and also has important socio-economic repercussions (along with farmer emotional suffering). The deficit in animal production due to reduced milk production, abortion, and slaughtering of infected animals [50] leads to important economic losses in developing countries estimated to hundreds of millions of dollars [51]. Brucellosis control measures have proven to be effective since many developed countries are now considered

free of brucellosis. Nevertheless, efforts must be focused on educating the population in order to acquire the barrier gestures and on the scientific community in order to better understand the mechanisms of virulence of the bacterium with the aim of developing more effective vaccines.

## 2. *Brucella* intracellular life

Like *Legionella*, *Listeria* and *Salmonella*, *Brucella* are classified as facultative intracellular pathogens, in contrast to obligate intracellular pathogens such as *Chlamidia*, *Rickettsia* or *Coxiella*. However, the term facultative extracellular pathogen might be more appropriate, as to date no environmental reservoirs have been identified and the intracellular environment is suitable to *Brucella* replication [52]. Indeed, *Brucella* is extremely well adapted to intracellular life style, it is able to manipulate intracellular traffic, immune response, and replicate within host cells without inducing cell death. Furthermore, hiding within eukaryotic host cells limits exposure to immune responses, competition with other microbes and protects *Brucella* against the effect of antibiotics making treatment more complicated.

This pathogen is able to enter, survive and replicate in a wide range of mammalian cell types, including professional phagocytes such as macrophages and dendritic cells and non-professional phagocytes such as epithelial cells, fibroblasts and trophoblasts [53] [54] .

### 1. Entry into the cells

Successful bacterial invasion depends on two consecutive steps: binding and internalization. The mechanism of attachment and entry into cells host by *Brucella* are not fully understood and is still controversial.

In non-professional phagocytic cells, *Brucella* is taken up within minutes after inoculation, with one or two bacteria per cell [55]. In this process, lipid-rafts are involved. *Brucella's* entry into the host cell is abolished by inhibiting clathrin, suggesting it plays a fundamental role in the entry [56]. *Brucella* uptake by HeLa cell leads to a slight reorganization of the membrane with enrichment of the F-actin cytoskeleton at the entry site. Previously it has been shown that infection performed in the presence of cytochalasin D and colchicine,



two specific inhibitors of microfilaments and microtubules respectively also hamper internalization [57].

Rho small GTPases (Rho, Rac and Cdc42) known to regulate the organization of actin cytoskeleton, are required for actin polymerization and *Brucella* penetration into cells. Cdc42 is directly recruited and activated by virulent *Brucella* [57]. Regulator BvrR and sensor protein BvrS coding by the two-component regulatory system BvrR/BvrS are involved in the invasion of *Brucella* in both professional and non-professional phagocytic cells. *Brucella* BvrR/BvrS mutants fail to recruit small GTPases of the Rho subfamily [58] [59].

In professional phagocytic cells, two cases can be distinguished depending on the opsonic condition of the bacteria. In the case of opsonized *Brucella*, internalization occurs via complement and Fc receptors. After recognition by the receptor, *Brucella* is internalized by phagocytosis which occurs by a zipper-like mechanism. In this case, *Brucella* is mostly phagocytized by activated macrophages which can efficiently destroy bacteria [52].

In the case of non-opsonized *Brucella*, internalization into host macrophages is mediated by components of lipid rafts such as cholesterol and ganglioside GM1 on the cell host plasma membrane [60] [61] [62]. In this case, internalization is dependent on toll like receptor 4 (TLR4) and PI3 kinases. Indeed, when TLR4 is disrupted internalization of *Brucella abortus* is suppressed [63] [64,65].

The LPS also plays an important role in bacterial adhesion and internalization. In smooth strains, the LPS O side chain interacts directly with the class A scavengers receptors (SR-A) present in lipid rafts of host cell plasma membrane [66]. Macrophages from SR-A-deficient mice hamper *Brucella* internalization and replication, showing internalization is SR-A dependent. Nevertheless, signal transduction mediated by SR-A remains unknown. In contrast, rough strains, whose LPS does not have O side chain, do not enter through lipid rafts and are quickly degraded by lysosomes [62].

Another receptor that has been shown to be involved in the internalization of *Brucella abortus* in macrophages is the cellular prion protein (PrPc) present on the surface of macrophages or M cells through Hsp60 a chaperone of the GroEL family [67] [68]. However, these studies remain controversial [69].

To enable adhesion to cells *Brucella* has developed surface molecules that target different cellular receptors. In HeLa cells as well as macrophages, *Brucella* adhesion is mediated by SP41 a surface marker of the brucellae which interact with eukaryotic receptors containing sialic acid [70] [71]. More recently, additional adhesins have been described, including BigA [72] and the trimeric autotransporter BtaE [73].

## 2. Intracellular traffic

Once inside phagocytic or non-phagocytic cells, *Brucella* is found in a membrane-bound compartment, the so-called *Brucella*-containing vacuole (BCV). These BCVs traffic along the endocytic and secretory pathway and mature over time (figure 2).

The initial stage of trafficking take place between 0- and 8-hours post-infection and the BCV is called endosomal BCV (eBCV). During this stage, eBCV fuses with early endosomes and acquires some of their markers such as the small GTPase Rab5 and Early endosome Antigen 1 (EEA1). Thereupon, eBCV partially fuses with late endosomes and lysosomes where it acquires late endosomal markers such as Lysosomal-Associated Membrane Protein 1 (LAMP-1) as well as the small GTPase Rab7 [74]. This transient fusion with the lysosome lead to an acidification of the BCV reaching a pH of 4.5 [75]. eBCV acidification is essential for correct traffic and replication in macrophages and HeLa cells during early stage of infection [75]. This acidification triggers the expression of the VirB type IV secretion system (T4SS) [76]. T4SS allows the translocation of several bacterial effector proteins into the cell host to modulate various cellular processes including BCV trafficking and host immune responses, which we will be discuss in the corresponding T4SS section. Several studies have shown that replication of *Brucella* in both macrophages and epithelial cells as well as *in vivo* models of infection requires the expression of the T4SS [52]. Additional virulence factors have also been implicated, such as the cyclic  $\beta$ -1,2-glucan (C $\beta$ G) synthesized by *Brucella* that is important for preventing total fusion with lysosomes and thus degradation [77]. It is important to note that at this early trafficking step, more than 90% of bacteria are killed inside the BCV in macrophages, meaning that only a few of the internalized bacteria are able to reach their replicating niche.

### 3. The endoplasmic reticulum: the replicating niche

Between 8 and 12 hours post-infection, eBCVs are redirected towards the endoplasmic reticulum (ER) and interacts with the Endoplasmic Reticulum Exit Sites (ERES). eBCVs lose the endosomal markers and acquires some specific markers of the ER such as calnexin, calreticulin, Sec61 $\beta$  [78] [54], giving rise to replicative BCVs (rBCV). This interaction is regulated by the small GTPase Sar1 involved in the formation of the COPII complex. This complex allows shuttling between the membranes of the ER towards the Golgi apparatus. Inhibition of Sar1 activity blocks replication, indicating that this interaction is essential for the establishment of the *Brucella* replication niche [79]. There is also other evidence that rBCVs interact with the vesicular traffic between the ER and the Golgi apparatus. Rab2 and the GAPDH are recruited to the BCV. These two proteins are involved in the vesicular transport between the ER and the Golgi apparatus [80]. *Brucella* effectors secreted by the VirB T4SS and that are involved in this process have been identified [81] [78] [82]. Studies have identified several effector proteins targeting host secretory functions among them, BspA, BspB and BspF that contribute to bacterial replication by impairing host secretory trafficking [83] and RicA [84]. For example, BspB interacts with the Golgi apparatus-associated conserved oligomeric Golgi (COG) complex which is a key regulator of vesicular traffic at the Golgi apparatus [85]. This conversion into rBCV, provides a suited environment for *Brucella* replication.

Interestingly, initiation of bacterial division occurs at the eBCV stage, suggesting sensing of changing conditions within the vacuole [86]. Indeed, it has been clearly shown that *Brucella* cell division is intimately connected to intracellular trafficking [87]. During the first stage of BCV maturation, the bacterial cell cycle is arrested. However, before conversion of eBCV to rBCVs, bacterial division is initiated, which then likely assists the action of the T4SS and enables further maturation of BCVs into a compartment suited for proliferation.

Once the intracellular niche of replication is established, the bacteria aim to remain in the cell for as long as possible by inhibiting apoptosis [88] [89]. Thereupon between 12 and 48 hours post-infection, *Brucella* extensively proliferate in rBCVs to occupy almost the entire cytoplasmic volume of the host cell.

#### 4. The exit of *Brucella* : The autophagic BCV

It has been proposed that *Brucella* completes its intracellular cycle by the formation of autophagosome-like structures, autophagic BCVs (aBCVs) [90].

Autophagy is a ubiquitous degradation mechanism, orchestrated by more than 30 specific proteins called ATG (for autophagy-related gene) in a multi-step process, involving at least three main phases: Initiation, nucleation and elongation. It is a dynamic membrane process that begins with the *de novo* formation of vacuoles called autophagosomes encompassing cytoplasmic fractions into a double-membrane compartment. This process allows the capture of aggregated/misfolded protein, damaged organelles or pathogens. Subsequently these autophagosomes fuse with the lysosomes where their contents will be degraded providing nutrients or elimination of the pathogen. Although it has a role against microbial invasions, all or part of the autophagic process can be blocked, or hijacked, by microorganisms for their own benefit [91].

As a result of rBCV proliferation, starting at 48 hours after infection, BCVs lose ER markers and gain features consistent with an autophagosome. The formation of these vacuoles, named aBCVs for autophagic BCVs, is dependent on nucleation proteins such as Beclin1, ULK1 and Atg14L, but independent on elongation proteins Atg5, Atg7, Atg4 or Atg16L [90]. Thus, *Brucella* is able to subvert part of the autophagy machinery by modulating specifically autophagy initiation/nucleation complexes to allow its exit from the host cell and the infection of new adjacent cells.

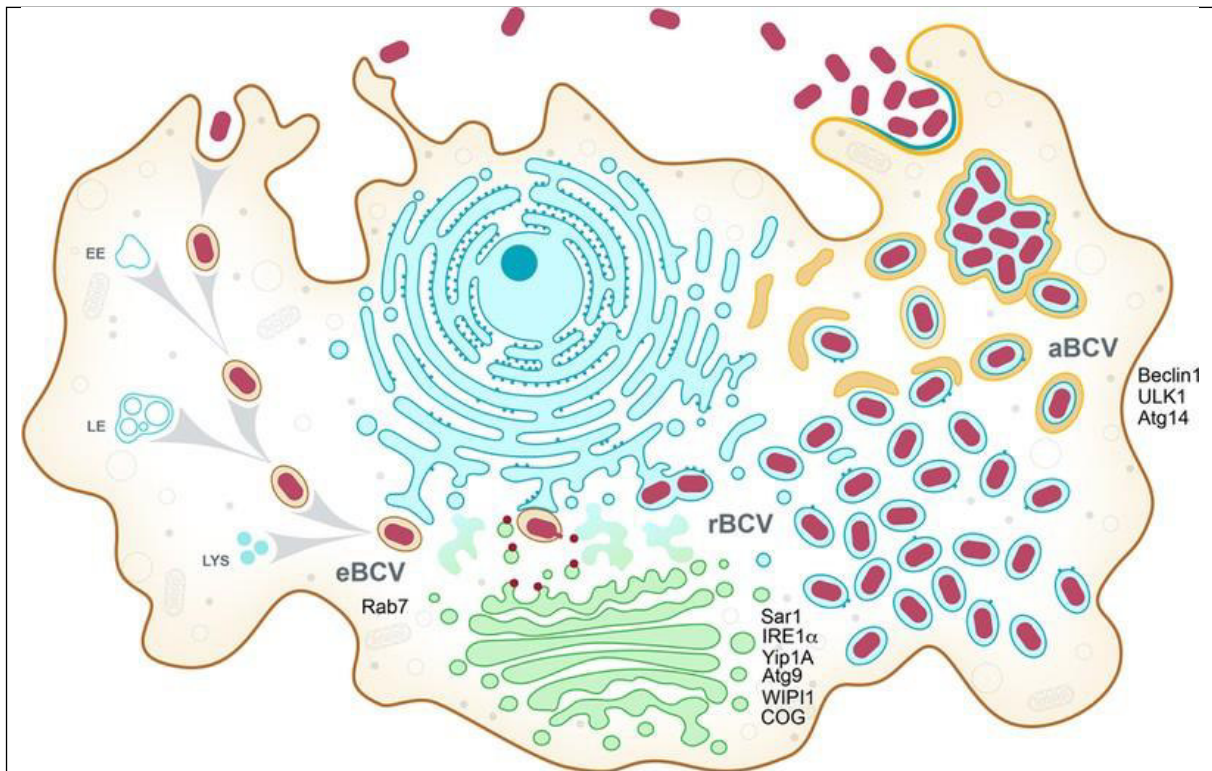


**Figure 2. *Brucella* intracellular lifecycle**

Once internalized by host cells, *Brucella* is contained in a vacuole named *Brucella*-containing vacuole (BCV). *Brucella* will follow the endosomal pathway and mature over time. BCV interacts with the host cell to first become endosomal BCV (eBCV), then replicative BCV (rBCV) and finally autophagic BCV (aBCV). [92].

### 3. Brucella T4SS and its effectors

Pathogenic bacteria are often able to secrete macromolecules necessary for virulence in the extracellular medium but also export them into host cells. These macromolecules must be able to cross the internal and external membranes of the bacteria, which are naturally hydrophobic and are therefore impermeable to hydrophilic macromolecules. Dedicated secretion systems make it possible to transport these macromolecules through the bacterial membranes and have an essential role in bacterial pathogenesis. Nine secretion systems are currently known in Gram-negative bacteria: types I to IX.

#### 1. Brucella T4SS

In 1999, thanks to the sequencing of the *Brucella suis* genome, O'callaghan et al. identified an operon coding for a type IV secretion system homologous to the *virB* system of *Agrobacterium tumefaciens* [93]. The *virB* operon is conserved in all the sequenced *Brucella* species.

- *T4SS functions*

Type 4 secretion systems are protein complexes that carry out the transfer of macromolecules (protein, DNA) across the two bacterial membranes. They are found in several pathogenic bacterial species such as *Agrobacterium*, *Legionella*, *Bartonella*, *Bordetella*, *Helicobacter* and *Brucella*. T4SS have several functions, namely: i) the transfer of an effector molecule from the pathogen to the host cell, ii) the release of DNA allowing the exchange of DNA with the extracellular medium, iii) bacterial conjugation, which ensures the transfer of DNA to a target receptor cell allowing the acquisition of a selective advantage [94] [95].

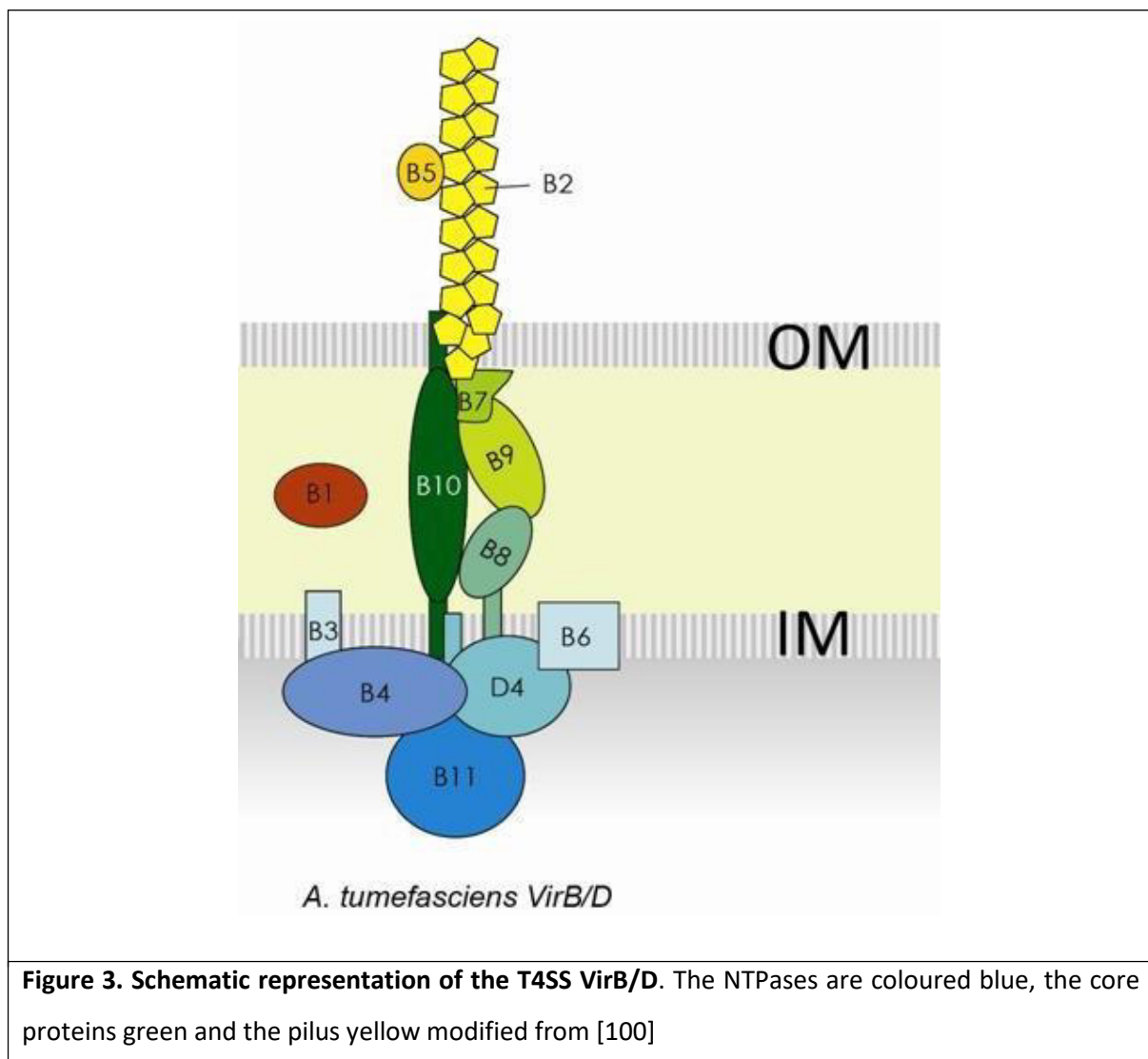
- *T4SS architecture*

The best characterized T4SS to date is the VirB/D4 system from *A. tumefaciens*. VirB/D4 is composed of 12 proteins called VirB1-11 and VirD4. This system serves as a reference for the study of effector translocation by T4SS in Gram-negative bacteria. The VirB/D4 system forms a dynamic protein complex consisting of three functional groups of proteins: i) the pilus, present on the bacterial surface, is formed by the VirB2 and VirB5 proteins and allows contact with the host cell. ii) the transmembrane or "core" channel (VirB7, VirB9 and VirB10) passes through the inner membrane, the periplasm and the outer membrane. This channel allows

the transport of the effector. iii) three NTPases provide the energy input necessary for the assembly of the complex as well as the transport of substrates through the pore (VirB4, VirB11 and VirD4) (Figure 3) [95,96] .

T4SSs are broadly classified as type IVA with structural components resembling the VirB/D4 complex of *Agrobacterium tumefaciens* or classified as type IVB, when they resemble the conjugal transfer system of the self-transmissible IncI plasmid, such as the case of *Legionella* and *Coxiella* [97]. Nevertheless, it is important to note that there are important differences between the systems even within the same class. This is nicely illustrated with the example of the type IVA T4SS of *Helicobacter pylori*. A pathogenicity island called cagPAI encodes for the T4SS known as cagT4SS, responsible for the translocation of the CagA oncoprotein [98,99]. This island encodes 28 proteins, 12 of which have similarities to the VirB proteins of *A. tumefaciens* and are essential for CagA translocation. This reveals that T4SS in *H. pylori* is more complex than its counterpart in *A. tumefaciens*.

Studies are currently being undertaken to characterize the *Brucella*'s T4SS, which has some intriguing features such as lacking the gene encoding for VirD4, an important ATPase in other systems and encoding for an additional protein (VirB12) with unknown function.



## 2. Brucella effectors

In *Brucella*, the VirB T4SS delivers into the host cells protein effectors that modify cellular functions in order for the bacterium to survive and proliferate [83]. Mutants lacking *virB* essential genes cannot survive or replicate in host cells and are attenuated in a mouse model of infection, showing that the *virB* encoded T4SS plays a major role in *Brucella* pathogenesis [101].

- *Brucella effectors identification:*

Since its discovery 20 years ago, only about twenty effectors have been identified and not all of them have yet been characterized. This contrasts with *Legionella*, whose T4SS was identified in 1998 [102], with more than 300 effectors characterized [103]. This shows how difficult it has been to identify effectors in *Brucella*. The Table 2 recapitulates briefly what is



known about *Brucella* VirB-secreted effectors. The majority of effectors in *Brucella* have been identified using a bioinformatic approach based on the sequenced *Brucella* genome. This approach aims to identify genes encoding proteins with eukaryotic-like domains, protein-protein interaction domains, domains present in other bacterial effectors known to be involved in virulence [104], potential horizontally transmitted regions encoding transposases or recombinases adjacent to transfer tRNAs [105] or presence of features similar to known VirB T4SS effectors (eg potential secretion sequences) or distinct GC content [83].

- *Brucella* effectors confirmation:

Once identified, these putative effectors must be confirmed as translocated in a T4SS-dependent manner during infection in the host cell. Several techniques have been successfully used: in particular the use of reporter systems such as CyaA adenylate cyclase or TEM1- $\beta$ -lactamase enzymatic translocation assays [104] [106] and more rarely by directly observing the effector fused to a tag [107]. The position of the N-terminal or C-terminal reporter tag of the putative effector can disturb the translocation of the protein. For example, only the position of the TEM1 in C-terminal of BspB, BspC, BspE showed a translocation while the translocation of BspA and BspF is independent of the position of the tag in N or C-terminal. In addition, several effectors have been shown to be translocated in the host cell but in a manner totally independent of the T4SS (BspG, BspH, BspI, BspK) [83].

This indicates the need for better characterization of the molecular mechanisms involved in effector translocation via T4SS in *Brucella* and the caveats associated with the use of reporter translocation systems.

### 3. Effector proteins secreted by *Brucella* T4SSs

The first reported effector protein were VceA and VceC, identified using TEM1-beta lacamase protein translocation reporter assay [106]. VceC interacts with Bip/Grp78, activating the Unfolded Protein Response (UPR) [108]. More recently, contradictory results have been reported related to the role of VceC. Some author found that VceC induces CHOP expression favoring ER stress in placenta trophoblast, and thus, inducing cell death and placenta inflammation, promoting abortion [109]. Other authors found that VceC inhibits the expression of CHOP protein inhibiting apoptosis mediated by ER stress and thus, protecting

cell from death by apoptosis and favoring intracellular persistence [110]. Also, very recently, it has been shown that a VceA mutant promotes autophagy and inhibits apoptosis in trophoblast during *Brucella* infection [111]. BPE005, BPE043, BPE275 and BPE123 were identified using CyaA adenylate cyclase assay [104]. BPE123 was shown to interact with alpha enolase (ENO-1), a host cell factor involved in *B abortus* intracellular replication [112]. Additionally, BPE005 was shown to induce collagen deposition and matrix metalloproteinase 9 down-modulation via transforming growth factor beta1 in hepatic stellate cells [113].

De Barsey et al. used a high-throughput yeast two-hybrid screen to identify interactions between *Brucella* proteins and human proteins predicted to be enriched in phagosomes such as RabGTPases. This screening identified RicA (Rab2 Interacting Conserved protein A) as putative effector confirmed by TEM1- $\beta$ -lactamase reporter assay. RicA preferentially interacts with GDP-bound inactive form of the Rab2. Rab2 is involved in membrane trafficking from the Golgi apparatus to the ER [114]. It has been shown that Rab2 is recruited onto BCVs during infection and is involved in the control of intracellular trafficking of BCVs [80].  $\Delta ricA$  mutant strain loses LAMP1 earlier than the wild type strain. By interacting with GDP-bound Rab2, RicA delays the conversion from eBCV to rBCV [84].

Later on, five more effector protein were described, BspA, BspB, BspC, BspE and BspF [83]. Some of them were shown to target the host cell secretion pathway, including BspA, BspB and BspF. These three effectors were predicted by bioinformatics approach and confirmed by TEM-1 and CyaA assays. Overexpressed in Hela cells or HEK293T, these effectors inhibit protein secretion. In infection, *Brucella* also interferes with host protein secretion and this inhibition takes place 8 hours after infection, just before the BCV joins the ER, its replication niche.  $\Delta bspB$  and  $\Delta bspF$  mutant strains failed to inhibit protein secretion in infection, whereas  $\Delta bspA$  mutant strain inhibit protein secretion similar to the wild type strain, suggesting that BspA is not involved in the inhibition of secretion in the context of infection. It seems that the inhibition of secretion in the host by these effectors promotes the formation of the *Brucella* ER-derived replication niche. Indeed, the triple  $\Delta bspABF$  mutant leads to a replication defect compared to the wild type strain [83].

The molecular mechanism by which BspB inhibits protein secretion and its involvement in bacterial replication has been recently studied. BspB interacts with an important complex in the coordination of vesicular trafficking in the host cell secretion pathway: the conserved

oligomeric Golgi (COG) complex, that regulates protein secretion and vesicular traffic at the Golgi apparatus. The interaction of BspB with the COG complex, leads to the diversion of COG-dependent vesicles towards the BCV to promote rBCV biogenesis. BspB and the COG complex are required for an optimal bacterial replication. Surprisingly, the replication defect of  $\Delta bspB$  mutant strains is restored by the depletion of Rab2 suggesting that BspB may affect retrograde secretory traffic to redirect COG-dependent Golgi vesicular traffic to the BCV [115].

Although individually the role of these effectors is becoming well established, the effect of the combined actions of these effectors is still unknown. Recently Smith et al have established a link between RicA and BspB during infection. They have shown that BspA and RicA show an epistatic interaction in the replication of *Brucella*. Although there are some discrepancies in relation to previous reports showing a role of Rab2 and RicA in rBCV biogenesis [80] [84], both effectors seem to be involved in modulation of Golgi apparatus associated vesicular transport dependent on Rab2. The currently proposed model is that RicA by interacting Rab2 inhibits the conversion of eBCV to rBCV, impacting rBCV biogenesis and replication, while BspB counters this effect to promote biogenesis and bacterial replication [116]. It will be important to establish the kinetics of secretion of these effectors. BtpA BtpB were identified together as T4SS effector protein [117]. BtpA was previously studied by several authors, who showed that BtpA has a TIR domain and is able to interfere with DC maturation [118] [119]. It was also reported that its target was TIRAP [120] [121] and that the protein could inhibit killing by CD8+T cells [122]. BtpA and BtpB through their TIR domain are able to modulate host inflammatory responses during infection specifically inhibiting TLR pathways [117], we will discuss BtpA and BtpB in more detail in the chapter on TIR proteins. Finally the T4SS effector protein of *Brucella* identified until now is SepA [123]. This protein inhibits the fusion of BCVs with the lysosome.

**Table 2 : *Brucella* T4SS effector proteins**

Name	Gene	Target	Function	Translocation Method	References
<b>VceA</b>	<i>bab1_1652</i>	Unknown	Inhibits autophagy and induces apoptosis	TEM1	[106]
<b>VceC</b>	<i>bab1_1058</i>	BiP	Activates UPR	TEM1	[106]
<b>BPE005</b>	<i>bab1_2005</i>	Unknown	Inhibition of matrix metalloproteinase 9	CyaA	[104]
<b>BPE043</b>	<i>bab1_1043</i>	Unknown	Unknown	CyaA	[104]
<b>BPE275</b>	<i>bab1_1275</i>	Unknown	Unknown	CyaA	[104]
<b>BPE123</b>	<i>bab1_0123</i>	ENO-1	Contributes to intracellular lifestyle. ENO1 recruitment to the BCV	CyaA	[104]
<b>RicA</b>	<i>bab1_1279</i>	Rab2	Regulation of vesicular trafficking. Rab2 recruitment at the BCV	TEM1	[84]
<b>BspA</b>	<i>bab1_0678</i>	Unknown	Inhibits the secretory pathways	TEM1 and CyaA	[83]
<b>BspB</b>	<i>bab1_0712</i>	COG complex	Inhibits the secretory pathway. Biogenesis of rBCV and bacterial proliferation	TEM1 and CyaA	[83]
<b>BspC</b>	<i>bab1_0847</i>	Unknown	Unknown	TEM1 and CyaA	[83]
<b>BspE</b>	<i>bab1_1671</i>	Unknown	Unknown	TEM1 and CyaA	[83]
<b>BspF</b>	<i>bab1_1948</i>	Unknown	Inhibits the secretory pathways	TEM1 and CyaA	[83]
<b>BtpA/TcpB/Btp1</b>	<i>bab1_0756</i>	TIRAP, Myd88	Inhibits TLR pathways Modulation of microtubule dynamics UPR induction	TEM1 and CyaA	[119]
<b>BtpB/Btp2</b>	<i>bab1_0279</i>	Myd88	Inhibits TLR pathways	TEM1 and CyaA	[117]
<b>SepA</b>	<i>bab1_1492</i>	Unknown	Inhibits BCV fusion with the lysosome	3xFLAG	[105]

#### 4. The different research projects of my thesis work:

The objective of this thesis is to characterize new bacterial effectors identified in *Brucella*. My work focused on 4 *Brucella* effectors, BtpA and BtpB, and two new effectors NyxA and NyxB.

BtpA and BtpB are two TIR domain-containing proteins known to interfere with TLR-mediated signalling and thereby inhibit the host's innate immune response. Recently, proteins containing TIR domains have been described as having NAD<sup>+</sup> hydrolase enzymatic activity *in vitro*. In collaboration with the team led by Dr. Victor Cid, we aimed to determine if this NAD<sup>+</sup> hydrolase activity is retained for BtpA and BtpB. Victor Cid's lab, using over-expression of these TIR effectors in yeast was able to show that both proteins resulted in NAD depletion in yeast cells. Our team, by measuring the intracellular level of NAD, confirmed these results in epithelial cells expressing BtpA and BtpB but also during *Brucella* infection. This collaborative work is included in the results, and was published in PloS Pathogens this year, in which I am joint-first author.

The second part of this thesis manuscript corresponds to my principle PhD project. This work was funded by a young researcher ANR project "NucPath" obtained by Dr Suzana Salcedo. This project aims at characterizing the cellular role of two new effectors in *Brucella*: NyxA and NyxB. To do this, we are using a multidisciplinary approach combining cell biology, cell imaging, structural biology and biochemistry. We had multiple objectives: to identify the target of these 2 effectors and to understand their role and mode of action in infection; to carry out a structural and functional study in order to define the functional domains involved in the modulation of host cell functions.

For this reason, we are going to present the TIR protein related to the first research project and in a second time introduce the nucleus and the sumoylation corresponding to a compartment and a post-translational modification targeted by the two new effectors identified during my major thesis project.

## 5. TIR proteins and innate immune system.

### 1. Immune system

The immune system is the body's biological defense system. It allows the identification of non-self (proteins, viruses, bacteria, parasitic fungi and other pathogens) and self-defense by controlling the invasion and proliferation of infectious agents. It is composed of a multitude of proteins, cells, tissues and organs forming a dynamic network capable of specifically recognizing and adapting a response to eliminate a wide variety of foreign microorganisms.

The immune system is able to recognize molecular patterns that characterize groups of pathogens with known characteristics, and to establish a rapid immune response directed against these pathogens. It is divided into two parts that differ according to the speed and specificity of the immune response: the innate immune system (non-specific) and the adaptive immune system (specific). The innate immune system is the body's first line of defense against infectious agents while the adaptive immune system acts as a second line of defense. Nevertheless, there is a strong interconnection between these two immune systems, so the innate immune response stimulates the adaptive response and influences its response [124] [125].

Despite these efficient barriers, some pathogens have developed strategies to circumvent immune defense mechanisms.

In most cases, the innate immunity is very effective and immediately brought into play, preventing most infections from spreading and thus allowing the infectious agent to be eliminated within a few hours of its encounter with the organism [126]. Innate immunity includes several non-specific protective mechanisms such as physical or mechanical barriers. A good example are epithelial cells (urogenital, bronchial or digestive epithelium). that form a barrier between the external environment where the microorganisms reside and the internal environment which is supposed to be pathogen-free. The pulmonary epithelium for instance, ensures a protective function against external aggressions by the secretion of mucus on which dust, particles and microbes will be trapped. Multiciliated cells, on which several hundred

vibrating lashes will beat in a coordinated manner, allow this mucus to be transported to the digestive tract where it will be broken down.

Once infectious agents have penetrated the body, the innate immune system is able to induce an inflammatory reaction using specific receptors. This mechanism involves different cell types such as: phagocytes (macrophages, neutrophils, monocytes and dendritic cells), natural killer (NK) cells and innate lymphoid cells. The innate immune system corresponds to a common defense mechanism in all multicellular animals and is thought to have evolved long before the adaptive immune system [127].

## 2. Recognition of microbes and pathogens by the innate immune system

The immune system is able to make “self” and “not self” this distinction by recognizing repeated molecular structural patterns present on the surface of invading microorganisms, whether pathogenic or not.

- *PAMPs* :

In mammals, the immune response is essentially via effector cells such as macrophages, which are able to detect particular patterns decorating pathogens. These particular patterns have been named by Charles Janeway, PAMPs which stands for Pathogen Associated Molecular Pattern [124]. Nevertheless, it is important to emphasize that PAMP is not entirely the right term to describe these structures, since they are also present on non-pathogenic microorganisms, especially commensal flora. These molecular signatures are conserved during evolution and are exclusively present on the microorganisms and totally absent from the host cells. These structures are also essential for the survival and proliferation of these microorganisms.

The recognition of the non-self will lead to the production of cytokines such as interleukin (IL)-1, TNF $\alpha$  (Tumor Necrosis Factor $\alpha$ ) and IL-6 leading to the inflammatory response and stimulate the adaptive immune response via lymphocytes.

Each group of microorganisms has one or more PAMPs. These unique molecular units present on the surface of the microbes can be: lipopolysaccharide (LPS) present on the outer membrane of Gram-negative bacteria, lipoteichoic acid and peptidoglycan present on the membrane of Gram-positive bacteria, flagellin in flagella of bacteria, dsRNA and ssRNA in viruses, or mannans on the wall of fungi. These PAMPs will be detected by our body to alert the immune system. How can the immune system recognize these PAMPs?

PAMPs are recognized by specific receptors present on the surface or inside cells of the innate immune system called PRRs (Pattern Recognition Receptors) [128].

- *PRRs* :

PRRs are receptors expressed in innate immune cells such as macrophages and dendritic cells. PRRs are also present in non-professional cells, as epithelial cells, endothelial cells and fibroblasts that contribute to the innate immune response. These are present at the plasma membrane or within cells, at the cytosol level but also in different cell compartments such as endosomes. This diversity of cellular localization of these PRRs corresponds to the different cellular compartments in which pathogens can be found. Thus, PRRs are able to recognize pathogens both extracellularly and intracellularly.

Each type of PRR can recognize a multitude of pathogenic species that share a particular molecular motif.

There are 4 main types of PRRs [129] (Figure 4):

-TLRs : Toll-Like Receptors : TLRs were the first family of PRRs to be discovered, they are also the best characterized. TLRs are related to defense against viral, bacterial and fungal infections. We will describe them in more detail later.

-CLRs : C-type Lectin Receptors :

CLRs are a large family of transmembrane receptors present mainly at the plasma membrane level of macrophages and dendritic cells. They are composed of one or more CTLDs (C-type lectin-like domains). They allow the detection of carbohydrate (polysaccharide) motifs contained mainly in fungal walls and leads to an inflammatory response.

-RLRs : RIG-1 like Receptors



RLR receptors essentially recognize viral components, mainly viral nucleic acids, and will activate all signaling pathways: NF- $\kappa$ B, MAP-kinases and interferon.

-NLRs : NOD-Like Receptors

NLRs are a large family of cytosolic receptors. They are present in cells where they act as sensors of bacterial invasion. They are subdivided into 3 subfamilies: NOD, NALP and NAIP. All three subfamilies recruit caspases that cleave a number of cytokines, in particular inflammatory cytokines such as interleukin 1, which is found in the inactive form in the cytoplasm and is thus activated.

Scavenger receptors can also be added to the PRR family because of their involvement in the recognition of PAMPs [130].

Activation of PRRs induces a cascade of intracellular signaling leading to activation and/or modulation of the immune response. This signaling cascade results in the production of antimicrobial peptides, the secretion of pro-inflammatory cytokines and the recruitment of neutrophils and macrophages that will together allow elimination of the invading pathogen.

Hereafter we are going to focus more particularly on the TLR.

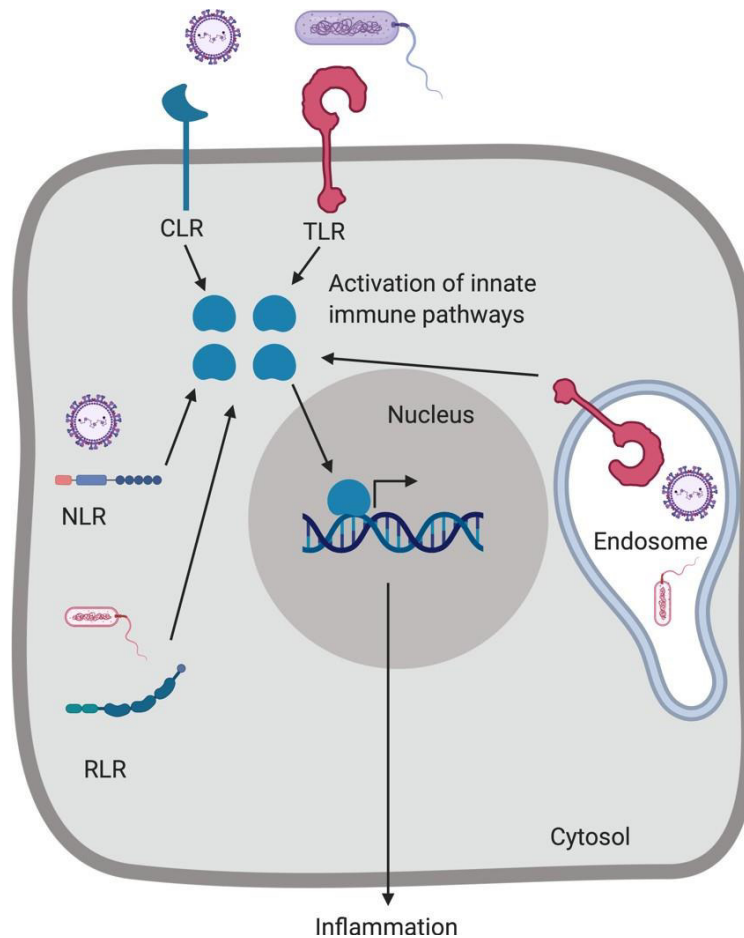


**Figure 4 : Location of the different classes of PRRs**

### 3. Toll-like receptors (TLRs)

The first Toll receptor was discovered in *Drosophila*. In *Drosophila*, the Toll gene plays a role in embryonic development, particularly during the establishment of dorso-ventral polarity [131] [132]. B. Lemaitre and co-workers have demonstrated the involvement of this receptor in innate immune functions against fungal infections [133]. Indeed, this study has shown that *Drosophila* deficient in toll genes are more susceptible to fungal infections. TLR have been discovered in mammals, insects, plants and also in *C. elegans* playing a role in the immune response [134-136] [134]. From an evolutionary point of view, it seems that this TLR recognition system is highly conserved over time.

In mammals, TLR receptors are mainly present on the surface of immune cells such as dendritic cells, macrophages, polynuclear cells, B and T lymphocytes. They can also be found in a large number of cells having contact with the external environment such as skin cells, epithelial cells or intestinal cells.

- *TLR structure:*

TLRs are type I membrane receptors in which three domains can be distinguished (Figure5):

-An extracellular N-terminal domain, which allows ligand recognition; this domain corresponds to a leucine-rich repeat (LRR).

-A transmembrane domain,

-An intracellular C-terminal domain that allows signal transduction, thanks to a specialized domain called TIR, for Toll/interleukin-1 receptor homology.

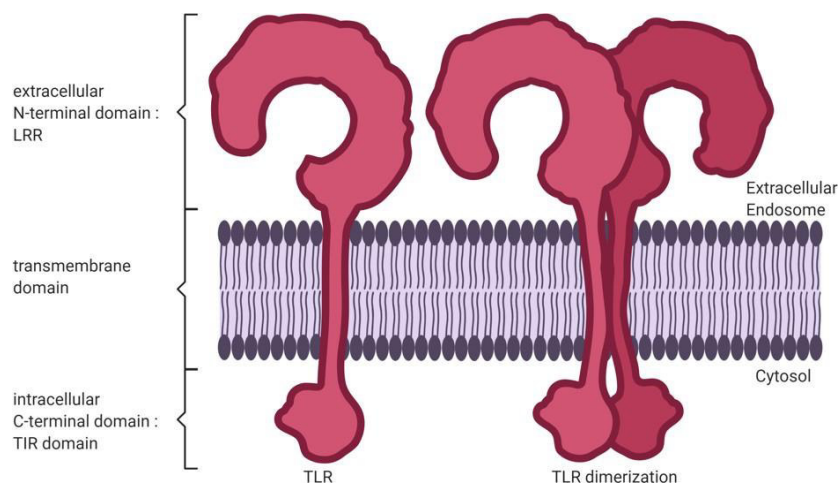


**Figure 5. Schematic representation showing structure of TLR family.** TLRs can be present at the plasma membrane of the cell but also in the endosomes present in the cell. The TIR domain of TLRs is always present in the cytosol.

### Extracellular domain :

The extracellular domain of TLRs is composed of approximately 800 amino acids in the form of leucine-rich repeats called Leucine-Rich Repeats or LRRs. This extracellular domain is involved in pathogen recognition and plays a key role in the initiation of TLR signaling [135]. The distribution and number of leucine-rich repeat units is specific to each TLR, which gives them their specificity in pathogen recognition [136,137]. It is composed of a beta-sheets and an alpha helix that forms a horseshoe structure, the beta-sheets are present on the concave side of the structure (Figure 6).

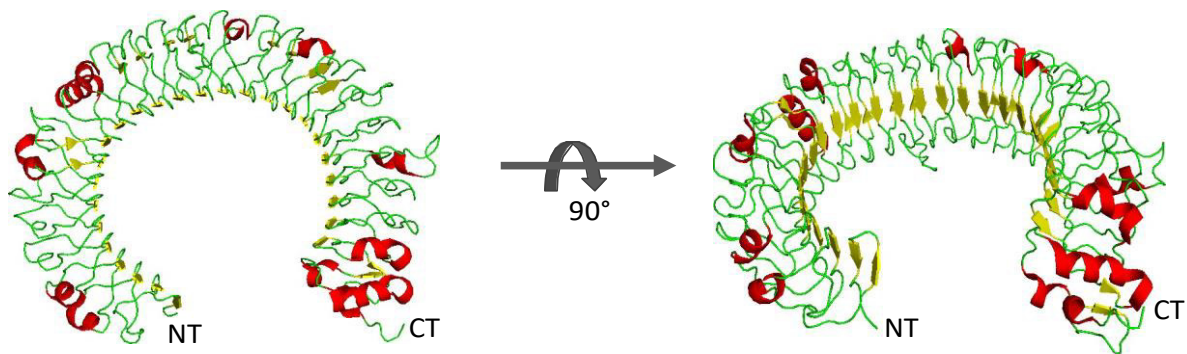


**Figure 6. Cartoon representation of the horseshoe-shaped structure of human TLR3** ectodomain (2a0z), depending on the secondary structural elements:  $\beta$ -sheet in yellow,  $\alpha$ -helices in red and loops in green. Structural representation were performed with Pymol.

### Intracellular domain :

The intracellular TIR domain of TLRs, consisting of 150 to 200 aa, is similar to that of the IL-1 receptor [138]. Three highly conserved sequences called box 1, box 2 and box 3 have been characterized in this TIR domain after alignment of sequences from different members of the IL-1R/TLR family[139] (Figure 7A). These sequences are involved in the signal transduction downstream of the receiver. The box 1 sequence is involved in the coupling of the TLR with another receptor [140], the box 2 sequence is involved in the interaction with the adaptor molecules involved in TLR signaling [141]. The box 3 sequence contains essential amino acids

for signaling and is involved in the localization of the receptor through interactions with elements of the cytoskeleton [142] and also in the interaction with the other TIR domain-

containing proteins : adaptor protein. There are 5 adaptor proteins : **MyD88** (Myeloid differentiation primary response protein), **TRIF** (Toll/IL-1 receptor domain containing adaptor inducing IFN- $\beta$  ou TICAM1 pour Toll-like receptor adaptor molecule 1), **TIRAP** (TIR domain containing adaptor protein ou MAL pour MyD88 adaptor-like), **TRAM** (TRIF-related adaptor molecule) et **SARM** (pour Sterile alpha- and armadillo-motif-containing protein) [126] [143]. These proteins allow, once the TLRs are activated, the transduction of the signal. Proteins containing TIR domains share 20-30% sequence identity. From a structural point of view, the TIR domains adopt approximately the same three-dimensional structure, with 5 parallel beta sheets surrounded on both sides by 5 alpha helices. The protein structure is more stable but also more conserved than the sequence during evolution. When comparing the structural alignment of the TIR domain of TLR2 (figure 7C) with that of the MyD88 TIR domain (Figure 7B) and calculating the Root-Mean-Square Deviation (RMSD) of each of the alpha carbons, an RMSD of 2.431Å is obtained, which allows us to consider that the two structures are relatively close to each other (Figure 7D). This is why we can say that the TIR domains are domains conserved during evolution.

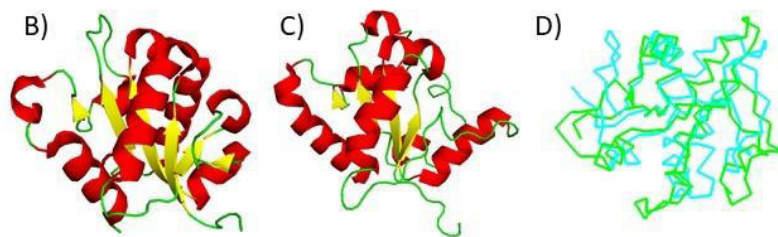
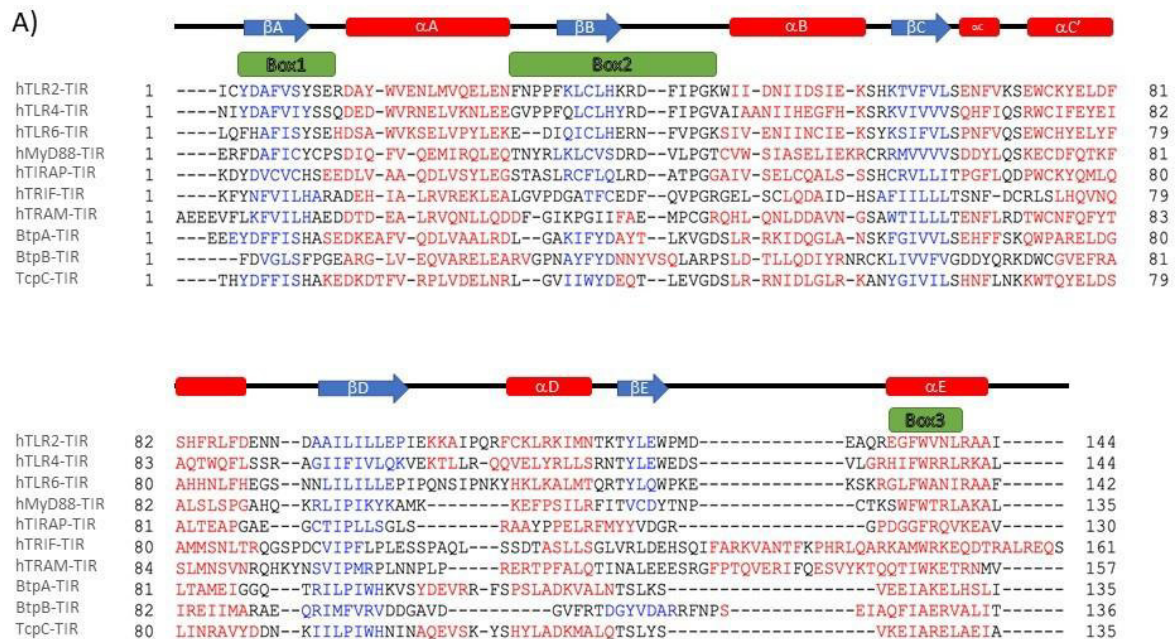


**Figure 7. Sequence and structure of TIR domains.** A) Multiple sequence alignment of TIR domain proteins from Human and bacterial : Human TLR2 (residues 639-782), Human TLR4 (residues 672-815), Human TLR6 (residues 640-781), Human MyD88 (residues 159-293), Human TIRAP (residues 84-213), Human TRIF (residues 393-553), Human TRAM (residues 73-229), Brucella abortus BtpA (residues 141-275), Brucella abortus BtpB (residues 156-292), Escherichia coli TcpC (residues 169-303). Structural features above the sequence are based on the MyD88. Blue arrows denote areas of beta sheet, red boxes denote alpha helices and black line denote connecting loops. The alignment and the prediction structure were performed with PROMALS3D. B) and C) Cartoon representation of the structure of human MyD88 TIR domain (4DOM) and human TLR2 TIR domain (1FYW) respectively, depending on the secondary structural elements:  $\beta$ -sheet in yellow,  $\alpha$ -helices in red and loops in green. D) Ribbon representation of the superposition of MyD88 TIR domain (4DOM) in cyan with TLR2 TIR domain (1FYW) with Root Mean Square Deviation (RMSD) of 2,431Å. Structural representation were performed with Pymol.

- *TLR and their Ligands :*

To date there are 10 different TLRs in humans (TLR1 to TLR10) and 12 TLRs have been identified in mice (TLR1 to TLR13), TLR10 is not present in mice [144]. Two different TLR groups can be distinguished according to their location in the cell. The TLRs present on the cell surface TLR1, TLR2, TLR4, TLR5, TLR6 and TLR10, and the TLRs present in the cell at the endosomes: TLR3, TLR7, TLR8, TLR9 [145] (Figure 8).

Each TLR is specific to a component of the microbes (Table 2). For example TLR2 recognizes bacterial lipoglycans, peptidoglycans TLR3,7 and 8 recognizes viral nucleic acids, TLR4 recognizes LPS, TLR5 recognizes flagellin, TLR 9 recognizes unmethylated oligonucleotide motifs.

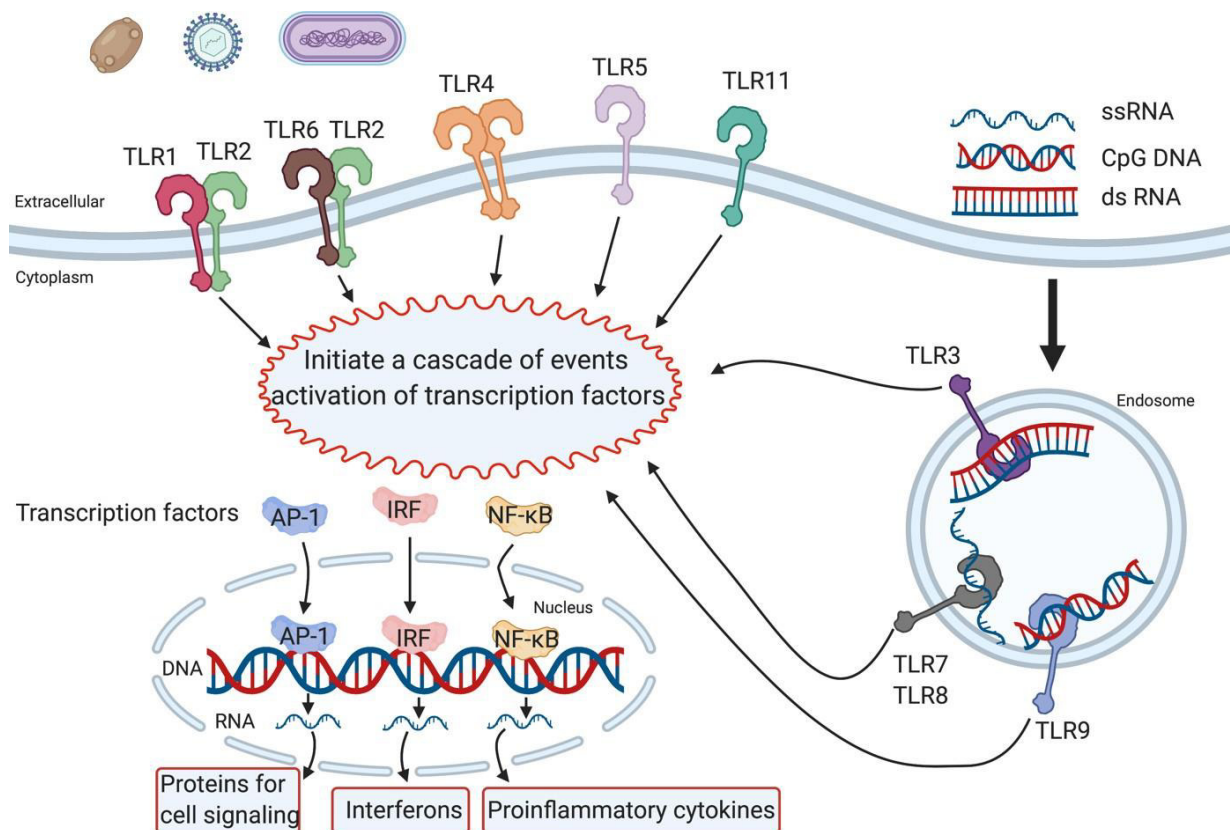


**Figure 8. Schematic representation of TLRs pathways.** Each receptor recognizes a specific ligand. TLR1, TLR2, TLR6, TLR5, TLR11 are at the cytoplasmic membrane, while TLR3, TLR7, TLR8, TLR8 and TLR9 are endosomal.



Once PAMP has been detected, TLR dimerize into either a homodimer or a heterodimer [146]. TLRs will activate an intracellular signaling cascade which is initiated by recruiting via TIR-TIR interactions between the TIR domain of the TLRs and the TIR domains adaptor proteins. This interaction allows the recruitment of IL-1R-associated protein kinases (IRAK) 1, 2, 4, M, TAB2 and TNF receptor-associated factor 6 (TRAF6). This signaling cascade leads to the translocation of transcription factors in the cell nucleus such as NF- $\kappa$ B [147], members of the IRF family (IRF3

<b>TLR</b>	<b>Ligand</b>	<b>Origin of the ligand</b>
<b>TLR1/TLR2</b>	Triacyl lipoprotein	Bacteria
<b>TLR2</b>	Lipoprotein Porine Lipoteichoic acid Lipoarabinomannan OmpA Porine	Bacteria, viruses, parasites,
<b>TLR3</b>	dsRNA	Virus
<b>TLR4</b>	LPS Viral protein Phosphatidylinositol mannoside	Bacteria Viruses mycobacteria
<b>TLR5</b>	Flagellin	Bacteria
<b>TLR6/TLR2</b>	Diacyl lipoprotein	Bacteria, viruses
<b>TLR7</b>	ssRNA	Virus, bacteria,
<b>TLR8</b>	ssRNA	Virus, bacteria,
<b>TLR9</b>	CpG-DNA	Virus, Bacteria, Protozoa,
<b>TLR10</b>	Unknown	Unknown

and IRF7) [148] and AP-1 [149] (Figure 8). These transcription factors allow the activation of genes and thus the production of inflammatory cytokines such as TNF alpha, IL-6, IL-1beta and IL-6 but also the production of chemokines (CXCL8 and CXCL10) and type I interferon (IFN) [150].

TLRs induce a specific response to their ligand. This specificity is mediated by the adaptor proteins involved in signal transduction. Two signaling pathways can be distinguished: a signaling pathway dependent on MyD88 and one independent of MyD88 but dependent on TRIF. It should be noted that the SARM adaptor protein acts as a negative regulator of the TRIF-dependent pathways. Indeed, SARM expression blocks the induction of TRIF-dependent genes, not those of MyD88[151].



- *The MyD88-Dependent Signaling Pathway:*

MyD88 is the first adaptor molecule identified in 1990 [152]. All TLRs except TLR3 are dependent on the recruitment of Myd88. Recruitment of Myd88 at the TLR-TIR domain can take place directly or by other adaptor molecules. Myd88 is recruited via TIRAP to initiate the signaling cascade of TLR4, the different heterodimers of TLR2, as well as the endosomal TLRs [153]. Subsequently, Myd88 recruits the IRAK (IL-1R-associated kinases) family of proteins to form what is known as the Myddosome. The myddosome corresponds to a multi-protein complex formed by 4 IRAK4 proteins and 4 IRAK2 proteins [149]. The myddosome activates the IRAK kinases by phosphorylation allowing interaction with TRAF6 (TNF receptor-associated factor 6). TRAF6 will thus be able to ubiquitinate itself. Ubiquitylated TRAF6 will be recognized by TAB2 (TAK1 binding protein) and TAB3, leading to the activation of the TAK1 complex (transforming growth factor [TGF]  $\beta$ -activated kinase 1). The activated TAK1 complex generates a phosphorylation cascade of the different members of the MAPK (Mitogen-activated protein kinase) pathway but also the induction of IB (inhibitor of NF- $\kappa$ B  $\alpha$ ) degradation via activation of the I $\kappa$ K (I $\kappa$ B kinase) complex, leading to the release of NF- $\kappa$ B and its nuclear translocation [154]. Activation of the MAPK pathways and the NF- $\kappa$ B transcription factor allows the expression of inflammatory cytokines.

- *TRIF-dependent signaling pathway*

The second TLR pathway induced following pathogen recognition is independent of Myd88 and is associated with TLR3 and TLR4[155]. This alternative pathway is dependent on TRIF, which is recruited directly at the TIR domain of TLR3 or indirectly via TRAM for TLR4. Subsequently TRIF interacts with TRAF6 and RIP1 (Receptor-interacting protein 1) to activate the MAPK and NF- $\kappa$ B pathways in the same way as the MyD88-dependent signalling pathway. However, TRIF also collaborates with TRAF3 which activates IKK $\epsilon$  (inhibitor of NF- $\kappa$ B kinase  $\epsilon$ ) and TBK1 (TRAF family member-associated NF- $\kappa$ B activator-binding kinase 1), both of which are responsible for phosphorylation and nuclear translocation of IRF3 and IRF7. This pathway thus allows the expression of type I IFNs and mainly IFN- $\beta$  [156].

#### 4. Microbial targeting of the TLR signaling pathway

Over the course of evolution, bacteria have developed different strategies to subvert immune responses from the host cell, including hijacking signaling pathways, modifying their PAMPs, and activation of others receptors that dampen the effect of TLR activation (Figure 9) [157].

Some pathogenic bacteria have evolved by modifying their PAMPs so that they are less

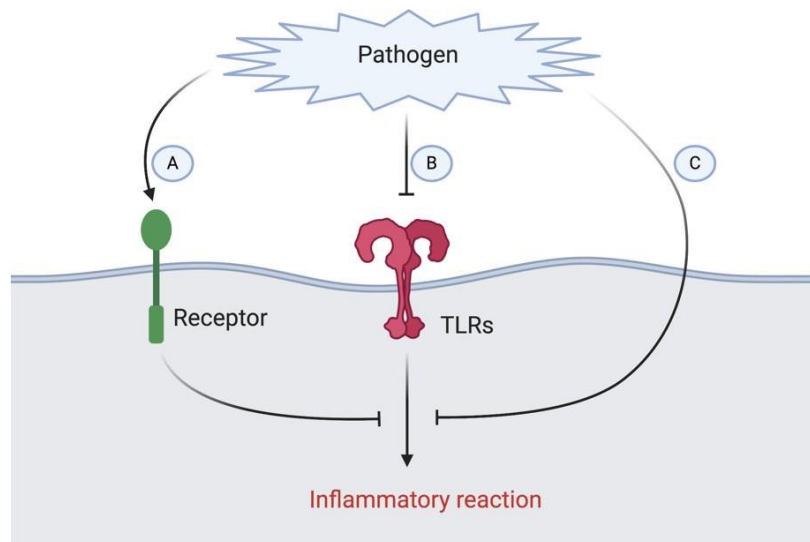


**Figure 9 : The different strategies used to manipulate TLRs.** (A) Microbes may stimulate other receptors that lead to a weakened immune response. (B) Microbes may modify their PAMPs in order to avoid TLR recognition. (C) Microbes may interfere with TLR signaling. Adapted from Sunderhill 20043

effective in stimulating TLRs. *Yersinia pestis*, for example, is capable of modifying the composition of its membrane lipid A, according to the growth temperature. Thus at 37°C, host temperature, the LPS of *Yersinia pestis* does not stimulate the TLR4 receptor [158] [159]. In addition, *Campylobacter jejuni*, *H. pylori* and *Bartonella bacilliformis* produce flagellins that do not activate TLR5 [160].

*Brucella* is also known to modify its PAMPs to escape the immune system or limit the host's immune response. Firstly, *Brucella* does not express pili, fimbriae or capsules which are recognized by the immune system. Furthermore, *Brucella melitensis* seems to produce a non-functional flagellum which limits its recognition by the TLR5 [161] [162]. In addition, the lipidA of *Brucella's* LPS has a longer fatty acid chain (C28) compared to the classical LPS of enterobacteria (C12-C16), resulting in a limited detection of this LPS by the TLR4. *Brucella* LPS is 1000 times less active and less toxic than *E.coli* LPS[163].

Some pathogens activate other receptors to indirectly manipulate the response of the TLR pathways. For example, *Mycobacterium tuberculosis* via mannose-capped lipoarabinomannan (ManLAM), a cell wall component, is able to activate a mannose receptor that inhibits pro-inflammatory cytokine production [164] [165].

Finally, microbes may directly target the TLR signaling pathway to modulate the inflammatory response. Indeed, TLRs are an excellent target as they are key elements in the regulation of the innate immune response against invading microorganisms. As discussed above, detection of microbial PAMPs by TLRs triggers a chain reaction that leads to the production of inflammatory mediators. This pathway is mediated by protein/protein interactions involving the TIR domains present on the cytoplasmic domains of the TLRs and on the adaptor proteins. Interestingly, pathogens also use bacterial TIR domain-containing proteins as molecular mimics to downmodulate TLR signaling [166].

#### 5. Bacterial TIR proteins

TIR domains are found in many bacteria, with more than 200 bacterial proteins with TIR domains estimated [167]. It has been shown that bacterial TIR domains from pathogenic bacteria can hijack TLR signalling pathways and thus prevent the translocation of the transcription factor NF- $\kappa$ B, inhibiting the production of inflammatory mediators. Among the bacterial pathogens containing TIR proteins we can cite *P. denitrifica*, *Brucella spp.*, *E. coli*, *Y. pestis*, *S. enterica*, *S. aureus*, *P. aeruginosa* (Table 1). Nevertheless, the mode of action of these different bacterial TIR proteins are not yet fully understood.

One of the best-characterized bacterial TIR-containing protein is TcpC, a virulence factor of uropathogenic *E. coli* responsible in urinary tract infections. TcpC interacts directly with Myd88 and TLR4 to impair TLR-induced cytokine secretion. In addition TcpC is able to interfere with TLR2 signaling [118]. TcpC is a virulence factor that increases acute mortality, bacterial persistence and tissue damage after infection [168].

BtpA and BtpB are two bacterial effectors secreted by *Brucella*'s T4SS. BtpA has been studied by numerous teams who have shown that BtpA possesses a TIR domain and is able of interfering with TLR signaling [119]. BtpA has been shown to interact with a eukaryotic

adaptor protein TIRAP and Myd88 [121] [169]. BtpA has also been shown to interact with specific phosphoinositides present in lipid raft [120]. BtpA and BtpB through their TIR domain are able to modulate the host inflammatory response during infection by specifically inhibiting TLR pathways and blocking the maturation of inflammatory dendritic cells [117]. In vitro experiments have shown that BtpB can strongly modulate the signaling pathways induced by TLR2, TLR4, TLR5 and TLR9. The authors also demonstrated by double hybrid experiments in yeast that BtpB interacts with Myd88 via their TIR domain. Contrary to BtpB, BtpA does not seem to block TLR9 [117]. Besides, the effect of BtpB on the modulation of the innate immune response appears to be greater than that of BtpA. In addition, infection experiments in mice with *Brucella* strains deleted for *btpA*, *btpB* or both, indicate that these effectors are able to modulating the inflammatory response *in vivo*. Consistently, BtpB was implicated in downmodulation of proinflammatory genes in chorioallantoic membrane explants from bovine placental tissues during early stages of the infection [170].

## 6. Bacterial TIR domain peptides as therapeutic agents

Stimulation of the innate immune response is necessary for host survival. Nevertheless, over-regulation of the immune response leading to uncontrolled inflammatory responses are observed in several mammalian diseases such as plaque sclerosis, rheumatoid arthritis or cystic fibrosis. In this context, before starting my thesis, with Dr Suzana Salcedo, we worked on a project funded by the association Vaincre La Mucoviscidose (VLM). Patients suffering from cystic fibrosis have exacerbated inflammatory reactions, which are highly disabling for the patients. Indeed, the inflammatory response to bacterial infections will damage the tissues and greatly reduce their respiratory capacity. The use of peptides based on TIR domains could be used as anti-inflammatory agents and represents a promising strategy for therapeutic application [171] [172]. Recently, use of a TIR domain peptide has proven successful in control of H1N1 infection in a mouse model [173] suggesting they may indeed provide powerful anti-inflammatory compounds.

**Table 3. Bacterial TIR domain-containing proteins and immune subversion** adapted from [169]

<b>Protein</b>	<b>Bacterium</b>	<b>Function</b>	<b>Interaction</b>	<b>References</b>
<b>BtpA (Btp1/TcpB)</b>	<i>Brucella spp.</i>	Inhibit TLR2, TLR4 and TLR5-mediated signaling Stabilization of microtubules Inhibition of dendritic cell maturation Induces the unfolded protein response (UPR) Facilitate bacterial colonization	TIRAP MyD88 TLR4 Microtubule Lipid raft	[169] [118] [174] [175] [120] [176] [119] [117] [121] [177] [178]
<b>BtpB</b>	<i>Brucella spp.</i>	Inhibit TLR2, TLR4, TLR5 and TLR9-mediated signaling Promote virulence	MyD88	[117]
<b>TipA</b>	<i>Salmonella enterica</i>	Inhibit TLR signaling responsible for activation of NF- $\kappa$ B Promotes bacterial survival	Not known	[167]
<b>TirS</b>	<i>Staphylococcus aureus</i>	Inhibit TLR2, TLR4, TLR5 and TLR9-mediated signaling Promote virulence	Not known	[179] [180]
<b>YpTdp</b>	<i>Yersinia pestis</i>	Suppresses NF- $\kappa$ B activation No role in virulence	MyD88	[181]
<b>PdTip</b>	<i>Paracoccus denitrificans</i>	Not known	MyD88 TLR4	[182]
<b>TcpC</b>	<i>Escherichia coli</i>	Inhibit TLR2 and TLR4-mediated signaling Facilitate bacterial colonization	MyD88 TLR4	[118] [168] [183] [184]
<b>PumA</b>	<i>Pseudomonas aeruginosa PA7</i>	Inhibit TLR4 and TLR5-mediated signaling Inhibit NF- $\kappa$ B activation Promote virulence	Myd88 TIRAP UBAP1 Lipid raft	[185]

## 7. Other roles of bacterial TIR domains

Numerous studies have shown the role of bacterial TIR domains in inhibiting TLR pathways, however these effectors can modulate other cellular functions. This is highlighted by TcpC, involved in control of the inflammasome and caspase-1 by interacting with the NACHT leucine-rich repeat PYD protein 3 (NLRP3) [186]. This is also the case for BtpA and BtpB that are closely associated with microtubules via their TIR domains when ectopically expressed, stabilizing the polymerized microtubules and preventing nocodazole-induced depolymerization of the microtubules [176]. In addition BtpA and BtpB present a WxxxE motif known in T3SS effectors to transiently subvert host actin dynamics [174]. BtpA also displayed an additional function as inducer of unfolded protein response [177].

Recently, studies have shown eukaryotic TIR domains of SARM1 (TLR adaptor protein) and several bacterial TIR protein have NAD<sup>+</sup> cleavage activity [187-190]. Enzymatic cleavage of NAD<sup>+</sup> by protein TIR domain constitute a new class of metabolic regulatory enzymes and could have important implications in control of host responses.

## 6. Foreword to the second part of the thesis

Before my arrival at the laboratory, a yeast two-hybrid screen was carried out by Jean-Paul Borg in Marseille in order to identify potential partners of the putative effector proteins studied during my thesis project. This technique allows detection of direct interactions between two proteins via the activation of a reporter gene. Although, this screen identified several potential targets, we chose to focus on SENP3, a deSUMOylase that is localized in a sub-structure of the nucleus, called nucleoli. This choice was based on three points. Firstly, SENP3 came out strongly from the double hybrid in yeast. Secondly, the subcellular localization of this potential partner of our effectors was really interesting. Indeed, the localization of SENP3 in the nucleus echoed the fact that preliminary experiments on NyxA, NyxB showed a nuclear localization in transfection. Finally, the function of SENP3, which is a deSUMOylase, seemed interesting to us because of the wide variety of cellular function involving this post-translational modification.

Therefore, in the introduction I have decided to briefly present the different structures of the nucleus and their functions, the process of SUMOylation and finish with a more detailed description of the functions of SENP3.

## 7. The nucleus :

The nucleus can be considered as the heart of the cell. It was the first cell compartment to be discovered in 1833 by Robert Brown. It contains the vast majority of the cell's genetic material, which is present as compacted DNA in the 23 pairs of chromosomes, with the rest of the genetic material found in the mitochondria. The chromosomes are present in defined regions of the nucleus in interphase [191]. The nucleus is highly organized and dynamic. It protects the genetic material and controls the physiology of the cell, particularly during cell division. It also performs major functions: DNA repair, transcription, RNA splicing, DNA replication, ribosome assembly, chromatin modifications, gene regulation and expression.

Only the cells of higher organisms (eukaryotes) have a nucleus, with the exception of red blood cells. The nucleus is the largest organelle of the cell, separated from the cytosol by a nuclear envelope corresponding to a double lipid membrane. The nuclear envelope has nuclear pores allowing the transport of biomolecules in both directions between the cytoplasm and the nucleus. The nucleus represents about 10% of the total volume of the cell with a diameter of about 10 $\mu$ m, however this value varies greatly depending on the cell type and the stage of the cell cycle. In HeLa cells the nucleus occupies 8-21% of the total cell volume. The protein atlas website (<https://www.proteinatlas.org/humanproteome/cell>) provides information on the expression and spatio-temporal distribution of proteins in human cells. They have been able to establish experimentally that 33% of all human proteins (i.e. 6523 proteins) are located in the nucleus. The presence of such a large number of proteins in a relatively small space underlines the need for structural organization in the nucleus.

### 1. Architecture of the nucleus :

Much is known regarding nuclear molecular mechanisms and processes, however it is only recently through molecular biology, biochemistry and cell biology techniques and especially through technological advances in the field of imaging using increasingly powerful microscopes that the architecture of the nucleus and its three-dimensional organization is beginning to be elucidated. In the 1980s, the use of fluorescent probes in microscopy made it possible to revive the study of the architecture of the nucleus by observing nuclear proteins



of chemically fixed cells [192]. This made it possible to highlight the presence of different structures within the cell with distinct and highly dynamic morphologies. To date, several nuclear sub-structures have been identified, also called nuclear bodies.

## 2. The different nuclear compartments: nuclear bodies

In a similar way to cytosol, where a compartmentalization of the different organelles can be observed according to different metabolic processes (i.e. mitochondria, Golgi apparatus, endoplasmic reticulum...), the cell nucleus presents different sub-structures [192] [193]. However, unlike the cytosol, the different nuclear sub-structures are not separated from their surroundings by a membrane. This compartmentalization facilitates metabolic processes, regulates the concentration of nuclear factors or serves as a hub for gene regulation. These nuclear bodies are extremely dynamic, reacting to different physiological processes and different forms of stress. They are formed at the exit of mitosis and maintained until the start of the next mitosis. Nuclear bodies are made up of proteins and RNAs whose structural

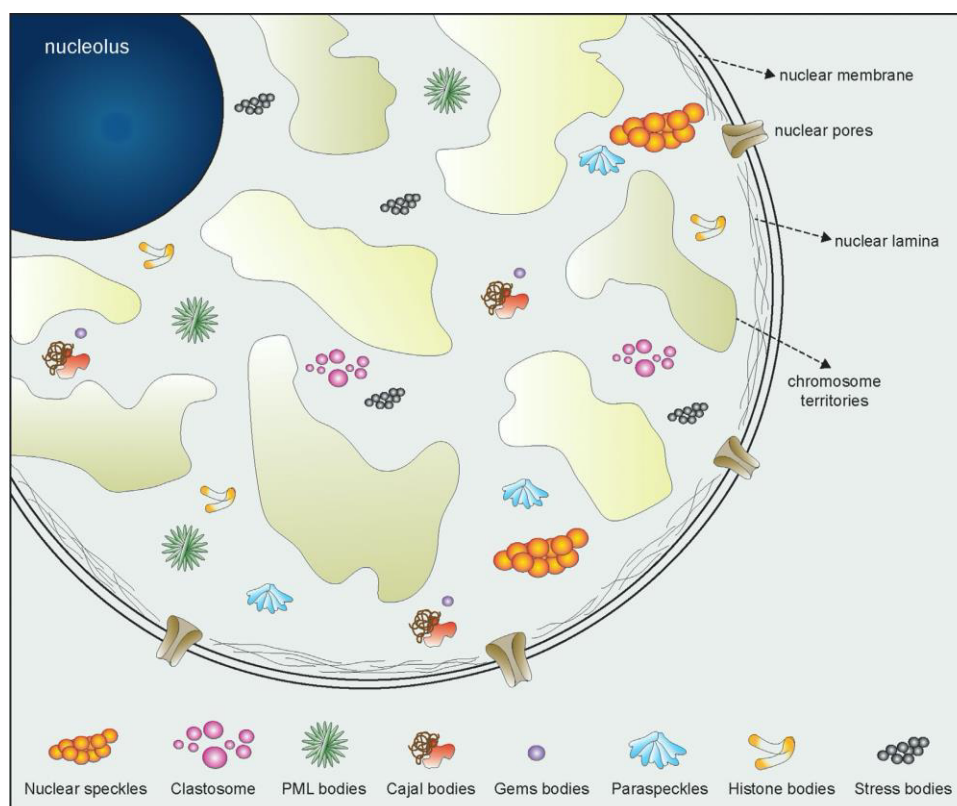


**Figure10. Schematic representation of the main nuclear subcompartments.**  
According to 3[198]

integrity is ensured by protein-protein and protein-RNA interactions, yet the mechanisms of formation of these structures are still poorly understood [194].

Numerous nuclear bodies have been described and characterized: nucleoli, nuclear speckles, clastosome, PML bodies, Cajal bodies, Gems bodies, paraspeckles, histone bodies and stress bodies [195] (figure10). Hereafter we will discuss only the nucleoli and PML nuclear bodies.

### 3. The nucleolus: an assembly platform

The nucleoli form the largest and most dense structures of the nucleus, first observed by microscopy at the end of the 18th century (Fontana, 1781). Fontana characterized it as an "oviform body with a spot in the middle". Most mammalian cells contain 1 to 5 nucleoli with a diameter of 0.5 to 5  $\mu\text{m}$ .

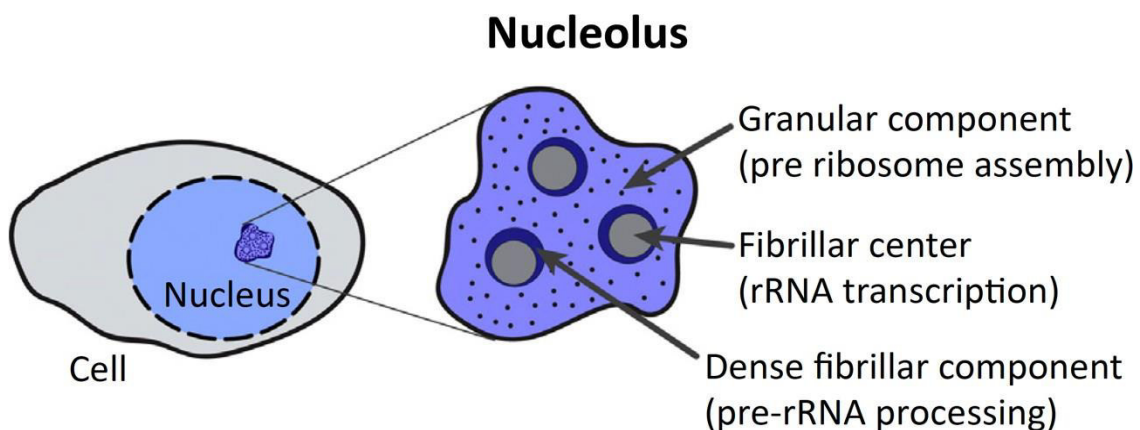


**Figure 11 : Schematic representation of the structure of the nucleolus** consisting of a fibrillar centre, a dense fibrillar component and a granular component. According to [198]

They are mainly known for their role in the production of ribosomal RNA (rRNA) and in the assembly of ribosomes. In addition, the nucleoli are involved of the cell's metabolic activity. Indeed, rRNA synthesis is linked to cell growth and activity [196]. Dividing cells generally have large nucleoli to ensure a high level of ribosome biogenesis for sustained protein synthesis. There is therefore a positive correlation between rRNA synthesis and nucleolar size. Conversely, cell cycle arrest leads to a reduction in nucleolar size [197]. The nucleolus adopts

a structure divided into three zones: a fibrillar centre, a dense fibrillar component and a granular component (figure 11) [198].

**The Fibrillary Centre (FC) :**

It is a rounded area of the nucleoli not very dense to electrons, located in the centre in quiescent cells, more in periphery and less regular in the most active cells. This zone contains the promoter regions of the rDNA genes and is the site of initiation of rRNA transcription.

**The dense fibrillar component (DFC) :**

DFC is very dense to electrons, which is adjacent to the fibrillar centre. Limited to a small proportion of the nucleolus in quiescent cells, it becomes more important in proliferating cells and forms filaments called nucleonemes. FC and DFC participate in the transcription of rRNA. The rRNA thus produced is called precursor or pre-rRNA. The pre-rRNA then undergoes several stages of maturation within DFC.

**The granular component (GC) :**

GC is an area larger than CF and CFD located at the periphery of the nucleoli. The granular aspect of GC is due to the large number of pre-ribosomal particles being assembled or stored.

Although it is clear that nucleoli play a role in cell growth via ribosome biogenesis, the notion of nucleoli multifunctionality is emerging. Indeed, proteomic analysis reveals that about 30% of nucleoli proteins are involved in ribosome biogenesis, suggesting that nucleolus are likely to be involved in various other cellular processes [199]. Nucleoli are believed to be involved in the maturation and export of certain mRNAs and tRNAs, DNA replication and repair, cell cycle progression, proliferation and apoptosis [200] [201]. Indeed, nucleoli are sensitive to a variety of stresses and trigger a rapid response by regulating the induction of p53, a key transcription factor regulating multiple cellular processes including proliferation and death [196].

- *The production of ribosomes by nucleoli :*

### **Ribosomes :**

Ribosomes are made up of proteins and ribosomal RNA (rRNA) to form ribonucleoprotein complexes. They are found in both eukaryotic and prokaryotic cells. These structures are relatively well preserved during evolution, mediating protein synthesis proteins by decoding the information contained in messenger RNA (mRNA). Ribosomes are the main effectors of translation and therefore are intimately linked to the capacity of cells to grow and divide [202].

The ribosomes are formed of two subunits: a small subunit that allows binding to the messenger RNA and a large subunit whose function is to carry out the polymerization of the amino acid residues to form the corresponding protein. These sub-units are designated according to the sedimentation coefficient expressed in Svedberg (S) units.

In eukaryotes, the large subunit has a sedimentation coefficient of 60S with a molar mass of 2.9 MDa. It consists of three ribosomal RNAs: 28S rRNA, 5.8S rRNA and 5S rRNA with 49 ribosomal proteins. The small subunit has a sedimentation coefficient of 40S with a molecular weight of 1.4 MDa. This sub-unit is composed of a single ribosomal RNA, the 18S rRNA associated with 33 ribosomal proteins. The rRNA is the major constituent of ribosomes, it represents 60% of the total mass of ribosomes.

### **Ribosome biogenesis**

Ribosome biogenesis in eukaryotes is a complex process of transcription, maturation, folding and post-translational modification of rRNAs. This process takes place in several stages with different locations in the cell: it starts in the nucleoli, then during their maturation the pre-ribosomal particles join the nucleoplasm and cross the nuclear pore to reach the cytosol where they are finally assembled [203]. It involves more than 200 partners (protein and small nucleolar RNAs (snoRNAs)) who coordinate the different stages of maturation, pre-rRNA cleavage, post-translational modifications of ribosomal proteins and the export of sub-units into the cytosol [206-209]. Although a large number of proteins have been identified as ribosome-associated by co-immunoprecipitation or mass spectrometry, the molecular functions of a large number of proteins involved in ribosome biogenesis are still unknown.

This process is extremely energy intensive for the cell. It is estimated that 80% of the cell's energy reserves are required for ribosome biogenesis [204].

Ribosome biogenesis is globally well conserved between eukaryotic species. The model is best established in yeast (*Saccharomyces cerevisiae*) and is often extrapolated to mammals and humans. Nevertheless, many differences can be observed in the structure, factors involved and maturation stages of pre-rRNAs [211-213]. In mammals, it involves the three RNA polymerases (I, II, III). RNA polymerase I allows the transcription of 28S, 18s and 5.8S rRNAs. RNA polymerase II synthesizes the mRNA of ribosomal proteins. RNA polymerase III synthesizes rRNA5S.

Biogenesis starts in the fibrillar center of the nucleoli, where RNA polymerase I allows the transcription of 47S RNA precursors. The latter contains the sequences of the 5.8S, 18S and 28S rRNAs surrounded by external transcribed spacers at the 5' and 3' ends (5'-ETS and 3'-ETS), and are separated from each other by internal transcribed spacers (ITS-1 and ITS2). This 47S transcript will undergo a succession of endonucleolytic cleavage and exonucleolytic digestions, these processing and cleavage steps performed by several ribosomal proteins that participate in the ribosome structure, different assembly factors as well as non-coding RNA species [205]. The assembly factors assist the formation of the maturation of the subunits but will not be present in the final architecture. Thus, the 47S rRNA precursor will first lose the 3' ETS then the 5' ETS to form the 45S rRNA precursor then the 41S rRNA precursor. At this stage the pre-rRNA processing will split in two pathways. The first will lead to the pre-rRNA18S which will be incorporated, together with ribosomal proteins, in the pre-ribosomal 40S subunit [206]. The second pathway will undergo additional cleavage steps to obtain the 5.8S and 28S rRNA. At the same time, the 5S rRNA that follows a different assembly pathway, will be transcribed by RNA polymerase III at the periphery of the nucleoli. Subsequently, it will be recognized by two ribosomal proteins uL18 (Rpl5) and uL5 (Rpl11). It will then join the nucleoli where it will associate with 28S and 5.8S rRNA and ribosomal proteins to form the 60S pre-ribosomal subunit. These steps of cleavage and maturation of the spacer regions are performed in the nucleoli. These pre-ribosomal particles (40S and 60S) undergo several steps of cleavage and maturation in nucleoplasm, and are exported to the cytoplasm to form the mature 40S and

60S sub-units and subsequently form the 80S ribosomal particle, capable of mRNA translation (figure 12) [207].

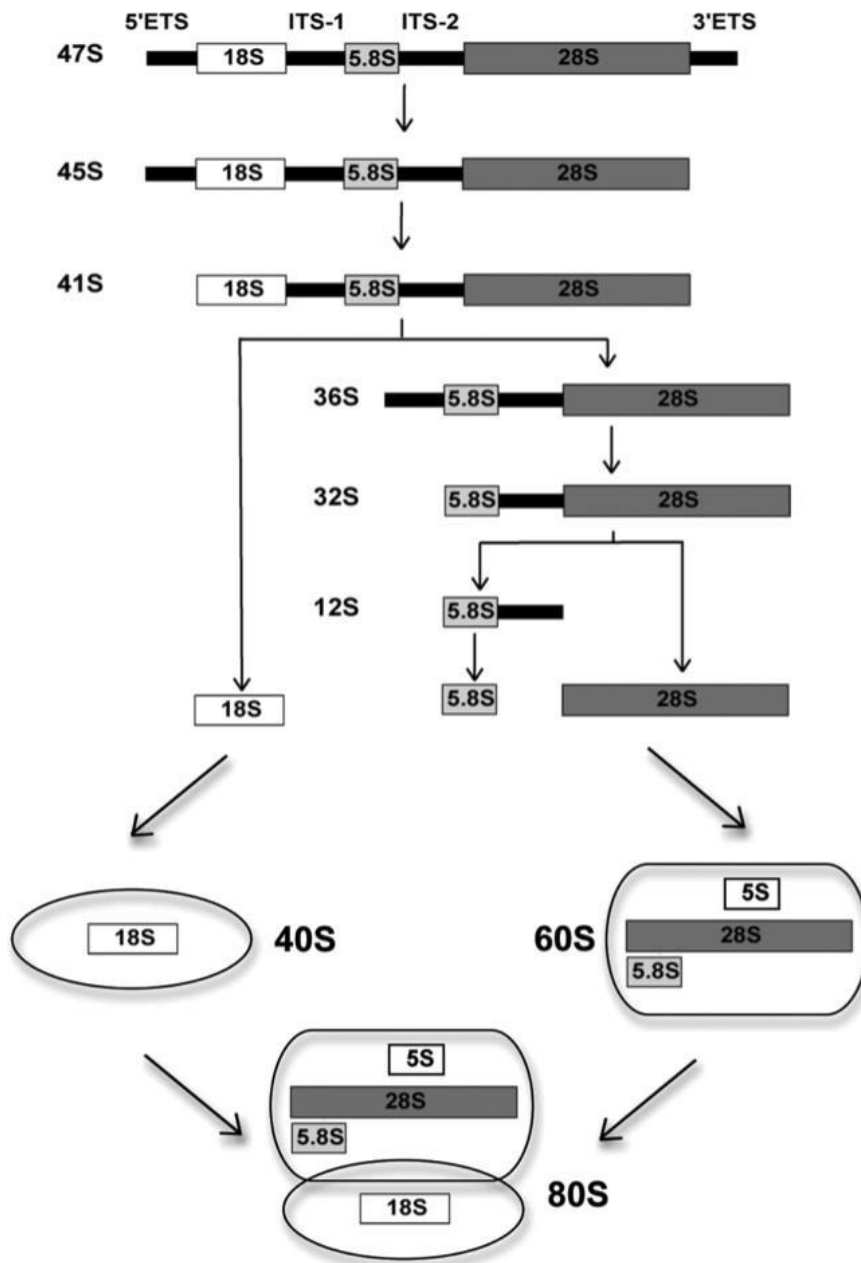


**Figure 12. Schematic view of ribosome biogenesis in mammals :** From the 47S precursor ribosomal RNA, a succession of treatment steps lead to the formation of the 40S and 60S subunits which will be assembled in the cytosol to form the mature 80S ribosome [316].

#### 4. The PML nuclear bodies:

PML nuclear bodies are structures composed of multi-protein complexes defined by the presence of the PML (promyelocytic leukaemia) protein itself. These bodies have a punctate appearance in the cell nucleus that vary in number from 5 to 20 per interphase nucleus, with a diameter of 0.5  $\mu\text{m}$ . The main organizing protein of these nuclear bodies is the PML protein, whose modification by SUMO is necessary for its stability and PML-NB formation [216,217]. Indeed, only the form of PML conjugated to SUMO is able to properly aggregate and induce the formation of nuclear bodies. PMLs are regulated by the desumoylases of the SENP family (SENP1, SENP3, SENP5 and SENP6) [218-220]. Nevertheless, the mechanisms of action of SENPs on PML are still poorly understood. In the presence of arsenic, the SUMOylation of PML is exacerbated, and an increase in the size of PML nuclear bodies is found [208].

PML nuclear bodies recruit different proteins, the only common characteristic of which is their ability to be sumoylated [209]. These include the proteins PML, SP100, BLM, Daax, LEF1, p53, CBP... [210]. PML nuclear bodies are proposed to be reservoirs of regulators involved in the control of many cellular processes such as stress response, apoptosis or response to DNA damage. They constitute hubs of further post-translational modifications, including ubiquitination. For the cell, PML nuclear bodies are likely to be a repository of nuclear factors and a specific site for modification and assembly of transcriptional factors [211] [212]. It is also interesting to note that the depletion of PML in cells leads to an acceleration of cell proliferation [213].

PMLs have been studied in particular because of the alteration of PML-NB in pathological conditions such as promyelocytic leukemia, viral infections or various cellular stresses [214] [215] [216]. *Shigella* infection was also shown to impact PML nuclear bodies by increasing the number of PMLs in infected cells [217], following decrease in the levels of host sumoylation. Recently, PML was identified as being targeted by the pore-forming toxin (LLO) of *Listeria monocytogenes*. LLO triggers a de-SUMOylation of PML, which leads to a de-structuring of the PML nuclear body and triggers an antibacterial response via activation of immune response genes and cytokine secretion [218]. Further studies with other intracellular bacterial pathogens need to be undertaken to determine whether PMLs play a general antimicrobial control mechanism.

## 8. SUMOYLATION :

The cell can mediate the dynamic regulation and biochemical functioning of its proteins through post-translational modifications (PTM), that correspond to the attachment of a group to a target protein, which will modify its properties and consequently its functions. These include: glycosylation, acylation, phosphorylation, acetylation, methylation, ubiquitination...

Sumoylation is also a post-translational modification of target proteins. It is an extremely dynamic and reversible process. SUMO was initially identified in 1995 in *Saccharomyces cerevisiae* with the *smt3* gene, a homologue of SUMO1, following genetic screening to identify suppressors of a mutation in MIF2, a protein associated with the centromere [219]. In 1996, three teams simultaneously discovered SUMO1, through yeast two-hybrid experiments. In these studies, SUMO1 was shown to interact with PML [220], Rad51 and Rad52 involved in DNA repair [221] and Fas protein playing a role in apoptosis [222], already suggesting a high diversity of mechanisms in which this PTM is involved.

In recent years many more SUMO substrates have been identified, underlining the importance of this SUMO modification within the eukaryotic cell [223] [224].

SUMOylation consists of the addition of a polypeptide called SUMO (Small Ubiquitin-like MOdifier) of about 10kDa which shares 20% identity with ubiquitin. Nevertheless, the three-dimensional structure of these two proteins is relatively close (Figure 13). The addition of this SUMO polypeptide is achieved by forming an isopeptide bond with the  $\epsilon$ -amino group of the lysine acceptor residues of the target protein.



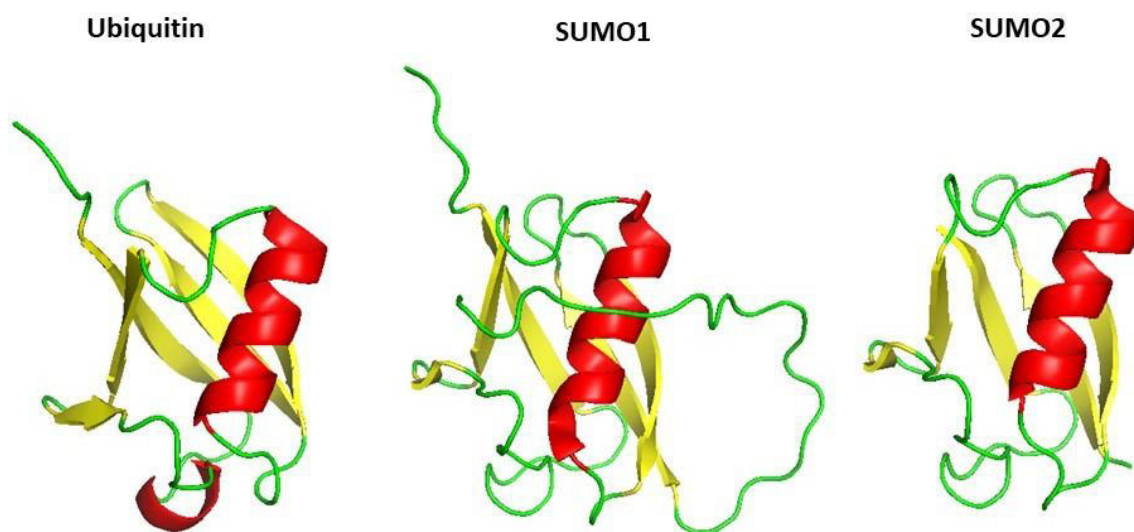


**Figure 13. Tridimensional structure of ubiquitin, SUMO1 and SUMO2.** Cartoon representation of the structure of human Ubiquitin (1UBI), human SUMO1 (2N1V) and human SUMO2 (4NPN), depending on the secondary structural elements:  $\beta$ -sheet in yellow,  $\alpha$ -helices in red and loops in green.

SUMOylation is involved in a multitude of cellular functions such as transport between the nucleus and the cytosol, transcriptional regulation, apoptosis, protein stability, immune response, DNA repair, stress response, cell cycle progression, cell proliferation and differentiation [235,237,238]. For example, mice in which expression of Ubc9, a key enzyme in the SUMOylation pathway, is turned off, die in the embryonic stage [239,240]. This underlines the importance of SUMOylation in cell proliferation and differentiation.

Initially, the scientific community thought that sumoylation occurred only in nuclear or perinuclear compartments [225], but it has become clear that it also regulates cytoplasmic and plasma membrane proteins [226]. SUMO proteins are present in all eukaryotes. Some organisms have only one SUMO gene such as yeasts (*SMT3*), *Caenorhabditis elegans* (*SMT-1*) and *Drosophila melanogaster* (*smt3*) [242-244], whereas plants and vertebrates have several SUMO genes. In humans, 5 paralogues of SUMO have been identified: SUMO1, SUMO2, SUMO3, SUMO4 and more recently SUMO5 [227] [246,247]. SUMOs are formed by about 100 amino acid residues. SUMO2 and SUMO3 are very strongly similar and share 97% identity, only three amino acids differ. As a result, it is very complicated to differentiate between them

and they are often referred to SUMO2/3. SUMO2/3 shares 47% identity with SUMO1 and 83% identity with SUMO4 [228] and 46% identity with SUMO5 (figure 14).

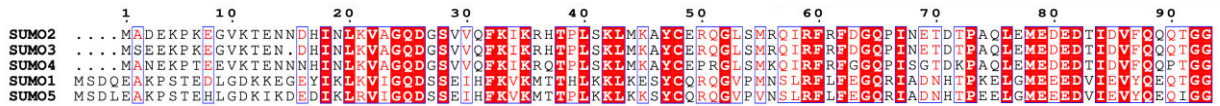


**Figure 14. Alignment of the five SUMO paralogs in humans.** The preserved amino acids are in red and the poorly preserved amino acids in black. Amino acids highlighted in red are preserved in all sequences. The sequence alignment was carried out with ClustalW and ESPrpt3.

SUMO1-3 are ubiquitously expressed whereas SUMO4 and SUMO5 are tissue- specific [227]. Proteomic analyses have shown that 2% of the mammalian proteome is SUMOylated underlining the importance of this PTM [229]. SUMO1 and SUMO2/3 perform very distinct functions in the cell, as they are conjugated to different target proteins *in vivo* [250-252]. The role of SUMO4 is more obscure, currently scientists are not sure whether it is in the mature *in vivo* form needed for conjugation [245,253]. Results suggest that SUMO4 is involved in the pathogenesis of type I diabetes [228]. The youngest member of the SUMO5 family seems to play a major role in the regulation of the nuclear PML bodies [230]. It should be noted that SUMO1, SUMO2/3 have been studied in more detail than the SUMO4 and SUMO5 paralogs. To date, the mechanisms and consequences of this specificity of conjugation of the SUMO paralogs to their substrate are not clearly established and many questions remain unanswered. Like ubiquitination, proteins can be modified with the addition of a single SUMO molecule (monoSUMOylation) or with several chains of SUMO molecules (polySUMOylation) [231]. Nevertheless, only SUMO2/3 and SUMO4 are capable of producing polySUMO chains, due to the presence of a lysine 11 present in a  $\psi$ KxD/E consensus sequence in SUMO2/3 and SUMO4 to which SUMO is added, but absent in SUMO1 and SUMO5 (Figure 14) [255,256]. On the contrary, lysine 18 can be observed on SUMO5, which could be SUMOylated, but to date no study has reported a polySUMOylation of SUMO5.

## 1. The enzymatic mechanism of SUMOylation :

The different paralogues of SUMO are conjugated by covalent binding to the target protein at the lysine level generally present in  $\psi$ KxD/E consensus motif (in which  $\psi$  is a branched aliphatic amino acid, K corresponds to lysine, x any amino acid, D corresponds to aspartic acid E corresponds to glutamic acid) [257,258]. It should be noted, however, that the literature reports an increasing number of sumoylated proteins on lysines not belonging to a consensus sumoylation site. In addition, many proteins with this motif are not sumoylated.

### ▪ *Maturation of the precursor:*

The various forms of SUMO are expressed as inactive precursors that require cleavage of the C-terminal part of the peptide to expose a di-glycine motif essential for conjugation. It is at the carboxy-terminal glycine doublet (GG) that the binding with the lysine of the target protein will take place. This cleavage is achieved by the hydrolase activity of specific enzymes of the SENPs family (SUMO/Sentrin-specific protease). Similar to ubiquitination, SUMOylation consists of a cascade of enzymatic steps involving three enzymes: SUMO activating enzyme (E1), SUMO conjugating enzyme (E2) and ligase (E3) (Figure 15).

### ▪ *-E1 the activating enzyme :*

Unlike ubiquitination, the E1 enzyme is not monomeric but heterodimeric. This heterodimeric E1 enzyme consists of two subunits: a small SAE1 subunit and a large SAE2 subunit (SUMO Activating Enzyme 1 and 2). This activation is ATP dependent. Initially E1 forms a high-potential energy connection between the C-terminal end of SUMO and SAE2 using ATP. Then, by releasing the AMP, the adenylated SUMO intermediate uses this binding energy to form a covalent thioester-type bond between the carboxyl group at the C-terminal end of SUMO and the sulphide group of the C173 residue of the SAE2 sub-unit [232].

- *-E2 conjugating enzyme:*

In contrast to ubiquitination, SUMOylation uses exclusively the conjugating enzyme E2: UBC9 (SUMO ubiquitin-conjugating enzyme 9). UBC9 is highly conserved in eukaryotes, it has 56% amino acid sequence identity between the human UBC9 sequence and its orthologue in *S. cerevisiae* [233]. By a transesterification reaction, "activated" SUMO is transferred from SAE2 to the cysteine C93 residue of the conjugating enzyme Ubc9, again forming a covalent thioether bond. Ubc9 serves as the donor of SUMO. Ubc9 will then create an isopeptide bond between the double glycine of SUMO and the lysine of the substrate

- *-E3 SUMO ligase :*

It is important to note that *in vitro* tests show that the activating enzyme E1 and the conjugating enzyme E2 are sufficient for SUMOylation of the substrate [261-263]. Nevertheless, the conjugation process can be assisted by E3 ligases which promote the interaction of the E2 enzyme with the substrate or act by positioning SUMO in a conformation that facilitates its transfer to the target lysine residue [234]. Thus, the conjugation of SUMO is generally increased in the presence of E3 ligases *in vivo* and *in vitro* [265,266]. The three main types of E3 SUMO ligases: the PIAS family (Protein Inhibitor of Activated STAT), the nucleoporin RanBP2 (Ran Binding Protein2) and the Polycombe PC2 complex, interact with Ubc9 and the substrate [236,267].

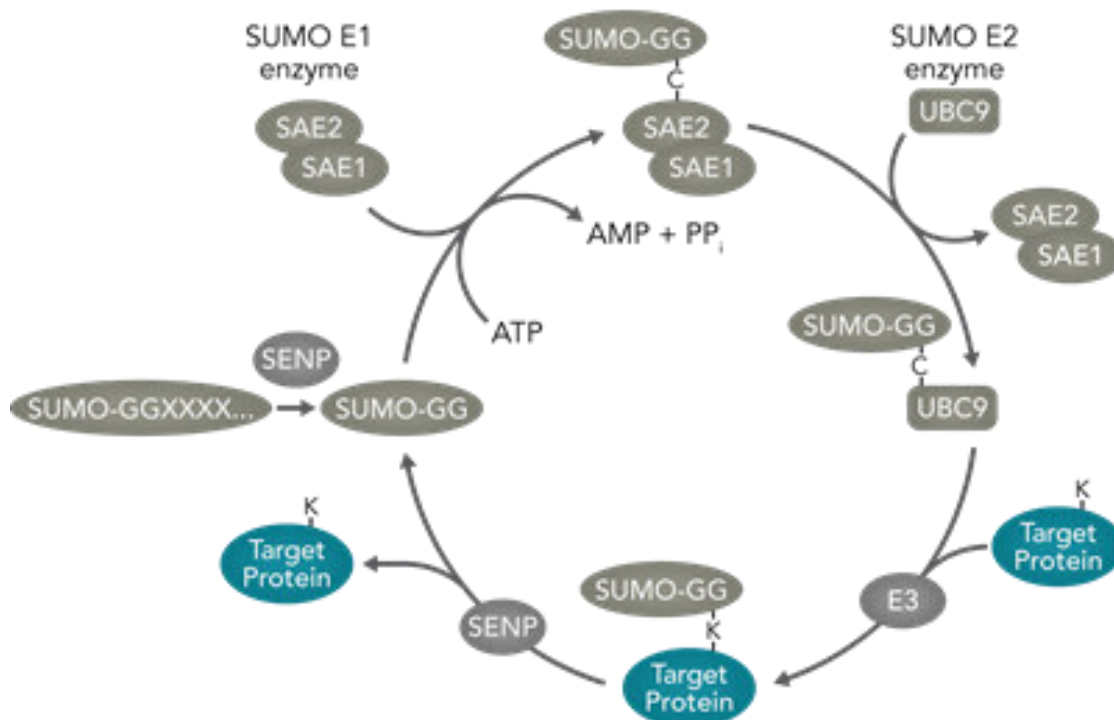


**Figure 15. Enzyme cascades involved in sumoylation** . SUMO-specific proteases (SENPs) catalyse the maturation of SUMO proteins by cleaving the amino acids that follow the double glycine residue at the C-terminal end of SUMO. Mature SUMO can then be conjugated to its substrate by following a cascade of enzymatic reactions: E1 the activating enzyme (SAE1/SAE2), E2 the conjugating enzyme (Ubc9) and E3 the ligase. The substrate can be deSUMOylated by the action of the protease of the SENPs family

- *-DeSUMOylase*

Post-translational modifications of SUMOylation are highly dynamic and transient processes. They are easily reversible by the action of SUMO proteases or hydrolases that remove SUMO or SUMO chains from sumoylated proteins [254,268].

In humans, deSUMOylation is carried out by proteins of the SENPs family (Sentrin/SUMO - specific protease), DESI1 and DESI2 (DeSUMOylating Isopeptidase 1 et2) [235] and USPL1 (Ubiquitin Specific Protease Like 1) [236]. These three enzyme families are all cysteine proteases. SENPs are the best characterized deSUMOylases. Discovered at the beginning of the 2000s by sequence homology with Ulp1 [237]. SENPs therefore play a double role in SUMOylation: firstly, they allow the maturation of newly translated SUMO into its active form

thanks to their hydrolase activity, which is necessary for conjugation, and secondly, they allow the removal of SUMO from their substrate by an isopeptidase activity.

DeSUMOylation seems to be essentially exercised by SENPs, in fact cells lacking members of the SENPs family present a large accumulation of SUMOylated proteins. Conversely, cells lacking DESI1, DESI2 or ULSPL1 do not present an alteration in the total SUMOylated protein profile. This suggests the major role of the SENPs family in the overall status of cell SUMOylation. However, the study of this post-translational modification is complicated by the fact that this event is highly dynamic. Only a small fraction of substrate is SUMOylated at any given time. It therefore seems that there is a SUMOylation/de-SUMOylation equilibrium for a specific substrate and that this equilibrium is finely regulated. To date many questions, remain unanswered about the understanding of the cellular signals that trigger de-SUMOylation and how SENPs are regulated under physiological as well as pathological conditions.

## 2. The SUMO Interacting Motif (SIM: SUMO Interacting Motif):

Interestingly, on some proteins, a SUMO interacting motif (SIM) has been identified to interact non-covalently with SUMOylated proteins [238]. The SIM motif corresponds to a short sequence not exceeding 10 amino acid residues, may contain phosphorylated amino acids, and interacts with a specific groove present on the surface of SUMO [239]. To date, two important characteristics of SIM motifs have emerged: Presence of a core formed by 3-4 hydrophobic residues (generally valine or isoleucine) and the presence of a close acidic region such as the side chains of glutamic or aspartic acids or phosphorylated residues such as serine or threonine [272,274].

A study on the PML protein showed that it has this non-covalent binding motif, which is involved in the formation of PML nuclear bodies [240].

Similar to the consensus site of SUMOylation  $\psi$ KxD/E, not all SUMO binding motifs are functional, due to poor exposure of the SIM motif, or because these SIM motifs are masked by interaction with other proteins.

### 3. Consequences of SUMOylation

Modification by SUMO can have several consequences on the target protein, and it can change its localization, activity or stability. SUMO can compete with other PTMs which modify the function of the protein, or SUMO can modify directly the conformation of the target protein. SUMO can also modulate the interaction with other proteins, by preventing protein-protein interactions or conversely by promoting new interactions by exposing a new binding domain or directly binding to another protein with a SIM (figure 16) [241].

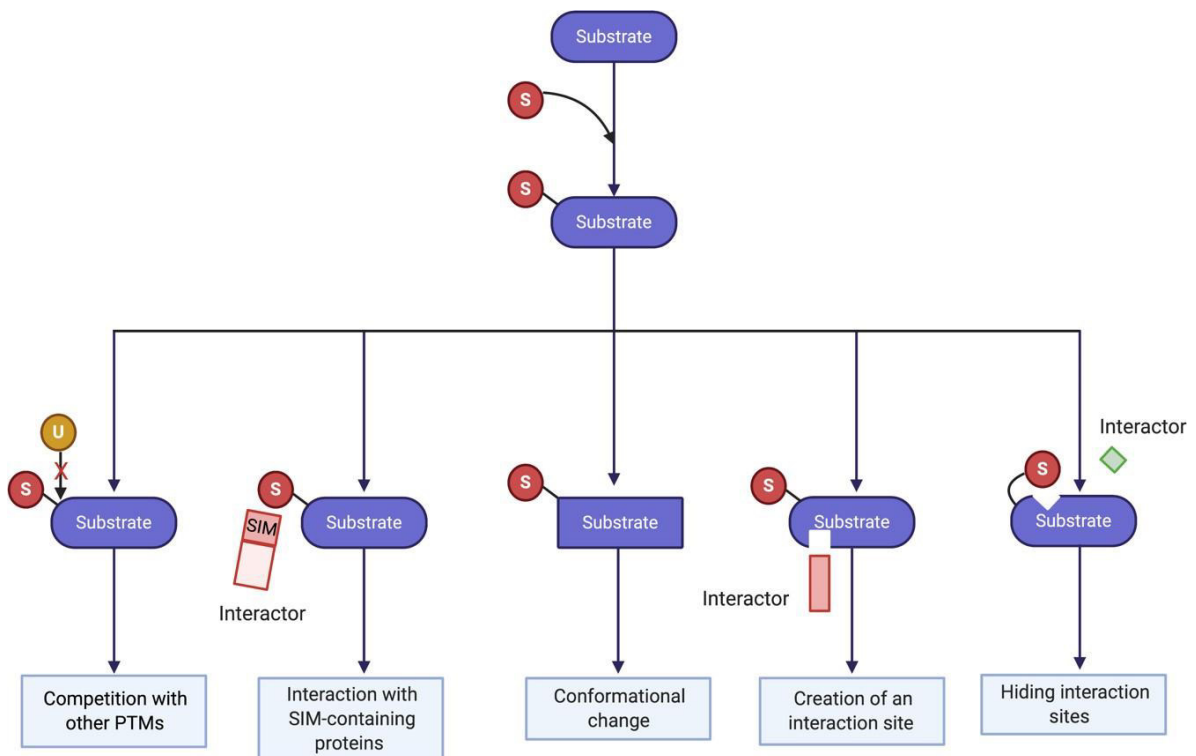


**Figure 16. Molecular consequences of modification by SUMO.** SUMO and ubiquitin are indicated respectively by S and U. Adapted from [241] Created with BioRender.com

### 4. The pathway of sumoylation targeted by bacteria:

SUMOylation is a conserved process in eukaryotes. In humans several thousand SUMOylated proteins have been identified. These proteins are involved in transcriptional regulation, stress response, immunity and other biological processes [229]. *In vitro* experiments have shown that overexpression of SUMO1 or SUMO2 in HeLa cells infected with *Listeria*

*monocytogenes* decreases the number of bacteria in the cell, suggesting that SUMOylation plays a negative role in the invasion and/or replication of *L. monocytogenes* and highlighting the importance of sumoylation for the host cell in the fight against bacterial infection [242]. Therefore, it is not surprising that this process is targeted by pathogens to promote their own survival and replication. Indeed, several studies have shown that viruses target this PTM [243], however little is known about the modulation of SUMO by pathogenic bacteria. Several strategies have recently been highlighted to modulate different stages of the SUMOylation cycle: activating enzymes E1, conjugating enzyme E2, and de-SUMOylases. In addition, some pathogens use the host machinery to sumoylate their own proteins.

- *Bacteria targeting SUMO E1*

*Shigella flexneri* the causative agent of human bacillary dysentery, modulates the overall sumoylation state of the host during infection. *In vitro* and *in vivo* experiments have shown that *Shigella* negatively alters SUMOylation. *Shigella* infection leads to activation of the calpain protease which targets and degrades the activating enzyme E1 SAE2, leading to inhibition of SUMOylation [244].

- *Bacteria targeting SUMO E2*

Infection of cells with *Listeria monocytogenes*, a human pathogen causing listeriosis, causes a global deSUMOylation by degrading the conjugating enzyme E2: Ubc9. This is achieved through its pore-forming toxin, Listeriolysin (LLO) [277,280]. Homologues of LLO are found in *Clostridium perfringens* and *Streptococcus pneumoniae* with PFO and PLY respectively. Like LLO, these two toxins cause the degradation of Ubc9 [242].

*Salmonella* Typhimurium, the causative agent of typhoid fever alters host SUMOylation through microRNA. *Salmonella* infection upregulate miRNA30c and miRNA30e which target Ubc9 [245] and lead to downregulation of Ubc9 [246]. In addition, Verma et al have shown that infection of cells with *Salmonella* Typhimurium is able to modulate the activity of PIAS1, an E3 ligase.



- *Bacterial effectors can mimic host deSUMOylases.*

This is the case for *Yersinia* outer membrane protein J (YopJ), the first bacterial protein identified to modulate SUMOylation. YopJ is a cysteine protease that mimics the isopeptide activity of SENPs. It will lead to the deconjugation of SUMO from their substrate and thus to a decrease in the overall level of SUMOylated proteins [283,284].

Similarly, XopD is an effector secreted by the T3SS of a plant pathogen, *Xanthomonas euvesicatoria*. XopD has an isopeptidase activity that allows it to deconjugate SUMO from the transcription factor SIERF4. Thus, the bacterium suppresses the ethylene response allowing it to escape the plant immune system and promote its proliferation [285,286] .

*Klebsiella pneumoniae* is a major multidrug-resistant pathogen causing nosocomial infections worldwide. Recently, it has been shown that *K. pneumoniae* decreases the level of SUMO-conjugated proteins in epithelial cells but also in macrophages. In epithelial cells, this decrease is not dependent on an alteration of the E1 or E2 enzymes. The authors have shown that SENP2 deSUMOylase is involved in the decrease of SUMO-conjugated proteins. *K. pneumoniae* triggers the delocalization of SENP2 from the nucleus to the cytosol. The bacterium leads to the deNEDDylation of E3 ubiquitin ligase which results in a defect of ubiquitylation of SENP2 by this ligase and thus prevents the degradation of SENP2 by the proteasome. On the other hand, in macrophages, the decrease in SUMOylation is mediated by type I interferon in a TLR4-dependent manner. The type I interferon stimulates the transcription of miRNA let-7 which prevents SUMOylation. This decrease in the SUMOylation status of epithelial cells and macrophages allows intracellular survival of *Klebsiella pneumoniae* and limitation of the inflammatory response [247].

- *Bacteria using the host's machinery to SUMOylate their own effectors*

This has been observed in *Ehrlichia chaffeensis* and *Anaplasma phagocytophilum* [288,289]. Thus the TRP120 and AmpA effectors belonging respectively to *Ehrlichia chaffeensis* and *Anaplasma phagocytophilum* are secreted in the host cell cytosol and localize to the membrane of the pathogen-containing vacuole. TRP120 and AmpA are sumoylated during the

infection. SUMOylation of TRP120 allows it to interact with host proteins and thus promote infection [248]. Inhibition of the SUMO pathway significantly decreases the interaction of TRP120 with its protein targets, resulting in decreased intracellular survival of *Ehrlichia chaffeensis*. However, the molecular mechanisms and repercussions of this modification are not yet established. *Shigella flexneri* also uses the host machinery for SUMOylation of OspF, an effector secreted during infection. The sumoylation of OspF allows it to be translocated into the nucleus of the infected cell where it can modulate proinflammatory cytokine expression [249].

Thus, by interfering with the SUMOylation of the host cell, bacterial pathogens can modulate the activity of proteins in order to promote the replication and dissemination of the bacterium in its host. It seems obvious today that the understanding of these interactions between the host and the pathogen modulating sumoylation is more than necessary and could be used in the future for the development of new therapeutic strategies

## 9. The SENP family

SENPs are cysteine proteases, discovered in the early 2000s [237]. They have a C-terminally conserved catalytic domain of about 200 amino acid residues and exhibit a characteristic papain-like folding. The cysteine residue of the active site is present at a catalytic triad (histidine, aspartic acid and cysteine). The N-terminal domain is different among members of the SENP family (Figure 17). This domain is variable in length and plays a major role in their regulatory function and location. It is often subject to post-translational modifications such as phosphorylation or ubiquitination, allowing regulation for partner recruitment or protein stability. We also find SIM motifs allowing them to target their substrates.



They also play a role in chromatin remodeling and control of gene expression. SENPs are also involved in cell cycle progression, inflammatory signalling and the adaptive immune response.

In the framework of this thesis project we will focus on the role of SENP3.

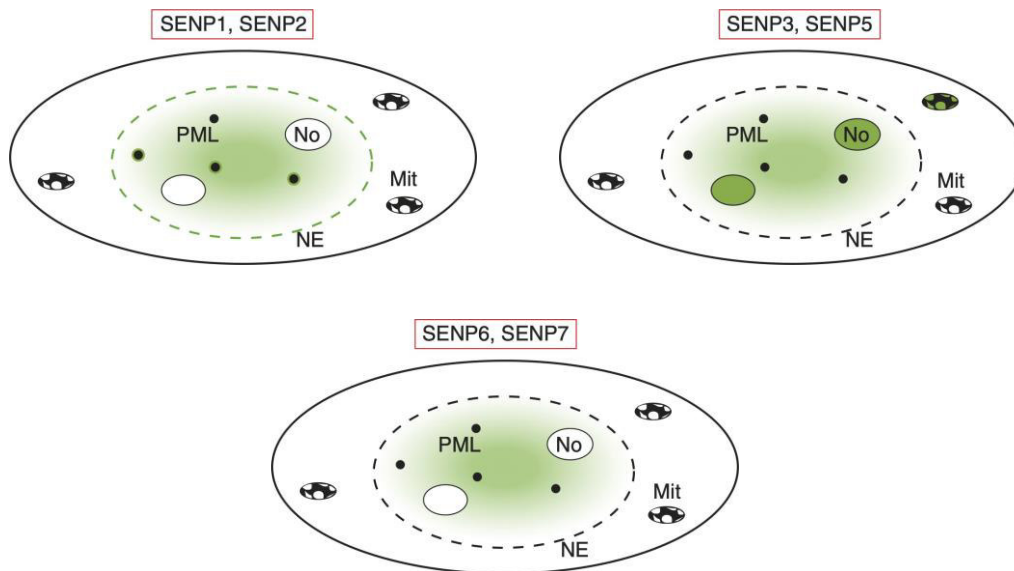


**Figure 18 : Schematic representation of the cellular distribution of the SENPs family members.** The preferential distribution of SENPs is shown in green. SENP1 and SENP2 are found at the level of the nuclear envelope (NE) of the nucleoplasm, and around the PML nuclear body. SENP3 and SENP5 are found in the nucleoli (No), nucleoplasm and also in the mitochondria (Mit). SENP6 and SENP7 is only found in the nucleoplasm [250]

## 10. SENP3

SENP3 is a cysteine protease. This protein is composed of 574 amino acid residues with a molecular weight of 65 kDA. Its catalytic domain is located at the C-terminus of the protein and presents a catalytic triad of cysteine, histidine and aspartic acid. Cysteine 532 is the key residue that enables it to attack the peptide bond between the glycine terminal residue of SUMO and the lysine residue of the substrate. The mutation of Cys532 to alanine leads to a total loss of its isopeptidase activity. SENP3 acts preferentially on substrates sumoylated by SUMO2/3 and has a very limited activity on SUMO1. Depletion of SENP3 by siRNA leads to a significant increase in SUMOylated substrate by SUMO2/3 in cells [293,296,297].

Furthermore, SENP3 does not possess hydrolase activity and therefore does not participate in the maturation process of SUMO.

The N-terminal part contains a domain responsible for its localization in the cell, a NoLS (Nucleolar Localization Site) domain, corresponding to a very acidic region of the protein. The absence of this domain leads to a redistribution of SENP3 from the nucleolus to the nucleoplasm. Nevertheless it seems that the localization of SENP3 is not exclusively in the nucleoli since it has been established that SENP3 may reside in the cytosol and is required for mitochondrial fission [297,298].

The biological processes in which SENP3 is involved are now well established, and include: inflammation [252], cell differentiation [253], cell stress response [297,301,302] and ribosome biogenesis [254]. Nevertheless, the identification of substrates and their physiological roles are still poorly characterized. This lack of knowledge stems in part from the difficulty of experimentally obtaining recombinant SENP3 proteins, especially the stable and active catalytic domain [255].

I will now present some of the most relevant discoveries relating to SENP3 to illustrate the multiple roles of this protease in various cellular processes.

#### 1. SENP3 as a redox-sensor under stress

It has been shown that SENPs can be redox sensors [256]. Reactive oxygen species (ROS) have been shown to modulate SENP3 and have an impact on its stability and localization. Indeed, the redox state of the cell regulates the level of SENP3 expression. HeLa cells under mild oxidative stress such as treated with oxygen peroxide (H<sub>2</sub>O<sub>2</sub>) present an increased level of SENP3 due to inhibition of ubiquitination, revealing that under normal conditions SENP3 is ubiquitinated by the ubiquitin ligase CHIP (for C-terminus of Hsc70-interacting protein) and sent to the proteasome for degradation [257] [258]. Under moderate oxidative stress, two SENP3 cysteines (Cys243 and Cys274) are oxidized [259], allowing recruitment of Hsp90 and preventing ubiquitination by CHIP (Figure 19) [260].

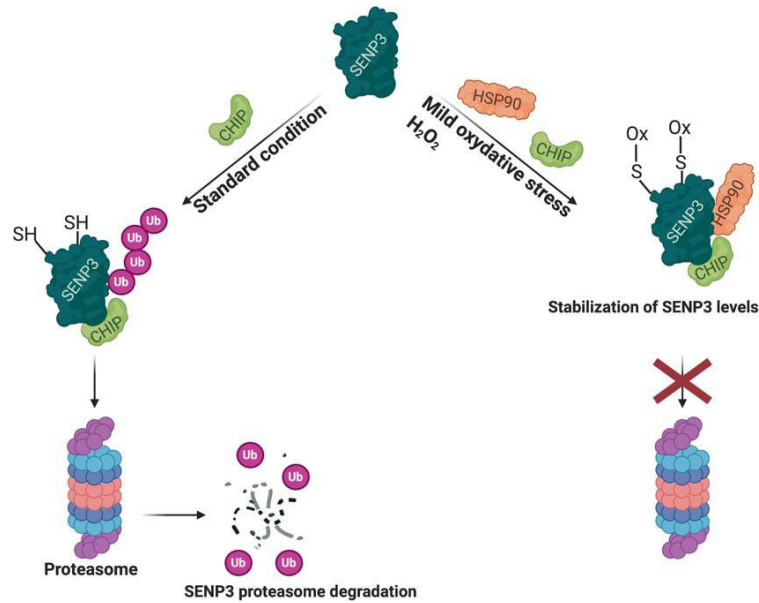


**Figure 19. Redox regulation of SENP3 :** SENP3 interacts with CHIP under standard and oxidative stress condition. Under oxidative condition SENP3 undergoes oxidative modification which is a signal for the recruitment of HSP90. Created with BioRender.com.

The result of this stabilization under oxidative stress is a redistribution of SENP3 from the nucleoli to the nucleoplasm where it will accumulate and participate in the de-SUMOylation of a large number of proteins. Notably, nucleoplasmic SENP3 will deconjugate SUMO2/3 from p300, a co-activator of HIF-1, a transcription factor sensitive to redox. This deSUMOylation by SENP3 will lead to a transactivation of HIF-1 [257]. A few years later the same team showed that SENP3 is induced under mild oxidative stress but under high oxidative stress its catalytic activity is inhibited due to the oxidation of catalytic cysteine532, preventing the transcriptional activity of HIF-1 [259].

Under oxidative stress, the delocalization of SENP3 from nucleoli leads to accumulation within PML nuclear bodies and thus deconjugation of PML from SUMO2/3. As a consequence, a decrease in the number of PML nuclear bodies, which requires the SUMOylation of PML for their formation is observed under oxidative stress.

## 2. SENP3 as a modulator of gene expression

Studies have shown that deSUMOylation mediated by the SENPs family has a role in bone metabolism. SENP3 is found associated with the MLL1/MLL2 histone methyltransferase complex and catalyzes the SUMO deconjugation of RbBP5 required for the activation of *Hox* gene. SENP3 promotes osteogenesis by deSUMOylating RbBP5, which activates the expression of HOX genes necessary for cell specialization and determine pathway such as osteogenesis [250]. Recently a study showed that in bone marrow-derived monocytes, SENP3 activity is decreased during osteoclastogenesis promoting osteoclast differentiation. The authors showed that SENP3 negatively regulates osteoclast differentiation by deconjugating SUMO2/3 present on IRF8 lysine K310. This suggests a potential role for SENP3 as a therapeutic target in diseases related to bone loss [261].

SENP3 is also phosphorylated by the CDK1 protein kinase before entering mitosis and is dephosphorylated by the protein phosphatase-1 (PP1) at the exit of mitosis. The phosphorylation of SENP3 negatively regulates its activity, so that it can no longer desumoylate chromosome-associated proteins such as Topoisomerase II  $\alpha$  (TopoII  $\alpha$ ). The expression of a mutant of SENP3 that cannot be phosphorylated decreases the SUMOylation of TopoII  $\alpha$ , leading to abnormal chromosome segregation, abnormal mitotic cell cycle and tumorigenesis [262]. These data show that SENP3 phosphorylation plays a crucial role in the regulation of chromosome stability in mitosis. Subsequently the same team showed that in response to DNA damage, p53 is activated and will suppress the phosphorylation of SENP3.

## 3. SENP3 and immune response :

It is well established that protein SUMOylation plays a role in the innate immune response. ROS are produced in abundance during macrophage activation and are necessary for inflammatory signaling by TLR4. As we have seen above, SENP3 is sensitive to ROS. SENP3 deficient cells markedly deregulate the activation of TLR4 inflammatory signaling and the production of pro-inflammatory cytokine in LPS-stimulated macrophages. SENP3 potentiates

LPS-induced TLR4 signaling via MKK7 desumoylation resulting in increased JNK phosphorylation and downstream events. This suggests that SENP3 may be the link between redox regulation and innate immune response [263].

Finally, NLRP3 (NOD-like receptor family, pyrin domain containing3) which is an inflammasome activating protein undergoes SUMOylation, essential for the regulation of its inflammatory activity [264]. Subsequently, it was shown that SENP3-mediated deSUMOylation of NLRP3 orchestrates the activation of the inflammasome [265].

---

#### 4. SENP3 as a regulator of macromolecular assemblies in the nucleus : ribosome biogenesis

As mentioned above, SENP3 is mainly localized in nucleoli, a major site of ribosome biogenesis due to the presence of a nucleolar localization sequence (NoLS). However, authors have also shown that this nucleolar localization is also dependent on the serine/threonine kinase activity of mTOR. Indeed, when HeLa cells were treated with mTOR inhibitors (Ku-0063794, Rapamycin), SENP3 was no longer able to localize into the nucleoli, revealing that phosphorylation of several N-terminal SENP3 serines and threonines (S25, S139, S141, T142, S143, T145) by mTOR was required for its localization. This delocalization of SENP3 is also observable in case of amino acid starvation, consistent with the fact that during starvation mTOR is no longer activated [266].

When SENP3 is phosphorylated, it interacts with its major partner nucleophosmin (NPM1/B23) which will allow SENP3 to be retained in the nucleolus [267] [268]. NPM1 is a 37kDa phosphoprotein that shuttles between the granular component of the nucleoli and the cytoplasm. The SENP3/NPM1 interaction has been shown by co-precipitation experiments in HeLa cells and by yeast two hybrid. In addition, the authors showed that NPM1 specifically interacted with SENP3, since other members of the SENPs family are not able to interact with NPM1 [269]. SENP3 catalyzes the deSUMOylation of NPM1 by removing SUMO2/3. Together SENP3 and NPM1 play a key role in ribosome biogenesis. Indeed, depletion of SENP3 or NPM1 by siRNA negatively impacts ribosome biogenesis by inhibiting the maturation of 32S rRNA into 28S [269].



In addition, a large protein complex associated with SENP3 has been identified, it is composed of PELP1, TEX10 and WDR18. PELP1 is found in the GC region of the nucleolus, associated with the precursor forms of 28S rRNA, and it interacts with LAS1L [270], a 28S rRNA maturation factor. When PELP1 is sumoylated it is localized in the nucleoplasm while when it is not conjugated to SUMO it is found in the nucleolus. Thus, SENP3 will regulate the nuclear distribution of this complex. The authors suggested that SENP3 via its activity on PELP1 allows a quality control mechanism by preventing the loading of the PELP1-WDR18-TEX10 complex on the maturing pre-ribosome [271] [272]. Thus, SENP3-mediated deSUMOylation makes it possible to coordinate the rate of ribosome formation with the physiological state of the cell. In addition, the absence of SENP3 leads to a localization error of the ribosomal transformation factor NVL (Nuclear VCP-like protein) [273]. NVL belongs to the AAA ATPase family [274]. The human genome codes for two NVL isoforms, NVL1 and NVL2, which differ in the length of their N-terminal sequence. Thus, NVL1 starts from the residue corresponding to the second methionine at position 107 of NVL2. NVL1 and NVL2 have distinct locations in the cell and more particularly in the nucleus. NVL2 is the more represented of the two, it is mostly found in the nucleoli while NVL1 is nucleoplasmic. Nagahama et al. were able to establish that NVL interacts with RPL5 in a manner dependent on ATP and their NoLS. This interaction allows NVL to have a nucleolar localization [275]. Depletion of NVL2 by siRNA inhibits ribosomal biosynthesis, highlighting that like SENP3, NVL2 plays a key role in this cellular process [275] [276].

## Chapter II: Results

---

1. The TIR-domain containing effectors BtpA and BtpB from *Brucella abortus* impact NAD metabolism

When I first joined the team, the topic of my research was centered on bacterial TIR domain proteins. During this time I participated in several projects that gave rise to 4 publications. My main contribution led to the publication included in this chapter, in which I am joint first author on the characterization of the *Brucella* TIR domain-containing proteins, BtpA and BtpB. In the work we show that the recently NADase activity described for TIR domains is retained in BtpA and BtpB and leads to intracellular NAD depletion during infection. This was a joint project with our long-term collaborators at the University of Madrid, the lab of Victor Cid and Maria Molina. I constructed several expression and complementation vectors as well as *Brucella* strains, participated in the assessment of the localization of BtpA/BtpB in transfected cells along with Paul Imbert, and carried out all the infection work, namely for the NAD measurements that were done with the help of Morgane Roussin. I also worked side-by-side on this project with Julia Coronas-Serna when she came for a 3 months stay at our lab.

## RESEARCH ARTICLE

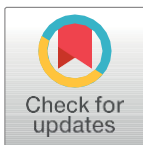
# The TIR-domain containing effectors BtpA and BtpB from *Brucella abortus* impact NAD metabolism

Julia Mar'ia Coronas-Serna<sup>1</sup>\*, Arthur Louche<sup>2\*</sup>, Mar'ia Rodr'iguez-Escudero<sup>1</sup>, Morgane Roussin<sup>2</sup>, Paul R. C. Imbert<sup>2</sup>, Isabel Rodr'iguez-Escudero<sup>1</sup>, Laurent Terradot<sup>2</sup>, Mar'ia Molina<sup>1</sup>, Jean-Pierre Gorvel<sup>3</sup>, V'ictor J. Cid<sup>1\*</sup>, Suzana P. Salcedo<sup>1,2\*</sup>

**1** Departamento de Microbiolog'ia y Parasitolog'ia, Facultad de Farmacia, Universidad Complutense de Madrid and IRYCIS, Madrid, Spain, **2** Laboratory of Molecular Microbiology and Structural Biochemistry, Centre National de la Recherche Scientifique UMR5086, Universit' de Lyon, Lyon, France, **3** Aix-Marseille University, CNRS, INSERM, CIML, Marseille, France

\* These authors contributed equally to this work.

\* vicjcid@ucm.es (VJC); suzana.salcedo@ibcp.fr (SPS)



## OPEN ACCESS

**Citation:** Coronas-Serna JM, Louche A, Rodr'iguez-Escudero M, Roussin M, Imbert PRC, Rodr'iguez-Escudero I, et al. (2020) The TIR-domain containing effectors BtpA and BtpB from *Brucella abortus* impact NAD metabolism. *PLoS Pathog* 16(4): e1007979. <https://doi.org/10.1371/journal.ppat.1007979>

**Editor:** Jean Celli, Washington State University, UNITED STATES

**Received:** July 9, 2019

**Accepted:** March 26, 2020

**Published:** April 16, 2020

**Peer Review History:** PLOS recognizes the benefits of transparency in the peer review process; therefore, we enable the publication of all of the content of peer review and author responses alongside final, published articles. The editorial history of this article is available here: <https://doi.org/10.1371/journal.ppat.1007979>

**Copyright:** © 2020 Coronas-Serna et al. This is an open access article distributed under the terms of the [Creative Commons Attribution License](https://creativecommons.org/licenses/by/4.0/), which permits unrestricted use, distribution, and reproduction in any medium, provided the original author and source are credited.

**Data Availability Statement:** All relevant data are within the manuscript and its Supporting Information files.

## Abstract

*Brucella* species are facultative intracellular Gram-negative bacteria relevant to animal and human health. Their ability to establish an intracellular niche and subvert host cell pathways to their advantage depends on the delivery of bacterial effector proteins through a type IV secretion system. *Brucella* Toll/Interleukin-1 Receptor (TIR)-domain-containing proteins BtpA (also known as TcpB) and BtpB are among such effectors. Although divergent in primary sequence, they interfere with Toll-like receptor (TLR) signaling to inhibit the innate immune responses. However, the molecular mechanisms implicated still remain unclear. To gain insight into the functions of BtpA and BtpB, we expressed them in the budding yeast *Saccharomyces cerevisiae* as a eukaryotic cell model. We found that both effectors were cytotoxic and that their respective TIR domains were necessary and sufficient for yeast growth inhibition. Growth arrest was concomitant with actin depolymerization, endocytic block and a general decrease in kinase activity in the cell, suggesting a failure in energetic metabolism. Indeed, levels of ATP and NAD<sup>+</sup> were low in yeast cells expressing BtpA and BtpB TIR domains, consistent with the recently described enzymatic activity of some TIR domains as NAD<sup>+</sup> hydrolases. In human epithelial cells, both BtpA and BtpB expression reduced intracellular total NAD levels. In infected cells, both BtpA and BtpB contributed to reduction of total NAD, indicating that their NAD<sup>+</sup> hydrolase functions are active intracellularly during infection. Overall, combining the yeast model together with mammalian cells and infection studies our results show that BtpA and BtpB modulate energy metabolism in host cells through NAD<sup>+</sup> hydrolysis, assigning a novel role for these TIR domain-containing effectors in *Brucella* pathogenesis.

**Funding:** This work was funded by the FINOVI foundation under a Young Researcher Starting Grant, the Cystic Fibrosis French Foundation Vaincre la Mucoviscidose grant RF20130500897 and the ANR (grant n°ANR-15-CE15-0011) to SS, and by grants BIO2016-75030-P from Ministerio de Economía y Competitividad (Spain) and S2017/BMD-3691 (InGEMICS-CM) from Comunidad de Madrid and European Structural and Investment Funds to VJC and MM. SS is supported by an INSERM staff scientist contract. J.M.C-S is supported by a predoctoral contract from UCM. The funders had no role in study design, data collection and analysis, decision to publish, or preparation of the manuscript.

**Competing interests:** The authors have declared that no competing interests exist.

## Author summary

*Brucella* is a genus of zoonotic bacteria that cause severe disease in a variety of mammals, ranging from farm animals (as bovines, swine and ovine) to marine mammals. Transmission to humans, often by ingestion of non-treated dairy products, leads to serious systemic infection. *Brucella abortus* invades host cells and replicates intracellularly. Such behavior relies on the injection of bacterial proteins into the host cytoplasm via specialized secretion systems. Our work focuses on the study of two of these factors, BtpA and BtpB, previously described to contain Toll/Interleukin-1 Receptor (TIR)-domains that modulate innate immunity. We use here two biological models: the yeast *Saccharomyces cerevisiae* and human cell lines. We found that the TIR domains of both *Brucella* proteins were necessary and sufficient to collapse energy metabolism in yeast by depleting ATP and NAD<sup>+</sup>. This result was translatable to higher cells and consistent with the recently described NADase activity of some TIR domains both in mammalian and bacterial proteins. Importantly, we demonstrate that *Brucella* down-regulates total NAD levels in host cells by using both BtpA and BtpB effectors. Our results show that NAD<sup>+</sup> is targeted by *Brucella* during infection, which may constitute a novel mechanism for its pathogenicity.

## Introduction

Several bacterial pathogens can circumvent host innate immune responses during infection, often by injecting effector proteins into host cells that target components of innate immune pathways. In many cases, these effectors contain eukaryotic-like domains capable of modulating receptor proximal events. This is the case of Toll/interleukin 1 receptor (TIR) domains present on the cytosolic faces of all Toll-like receptors (TLRs) and corresponding adaptor proteins, enabling the formation of a scaffold for the assembly of intricate protein signaling complexes [1]. The formation of these supramolecular organizing complexes (SMOCs) involves both self-interactions and interactions with other TIR domains [2]. TIR domains are also present in plants, where they mediate disease resistance, in amoebas with a role in ingestion of bacteria and immune-like functions, as well as in many bacterial genera [3].

Several Gram-negative and Gram-positive bacterial pathogens are known to rely on TIR domain-containing protein effectors for down-regulation of TLR-signaling during infection [4]. One of the best characterized is the TIR-containing protein of uropathogenic *E. coli* (TcpC), prevalent in clinical isolates associated with acute pyelonephritis in children. TcpC was shown to contribute to kidney pathology by hijacking the MyD88 TLR adaptor, resulting in inhibition of TLR4 and TLR2 signaling [5]. TcpC inhibition of TRIF- and IL-6/IL-1-dependent pathways has also been described [6]. Interestingly, the observation that expression of TirS from *Staphylococcus aureus*, present in a multi-drug resistant (MDR) island of numerous clinical isolates, is induced by specific antibiotic treatment [7] raises the possibility that these bacterial proteins may be tightly regulated, enhancing virulence, persistence or dissemination in particular clinical contexts such as exposure to selective pressure.

For some pathogens, additional functions have been assigned to bacterial TIR domains other than the downregulation of TLR pathways, as in the case of PumaA from *Pseudomonas aeruginosa*, which interferes with TNF receptor signaling by targeting UBAP1 [8], a component of the endosomal-sorting complex required for transport I (ESCRT-I). Also, *E. coli* TcpC directly interacts with the NACHT leucine-rich repeat PYD protein 3 (NLRP3) inflammasome and caspase-1 resulting in inflammasome perturbation [9].

Recent work on mammalian TLR adaptor SARM1 and plant nucleotide-binding leucine-rich repeat (NLR) immune receptors, such as RUN1, unveiled that their TIR domains possess enzymatic activity [10, 11]. Authors went on to demonstrate that not only eukaryotic but also prokaryotic TIR domains, in general, constitute a new family of nicotinamide adenine dinucleotide (NAD<sup>+</sup>) hydrolase enzymes [12]. Although this NADase activity is efficiently neutralized in the bacteria by an unknown mechanism, when heterologously expressed in laboratory *E. coli* strains or assayed *in vitro* these prokaryotic TIR domains were able to cleave NAD<sup>+</sup>. Loss of NAD<sup>+</sup> was also detected when full-length *S. aureus* TirS was ectopically expressed in mammalian cultured cells [12].

One of the bacterial TIR domains shown to have NAD<sup>+</sup>-consuming activity when expressed in *E. coli* was that of BtpA (also known as TcpB) from *Brucella* spp. [12]. In *Brucella abortus*, a clear role in virulence has been established not only for BtpA but also for BtpB, the second TIR domain-containing protein of *Brucella*. Together, these effectors have been shown to down-modulate dendritic cell activation contributing to the stealthy characteristics of this pathogen in the context of chronic brucellosis [13, 14].

The precise target of *Brucella* TIR-containing effector proteins remains unclear. BtpA has been proposed to act as a mimic of the TLR adaptor TIRAP by binding specific phosphoinositides of the plasma membrane [15] and increasing TIRAP ubiquitination and degradation during infection [16]. However, preferential binding to MyD88 was also demonstrated [17]. It is likely that these *Brucella* TIR-containing proteins display additional targets or functions, as they modulate microtubule dynamics when ectopically expressed [18, 19] and BtpA was shown to induce the unfolded protein response [20].

Given all the possible roles proposed for these *Brucella* TIR effectors and their potential NADase activity we set out to investigate in greater detail their functions. By combining ectopic expression in the model eukaryotic organism *Saccharomyces cerevisiae* and human cells, as well as *in vitro* infection studies we have found that BtpA and BtpB reduce total NAD levels during infection, suggesting their NADase activities are an integral part of their role in *Brucella* pathogenesis. Our results point towards a novel function of these effectors in modulation of host metabolism through the modulation of intracellular NAD levels during infection.

## Results

### Expression of *Brucella abortus* TIR-domain containing BtpA and BtpB proteins in *S. cerevisiae* induces toxicity

To gain insight into the roles of BtpA and BtpB in modulation of cellular functions, *btpA* and *btpB* genes were cloned in a yeast expression vector under the control of the inducible *GALI* promoter to produce the corresponding GFP fusion proteins. Thus, expression was repressed in glucose-based media, but incubation of yeast transformants in galactose-based media led to the expression of GFP-BtpA and GFP-BtpB, as verified by Western blotting (S1A and S1B Fig). Both GFP-BtpA and GFP-BtpB were inhibitory for yeast growth, but expression of the latter was much more toxic (Fig 1A). At the fluorescence microscope, GFP-BtpB displayed a punctate cytoplasmic pattern, whereas GFP-BtpA was clearly enriched in yeast nuclei (Fig 1B and 1C). In sum, when expressed in yeast, *Brucella* TIR-containing domain proteins lead to different degrees of toxicity and distinct subcellular localization.

### TIR domains of BtpA and BtpB are necessary and sufficient for toxicity, and form filamentous structures in the yeast cell

BtpA and BtpB have divergent N-terminal regions, while their C-terminal fractions display their respective TIR domains. To learn whether cytotoxicity relied on their TIR domains or

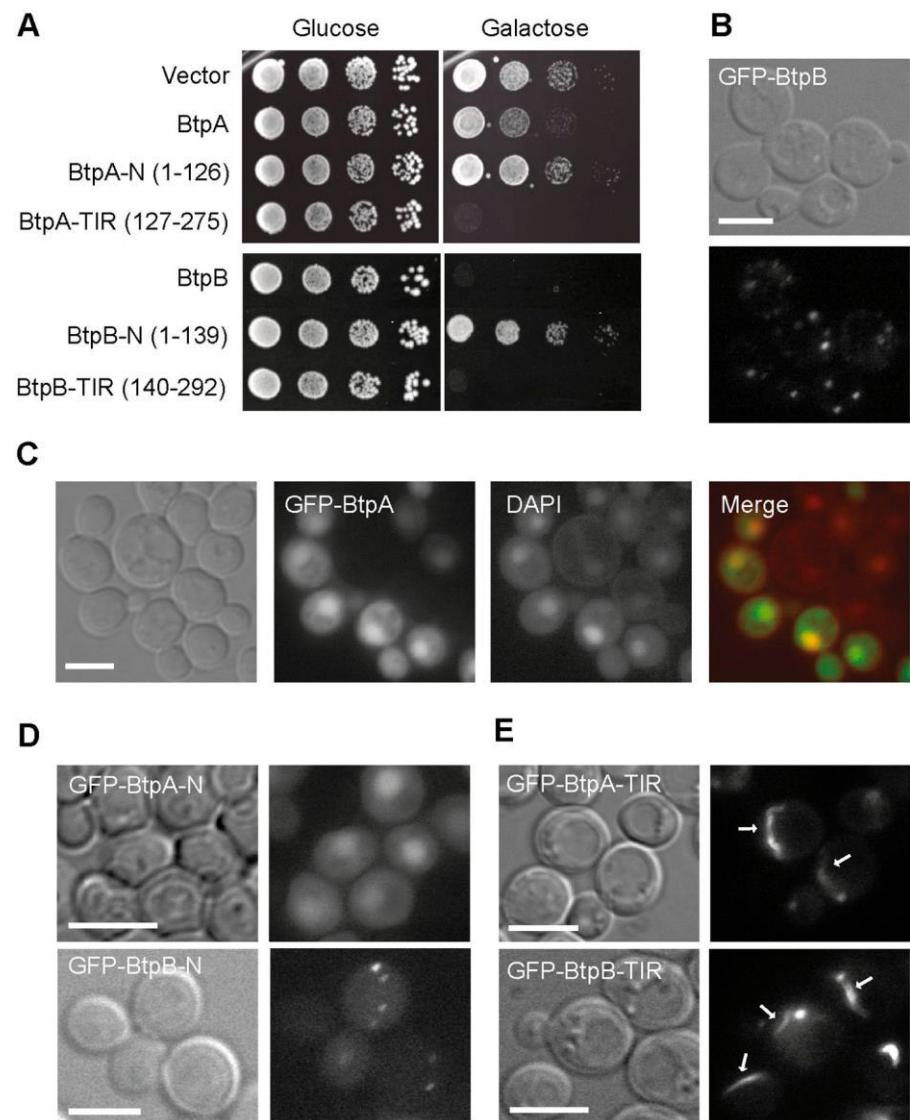


**Fig 1. Expression and localization of *B. abortus* BtpA and BtpB in *S. cerevisiae*.** (A) BtpA and BtpB induce different levels of toxicity when expressed in yeast. Ten-fold serial dilution assay to monitor growth in YPH499 yeast strain expressing the pYES2 empty vector or the BtpA or BtpB indicated versions (full-length, N and TIR) from pYES2-GFP plasmid derivatives, under control (Glucose) and induction (Galactose) conditions. Nomarski and fluorescence microscopy of YPH499 yeast strain expressing from pYES2 plasmid derivatives the following fusion proteins: (B) full-length GFP-BtpB after 4h induction; (C) full-length GFP-BtpA (green) and stained with DAPI (red), after 6h induction; (D) the GFP-fused N-terminal regions of BtpA and BtpB after 5h induction; (E) the GFP-fused C-terminal regions containing TIR domains of BtpA and BtpB after 4h induction. Scale bars correspond to 5  $\mu$ m.

<https://doi.org/10.1371/journal.ppat.1007979.g001>

their N-terminal extensions, we split both proteins to individually express the N- and C-terminal halves of the proteins. Thus, we produced GFP fusions to BtpA-N (1–126) and BtpA-TIR (127–275), and BtpB-N (1–139) and BtpB-TIR (140–292) and confirmed their expression in yeast cells (S1A and S1B Fig). As shown in Fig 1A, both TIR domains alone were sufficient for toxicity. Interestingly, the TIR domain of BtpA was more toxic than the full-length protein. In contrast, the N-terminal regions of BtpA and BtpB were innocuous for the yeast cell. However,

the N-terminal extensions defined subcellular localization of the proteins, as BtpA-N maintained the predominant nuclear localization and BtpB-N formed cytoplasmic dots, like the corresponding full-length proteins (Fig 1D). In spite of the limited identity (19.92%) between the TIR domains of BtpA and BtpB, fluorescence microscopy revealed that both GFP-BtpA-TIR and GFP-BtpB-TIR assembled into long cytoplasmic filaments (Fig 1E), occasionally contacting or surrounding the nucleus (S2 Fig). Both GFP-BtpA-TIR and GFP-BtpB-TIR conspicuous filaments resembled cytoplasmic microtubule bundles. However, immunofluorescence with anti-tubulin antibodies revealed that they did not co-localize with tubulin (S2 Fig). Although we cannot rule out that *Brucella* TIR domains are interacting with filamentous structures other than tubulin in yeast, our results suggest that they are prone to forming highly ordered structures by self-interaction, and that their N-terminal extensions negatively influence this behaviour.

### BtpB depolarizes actin patches, blocks endocytosis and down-regulates signaling in *S. cerevisiae*

To understand the mechanisms underlying growth inhibition in yeast expressing *Brucella* TIR proteins, we chose to analyze the effects of full-length BtpB. The actin cytoskeleton supports polarized growth in yeast during budding, so growth arrest could be caused by actin dysfunction. Indeed, as shown in Fig 2A, staining of actin cortical patches with rhodamine-conjugated phalloidin revealed a dramatic loss of polarization of actin structures towards the growing bud and septum region. Moreover, the BtpB TIR domain was fully responsible for this phenotype (Fig 2A). Besides supporting growth along the budding cycle, actin function is important for endocytosis. We used the FM4-64 fluorochrome to monitor endocytic traffic. Internalization of this non-permeable molecule via the endocytic pathway leads to staining of the vacuolar membrane in cells after 1 hour of incubation [21]. We observed that cells that efficiently expressed GFP-BtpB, as judged by the presence of intense green fluorescent cytoplasmic spots, were unable to internalize this marker, as compared to those lacking green fluorescence or control cells expressing GFP alone (Fig 2B), indicating that BtpB severely blocked endocytosis. This phenotype also relies on BtpB TIR domain, as shown in S1C Fig.

Often, cellular stresses that lead to actin depolarization in yeast trigger the activation of signaling cascades involving mitogen-activated protein kinase (MAPK) modules, such as the cell wall integrity (CWI) pathway, engaging the Sit2 MAPK [22]. Also, we have previously described that some bacterial effectors, such as *Salmonella* SteC and SopB [23, 24], depolarize actin by down-regulating small GTPases when expressed in yeast, leading to concomitant dephosphorylation of downstream Fus3 and Kss1 MAPKs of the mating pathway. Thus, we tested MAPK activation levels in BtpB-expressing cells by immunoblot using anti-phospho-MAPK antibodies. Peculiarly, all Sit2, Fus3 and Kss1 MAPK basal phosphorylation levels were downregulated in BtpB-expressing cells, but not upon BtpA expression (S3A Fig). Then we investigated whether BtpB would be able to downregulate MAPK activation upon stimulation of these pathways, by incubation at 39 °C or in the presence of the cell wall-stressing compound Congo red to stimulate the CWI pathway, and by using the mating pheromone  $\alpha$ -factor to activate Fus3 and Kss1. Although BtpB still allowed activation of these pathways by the stimuli, MAPK phosphorylation was always less efficient (S3B Fig). A fourth MAPK, Hog1, a p38 homolog, operates in budding yeast responding to high osmolarity challenges [25]. As observed for the other MAPKs, phosphorylation of Hog1 was less efficient in the presence of BtpB when this pathway was stimulated by osmotic stress (S3C Fig). Since these MAPK pathways do not share upstream components, it is striking that they all were simultaneously down-regulated by BtpB expression. Such a general effect in MAPK phosphorylation might reflect



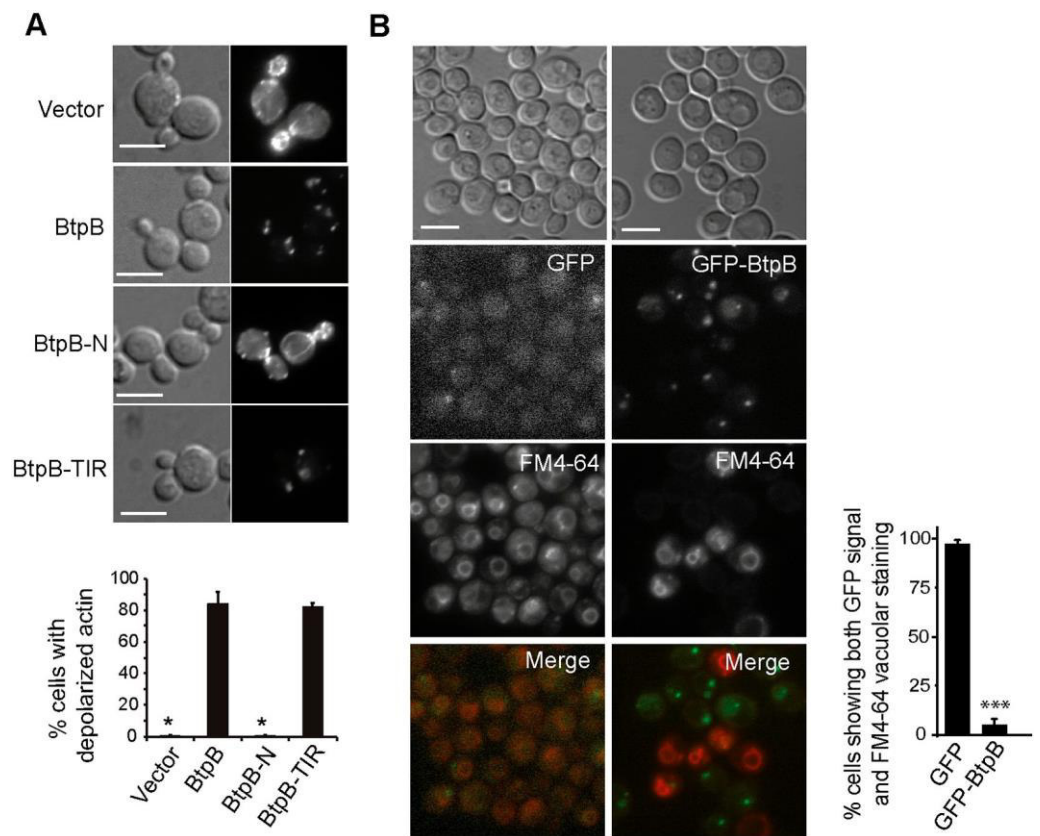


**Fig 2. BtpB expression causes severe defects in actin cytoskeleton and endocytosis in *S. cerevisiae*.** (A) Nomarski and fluorescence microscopy images (upper panel) and graph showing the percentage of small- to medium-budded cells with depolarized actin (lower panel) after rhodamine-phalloidin staining of YPH499 cells expressing pYES2-GFP empty vector, BtpB, BtpB-N or BtpB-TIR from pYES2-GFP plasmid derivatives after 4h induction. Data correspond to means  $\pm$  standard deviation of three independent transformants ( $n \geq 100$ ) and statistical comparison was done with Kruskal-Wallis ANOVA with p-values referring to BtpB of 0.024 (\*) for vector and BtpB-N. Scale bars indicate 5  $\mu$ m. (B) Nomarski and fluorescence microscopy images (left panel) and graph representing the percentage of cells showing both GFP and FM4-64 vacuolar signal (right panel) of YPH499 cells expressing pYES2-GFP or pYES2-GFP-BtpB, after 4h induction, stained with the endocytic marker FM4-64 for 1h. Data correspond to means  $\pm$  standard deviation of three independent transformants ( $n \geq 100$ ) and statistical comparison was done with Student's t-test,  $p < 0.0001$  (\*\*\*). Scale bars indicate 5  $\mu$ m.

<https://doi.org/10.1371/journal.ppat.1007979.g002>

inability of the cell to properly undergo phosphorylation events. In support of this view, when heterologous mammalian Akt1 (which undergoes phosphorylation in its activation site by conserved yeast PDK-like kinases [26]), was co-expressed with BtpB, a reduced phosphorylation was also observed (S3D Fig). The TIR domain of BtpB alone was fully responsible for signaling down-regulation (S1B Fig). Interestingly, such effect was also observed when expressing the TIR domain of BtpA (S1A Fig).

In sum, BtpB and BtpB-TIR expression in yeast result in severe actin disorganization, endocytic block and a general defect in the phosphorylation of all signaling kinases tested.

### Genetic screen for yeast genes that suppress BtpB-induced lethality

We pooled three non-overlapping libraries obtained from the whole genome yeast ORF collection, consisting of all *S. cerevisiae* predicted ORFs cloned in an expression vector under the

control of the inducible *GALI* promoter transformed in *E. coli*. This pooled whole genome expression library was co-transformed with a GFP-BtpB *GALI*-based expression plasmid and positive selection allowed the recovery of genes suppressing BtpB toxicity in galactose-based medium. Suppressor genes listed in [S4A Fig](#) and [S3 Table](#) were selected when growth rescue (i) was confirmed after individual re-transformation, (ii) was specific for BtpB-induced growth inhibition, but not that of other toxic heterologous protein (PI3K $\alpha$ -CAAX)[26], and (iii) was not due to a lower production of GFP-BtpB, as verified by immunoblot ([S4B Fig](#)). As shown in [S4A Fig](#), suppression was partial in all cases. Co-transformation of these suppressors with BtpB-TIR led to the same rescue levels, although no growth recovery was detected when co-expressed with BtpA-TIR ([S4C and S4D Fig](#)). Thus, either these suppressors are specific for BtpB-TIR domain derived toxicity in yeast or the effect of BtpA-TIR is too strong to allow partial suppression. Although most of these genes have not been yet assigned a bona fide function in yeast, a subset of them, *INM2*, *RBK1*, and *DOG2* are sugar or inositol phosphorylating/dephosphorylating enzymes related to metabolic pathways ([S3 Table](#)). *DOG2* encodes a 2-deoxyglucose-6 phosphate phosphatase and its overexpression overcomes toxicity of this glycolytic inhibitor [27], and *RBK1* encodes a putative ribokinase, which has been recently shown to be catalytically active [28]. These results suggest that metabolic shifts related to carbon source usage partially counteract BtpB toxicity.

### BtpA and BtpB deplete ATP and NAD<sup>+</sup> in the yeast cell

Our results on BtpB expression in yeast affecting dynamic cellular events such as cytoskeletal function and vesicle traffic as well as general kinase function would be consistent with limiting intracellular ATP levels. Furthermore, the fact that sugar kinase/phosphatases were isolated as *btpB* overexpression suppressors suggest that energetic metabolism is compromised in BtpB-expressing yeast cells. Recently, Essuman *et al.* [12] reported that the TIR-domain of proteins from phylogenetically diverse bacteria, including *Brucella* BtpA, displayed enzymatic activity as NAD<sup>+</sup> hydrolases. Thus, we were prompted to study ATP and NAD<sup>+</sup> levels in yeast cells expressing BtpA and BtpB. Yeast cells expressing BtpB or the TIR domains of either BtpB or BtpA, showed significant losses of both ATP and NAD<sup>+</sup> intracellular levels, as determined by luciferase assay or quantitative mass spectrometry respectively ([Fig 3](#)). This effect was especially dramatic in NAD<sup>+</sup> levels, which were lowered about one order of magnitude upon BtpB overexpression. We also observed a slight but significant reduction of NAD<sup>+</sup> in the case of full-length BtpA ([Fig 3B](#)). The decrease in NAD<sup>+</sup> and ATP correlated very well with the differential toxicity for yeast cells of each protein version ([Fig 1A](#)), as full-length BtpB had the strongest effect on intracellular NAD<sup>+</sup> and ATP levels while, in the case of BtpA, the TIR domain alone had a more dramatic effect than the full-length protein. This raises the idea that the N-terminal extension of BtpA, but not that of BtpB, has a negative regulatory effect on the C-terminal TIR/NAD<sup>+</sup> hydrolase domain.

As a control, we generated a BtpB E234A catalytically inactive mutant, by changing to Ala the equivalent Glu residue described by Essuman *et al.* [12] to be essential for catalysis in other TIR domains. BtpB E234A was no longer toxic for yeast ([Fig 4B](#)), and it did not lead to reduced MAPK phosphorylation ([S1B Fig](#)), or endocytosis defects ([S5D–S5E Fig](#)). In agreement with its lower toxicity, this BtpB mutant was expressed at higher levels than the toxic wild-type version ([S1B Fig](#)). Expression of the BtpB E234A mutant had no effect on ATP or NAD<sup>+</sup> intracellular levels ([Fig 3](#)), strongly suggesting that, as described for other TIR domains [12], this residue is essential for the catalytic activity of BtpB.

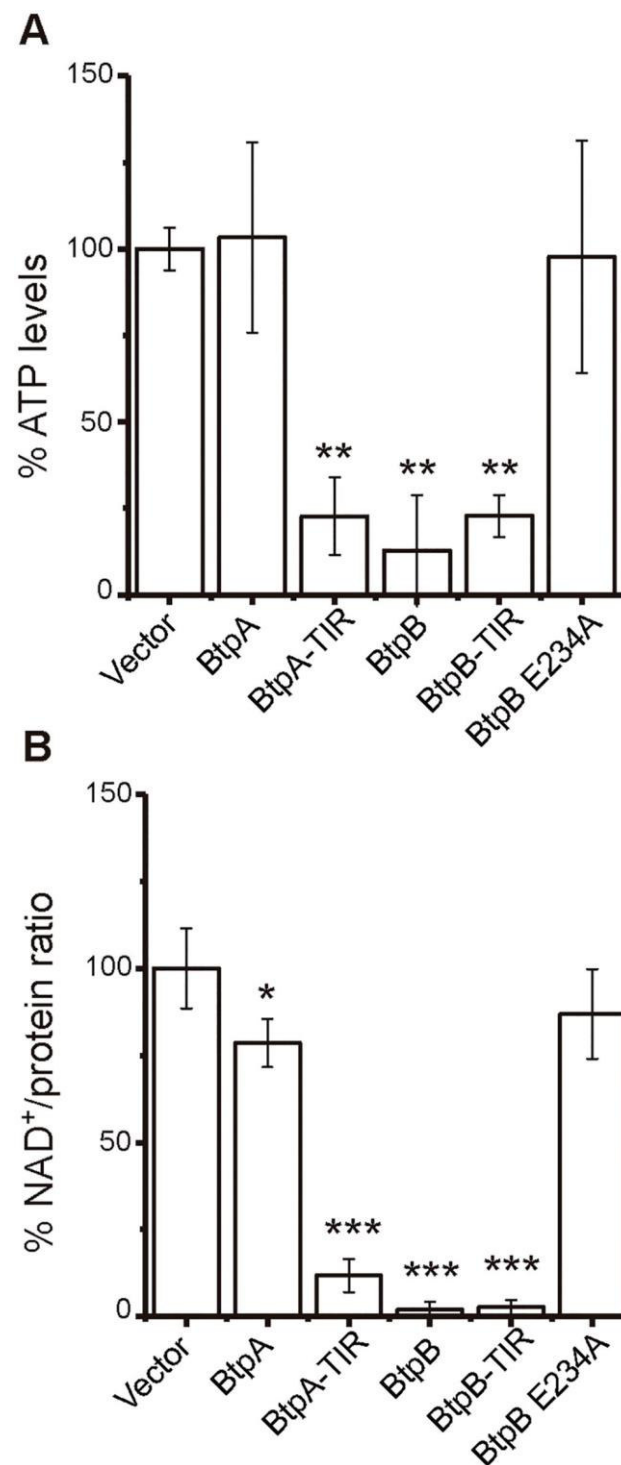


**Fig 3. BtpB, BtpA-TIR and BtpB-TIR reduce NAD<sup>+</sup> and ATP levels when expressed in yeast.** (A) Cellular ATP measurement by luciferase assay in YPH499 cells transformed with pYES2 empty vector and pYES2 plasmid derivatives bearing: both full-length and TIR domain versions of BtpA and BtpB and the catalytically inactive BtpB E234A mutant. Graph shows ATP levels as a percentage relative to the ATP levels measured on empty vector control cells. Results correspond to means  $\pm$  standard deviation of three different transformants and statistical comparison was done with one-way ANOVA with p-values referred to vector of 0.0045 (<sup>ns</sup>) for BtpA-TIR, 0.0017 (<sup>ns</sup>) for BtpB and

0.0046 (<sup>\*\*\*</sup>) for BtpB-TIR. (B) Cellular NAD<sup>+</sup> levels measured by mass spectrometry, standardized as a NAD<sup>+</sup>/extract protein ratio, from YPH499 cells transformed with the same plasmids as in A. Graph shows NAD<sup>+</sup>/protein ratio as a percentage of the empty vector control cells NAD<sup>+</sup>/protein ratio. Data correspond to means  $\pm$  standard deviation of four different transformants and statistical comparison was done with one-way ANOVA with p-values referred to vector <0.0001 (<sup>\*\*\*\*</sup>) for BtpA-TIR, BtpB and BtpB-TIR, and 0.0134 (<sup>\*</sup>) for BtpA.

<https://doi.org/10.1371/journal.ppat.1007979.g003>

## Mapping of residues essential for NAD<sup>+</sup> hydrolase function at the TIR domain of BtpB

Taking advantage of the severe toxicity of BtpB in yeast, we devised a screen for the isolation of loss-of-function mutations by random mutagenesis. This was performed by plasmid gap-repair [29], forcing *in vivo* homologous recombination between an open gapped plasmid and a partially overlapping insert encoding BtpB, which had been generated by error-prone PCR. Such strategy allows direct selection in galactose-based medium for recombinant clones bearing mutations in *btpB* that yield the protein non-toxic. Ten single and two double mutants were recovered and sequenced (S4 Table). As shown in S5A Fig, most mutations corresponded to non-conservative amino acid changes in highly conserved regions between BtpA and BtpB TIR domains. Some of these residues are also conserved in the TIR-domain of human SARM1 and plant RUN1, in which the NAD<sup>+</sup> hydrolytic activity was recently described [10, 11].

To decipher the effects of the mutations on BtpB properties, we mapped the corresponding residues on the BtpA-TIR domain structure (PDB: 4LZP) [30], as BtpB structure is not yet solved. As seen in Fig 4A, none of the residues mutated belonged to the TIR-TIR interface. S162 (S149 in BtpA) and F163 (H150 in BtpA) belong to the pA strand. Y225 (F208 in BtpA) and Q226 (F209 in BtpA) are part of the small helix  $\alpha$ C. Mutations of these residues are likely to disrupt the inner core and thus destabilize the whole structure.

Mutation of BtpB S201P (S185 in BtpA) is likely to perturb the NAD<sup>+</sup> catalytic site. In the recent crystal structure of NADP<sup>+</sup>-bound RUN1-Tir domain [11] (PDB: 6O0W), the substrate lies in a pocket formed by the BB-loop and the loop containing the conserved catalytic WxxxE motif [19] (S5B Fig). In BtpA structure S185 lies in the BB loop and interacts with the W213 (W231 in BtpB) of the WxxxE motif, which contains the essential catalytic E217 residue (E234 in BtpB). Finally, D158 (D145 in BtpA), F188 (F174 in BtpA), Y193 (Y178 in BtpA), and I291 (I275 in BtpA) residues clustered in two patches at the protein surface (Fig 4A).

In order to determine whether NAD<sup>+</sup> hydrolase and filament formation of TIR domains were separable features, we transferred mutations D158G, S162P and Y255C, as well as the mutation in the catalytic residue E234A, to GFP-BtpB-TIR to study whether loss of toxicity correlated with the ability of the TIR domain alone to produce filaments. Interestingly, only E234A, S162P and, partially, Y225C mutations eliminated BtpB-TIR toxicity in yeast cells (Fig 4B), despite the fact that all four mutations fully prevented toxicity and endocytosis defects in full-length BtpB (S5C–S5E Fig). Moreover, only the GFP-BtpB-TIR S162P mutant significantly lost the ability to form protein filaments (Fig 4C and 4D), probably because that mutation damaged the inner core (Fig 4A) These results indicate segregation between filament formation and growth inhibitory functions of BtpB-TIR in yeast and highlight the importance of the Glu234 residue specifically for NAD<sup>+</sup> hydrolase activity, while Ser162 is key for both features.

We also changed by site-directed mutagenesis the catalytic E217 residue to Ala in both full-length and the TIR domain alone of BtpA. Both mutants lost their toxicity on yeast (Fig 4E). Moreover, BtpA-TIR E217A did not reduce MAPK phosphorylation and yeast cells sustained higher levels of expression as compared to WT BtpA-TIR (S1A Fig). Although a statistically significant reduction in the percentage of cells showing BtpA-TIR filaments was found (45.1%

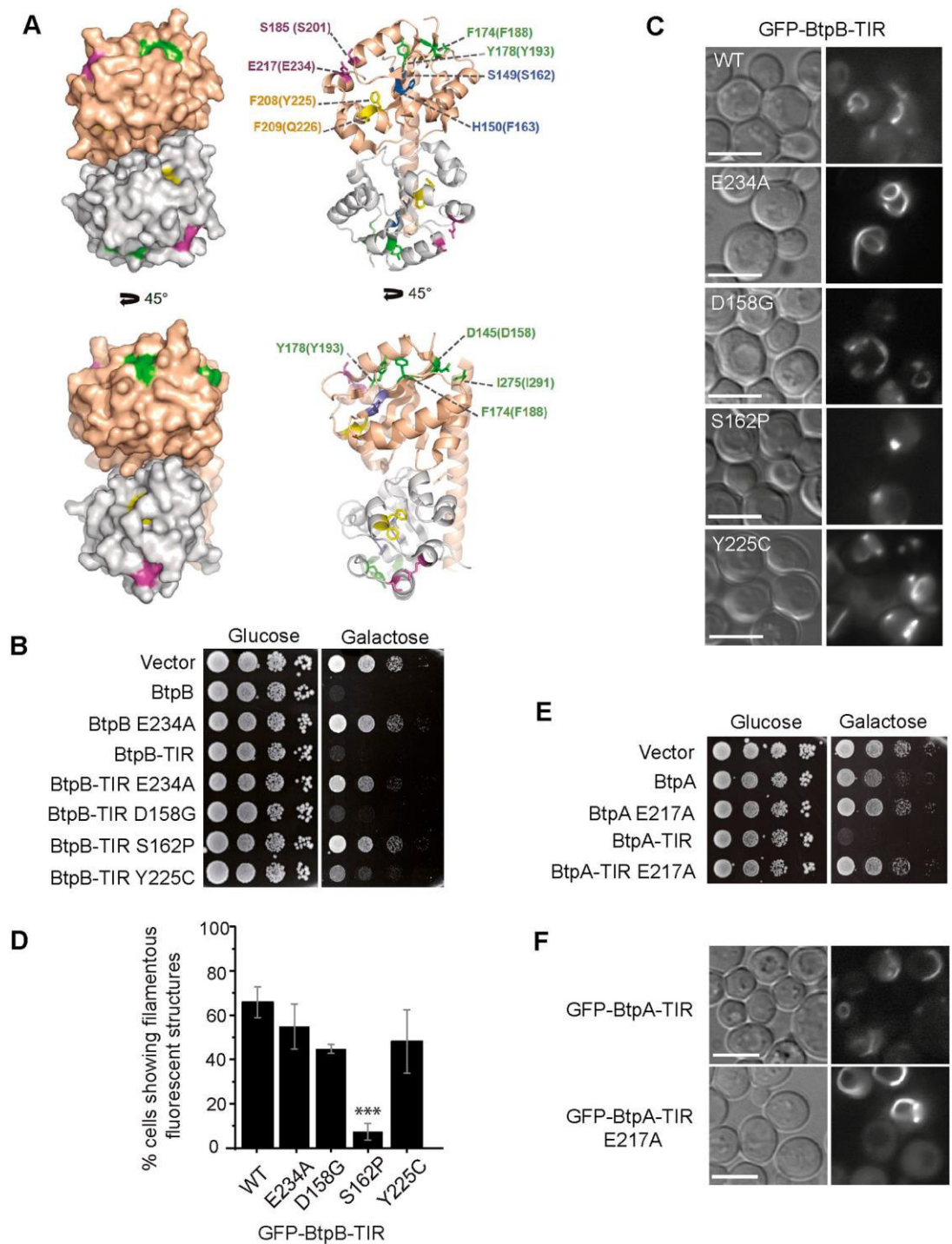


**Fig 4. Functional analysis of BtpB and BtpA mutations in yeast.** (A) Structure of BtpA-TIR domain showing the positions equivalent to those identified as loss-of-function in BtpB by yeast random mutagenesis screening. Left panels: two views of BtpA-TIR dimer structure (PDB: 4LZP) with chain A colored in wheat and chain B in grey. Residues identified are colored according to their assigned properties. Positions of the mutations putatively affecting protein folding are colored in blue (pA strand) and yellow (αC helix). Mutations at the active site are colored in magenta. Mutations at the surface outside the active site are colored in green. Right panels: views in the same orientation of the BtpA dimer depicted as cartoon with the side chains of mutated residues displayed as ball-and-sticks. Residue numbers are indicated for BtpA and the corresponding residues in BtpB are in parenthesis. (B) Ten-fold serial dilution growth assay of YPH499 cells expressing pYES2 empty vector, BtpB full-length, BtpB-TIR and the indicated mutants



from pYES2 plasmid derivatives, under control (Glucose) and induction (Galactose) conditions. (C) Normarski and fluorescence microscopy of YPH499 cells expressing GFP-BtpB-TIR and the indicated mutants, after 4h induction. Scale bars correspond to 5  $\mu\text{m}$ . (D) Graph displaying percentage of cells showing filamentous fluorescent structures. Data corresponds to means  $\pm$  standard deviation of three independent transformants and statistical comparison was done with one-way ANOVA with a p-value  $< 0.0001$  (<sup>\*\*\*</sup>) between BtpB-TIR WT and S162P. (E) Ten-fold serial dilution growth assay of YPH499 yeast strain bearing pYES2 empty vector and pYES2 plasmid derivatives expressing BtpA, BtpA-TIR and their corresponding catalytically inactive mutants E217A, under control (Glucose) and induction (Galactose) conditions. (F) Normarski and fluorescence microscopy of yeast cells expressing pYES2-GFP-BtpA-TIR and its E217A mutant version. Scale bars correspond to 5  $\mu\text{m}$ .

<https://doi.org/10.1371/journal.ppat.1007979.g004>

$\pm 7.7$  for BtpA-TIR vs.  $26\% \pm 12$  for BtpA-TIR E217A), these structures were larger and more intense for the mutant than for the wild type version (Fig 4F). Importantly, these results indicate that, as observed for BtpB, the catalytic E217 residue is essential for toxicity in yeast but still allows assembly of the BtpA TIR domain into ordered structures.

### Inhibition of endocytosis occurs upon ectopic expression of BtpB in human cells but not during infection

To investigate whether the results obtained in yeast were translatable to mammalian cells, we began by overexpressing BtpB in human epithelial cells (HeLa). As previously described [19] and consistent with the yeast model, a punctate accumulation of BtpB was observed in the cytosol of HeLa cells. These results were obtained for GFP-BtpB (Fig 5), as well as Myc-expressing BtpB (S6A Fig), indicating that this localization is independent of the tag. To gain insight into the type of structures BtpB was forming, we labelled for different endocytic markers. Some of these structures were enriched in mono- and poly-ubiquitinated proteins as recognized by the FK2 antibody (Fig 5A), which could correspond to either aggregates of misfolded protein or sites with densely ubiquitinated proteins as previously described [19]. However, some of the BtpB compartments did not show labelling with the FK2 antibody and were also negative for the lysosomal associated membrane protein 1 (LAMP1) (Fig 5A), suggesting BtpB associates with multiple intracellular structures. Unlike the yeast model, expression of BtpB neither resulted in significant perturbation of the actin cytoskeleton (Fig 5B) nor the microtubule network morphology (Fig 5C). Consistent with results from Felix and colleagues [19], we also observed localization of BtpB between cells, at sites of intercellular bridges that form during cell division (S6B Fig).

As the yeast model revealed a potential role for the N-terminal domain of BtpB in intracellular localization whereas the TIR domain for its toxicity, we next analyzed the fate of truncated BtpB versions in HeLa cells. As in yeast, expression of BtpB-N resembled that of full-length BtpB, with cytosolic aggregates being formed (Fig 6). Expression of the TIR domain alone (BtpB-TIR) resulted in the formation of long filament-like structures that showed no co-localization with tubulin (Fig 6), consistent with the results obtained in the yeast model. In some cells, BtpB-TIR induced disorganization of the microtubule network (S6C Fig). These filamentous structures did not co-localize with vimentin either, a marker of intermediate filaments (S6D Fig), strongly reminiscent of what has been previously described for the *Staphylococcus aureus* TirS protein [7]. Most likely, as also inferred from the above yeast data, these structures correspond to self-assembled ordered filaments consisting of the TIR domain, which are absent when stabilized by the presence of the N-terminal domain. These results confirm that the N-terminal portion of BtpB plays an important role in subcellular localization. Interestingly, the BtpB E234A mutant retained the dot-like distribution observed for BtpB in HeLa cells (S6E Fig).

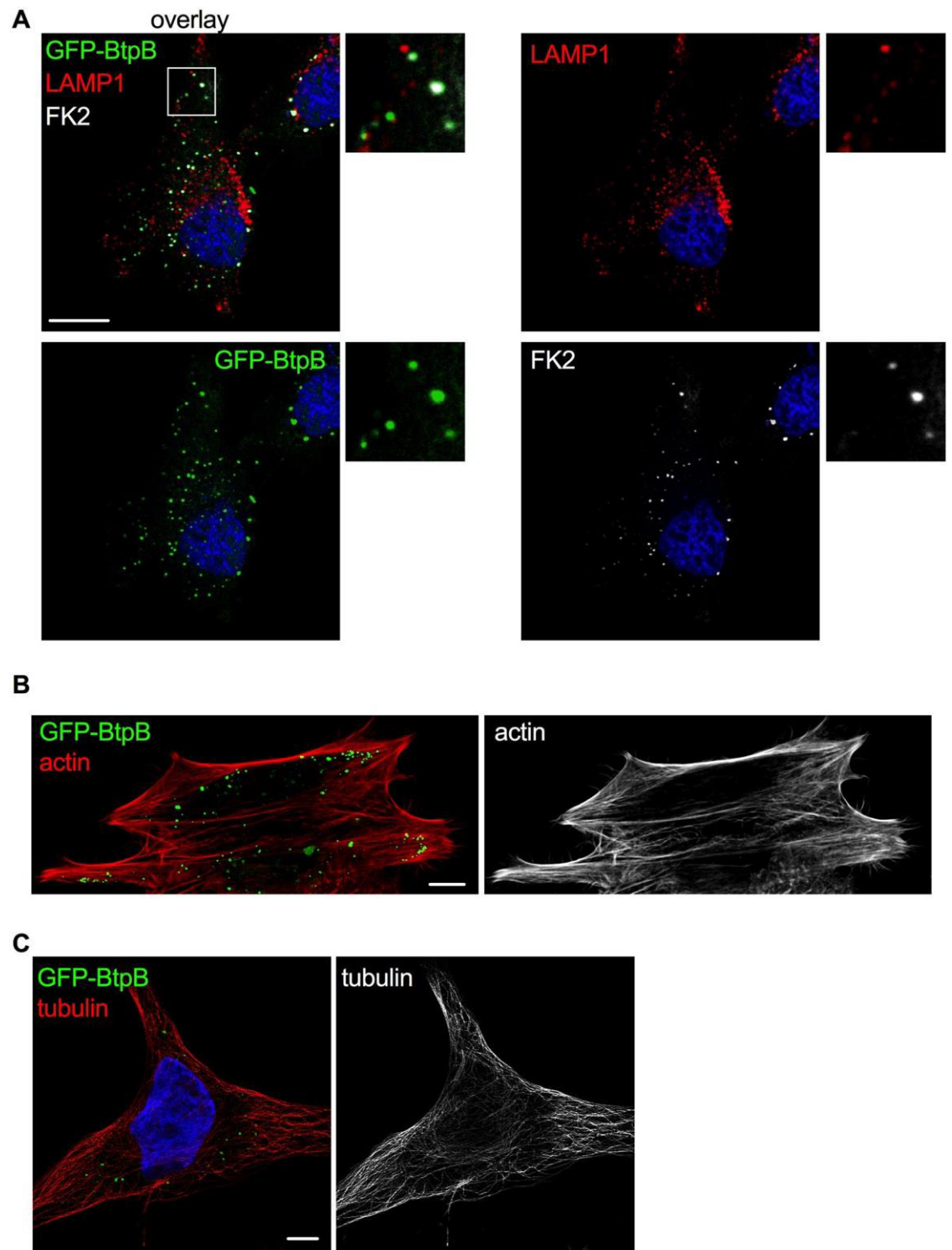


**Fig 5. Localization of ectopically expressed BtpB in human cells.** HeLa cells expressing GFP-BtpB (green) were labelled and analyzed by confocal immunofluorescence microscopy. Representative images are shown. (A) Cells were labelled with FK2 (cyan) along with LAMP1 (red) antibodies. The nuclei are labelled with DAPI (blue). (B) Cells were labelled with phalloidin for visualization of the actin cytoskeleton (red) and (C) with anti-tubulin antibody for visualization of the microtubules (red). Scale bars correspond to 5  $\mu$ m. The tubulin image was obtained with Airyscan confocal imaging mode.

<https://doi.org/10.1371/journal.ppat.1007979.g005>

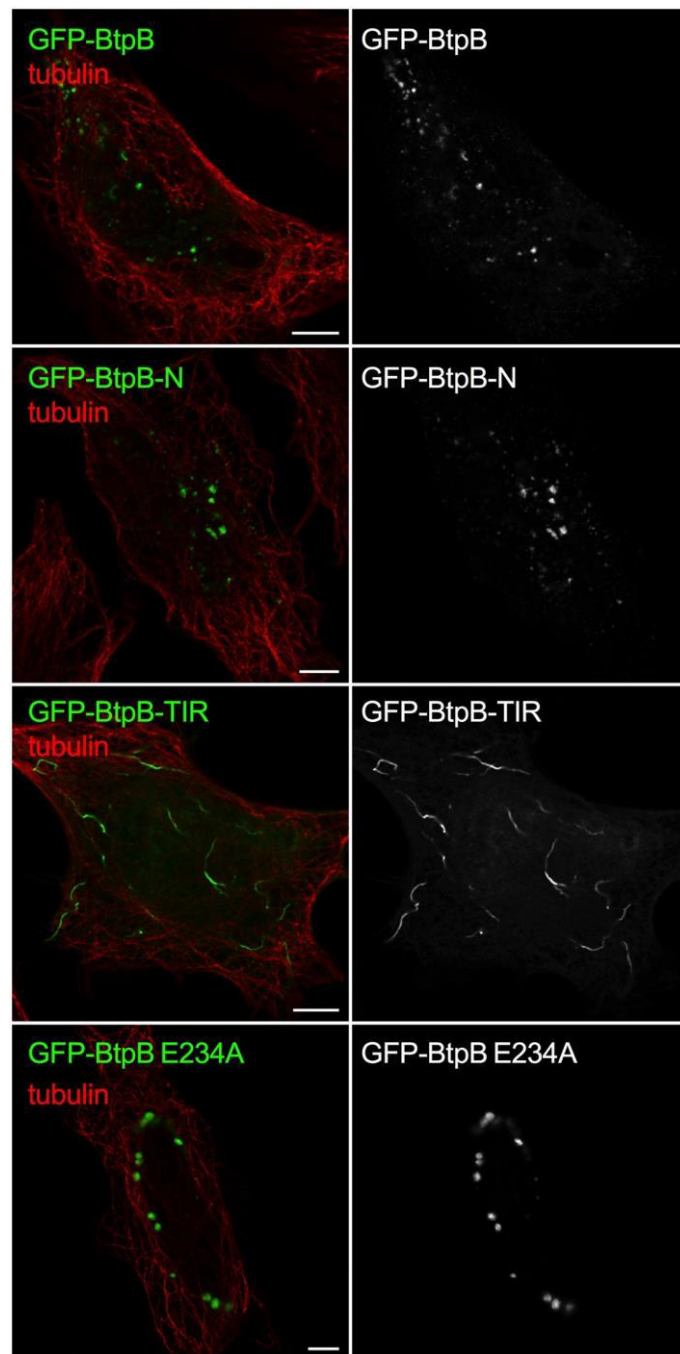


**Fig 6. BtpB N-terminal domain is required for intracellular localization when ectopically expressed.** The HeLa cells were transfected with GFP-BtpB, GFP-BtpB-N (1–139), GFP-BtpB-TIR (140–292) and GFP-BtpB E234A. Cells were then labelled for tubulin (red). Scale bars correspond to 5  $\mu$ m and all images obtained with Airyscan confocal imaging mode.

<https://doi.org/10.1371/journal.ppat.1007979.g006>



We next determined if BtpB expression resulted in perturbation of endocytosis in human cells as observed in yeast. Fluorescently labeled transferrin or Epidermal Growth Factor (EGF) were incubated with HeLa cells expressing GFP-BtpB or GFP alone and the percentage of cells with uptake of these endocytosis markers quantified by microscopy. The expression of GFP-BtpB significantly decreased endocytosis of both markers in comparison to GFP alone (Fig 7A–7C) consistent with the yeast model.

Although overexpression of individual effectors provides a powerful tool to investigate direct functions of these proteins, to thoroughly investigate the capacity of BtpA and BtpB to inhibit endocytosis, we analyzed this phenotype during infection. Although we could observe a slight decrease of endocytosis after 24 h of infection of HeLa cells, this phenotype was neither statistically significant nor abrogated by deletion of *btpA* nor *btpB* (S7A Fig). Furthermore, no significant differences were observed at 48 h post-infection for HeLa cells infected with WT *Brucella* in comparison to cells infected with mutants lacking either *btpA*, *btpB* or both genes (Fig 7D). Finally, no impact on endocytosis was observed in immortalized bone marrow-derived macrophages (iBMDM) at 24 nor 48 h post-infection (S7B Fig and Fig 7E, respectively), suggesting that *Brucella* TIR proteins do not interfere with endocytosis during infection.

### BtpA and BtpB deplete cellular NAD when ectopically expressed in human cells and during infection

As previous studies attributed a NAD<sup>+</sup>-consuming activity to the BtpA TIR domain when expressed in *E. coli* [12] and our experiments using the eukaryotic yeast model showed that both BtpB and BtpB-TIR strongly reduce intracellular NAD<sup>+</sup> content, we next assessed total NAD levels in HeLa cells expressing either Myc-BtpB or Myc-BtpA in comparison to Myc alone by using a colorimetric assay. Both Myc-tagged proteins were well expressed in epithelial cells although BtpA always migrated as a double band, potentially indicative of post-translational modifications occurring in the cell (Fig 8A). As shown in Fig 8B, both BtpA and BtpB strongly reduced total NAD levels in HeLa cells validating the results obtained with the yeast model.

To determine whether *Brucella* could impact intracellular NAD levels during infection, we first established that all bacterial strains had equivalent levels of total NAD in the inocula (S7C Fig), which corresponds to a 16h culture, the time required to reach early stationary phase used for our infection studies. We next infected HeLa cells with wild-type or mutant strains lacking either *btpA* or *btpB* and quantified the levels of total NAD. Although we did not observe any differences at 24h post-infection, we could observe that *B. abortus* infection for 48h resulted in reduction of total NAD levels in a manner dependent on BtpA and BtpB (Fig 9A). As it is well established that *btp* mutants replicate to the same levels as wild-type *Brucella* [14] and we have found they have equivalent bacterial total NAD levels (S7C Fig) we can conclude that BtpA and BtpB NAD-consuming activities are likely to impact host intracellular NAD levels. To confirm these phenotypes were specifically due to the absence of BtpA and BtpB, we attempted to complement the mutant strains. The phenotype of the *btpA* mutant strain could be restored by expressing *btpA* from a plasmid (Fig 9B). Although the same tendency could be observed for the complementation of the *btpB* mutant, due to a lower effect on the NAD concentration in HeLa cells infected with the *btpB* mutant we could not obtain statistical significance with the number of experiments performed (Fig 9C). We therefore infected iBMDM, as a much higher rate of infection can be attained with phagocytic cells. In this cellular model, wild-type *B. abortus* infection also resulted in the reduction of intracellular NAD levels, in a manner dependent on BtpA and BtpB. The expression of each gene from a plasmid

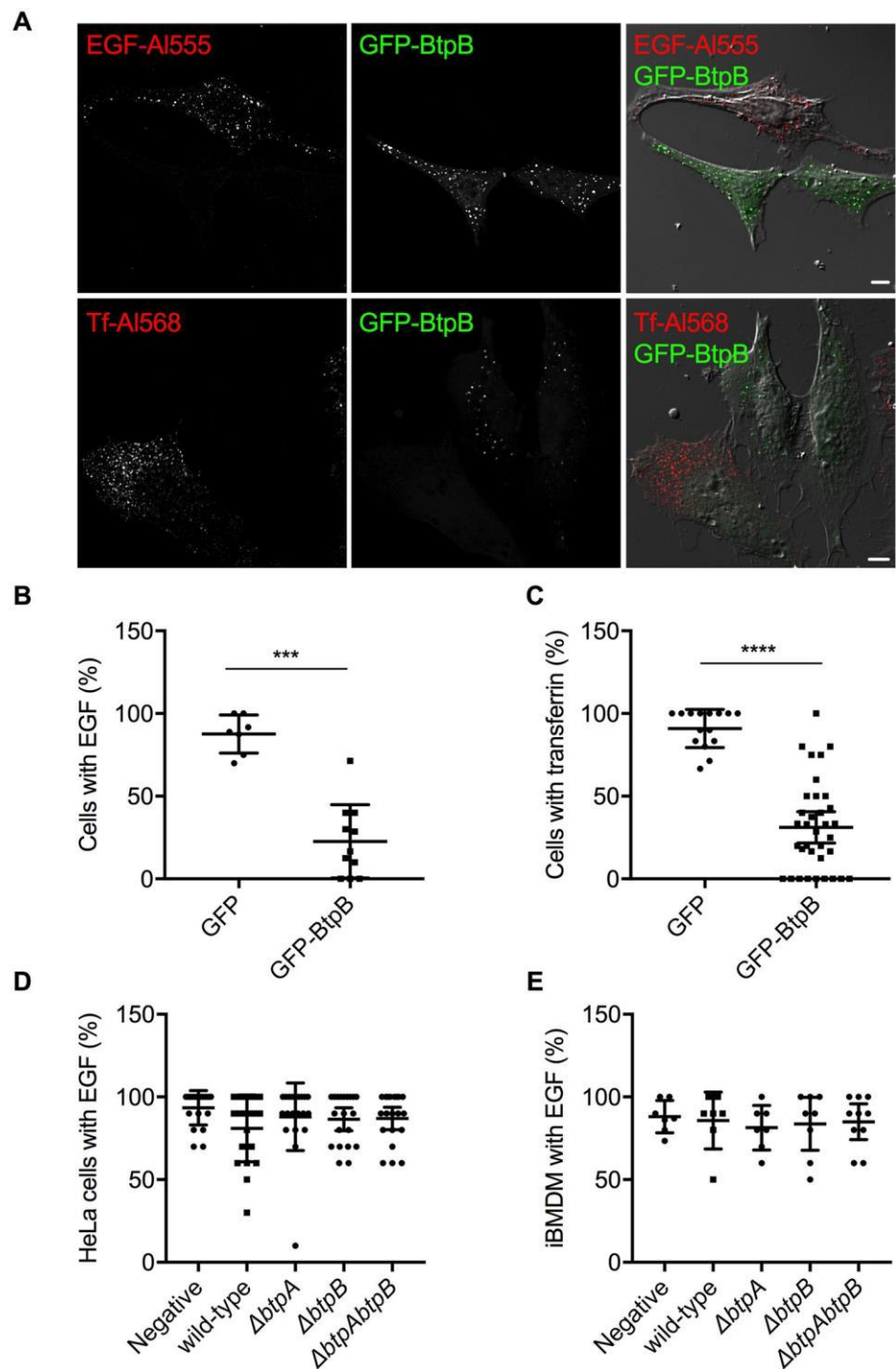


**Fig 7. Inhibition of endocytosis occurs upon ectopic expression of BtpB but not during infection.** HeLa cells expressing GFP-BtpB (green) were incubated with either EGF conjugated with Alexa Fluor 555 (red) or transferrin conjugated with Alexa Fluor 568 (red) for 10 minutes. (A) Cells were then analyzed by confocal microscopy and (B) and (C) the percentage of cells showing uptake of either fluorescent marker quantified. A cell was considered positive when clear labelling of endocytic vesicles was observed throughout the cell. Counts correspond to individual microscopy fields, obtained from three independent experiments. Data correspond to means  $\pm$  standard deviation and statistical comparison was done with Mann-Whitney test,  $p = 0.0001$  (\*\*\*) for EGF (left) and  $p < 0.0001$  (\*\*\*\*) for transferrin (right). (D) HeLa cells or (E) immortalized bone marrow-derived macrophages (iBMDM) were infected for

48 h with either wild-type *B. abortus* or a mutant strain lacking *btpA*, *btpB* or both genes. Cells were then incubated with EGF conjugated with Alexa Fluor 555 for 10 minutes and the percentage of infected cells showing uptake of this fluorescent marker quantified by microscopy. Counts correspond to individual microscopy fields, with a total of at least 200 cells counted for each, from three independent experiments. Mock infected cells are included as a control. Data correspond to means  $\pm$  standard deviation and statistical comparison was done with one-way ANOVA test, with no statistical significance observed.

<https://doi.org/10.1371/journal.ppat.1007979.g007>

fully restored the wild-type phenotype in the case of BtpA (Fig 10A) and partially in the case of BtpB (Fig 10B).

Finally, to determine if the observed reduction of NAD was due to the catalytic activity of the TIR domain we complemented the *btpA* mutant with a plasmid carrying a E217A mutation in *btpA* ( $\Delta btpA btpA$  E217A) and the *btpB* mutant with a plasmid expressing a E234A mutation in *btpB* ( $\Delta btpB btpB$  E234A). We first controlled that these catalytic mutant versions of BtpA and BtpB could be efficiently translocated into host cells. We constructed TEM1 fusions as previously reported [14] and determined the percentage of cells emitting coumarin fluorescence at 24 h post-infection (S7D Fig). We had to use RAW macrophages for these experiments as previously described [14] because CCF2 was toxic for iBMDM. In the case of BtpA we observed a level of translocation of TEM-BtpA E217A consistent with what was previously reported for the wild-type TEM-BtpA [14]. In the case of BtpB, a lower percentage of infected cells showed translocation of the TEM-BtpB E234A, consistent with what has been observed for the wild-type TEM-BtpB (less than 2% of infected cells) [14].

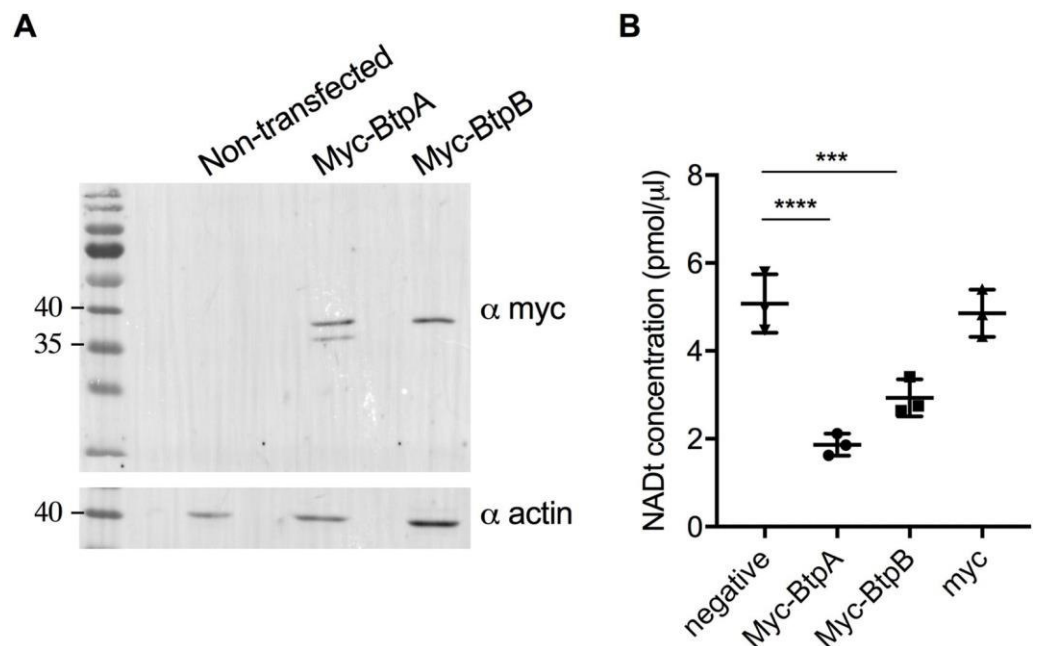


**Fig 8. Ectopic expression of BtpB results in reduction of total NAD<sup>+</sup> in HeLa cells.** (A) Representative Western blot showing levels of Myc-BtpA and Myc-BtpB expression revealed with an anti-Myc antibody and anti-actin antibodies, as a loading control. Myc-BtpA has a predicted molecular weight of 33 kDa whereas BtpB 38 kDa. (B) Measurement of total NAD levels using a colorimetric assay from HeLa cells expressing either Myc-tagged BtpA or BtpB. Non-transfected cells (negative) and cells transfected with Myc vector alone are also included as controls. Data correspond to means  $\pm$  standard deviation from three independent experiments and statistical comparison was done with one-way ANOVA, with a p-value for the negative control *versus* Myc-BtpA of  $<0.0001$  (\*\*\*\*) and *versus* Myc-BtpB of  $0.0006$  (\*\*\*).

<https://doi.org/10.1371/journal.ppat.1007979.g008>

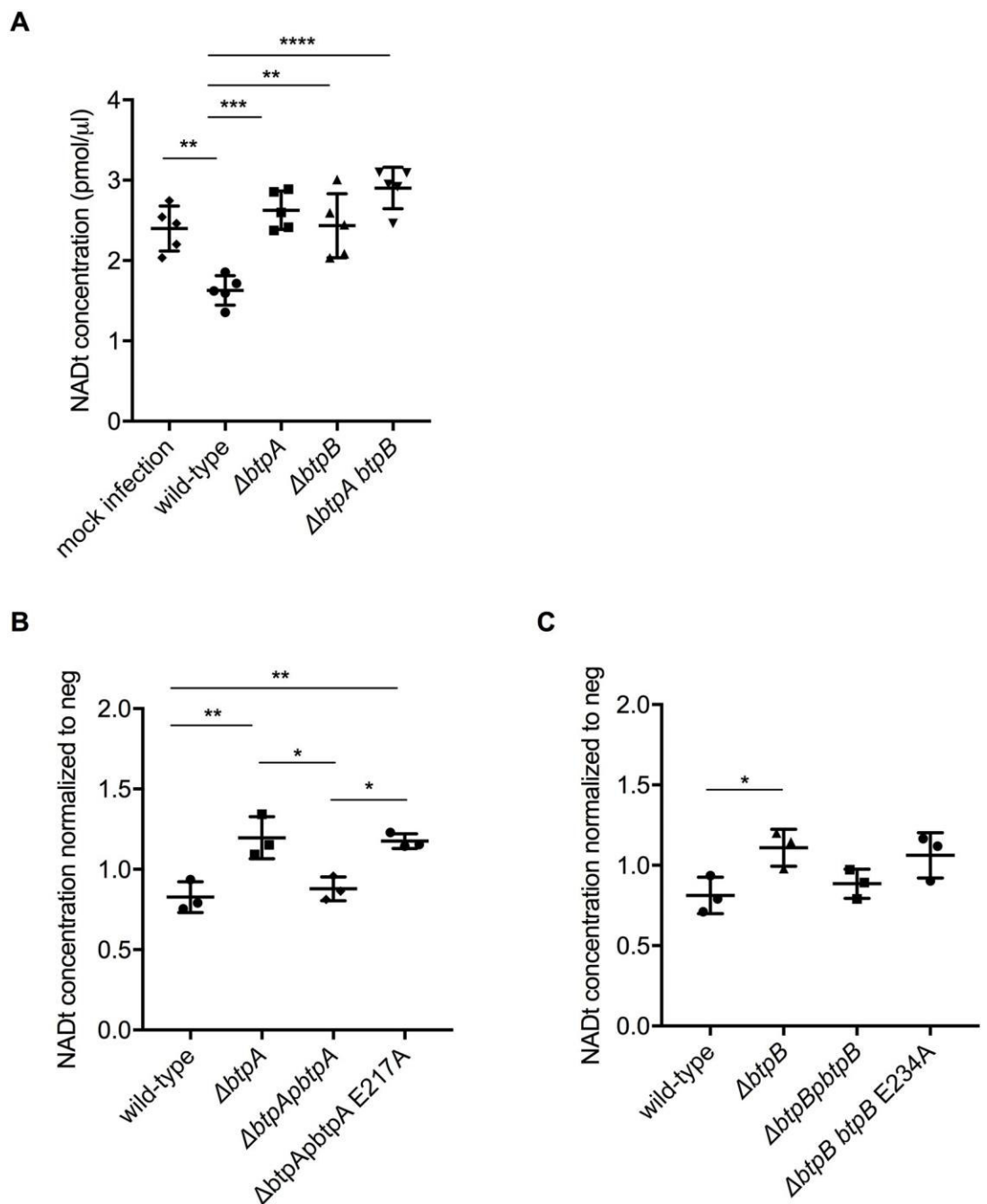


**Fig 9. *B. abortus* TIR domain-containing proteins control intracellular total NAD levels during infection of cultured epithelial cells.** (A) HeLa cells were infected for 48 h with either wild-type *B. abortus*, or strains lacking *btpA*, *btpB* or both genes. Mock infected cells are also included. Total NAD levels were measured using a colorimetric assay and data correspond to means  $\pm$  standard deviation from five independent experiments and statistical comparison was done with a one-way ANOVA test, with statistical significance indicated in the graph. Between mock and wild-type  $p = 0.0028$  (\*\*); between the wild-type and *btpA*, *btpB* or *btpAbtpB* mutants  $p = 0.0002$  (\*\*\*),  $0.0018$  (\*\*\*) and  $<0.0001$  (\*\*\*\*), respectively. Higher NAD levels in the infected cells than in the mock experiment are likely attributable to the fact that intracellular NAD levels from bacterial cells are added up to those of the cell line. (B) HeLa cells were infected for 48 h with either wild-type *B. abortus*, a *ΔbtpA* mutant, the complemented strain *ΔbtpAbtpA* and a *ΔbtpA* complemented with a catalytic mutant *ΔbtpAbtpA* E217A. Results are normalized to mock infected cell values and correspond to means  $\pm$  standard deviation from three independent experiments and statistical comparison was done with a one-way ANOVA test, with statistical significance indicated in the graph. For wild-type versus *ΔbtpA*  $p = 0.0052$ , *ΔbtpA* versus

$\Delta btpA$   $p = 0.0124$ ,  $\Delta btpA$   $p$  versus  $\Delta btpA$   $p$  E217A  $p = 0.0177$  and wild-type versus  $\Delta btpA$   $p$  E217A  $p = 0.0072$ . (C) HeLa cells were infected for 48 h with either wild-type *B. abortus*, a  $\Delta btpB$  mutant, the complemented strain  $\Delta btpB$   $p$  and a  $\Delta btpB$  complemented with a catalytic mutant  $\Delta btpB$   $p$  E234A. Results are normalized to mock infected cell values and correspond to means  $\pm$  standard deviation from three independent experiments and statistical comparison was done with a one-way ANOVA test, with a slight statistical significance only observed between wild-type and  $\Delta btpB$  ( $p = 0.0491$ ).

<https://doi.org/10.1371/journal.ppat.1007979.g009>

We next measured the concentration of total NAD in both HeLa and iBMDM infected cells. In HeLa cells, catalytically inactive BtpA failed to complement the mutant strain (Fig 9B). Consistently, this is also the case in iBMDM for both BtpA and BtpB (Fig 10A and 10B). Together these results indicate that BtpA and BtpB contribute to depletion of intracellular total NAD levels via direct enzymatic cleavage of this metabolic co-factor during infection, assigning a novel function for these two effectors during *Brucella* infection.

## Discussion

Bacterial TIR domain-containing proteins have been shown to be major contributors to the evasion of innate immunity for a variety of bacterial pathogens, mainly by interfering with the assembly of innate immune signaling complexes involving TIR domains [4]. However, certain

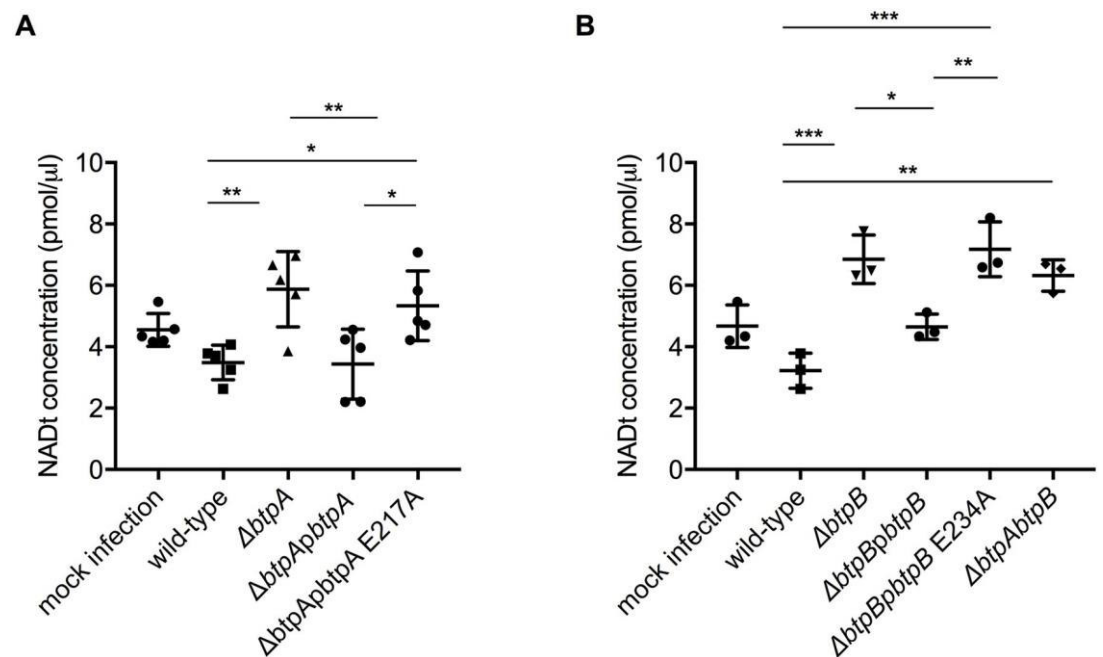


**Fig 10. *B. abortus* TIR domain-containing proteins control intracellular total NAD levels during macrophage infection.** (A) and (B) Immortalized bone marrow-derived macrophages (iBMDM) were infected for 48 h with either wild-type *B. abortus* or strains lacking *btpA*, *btpB* or both genes or complemented strains expressing *btpA* and *btpB* or the corresponding catalytic mutants. Mock infected cells are also included as a control. Total NAD levels were measured using a colorimetric assay and data correspond to means  $\pm$  standard deviation from five (A) or three (B) independent experiments and statistical comparison was done with a one-way ANOVA test, with statistical significance indicated in the graph. Higher NAD levels in the infected cells than in the mock experiment are likely attributable to the fact that intracellular NAD levels from bacterial cells are added up to those of the cell line. In (A) for wild-type versus  $\Delta btpA$   $p = 0.0071$ , wild-type versus  $\Delta btpA$   $p$  btpA E217A  $p = 0.0476$ ,  $\Delta btpA$  versus  $\Delta btpA$   $p$  btpA  $p = 0.0058$  and  $\Delta btpA$   $p$  btpA versus  $\Delta btpA$   $p$  btpA E217A  $p = 0.0398$ . In (B) for wild-type versus  $\Delta btpB$   $p = 0.0011$ , wild-type versus  $\Delta btpB$   $p = 0.0003$ , wild-type versus  $\Delta btpB$   $p$  btpB E217A  $p = 0.0001$ ,  $\Delta btpB$  versus  $\Delta btpB$   $p$  btpB  $p = 0.0156$  and  $\Delta btpB$   $p$  btpB versus  $\Delta btpB$   $p$  btpB E217A  $p = 0.0058$ . Statistical significances in relation to the negative control are not shown.

<https://doi.org/10.1371/journal.ppat.1007979.g010>

TIR domains have recently been demonstrated to possess a NAD<sup>+</sup> hydrolase activity which may contribute to their function, as for example the case of mammalian SARM1 [12] or plant NLR immune receptors [11]. We have found that both the *Brucella* TIR domain-containing proteins BtpA and BtpB retain this NAD<sup>+</sup> hydrolase activity inside cells when ectopically expressed in yeast or human cells, as well as during infection, resulting in reduction of intracellular total NAD levels at late stages of the infection. Furthermore, we have highlighted that the N-terminal non-TIR domains of these proteins are necessary for intracellular targeting of the effectors. Remarkably, BtpA-TIR and BtpB-TIR resulted in formation of long filament-like structures when ectopically expressed in yeast and human cells. Since this phenomenon can only be observed in the absence of their N-terminal regions it is likely that such N-terminal extensions may function to modulate intrinsic TIR self-assembly. Furthermore, genetic analyses in yeast revealed that such highly ordered structures formed by expression of the TIR domains alone are still achieved when expressing point mutants that lose their NADase activity, suggesting that distinct features of TIR domains rely in different structural determinants.

NAD<sup>+</sup> is an important coenzyme participating in hundreds of enzymatic reactions, notably glycolysis, the TCA cycle and mitochondrial oxidative phosphorylation. NAD<sup>+</sup> homeostasis is essential for metabolic balance and cell survival either being used as an electron carrier in redox reactions or being consumed as a substrate for numerous reactions. Beyond its well-known role in bioenergetics, NAD<sup>+</sup> has been found to have a prominent function in cell signaling, with sirtuins, poly ADP-ribose polymerases (PARPs) and CD38 using NAD<sup>+</sup> as substrate [31, 32]. NAD<sup>+</sup> has also been shown to be a key modulator of immune metabolism, acting as an important metabolic switch. In macrophages, it has been shown that increased NAD<sup>+</sup> levels are associated with activation and control of inflammatory responses, particularly involving regulation of TNF $\alpha$  transcription in classically activated pro-inflammatory (M1) macrophages [33, 34]. Interestingly, NAD<sup>+</sup> limitation also prompts important cellular changes such as the Warburg effect, a cellular state in which consumption of glucose is increased and aerobic glycolysis is favoured instead of the more energy efficient mitochondrial oxidative phosphorylation [35]. A switch to Warburg metabolism has also been observed upon immune activation of many cell types, for example macrophages, following pattern recognition receptor activation [36]. In addition, low NAD<sup>+</sup> levels are a trigger for cell death via necroptosis in macrophages [37].

Our work highlights that *Brucella* is decreasing total NAD levels in the host cell, likely contributing to modulation of cellular metabolism and signaling. This is dependent on two translocated effectors, BtpA and BtpB, containing a TIR domain that had previously been shown to down-modulate innate immune signaling in specific *in vitro* differentiated mouse bone marrow-derived dendritic cells [13, 14]. It is possible that the two phenotypes, NAD reduction and blocking of TIR-TIR interactions along the TLR signaling pathways are intimately connected. Indeed, targeting of these *Brucella* effectors to the vacuolar membrane or innate immune signaling platforms might locally impact NAD<sup>+</sup> levels inhibiting specific enzymatic reactions. Interestingly, the first enzyme to use NAD<sup>+</sup> in glycolysis, glyceraldehyde 3-phosphate dehydrogenase (GAPDH) has been shown to be recruited to the membrane of *Brucella*-containing vacuoles playing an essential role in intracellular replication [38]. Previous studies have also reported the role of the specific T4SS effector BPE123 in targeting the host enolase, another enzyme of the glycolysis pathway, which was also shown to be essential for *Brucella* intracellular multiplication in human cultured epithelial cells [39].

Host metabolism during *Brucella* infection has only recently started to be unravelled. In classically activated macrophages, *Brucella* infection was shown to induce a Warburg-like effect, with high consumption of glucose and generation of lactate efficiently used as a carbon source by intracellular replicating bacteria [40]. Interestingly, in alternatively activated



macrophages, abundant during chronic brucellosis, a shift from oxidative metabolism of glucose to oxidation of fatty acids occurs, enhancing the availability of glucose to promote intracellular bacterial replication [41]. In this study, we now highlight the role of the innate immune regulator effectors BtpA and BtpB in direct control of host energy metabolism.

Both BtpA and BtpB TIR domains were robust enough as NADases in the yeast heterologous model as to drop NAD<sup>+</sup> levels over one order of magnitude, causing a severe decrease of ATP availability in the cell and strong toxicity when overexpressed. The fact that full length BtpA is not as toxic for the yeast cell suggests that the N-terminal domains of BtpA negatively regulate BtpA catalytic activity. BtpB, on the contrary, is intrinsically active both in the absence and in the presence of its N-terminal extension. We show here that catalytically dead mutants in BtpA and BtpB TIR domains, still have the ability to self-aggregate and form filaments, proving that both features can be segregated. BtpA has been related to tubulin structures in host cells, specifically by protecting microtubules from depolymerization [19, 42]. However, we did not see coincidence of TIR cytoplasmic filaments with tubulin. ATP is necessary to achieve depolymerization of microtubules by nocodazole [43], so NAD<sup>+</sup> depletion and low ATP levels could contribute to the microtubule-stabilizing properties assigned to BtpA. Similar ATP-dependent phenomena could account for the inhibition of endocytosis in yeast and human cells. It is important to note however, that no impact of BtpA and BtpB on endocytosis was observed in infected cells. Therefore, ectopic over-expression of these effectors and its strong effect on ATP and NAD could be responsible for this phenotype, absent when a much smaller amount of protein is translocated into host cells during infection. Alternatively, *Brucella* infection may induce compensatory effects that would mask this phenotype, for example translocate other effectors that would enhance endocytosis.

Why *Brucella* may limit NAD<sup>+</sup> levels and energy metabolism in particular subcellular compartments and stages of the establishment of the intracellular niche? This is a challenging question and at this stage we can only speculate. NADase activity may contribute to evading the innate immune response. Importantly, NAD<sup>+</sup> levels are sensed by sirtuin proteins, like SIRT1, leading to the activation of several signaling pathways, some related to immunomodulation [44]. NAD<sup>+</sup>-dependent SIRT1 has recently been shown to be an important hub for cellular defence against *M. tuberculosis* intracellular survival. *M. tuberculosis* infection reduces intracellular NAD<sup>+</sup> and down-regulates SIRT1, which can be reversed by the addition of SIRT1-activating compounds that represent a potential therapeutic option [45]. The Tuberculosis Necrotizing Toxin (TNT) of *M. tuberculosis* bears NAD<sup>+</sup> glycohydrolase activity, which was shown to be important for mycobacterial replication in macrophages, and is involved in triggering necroptosis as a consequence of NAD<sup>+</sup> depletion [37, 46]. In addition, it has been proposed that reduced NAD<sup>+</sup> and ATP levels in *Salmonella*-infected macrophages, a process dependent on the *Salmonella* Pathogenicity Island 2 (SPI-2) type 3 secretion system [47], trigger the modulation of TORC1 to protect intracellular bacteria from xenophagy via lysosomal degradation of its upstream SIRT1/LKB1/AMPK regulators [47]. Thus, NAD<sup>+</sup> depletion could eventually be understood as a strategy to evade cellular innate immunity responses and promote bacterial intracellular survival.

To our knowledge, this is the first report on bacterial TIR domain-containing proteins showing NAD<sup>+</sup> hydrolase activity on the host cell during infection. Our results on the comparison of the divergent behaviour of full length and TIR domains alone in the case of BtpA and BtpB, together with the observation that the N-terminal non-TIR extensions determine subcellular localization and prevent filament formation, suggests that these extensions may finely tune NADase activity in the context of infection, likely by negatively modulating TIR-TIR assembly and by directing NADase activity to specific intracellular compartments. Further work is now necessary to better understand the control of NAD<sup>+</sup> homeostasis during *Brucella*

infection. Knowledge on how metabolic switches occur during infection at a molecular level could provide clues for the development of therapeutic strategies and vaccines.

## Materials and methods

### *Saccharomyces cerevisiae* strains and growth conditions

YPH499 (*MATa ade 2–101 trp1-63 leu2-1 ura3-52 his3-200 lys2-801*) [48] was the *S. cerevisiae* strain for general use in these studies, unless otherwise stated. W303-1A (*MATa leu2-3,112 trp1-1 can1-100 ura3-1 ade2-1 his3-11,15*) [49] was used for the Yeast ORF overexpression library screening. The *E. coli* strain DH5 $\alpha$  F<sup>0</sup>(K12 $\Delta$ (*lacZYA-argF*)U169 *deoR supE44 thi-1 recA1 endA1 hsdR17 gyrA96 relA1* (*S80lacZ $\Delta$ M15*)F<sup>0</sup>) was used for general molecular biology. As a general medium, YPD (1% yeast extract, 2% peptone and 2% glucose) broth or agar was used for growing yeast cells. For plasmid selection, synthetic complete medium (SC) contained 0.17% yeast nitrogen base without amino acids, 0.5% ammonium sulphate, 2% glucose and the appropriate amino acids and nucleic acid bases supplements. SG and SR were SC with 2% galactose or 1.5% raffinose, respectively, instead of glucose. For galactose induction experiments in liquid media cells were grown in SR medium to log phase and then galactose was added to 2% for 4–6 h. Effects of the expression of *Brucella* genes on yeast growth were tested by ten-fold serial dilution assay: spotting cells onto SC or SG plates lacking the appropriate auxotrophic markers to maintain the corresponding plasmids, and incubating them at 30 °C for 72 h [26].

### Cell culture and transfections

HeLa cells (from ATCC) were grown in DMEM supplemented with 10% of fetal calf serum (FCS) and were transiently transfected using Fugene (Roche) for 24 h, according to manufacturer's instructions. Immortalized bone marrow-derived macrophages from C57BL/6J mice were grown in DMEM supplemented with 10% of fetal calf serum (FCS) and 10% of spent supernatant of L929 cells (that provides M-CSF). RAW 264.7 macrophages (ATCC) were grown in DMEM supplemented with 10% of fetal calf serum (FCS). The *Brucella abortus* 2308 strain was used for transfection and genetic manipulation.

### Construction of yeast expression plasmids

General molecular biology techniques, as well as transformation of yeast by the lithium acetate method were performed according to standard procedures. All plasmids and oligonucleotides used in this work are listed in S1 and S2 Tables respectively. pYES2-GFP, pYES3-GFP-Akt1 and YCpLG-PI3K $\alpha$ -CAAX were previously described [26, 29, 50]. To clone *B. abortus* *btpA* into the *URA3*-based pYES2-GFP plasmid, this gene was amplified from pGEM-T-easy-BtpA plasmid [13]. The primers used for amplification of *btpA* (named BtpA-UP and BtpA-LO) had *Bam*HI respectively and *Eco*RI sites. PCR products were cleaved by these restriction enzymes to be inserted in the same sites of pYES2-GFP, generating the pYES2-GFP-BtpA plasmid. To obtain the pYES2-GFP-BtpB construction, *btpB* was amplified from pGEM-T-Easy-BtpB plasmid [13] using primers BtpB-UP and BtpB-LO, cleaved with *Bam*HI and *Xba*I restriction enzymes and the insert obtained was cloned into the pYES2-GFP plasmid. pYES3-GFP-BtpB was generated on a similar way but using primers BtpB-UP-pYES3 and BtpB-LO-pYES3 and *Bam*HI sites to clone into the *TRP1*-based pYES3-GFP plasmid. The latter plasmid had been constructed by subcloning the GFP sequence of pYES2-GFP with *Hind*III/*Bam*HI sites into pYES3 (Invitrogen).



In order to obtain the truncated versions of both BtpA and BtpB, we generated pYES2-GFP-BtpA-N (1–126), pYES2-GFP-BtpA-TIR (127–275), pYES2-GFP-BtpB-N (1–139) and pYES2-GFP-BtpB-TIR (140–292) by amplifying the corresponding DNA fragments from pYES2-GFP-BtpA and pYES2-GFP-BtpB using for the N-terminal regions BtpA-UP + BtpA-126stop-LO and BtpB-UP + BtpB-140stop-LO primers, respectively. In the case of the C-terminal regions, BtpA-BamHI127-UP + BtpA-LO and BtpB-BamHI140-UP and BtpB-LO primers were used. All upper primers carried *Bam*HI restriction site and lower primers had *Eco*RI site, except in the case of BtpB-LO, which carried an *Xba*I sequence. The PCR products were cleaved with their corresponding restriction enzymes and inserted in the same sites in the pYES2-GFP plasmid. Additionally, both C-terminal regions were also cloned into pYES3-GFP vector: BtpA-TIR (127–275) fragment was directly subcloned from pYES2-GFP-BtpA, whereas BtpB-TIR (140–292) was PCR amplified with BtpB-BamHI140-UP and BtpB-EcoRI-LO primers and then inserted on BamHI-EcoRI sites on pYES3-GFP.

*Dpn*I-based site directed mutagenesis was performed using the QuikChange kit (Agilent). To generate the catalytically inactive mutants in both full length and TIR domain of BtpA and BtpB in the pYES2-GFP and pYES3-GFP backbones, the mutations were introduced with primers Mut-BtpAE217A-UP and Mut-BtpAE217A-LO and Mut-BtpBE234A-UP and Mut-BtpBE234A-LO respectively. To introduce the three selected loss-of-function BtpB mutations into the TIR domain construct, primers Mut-BtpBD158G-UP and Mut-BtpBD158G-LO, Mut-BtpBS162P-UP and Mut-BtpBS162P-LO, or Mut-BtpBY225C-UP and Mut-BtpBY225C-LO were used.

### Construction of mammalian expression vectors

The DNA fragment encoding amino acid residues 1–139 of BtpB (BtpB-N), 140–292 of BtpB (BtpB-TIR) and BtpB full-length from *Brucella abortus* were cloned into the Gateway pDONR (Life Technologies, ThermoFisher Scientific) and then cloned into the pENTRY (Life Technologies, ThermoFisher Scientific) GFP vectors according to the manufacturer. The following primers were used: BtpB Fw, BtpB Rv, BtpB-TIR Fw and BtpB-N Rv. BtpB E234A was constructed as above from the pYES3-GFP-BtpB E234A with primers used to amplify BtpB.

### Construction of *Brucella* complementing vectors

The DNA fragments encoding *btpA*, and *btpB* were cloned into the plasmid pBBR-1-MCS4. The primers used for amplification of *btpA* had for the forward primer a *Spe*I restriction site and for the reverse primer a *Eco*RI restriction site. The primers used for amplification of *btpB* had for the forward primer a *Sac*I restriction site and for the reverse primer a *Spe*I restriction site. The following primers were used BtpA Fw-pBBR-1-MCS4, BtpA Rv-pBBR-1-MCS4, BtpB Fw-pBBR-1-MCS4, BtpB Rv-pBBR-1-MCS4. The PCR products were cleaved with their corresponding restriction enzymes and inserted in the same site in the digested pBBR-1-MCS4 plasmid. The BtpA E217A and BtpB E234A complementation vectors were obtained from pBBR-1-MCS4-BtpA and pBBR-1-MCS4-BtpB, respectively using QuickChange Site-Directed Mutagenesis.

The mutations were introduced with primers BtpA<sub>E217A</sub> Fw, BtpA<sub>E217A</sub> Rv, BtpB<sub>E234A</sub> Fw, BtpB<sub>E234A</sub> Rv.

To clone BtpA E217A and BtpB E234A into the pFlag-TEM, this genes were amplified from pBBR-1-MCS4-BtpA E217A and pBBR-1-MCS4-BtpB E234A, respectively. The primers used for amplification of *btpA*<sub>E217A</sub> and *btpB*<sub>E234A</sub> had for the forward primer a *Xba*I restriction site and for the reverse primer a *Pst*I restriction site. The PCR products were cleaved with their corresponding restriction enzymes and inserted in the same site in the pFlag-TEM plasmid.

The primers used were: TEM-BtpA<sub>E217A</sub> FW-pFlagTEM, TEM-BtpA<sub>E217A</sub> Rv-pFlagTEM, TEM-BtpB<sub>E234A</sub> FW-pFlagTEM, TEM-BtpB<sub>E234A</sub> Rv-pFlagTEM.

### Yeast cells microscopy and immunofluorescence

For fluorescence microscopy of live yeast to visualize GFP, cells were cultured in SR medium for 18 h at 30 °C, then, the appropriate amount of these cultures was suspended into fresh SG to reach an OD<sub>600</sub> of 0.3, and they were incubated for additional 4–6 h for *GALI* promoter induction. Cells were harvested by centrifugation and observed directly. To monitor vacuolar morphology and endocytosis, staining with FM4-64 was performed as described [21]. Nuclear labelling was performed by adding DAPI at 1:1000 directly to the harvested cells *in vivo* and washed once with PBS. To observe actin, yeast cells were fixed and treated with rhodamine-conjugated phalloidin (Sigma) as described [23].

Indirect immunofluorescence on yeast cells was performed as previously described [51]. Antibodies were used as follows: As primary antibody, monoclonal rat anti-alpha-tubulin (Serotec, YOL1/34) at 1:500 dilution; as secondary antibody, Alexa Fluor 594 anti-rat dye (Life Technologies) at 1:1000 dilution. DAPI was added at 1:1000 for nuclear labelling. Cells were examined in Eclipse TE2000U microscope (Nikon, Tokyo, Japan) and digital images were acquired with an Orca C4742-95-12ER charge-coupled-device camera (Hamamatsu Photonics, Hamamatsu City, Japan) and processed by HCLImage and ImageJ software.

### HeLa cells immunofluorescence, antibodies and microscopy

Cells were fixed in Antigenfix (DiaPath), at room temperature for 10 min or methanol at -20 °C for 3 min for tubulin staining. Cells were then labelled at RT with primary antibody mix diluted in 0.1% saponin in PBS with 1% BSA and 10% horse serum for blocking. Primary antibody was incubated for 1 h followed by two washes in 0.1% saponin in PBS. Secondary antibodies were then mixed and incubated for a further 30 min, followed by two washes in 0.1% saponin in PBS, one wash in PBS and one wash in distilled water before mounting with Prolong Gold. Samples were examined on a Zeiss LSM800 laser scanning confocal microscope for image acquisition. Images of 1024×1024 pixels were then assembled using ImageJ.

Primary antibodies used were mouse anti-beta-tubulin clone E7 (Developmental Studies Hybridoma Bank) at 1:250 or mouse anti-vimentin (V9) at 1:100 (Sigma). Secondary antibodies used were anti-rabbit or mouse conjugated with Alexa Fluor 488, 555 or 647 all from Jackson ImmunoResearch. When necessary phalloidin-568 (1:1000) was used to label the actin cytoskeleton and DAPI nuclear dye (1:1000) for the host cell nucleus. When indicated, cytochalasin D was added for 2 h at a final concentration of 1 µg/ml.

### HeLa cells endocytosis assay

Transferrin conjugated with Alexa Fluor 568 (Invitrogen) and EGF conjugated with Alexa Fluor 555 (Invitrogen) were added at 10 µg/ml and 50 µg/ml respectively, for 10 min at 37 °C. Cells were then placed on ice, washed with ice cold PBS twice and fixed in 3% paraformaldehyde for 15 min, followed by three washes with PBS.

### Immunodetection by western blotting

Standard procedures were used for yeast cell growth, collection, breakage, protein separation by SDS-PAGE, and transfer to nitrocellulose membranes. Anti-P-MAPK antibody (Anti-phospho-p44/ p42 MAPK (Thr-202/Tyr-204), New England Biolabs) was used to detect dually phosphorylated Slt2, Kss1 and Fus3 MAPKs diluted 1:1000. Slt2 protein was detected using a

polyclonal anti-Slt2 antibody [52], diluted 1:1000. To detect phosphorylated Hog1 high osmolarity pathway MAPK, antibody Anti-P-p38 (Sigma) at 1:1000 was used. Heterologous expressed Akt1 was detected with Anti-Akt1 (Cell Signalling) as total protein and with anti-P-Akt1(Thr)308 (Cell Signalling) for the phosphorylated forms. GFP fusion proteins were detected using monoclonal anti-GFP antibodies (Living Colors, JL-8) diluted 1:2000. As loading control either a monoclonal anti-actin (MP Biomedicals) diluted 1:2000 or a yeast specific polyclonal anti-Glucose-6-Phosphate Dehydrogenase (Sigma) diluted 1:50000 were used. In all cases, primary antibodies were detected using IRDye-680 or -800 anti-rabbit or anti-mouse antibodies (Li-Cor Biosciences), or Alexa-680 anti-mouse (Invitrogen) with an Odyssey Infra-red Imaging System (Li-Cor Biosciences).

### Yeast whole genome ORF overexpression library screening

A pooled *S. cerevisiae* whole genome ORF library (Yeast ORF collection, GE Healthcare), 4500 *URA3*-based plasmids, for overexpression under *GALI* promoter and protein A-tagged, was split into three groups. W303-1A wild type yeast strain (was co-transformed with pYES3-GFP-BtpB and one of the three library pools (S3A Fig). BtpB toxicity suppression by overexpression of a specific cDNA was tested by its ability to grow in SG agar plates. 20 different candidates were selected and tested for specificity by co-transformation with YCpLG-PI3K $\alpha$ -CAAX [26], another toxic construct for yeast cells that acts by a different mechanism. Eventually 7 positive ORF, listed on S3 Table, were found to specifically rescue BtpB toxicity.

### Random mutagenesis of *btpB* and isolation of mutants

The region of pYES2-GFP-BtpB including amino acids 118 to 292 delimited by the mutazarUP and mutazarLO primers was amplified by PCR using low-fidelity Taq DNA Polymerase (BioTools) under standard conditions. The PCR products were purified with a QIAquick Gel Extraction kit (250) kit (Qiagen) and 5  $\mu$ g of DNA were co-transformed into YPH499 yeast cells with 1  $\mu$ g of the largest fragment of pYES2-GFP-BtpB plasmid, resulting from digestion with *BsiWI/XbaI*. Such *BsiWI/XbaI* digestion of pYES2-GFP-BtpB produces a gap, so the *btpB* allele can only be reconstructed upon recombination with the amplicon by *in vivo* gap repair. Recombinants were recovered by positive selection, plating the transformation mixture onto galactose-based agar medium. The pYES2-GFP-BtpB-derived plasmids were isolated from growing clones, amplified in *E. coli*, verified by restriction analysis and transformed again in yeast cells to verify that they had lost the ability to inhibit yeast cell growth. Mutations were identified on the positive clones by DNA sequencing.

### Yeast cellular ATP measurement by luciferase assay

ATP levels were measured using ENLITEN ATP Assay System (Promega) following manufacturer's instructions. Yeast cells were cultured in SR for 18 h and then new SG was added for *GALI*-driven gene expression to a final OD<sub>600</sub> of 0.3 and cultured for 3 h at 30 °C. Approximately 1.8x10<sup>7</sup> cells were harvested in 3 mL of culture and then concentrated by centrifugation for 3 min at 2500 rpm at 4 °C. Pellets were washed with 1 mL PBS at 4 °C and stored at -80 °C for further analysis. For ATP extraction, pellets were resuspended with trichloroacetic acid (TCA, 5%, 10  $\mu$ L) and immediately neutralized using 500  $\mu$ L of Tris-acetate-EDTA buffer (TAE 1 $\times$ ; 40 mM Tris base, 20 mM acetic acid, and 1 mM EDTA, pH 7.75). The samples were centrifuged for 15 sec at 13000 rpm and then 1:100 diluted in more TAE 1 $\times$ . Ten  $\mu$ L of this solution was mixed with 100  $\mu$ L of the rL/L reagent provided by the kit and luminescence was measured using OPTOCOMP1 luminometer (MGM instruments). A standard curve for quantification was prepared using the kit's reagents.

### Yeast cellular NAD<sup>+</sup> measurement by mass spectrometry

Yeast cells were cultured as stated for the ATP luciferase assay. Approximately  $6 \times 10^7$  cells were harvested in 10 mL of culture and then concentrated by centrifugation for 3 min at 2500 rpm at 4 °C. Pellets were washed with 1 mL PBS at 4 °C and stored at -80 °C for further analysis.

Our yeast NAD<sup>+</sup> extraction protocol is a simplified version of the one described by Sporty et al. [53]. Pellets were resuspended in ammonium acetate (600  $\mu$ L of 50 mM in MS grade water) and approximately 300  $\mu$ L of 0.5–0.75 mm diameter glass beads (Reesch) were added to the tube. Cells were bead blasted at 5.5 m/s using a FastPrep-24 (MP Biomedicals) for 30 sec twice, allowing a 5 min incubation on ice in between. Supernatant was recovered by perforation of the bead-blasting tube's base with a red-hot 0.9 x 40 mm needle. The pierced tube was placed inside a capless 1.5 mL microfuge tube and both tubes were centrifuged together for 3 min at 2000 rpm at 4 °C. This first cell lysate was stored in a new 1.5 microfuge tube on ice. The glass beads in the bead-blasting tube were then washed one more time with 600  $\mu$ L of a 3:1 v/v mixture of acetonitrile (MS grade) and ammonium acetate (50 mM in MS grade water). The rinsate was then mixed with the first lysate. The mixture was clarified by centrifugation for 3 min at 13000 rpm at 4 °C and the supernatant was transferred to an ice-cold 1.5 mL microfuge tube. To standardize results, 150  $\mu$ L of these lysate were kept for protein concentration measurement by Bradford method.

Samples were filtered with a 0.22  $\mu$ m PTFE filter (JASCO) and analyzed by liquid chromatography (LC) coupled to a QQQ mass spectrometer equipped with a turbo ion spray source operating in positive ion mode (LCMS 8030, Shimadzu). Chromatographic separation was performed on a Gemini C18 analytical column (50 mm x 2.1 mm I.D., 2.7  $\mu$ m particle size; Poroshell 120 PhenylHexyl). Injection volume was 10  $\mu$ L. Samples were delivered over 11 min at a flow rate of 0.3 mL/min through the analytical column at 45 °C. The mobile phase was composed of A (3% methanol, 10 mM tributylamine, 3 mM acetic acid in water LC grade, 0.1% formic acid in water) and B (methanol). Mobile phase composition began with 0% B and was increased to 45% B in 2 min, to 50% in 5 more minutes and up to 95% in one minute. The mobile phase was then maintained at 95% B for 2 min and followed by re-equilibration with 0% B over the next 2 min, before injection of the next sample. Quantification of NAD<sup>+</sup> was performed by multiple reactions monitoring (MRM) mode to monitor the parent ion-product ion (m/z) of the analyte. Mass transitions of m/z 662.10 to 540.00 (CE = +16 V) were used for quantification and m/z 662.10 to 407.90 (CE = +30 V) for identification with a dwell-time of 100 ms. The calibration curve was determined by plotting the peak area of the analyte (Y) versus the nominal concentration (X) with least square linear regression. All analyses were made under ISO 9001:2008 quality management system certification.

### Brucella infection of HeLa and iBMDM cells

Immortalized Bone Marrow-Derived Macrophages (iBMDM) were obtained as previously described [54]. HeLa cells were seeded at  $1 \times 10^5$  cells/well for HeLa or  $0.8 \times 10^5$  cells/well for iBMDM (6 - well plates) overnight and tryptic soy broth *Brucella* cultures inoculated and incubated for 16 h with agitation at 37 °C. Cells were inoculated at an MOI of 500, centrifuged at 400 g for 10 min and incubated for a further 1 h at 37 °C for HeLa cells and 30 min for iBMDM and RAW cells. Cells were then washed 3 times with media and incubated for 1 h with media containing gentamycin 50  $\mu$ g/ml and streptomycin 100  $\mu$ g/ml. After this time media was replaced to reduce the gentamycin concentration to 10  $\mu$ g/ml streptomycin 20  $\mu$ g/ml.

### Total NAD colorimetric assay

Total NAD (NAD<sup>+</sup> and NADH) was extracted and quantified from cell lysates (from 2 wells of a 6-well plate for each sample) using the NAD<sup>+</sup>/NADH Colorimetric Assay Kit (Abcam, ab65348) following the manufacturer's instructions. Briefly, the amount of total NAD was calculated from a standard curve (pmol) divided by the sample volume added to the reaction well ( $\mu$ l) and multiplied by the dilution factor.

### TEM assay

RAW cells were seeded in a 96 well plate at  $1 \times 10^4$  cells/well overnight. Cells were then infected with an MOI of 500 by centrifugation at 4 °C, 400 g for 5 min and 1 at 37 °C 5% CO<sub>2</sub>. Cells were washed with HBSS containing 2.5 mM probenidicid. Then CCF2 mix (as described in the Life Technologies protocol) and probenidicid were added to each well, and incubated for 1.5 h at room temperature in the dark. Cells were finally washed with PBS, fixed using 3% PFA and analysed immediately by confocal microscopy (Zeiss LSM800).

### Statistical analysis and software

All data sets were tested for normality using Shapiro-Wilkinson test. When a normal distribution was confirmed a One-Way ANOVA test with a Tukey correction was used for statistical comparison of multiple data sets and Students t-test for two sample comparison. For data sets that did not show normality, a Kruskal-Wallis test was applied, with Dunn's correction, or Mann-Whitney U-test for two sample comparison. 3D protein images were generated using PyMOL (Schödinger), taking advantage of previously published structural data of BtpA (PDB: 4LZP) and RUN1-TIR + NADP<sup>+</sup> (PDB: 6O0W).

### Supporting information

**S1 Fig. Expression of BtpB and BtpA versions in yeast and in inhibition of yeast endocytosis by the TIR domain of BtpB.** Western blotting of YPH499 cells extracts bearing the indicated BtpA (A) and BtpB (B) versions from pYES2-GFP plasmid derivatives, using antibodies anti-GFP (upper panels), anti-P-MAPK to show dual phosphorylation of Slt2 yeast MAPK and anti-G6PDH as loading control (lower panels). (C) Normarski and fluorescence microscopy of YPH499 cells expressing GFP-BtpB, GFP-BtpB-N and GFP-BtpB-TIR after 4h induction, stained with the endocytic marker FM4-64 for 1h. Scale bars indicate 5  $\mu$ m.  
(PDF)

**S2 Fig. BtpA and BtpB TIR filaments are not coincident with yeast tubulin.** Indirect immunofluorescence of YPH499 yeast cells expressing GFP-BtpA-TIR, GFP-BtpB-TIR, and their corresponding E234A mutant versions from pYES2 plasmid derivatives (green). Microtubules are stained using anti-tubulin antibody (red). Nuclei are labelled with DAPI (blue). Scale bars correspond to 5  $\mu$ m.  
(PDF)

**S3 Fig. Inhibitory effect of BtpB on phosphorylation of yeast signaling proteins.** (A) Western blotting from cells bearing the empty vector pYES2 (control), BtpA or BtpB from pYES2-GFP plasmid derivatives, developed with anti-P-MAPK antibody to detect dually-phosphorylated Slt2, Kss1 and Fus3 (upper panel) and anti-actin to detect actin as loading control. (B) Upper part: representative immunoblot from yeast cell lysates bearing pYES2-GFP-BtpB (+) or pYES2 (-) and upon different conditions: 30°C (control), high temperature (39°C), pheromone ( $\alpha$ -factor) or Congo red, using anti-P-MAPK (upper panel), anti-

Slt2 (medium panel) and anti-actin (lower panel). Lower part: densitometric measurement of WB bands corresponding to phosphorylated MAPKs Slt2, Kss1 and Fus3. The graph displays densitometric data of phosphorylated MAPKs normalized against actin and error bars show the standard deviation from three independent experiments on different transformant clones. (C) Western blotting of cells containing the pYES2 empty vector (control) or pYES2-GFP-BtpB, developed with anti-P-p38 antibody to detect MAPK Hog1 under high osmolarity conditions (0.6M KCl). (D) Western blotting of cells expressing heterologous Akt1 (pYES3-GFP-Akt1) with either pYES2 empty vector (control) or pYES2-GFP-BtpB, using anti-P-Akt1(Thr)308 (upper panel) and anti-Akt1 antibodies. All immunoblots were performed on protein extracts from transformants of the YPH499 yeast strain after 4 h of galactose induction.

(PDF)

**S4 Fig. Partial suppression of BtpB toxicity by overexpression of yeast genes.** (A) Ten-fold serial dilution assay of yeast cells co-expressing BtpB and each of the seven suppressor ORFs isolated from a yeast genetic screen. pYES3 and pYES2 are the corresponding empty vectors for BtpB and for the overexpressed genes, respectively. (B) Western blotting of W303-1A yeast strain co-expressing GFP-BtpB and each of the proteins encoded by the suppressor genes. Antibodies anti-GFP to detect GFP-BtpB (upper panel) and Anti-G6PDH as loading control (lower panel) were used. Anti-GFP antibody allows the detection of the indicated protein A-tagged proteins due to affinity of the tag with the Fc region of IgG-type antibodies. (C) and (D) Ten-fold serial dilution assays of yeast cells co-expressing BtpB-TIR (C) or BtpA-TIR (D) and the suppressor genes. pYES3 and pYES2 are the corresponding empty vectors for BtpB- or BtpA-TIR and for the overexpressed genes, respectively.

(PDF)

**S5 Fig. Functional analyses in yeast loss-of-function mutations in conserved residues of BtpB.** (A) Alignment of protein sequences of the TIR domains of BtpB, BtpA, human SARM1 and plant RUN1. Conserved residues relevant for this study are marked with the same color code as in Fig 4, except for the catalytic site residues W213 and E217, that are colored in pink. (B) Structure of BtpA-TIR (left; PDB: 4LZP) and RUN1-NADP<sup>+</sup> complex (right; PDB: 6OOW), showing the equivalent positions of residues mutated in BtpB isolated in the yeast screen. Both structures cartoons are displayed in the same orientation. Side chain of mutated residues of BtpA relevant for this study are colored as in (A). The side chains of residues of the catalytic site of RUN1 are shown as ball-and-sticks and colored in pink and the NADP<sup>+</sup> ligand is colored in cyan. Specific atoms are colored as follows: nitrogen in blue, oxygen in red and phosphorus in orange. (C) Phenotype of selected loss-of-function BtpB mutants. Ten-fold serial dilution growth assay of YPH499 cells transformed with pYES2 empty vector and pYES2 plasmid derivatives expressing full-length BtpB wild-type and mutants D158G, S162P and Y225C, under control (Glucose) and induction (Galactose) conditions. (D) Nomarski and fluorescence microscopy images of YPH499 cells expressing the GFP-BtpB indicated mutants, after 4h induction, stained with the endocytic marker FM4-64 for 1h. Scale bars indicate 5  $\mu$ m. (E) Graph from the same experiment as in C representing the percentage of cells showing both GFP and FM4-64 vacuolar signal. Results correspond to means  $\pm$  standard deviation of three independent transformants ( $n \geq 100$ ) and statistical comparison was done with one-way ANOVA with a p-value  $< 0.0001$  (<sup>\*\*\*</sup>) for all four mutants *versus* wild-type.

(PDF)

**S6 Fig. Localization and effects of GFP-BtpB versions in HeLa cells.** (A) Representative micrograph of HeLa cells expressing Myc-BtpB revealed with an anti-Myc antibody (red) and



phalloidin for labelling actin (cyan). (B) GFP-BtpB (green) can be detected at intercellular contacts (arrow and zoomed image). Cells were labeled with an anti-tubulin antibody (red). (C) HeLa cells were transfected with GFP-BtpB-TIR (green) and then labelled for tubulin (red) or (D) vimentin (red). (E) Representative image of cells labelled with anti-tubulin antibody (red) expressing aggregates of GFP-BtpB E234A (green). Scale bars correspond to 5  $\mu$ m. (TIF)

**S7 Fig. Studies on endocytic function in *Brucella*-infected cells and NAD levels of wild-type and *btp* mutant bacteria.** (A) HeLa cells or (B) iBMDM infected with either wild-type or a mutant strain lacking *btpA*, *btpB* or both genes were incubated with EGF conjugated with Alexa Fluor 555 for 10 minutes and the percentage of infected cells showing uptake of this fluorescent marker quantified by microscopy at 24h post-infection. Counts correspond to individual microscopy fields, obtained from three independent experiments. Mock infected cells are included as a control (negative). Data correspond to means  $\pm$  standard deviation and statistical comparison was done with one-way ANOVA test, with no statistical significance observed. (C) Control total NAD levels from the inocula, corresponding to bacterial cultures of wild-type *B. abortus*, or strains lacking *btpA*, *btpB* or both *btpAbtpB*. Data correspond to means  $\pm$  standard deviation from three independent experiments and statistical comparison was done with Kruskal-Wallis test, with no statistical significance observed. (D) RAW macrophages were infected with wild-type *B. abortus* carrying N-terminal TEM-1 fused BtpA E217A or BtpB E234A catalytic mutants for 24 h. Data represents the means  $\pm$  standard errors of the percentage of cells with coumarin fluorescence from 5 independent experiments, in which at least 100 cells were analyzed per experiment and condition. (TIF)

**S1 Table. Plasmids generated and used in this work.**  
(DOCX)

**S2 Table. Oligonucleotides used in this work.**  
(DOCX)

**S3 Table. Yeast genes that suppress BtpB-induced toxicity when overexpressed.**  
(DOCX)

**S4 Table. BtpB loss-of-function mutants found by random mutagenesis screening on yeast.**  
(DOCX)

## Acknowledgments

We wish to acknowledge the Genomics and Mass Spectrometry Units at Universidad Complutense de Madrid (UCM) for sequencing and NAD<sup>+</sup> analyses, respectively. We would like to thank Thomas Henry (CIRI, Lyon) for providing us with iBMDM and Diego Comerici (CONICET, Argentina) for helping us with the complementation constructs. We also thank Lucia Sastre for technical assistance in molecular cloning and yeast growth assays and members of U3 Research Lab for help and discussion.

## Author Contributions

**Conceptualization:** Julia Mar'ia Coronas-Serna, Arthur Louche, Mar'ia Molina, Jean-Pierre Gorvel, V'ictor J. Cid, Suzana P. Salcedo.

**Formal analysis:** Julia Mar'ia Coronas-Serna, Arthur Louche, Mar'ia Rodr'iguez-Escudero, Morgane Roussin, Laurent Terradot, Mar'ia Molina, Jean-Pierre Gorvel, V'ictor J. Cid, Suzana P. Salcedo.

**Funding acquisition:** Mar'ia Molina, V'ictor J. Cid, Suzana P. Salcedo.

**Investigation:** Julia Mar'ia Coronas-Serna, Arthur Louche, Mar'ia Rodr'iguez-Escudero, Morgane Roussin, Paul R. C. Imbert, Isabel Rodr'iguez-Escudero, Suzana P. Salcedo.

**Supervision:** Mar'ia Molina, V'ictor J. Cid, Suzana P. Salcedo.

**Writing – original draft:** Julia Mar'ia Coronas-Serna, Arthur Louche, Mar'ia Molina, V'ictor J. Cid, Suzana P. Salcedo.

**Writing – review & editing:** Julia Mar'ia Coronas-Serna, Arthur Louche, Mar'ia Rodr'iguez-Escudero, Morgane Roussin, Paul R. C. Imbert, Isabel Rodr'iguez-Escudero, Laurent Terradot, Mar'ia Molina, Jean-Pierre Gorvel, V'ictor J. Cid, Suzana P. Salcedo.

## References

1. Kagan JC, Magupalli VG, Wu H. SMOCs: supramolecular organizing centres that control innate immunity. *Nat Rev Immunol.* 2014; 14(12):821–6. Epub 2014/11/02. <https://doi.org/10.1038/nri3757> PMID: 25359439
2. Ve T, Williams SJ, Kobe B. Structure and function of Toll/interleukin-1 receptor/resistance protein (TIR) domains. *Apoptosis.* 2015; 20(2):250–61. Epub 2014/12/03. <https://doi.org/10.1007/s10495-014-1064-2> PMID: 25451009.
3. Zhang Q, Zmasek CM, Cai X, Godzik A. TIR domain-containing adaptor SARM is a late addition to the ongoing microbe-host dialog. *Dev Comp Immunol.* 2011; 35(4):461–8. Epub 2010/11/30. <https://doi.org/10.1016/j.dci.2010.11.013> PMID: 21110998
4. Rosadini CV, Kagan JC. Microbial strategies for antagonizing Toll-like-receptor signal transduction. *Curr Opin Immunol.* 2015; 32:61–70. Epub 2015/01/24. <https://doi.org/10.1016/j.coi.2014.12.011> PMID: 25615700
5. Cirl C, Wieser A, Yadav M, Duerr S, Schubert S, Fischer H, et al. Subversion of Toll-like receptor signaling by a unique family of bacterial Toll/interleukin-1 receptor domain-containing proteins. *Nat Med.* 2008; 14(4):399–406. Epub 2008/03/11. <https://doi.org/10.1038/nm1734> PMID: 18327267.
6. Yadav M, Zhang J, Fischer H, Huang W, Lutay N, Cirl C, et al. Inhibition of TIR domain signaling by TcpC: MyD88-dependent and independent effects on Escherichia coli virulence. *PLoS Pathog.* 2010; 6(9):e1001120. Epub 2010/10/05. <https://doi.org/10.1371/journal.ppat.1001120> PMID: 20886104
7. Patot S, Imbert PR, Baude J, Martins Simoes P, Campergue JB, Louche A, et al. The TIR Homologue Lies near Resistance Genes in Staphylococcus aureus, Coupling Modulation of Virulence and Antimicrobial Susceptibility. *PLoS Pathog.* 2017; 13(1):e1006092. Epub 2017/01/07. <https://doi.org/10.1371/journal.ppat.1006092> PMID: 28060920
8. Imbert PR, Louche A, Luizet JB, Grandjean T, Bigot S, Wood TE, et al. A Pseudomonas aeruginosa TIR effector mediates immune evasion by targeting UBAP1 and TLR adaptors. *EMBO J.* 2017; 36(13):1869–87. Epub 2017/05/10. <https://doi.org/10.15252/emboj.201695343> PMID: 28483816
9. Waldhuber A, Puthia M, Wieser A, Cirl C, Durr S, Neumann-Pfeifer S, et al. Uropathogenic Escherichia coli strain CFT073 disrupts NLRP3 inflammasome activation. *J Clin Invest.* 2016; 126(7):2425–36. Epub 2016/05/24. <https://doi.org/10.1172/JCI81916> PMID: 27214553
10. Essuman K, Summers DW, Sasaki Y, Mao X, DiAntonio A, Milbrandt J. The SARM1 Toll/Interleukin-1 Receptor Domain Possesses Intrinsic NAD(+) Cleavage Activity that Promotes Pathological Axonal Degeneration. *Neuron.* 2017; 93(6):1334–43 e5. Epub 2017/03/24. <https://doi.org/10.1016/j.neuron.2017.02.022> PMID: 28334607
11. Horsefield S, Burdett H, Zhang X, Manik MK, Shi Y, Chen J, et al. NAD(+) cleavage activity by animal and plant TIR domains in cell death pathways. *Science.* 2019; 365(6455):793–9. Epub 2019/08/24 <https://doi.org/10.1126/science.aax1911> PMID: 31439792.
12. Essuman K, Summers DW, Sasaki Y, Mao X, Yim AKY, DiAntonio A, et al. TIR Domain Proteins Are an Ancient Family of NAD(+)-Consuming Enzymes. *Curr Biol.* 2018; 28(3):421–30 e4. Epub 2018/02/06. <https://doi.org/10.1016/j.cub.2017.12.024> PMID: 29395922



13. Salcedo SP, Marchesini MI, Lelouard H, Fugier E, Jolly G, Balor S, et al. Brucella control of dendritic cell maturation is dependent on the TIR-containing protein Btp1. *PLoS Pathog.* 2008; 4(2):e21. Epub 2008/02/13. <https://doi.org/10.1371/journal.ppat.0040021> PMID: 18266466
14. Salcedo SP, Marchesini MI, Degos C, Terwagne M, Von Bargen K, Lepidi H, et al. BtpB, a novel Brucella TIR-containing effector protein with immune modulatory functions. *Front Cell Infect Microbiol.* 2013; 3:28. Epub 2013/07/13. <https://doi.org/10.3389/fcimb.2013.00028> PMID: 23847770
15. Radhakrishnan GK, Yu Q, Harms JS, Splitter GA. Brucella TIR Domain-containing Protein Mimics Properties of the Toll-like Receptor Adaptor Protein TIRAP. *J Biol Chem.* 2009; 284(15):9892–8. Epub 2009/02/07. <https://doi.org/10.1074/jbc.M805458200> PMID: 19196716
16. Sengupta D, Koblansky A, Gaines J, Brown T, West AP, Zhang D, et al. Subversion of innate immune responses by Brucella through the targeted degradation of the TLR signaling adapter, MAL. *J Immunol.* 2010; 184(2):956–64. Epub 2009/12/19 <https://doi.org/10.4049/jimmunol.0902008> PMID: 20018612
17. Chaudhary A, Ganguly K, Cabantous S, Waldo GS, Micheva-Viteva SN, Nag K, et al. The Brucella TIR-like protein TcpB interacts with the death domain of MyD88. *Biochem Biophys Res Commun.* 2012; 417(1):299–304. Epub 2011/12/14. <https://doi.org/10.1016/j.bbrc.2011.11.104> PMID: 22155231
18. Radhakrishnan GK, Harms JS, Splitter GA. Modulation of microtubule dynamics by a TIR domain protein from the intracellular pathogen Brucella melitensis. *Biochem J.* 2011; 439(1):79–83. Epub 2011/06/23. <https://doi.org/10.1042/BJ20110577> PMID: 21692747
19. Felix C, Kaplan Turkoz B, Ranaldi S, Koelblen T, Terradot L, O'Callaghan D, et al. The Brucella TIR domain containing proteins BtpA and BtpB have a structural WxxxE motif important for protection against microtubule depolymerisation. *Cell Commun Signal.* 2014; 12:53. Epub 2014/10/12. <https://doi.org/10.1186/s12964-014-0053-y> PMID: 25304327
20. Smith JA, Khan M, Magnani DD, Harms JS, Durward M, Radhakrishnan GK, et al. Brucella induces an unfolded protein response via TcpB that supports intracellular replication in macrophages. *PLoS Pathog.* 2013; 9(12):e1003785. Epub 2013/12/18. <https://doi.org/10.1371/journal.ppat.1003785> PMID: 24339776
21. Vida TA, Emr SD. A new vital stain for visualizing vacuolar membrane dynamics and endocytosis in yeast. *J Cell Biol.* 1995; 128(5):779–92. Epub 1995/03/01. <https://doi.org/10.1083/jcb.128.5.779> PMID: 7533169
22. Harrison JC, Bardes ES, Ohya Y, Lew DJ. A role for the Pkc1p/Mpk1p kinase cascade in the morphogenesis checkpoint. *Nat Cell Biol.* 2001; 3(4):417–20. Epub 2001/04/03. <https://doi.org/10.1038/35070104> PMID: 11283616.
23. Rodríguez-Escudero I, Rotger R, Cid VJ, Molina M. Inhibition of Cdc42-dependent signalling in *Saccharomyces cerevisiae* by phosphatase-dead SigD/SopB from *Salmonella typhimurium*. *Microbiology.* 2006; 152(Pt 11):3437–52. Epub 2006/11/01. <https://doi.org/10.1099/mic.0.29186-0> PMID: 17074912.
24. Fernández-Pinar P, Aleman A, Sondek J, Dohlman HG, Molina M, Martin H. The *Salmonella Typhimurium* effector SteC inhibits Cdc42-mediated signaling through binding to the exchange factor Cdc24 in *Saccharomyces cerevisiae*. *Mol Biol Cell.* 2012; 23(22):4430–43. Epub 2012/09/28. <https://doi.org/10.1091/mbc.E12-03-0243> PMID: 23015760
25. Brewster JL, Gustin MC. Hog1: 20 years of discovery and impact. *Sci Signal.* 2014; 7(343):re7. Epub 2014/09/18. <https://doi.org/10.1126/scisignal.2005458> PMID: 25227612.
26. Rodríguez-Escudero I, Roelants FM, Thorner J, Nombela C, Molina M, Cid VJ. Reconstitution of the mammalian PI3K/PTEN/Akt pathway in yeast. *Biochem J.* 2005; 390(Pt 2):613–23. Epub 2005/05/26. <https://doi.org/10.1042/BJ20050574> PMID: 15913452
27. Rande-Gil F, Prieto JA, Sanz P. The expression of a specific 2-deoxyglucose-6P phosphatase prevents catabolite repression mediated by 2-deoxyglucose in yeast. *Curr Genet.* 1995; 28(2):101–7. Epub 1995/07/01. <https://doi.org/10.1007/bf00315774> PMID: 8590459.
28. Schroeder RY, Zhu A, Eubel H, Dahncke K, Witte CP. The ribokinases of *Arabidopsis thaliana* and *Saccharomyces cerevisiae* are required for ribose recycling from nucleotide catabolism, which in plants is not essential to survive prolonged dark stress. *New Phytol.* 2018; 217(1):233–44. Epub 2017/09/19. <https://doi.org/10.1111/nph.14782> PMID: 28921561.
29. Andres-Pons A, Rodríguez-Escudero I, Gil A, Blanco A, Vega A, Molina M, et al. In vivo functional analysis of the counterbalance of hyperactive phosphatidylinositol 3-kinase p110 catalytic oncoproteins by the tumor suppressor PTEN. *Cancer Res.* 2007; 67(20):9731–9. Epub 2007/10/19. <https://doi.org/10.1158/0008-5472.CAN-07-1278> PMID: 17942903.
30. Kaplan-Turkoz B, Koelblen T, Felix C, Candusso MP, O'Callaghan D, Vergunst AC, et al. Structure of the Toll/interleukin 1 receptor (TIR) domain of the immunosuppressive Brucella effector BtpA/Btp1/TcpB. *FEBS Lett.* 2013; 587(21):3412–6. Epub 2013/10/01. <https://doi.org/10.1016/j.febslet.2013.09.007> PMID: 24076024.

31. Yang Y, Sauve AA. NAD(+) metabolism: Bioenergetics, signaling and manipulation for therapy. *Biochim Biophys Acta*. 2016; 1864(12):1787–800. Epub 2016/10/21. <https://doi.org/10.1016/j.bbapap.2016.06.014> PMID: 27374990
32. Canto C, Menzies KJ, Auwerx J. NAD(+) Metabolism and the Control of Energy Homeostasis: A Balancing Act between Mitochondria and the Nucleus. *Cell Metab*. 2015; 22(1):31–53. Epub 2015/06/30. <https://doi.org/10.1016/j.cmet.2015.05.023> PMID: 26118927
33. Iqbal J, Zaidi M. TNF regulates cellular NAD+ metabolism in primary macrophages. *Biochem Biophys Res Commun*. 2006; 342(4):1312–8. Epub 2006/03/07. <https://doi.org/10.1016/j.bbrc.2006.02.109> PMID: 16516847.
34. Al-Shabany AJ, Moody AJ, Foey AD, Billington RA. Intracellular NAD+ levels are associated with LPS-induced TNF-alpha release in pro-inflammatory macrophages. *Biosci Rep*. 2016; 36(1):e00301. Epub 2016/01/15. <https://doi.org/10.1042/BSR20150247> PMID: 26764408
35. Gomes AP, Price NL, Ling AJ, Moslehi JJ, Montgomery MK, Rajman L, et al. Declining NAD(+) induces a pseudohypoxic state disrupting nuclear-mitochondrial communication during aging. *Cell*. 2013; 155(7):1624–38. Epub 2013/12/24. <https://doi.org/10.1016/j.cell.2013.11.037> PMID: 24360282
36. Kelly B, O'Neill LA. Metabolic reprogramming in macrophages and dendritic cells in innate immunity. *Cell Res*. 2015; 25(7):771–84. Epub 2015/06/06. <https://doi.org/10.1038/cr.2015.68> PMID: 26045163
37. Pajuelo D, Gonzalez-Juarbe N, Tak U, Sun J, Orihuela CJ, Niederweis M. NAD(+) Depletion Triggers Macrophage Necroptosis, a Cell Death Pathway Exploited by Mycobacterium tuberculosis. *Cell Rep*. 2018; 24(2):429–40. Epub 2018/07/12. <https://doi.org/10.1016/j.celrep.2018.06.042> PMID: 29996103
38. Fugier E, Salcedo SP, de Chastellier C, Pophillat M, Muller A, Arce-Gorvel V, et al. The glyceraldehyde-3-phosphate dehydrogenase and the small GTPase Rab 2 are crucial for Brucella replication. *PLoS Pathog*. 2009; 5(6):e1000487. Epub 2009/06/27. <https://doi.org/10.1371/journal.ppat.1000487> PMID: 19557163
39. Marchesini MI, Morrone Seijo SM, Guaimas FF, Comerici DJ. A T4SS Effector Targets Host Cell Alpha-Enolase Contributing to Brucella abortus Intracellular Lifestyle. *Front Cell Infect Microbiol*. 2016; 6:153. Epub 2016/12/03. <https://doi.org/10.3389/fcimb.2016.00153> PMID: 27900285
40. Czyz DM, Willett JW, Crosson S. Brucella abortus Induces a Warburg Shift in Host Metabolism That Is Linked to Enhanced Intracellular Survival of the Pathogen. *J Bacteriol*. 2017; 199(15). Epub 2017/06/01. <https://doi.org/10.1128/JB.00227-17> PMID: 28559292
41. Xavier MN, Winter MG, Spees AM, den Hartigh AB, Nguyen K, Roux CM, et al. PPARgamma-mediated increase in glucose availability sustains chronic Brucella abortus infection in alternatively activated macrophages. *Cell Host Microbe*. 2013; 14(2):159–70. Epub 2013/08/21. <https://doi.org/10.1016/j.chom.2013.07.009> PMID: 23954155
42. Alves-Silva J, Tavares IP, Guimaraes ES, Costa Franco MM, Figueiredo BC, Marques JT, et al. Modulation of Microtubule Dynamics Affects Brucella abortus Intracellular Survival, Pathogen-Containing Vacuole Maturation, and Pro-inflammatory Cytokine Production in Infected Macrophages. *Front Microbiol*. 2017; 8:2217. Epub 2017/12/01. <https://doi.org/10.3389/fmicb.2017.02217> PMID: 29184543
43. Bershadsky AD, Gelfand VI. ATP-dependent regulation of cytoplasmic microtubule disassembly. *Proc Natl Acad Sci U S A*. 1981; 78(6):3610–3. Epub 1981/06/01. <https://doi.org/10.1073/pnas.78.6.3610> PMID: 6943561
44. Yu Q, Dong L, Li Y, Liu G. SIRT1 and HIF1alpha signaling in metabolism and immune responses. *Cancer Lett*. 2018; 418:20–6. Epub 2018/01/07. <https://doi.org/10.1016/j.canlet.2017.12.035> PMID: 29306019.
45. Cheng CY, Gutierrez NM, Marzuki MB, Lu X, Foreman TW, Paleja B, et al. Host sirtuin 1 regulates mycobacterial immunopathogenesis and represents a therapeutic target against tuberculosis. *Sci Immunol*. 2017; 2(9). Epub 2017/07/15. <https://doi.org/10.1126/sciimmunol.aaj1789> PMID: 28707004
46. Tak U, Vlach J, Garza-Garcia A, William D, Danilchanka O, de Carvalho LPS, et al. The tuberculosis necrotizing toxin is an NAD(+) and NADP(+) glycohydrolase with distinct enzymatic properties. *J Biol Chem*. 2019; 294(9):3024–36. Epub 2018/12/30. <https://doi.org/10.1074/jbc.RA118.005832> PMID: 30593509
47. Ganesan R, Hos NJ, Gutierrez S, Fischer J, Stepek JM, Daglidu E, et al. Salmonella Typhimurium disrupts Sirt1/AMPK checkpoint control of mTOR to impair autophagy. *PLoS Pathog*. 2017; 13(2):e1006227. Epub 2017/02/14. <https://doi.org/10.1371/journal.ppat.1006227> PMID: 28192515
48. Sikorski RS, Hieter P. A system of shuttle vectors and yeast host strains designed for efficient manipulation of DNA in Saccharomyces cerevisiae. *Genetics*. 1989; 122(1):19–27. Epub 1989/05/01. PMID: 2659436
49. Thomas BJ, Rothstein R. Elevated recombination rates in transcriptionally active DNA. *Cell*. 1989; 56(4):619–30. Epub 1989/02/24. [https://doi.org/10.1016/0092-8674\(89\)90584-9](https://doi.org/10.1016/0092-8674(89)90584-9) PMID: 2645056.

50. Rodriguez-Escudero I, Andres-Pons A, Pulido R, Molina M, Cid VJ. Phosphatidylinositol 3-kinase-dependent activation of mammalian protein kinase B/Akt in *Saccharomyces cerevisiae*, an in vivo model for the functional study of Akt mutations. *J Biol Chem*. 2009; 284(20):13373–83. Epub 2009/03/25. <https://doi.org/10.1074/jbc.M807867200> PMID: 19307184
51. Cid VJ, Shulewitz MJ, McDonald KL, Thorner J. Dynamic localization of the Swe1 regulator Hsl7 during the *Saccharomyces cerevisiae* cell cycle. *Mol Biol Cell*. 2001; 12(6):1645–69. Epub 2001/06/16. <https://doi.org/10.1091/mbc.12.6.1645> PMID: 11408575
52. Martin H, Arroyo J, Sanchez M, Molina M, Nombela C. Activity of the yeast MAP kinase homologue Slit2 is critically required for cell integrity at 37 degrees C. *Mol Gen Genet*. 1993; 241(1–2):177–84. Epub 1993/10/01. <https://doi.org/10.1007/bf00280215> PMID: 8232202.
53. Sporty JL, Kabir MM, Turteltaub KW, Ognibene T, Lin SJ, Bench G. Single sample extraction protocol for the quantification of NAD and NADH redox states in *Saccharomyces cerevisiae*. *J Sep Sci*. 2008; 31(18):3202–11. Epub 2008/09/03. <https://doi.org/10.1002/jssc.200800238> PMID: 18763242
54. Blasi E, Mathieson BJ, Varesio L, Cleveland JL, Borchert PA, Rapp UR. Selective immortalization of murine macrophages from fresh bone marrow by a raf/myc recombinant murine retrovirus. *Nature*. 1985; 318(6047):667–70. <https://doi.org/10.1038/318667a0> PMID: 4079980.



## 2. *Brucella* effectors target SENP3, inducing subcellular mislocalisation of nucleolar proteins and induction of ribophagy

1. Two newly identified *B. abortus* effectors, NyxA and NyxB, accumulate in cytosolic and nuclear structures

Bacterial effectors often contain eukaryotic-like domains to enable efficient modulation of cellular pathways. Previous work highlighted a subgroup of *Brucella* candidate effectors containing a carboxyl-terminal CAAX tetrapeptide motif (C corresponds to cysteine, A to aliphatic amino acids and X to any amino acid) [277]. Several bacterial effectors rely on this kind of motif as a lipidation site to facilitate membrane attachment, such as SifA from *Salmonella enterica* [278] [279] and AnkB from *Legionella pneumophila* [277,280]. We have recently confirmed that one of these *Brucella* candidate effectors, BspL, is translocated into host cells during infection although no function has yet been assigned for its CAAX sequence [281]. Therefore, we set out to determine if other *B. abortus* encoded proteins with a potential CAAX box could be translocated into host cells during infection. We relied on the TEM1  $\beta$ -lactamase reporter, widely used to assess *Brucella* effectors' translocation, to test two CAAX-containing proteins encoded by the genes BAB1\_0296 (BAB\_RS17335) and BAB1\_0466 (BAB\_RS18145). The time-point of 4h was selected to enable a comparison between the wild-type and the  $\Delta virB9$  mutant strain, which lacks a functional type 4 secretion system (T4SS). These experiments were carried out in RAW macrophages, allowing infection of most cells with *B. abortus*. BAB1\_0296 was efficiently translocated into host cells in a manner significantly dependent on the T4SS, in contrast to BAB1\_0466 (Figure 20A and B). We should note that a small number of cells infected with the  $\Delta virB9$  expressing BAB1\_0296 were positive for CCF2 compared to BAB1\_0466 (Figure 20B). These first TEM experiments were carried out by a formal postdoc in the lab, Thais Lacerda, prior to my arrival.

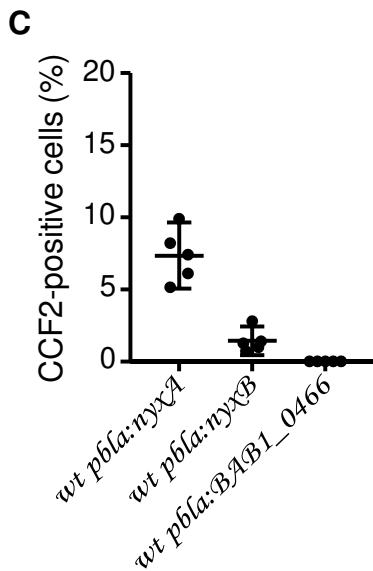
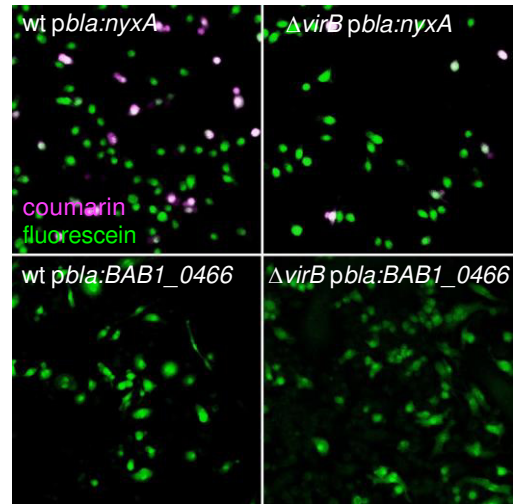
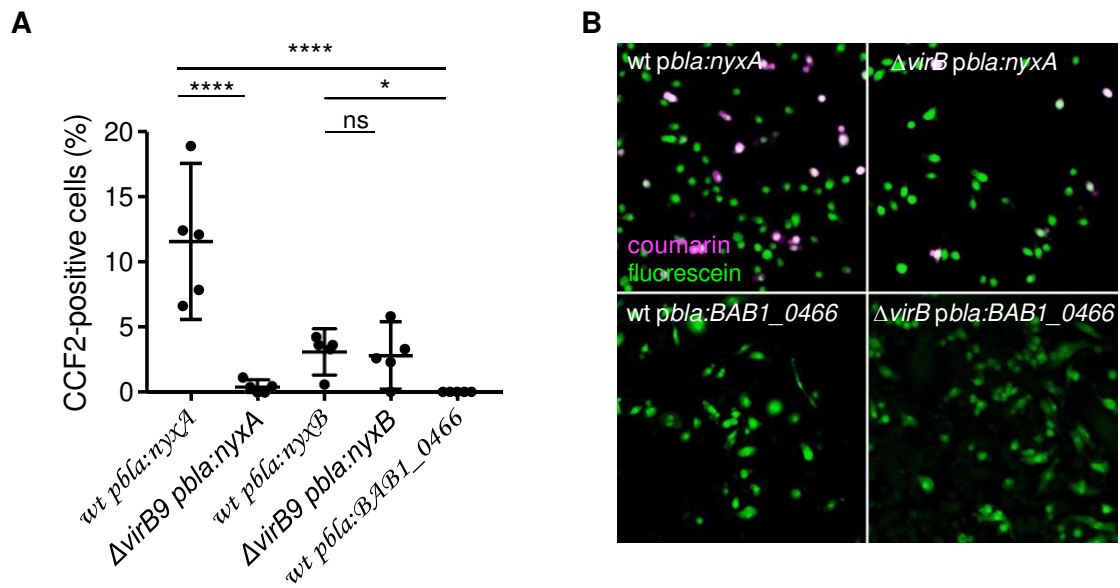


**Figure 20. The *Brucella* NyxA and NyxB proteins are translocated into host cells during infection. (A)** RAW macrophage-like cells were infected for 4h with either *B. abortus* wild-type or  $\Delta virB9$  expressing TEM1 (encoded by the *bla* gene) fused with NyxA, NyxB or BAB1\_0466. The percentage of cells with coumarin emission, which is indicative of translocation, was quantified after incubation with the CCF2-AM substrate. Data represent means  $\pm$  95% confidence intervals from 5 independent experiments, with more than a 500 cells counted for each condition. Kruskal-Wallis with Dunn's multiple comparisons test was used. Not all statistical comparisons are shown. **(B)** Representative images for *B. abortus* wild-type or  $\Delta virB9$  carrying *pbla:nyxA* or *pbla:nyxB* to exemplify the presence of effector translocation visible in coumarin-positive cells (violet) or absence of translocation. **(C)** NyxA and NyxB translocation at 24h post-infection, as in A.

At 24h post-infection, we could still not detect translocation of BAB1\_0466 with this reporter system (Figure 20C). Hence, we can conclude that BAB1\_0296 is likely to be a *B. abortus* effector, and we have named it as NyxA, inspired by Greek mythology. Nyx is the Greek personification of the night, daughter of Chaos, that seemed appropriate to us after remaining in the dark for so long regarding its function.

A *Brucella* genome analysis then identified another gene, BAB1\_1101 (BAB\_RS21200), encoding for a protein with 82% identity to NyxA, but without a potential CAAX motif (Figure 21). For consistency, we have named this second protein NyxB and that we found was also translocated by *B. abortus* into host cells, albeit to lower levels than NyxA at both 4 and 24h post-infection (Figure 20A and C). Curiously, the translocation of NyxB was independent of the T4SS (Figure 20A).

```

NyxA  1 MNAHTNISGSAA----FDPNAWHHSQMTIREAIDLSQLSGGHPYSSPNVPK 46
      ||...|.:.|.  |||...|...|.:.|:|:|...|...|
NyxB  1 MNTQATIDTAAVAPLNFDPNAWHHSQMTTLEAIELSRSGGHPYSSPNVPK 50

NyxA  47 GFNTVVGFFFDYDWYPAAYDDEEGNAMKDRELIQYEEWCAKYARKLGLE 96
      |||...|...|.:.|:|:|...|...|:|...|.:.|
NyxB  51 GFNTVVGFFFDYDWYPAAYDDEEGNAMKDRELIQYEDWCAKYARTLGLE 100

NyxA  97 VKEVEAPAALKVHGIMTLKAYPEALLEIRCLEL- 129
      |||...|...|.:.|:|:|...|...|:|.:.|
NyxB 101 VKEVEAPAALKVHGIMALKAYPEALLEIRLIEMP 134

```

**Figure 21.** Amino acid sequence alignment of NyxA and NyxB obtained with ClustalW, matrix EBLOSUM62, showing 82.1% identity, 86.6% similarity and 3.7% gaps.

To confirm that NyxA was indeed translocated across the vacuolar membrane during infection, we created new strains with NyxA fused on its N-terminus with either HA or 4HA epitope tags. We then infected HeLa cells, a well-characterized model of *B. abortus* infection nicely suited for microscopy studies. We could not detect any HA-NyxA at any of the time-points analysed. However, we could observe translocated 4HA-NyxA at 48h post-infection, accumulating in cytosolic structures in the vicinity of multiplying bacteria (Figure 22A). This was also the case for 4HA-NyxB (Figure 22A, bottom panel). Analysis of fluorescence intensity profiles along a defined straight line across the 4HA-positive structures confirmed the majority of the 4HA signal detected does not correspond to intra-vacuolar NyxA or NyxB. In a proportion of infected cells, 4HA-NyxA and NyxB positive structures could be detected in the nucleus (Figure 22B), suggesting these effectors may also be targeting the host nuclei.

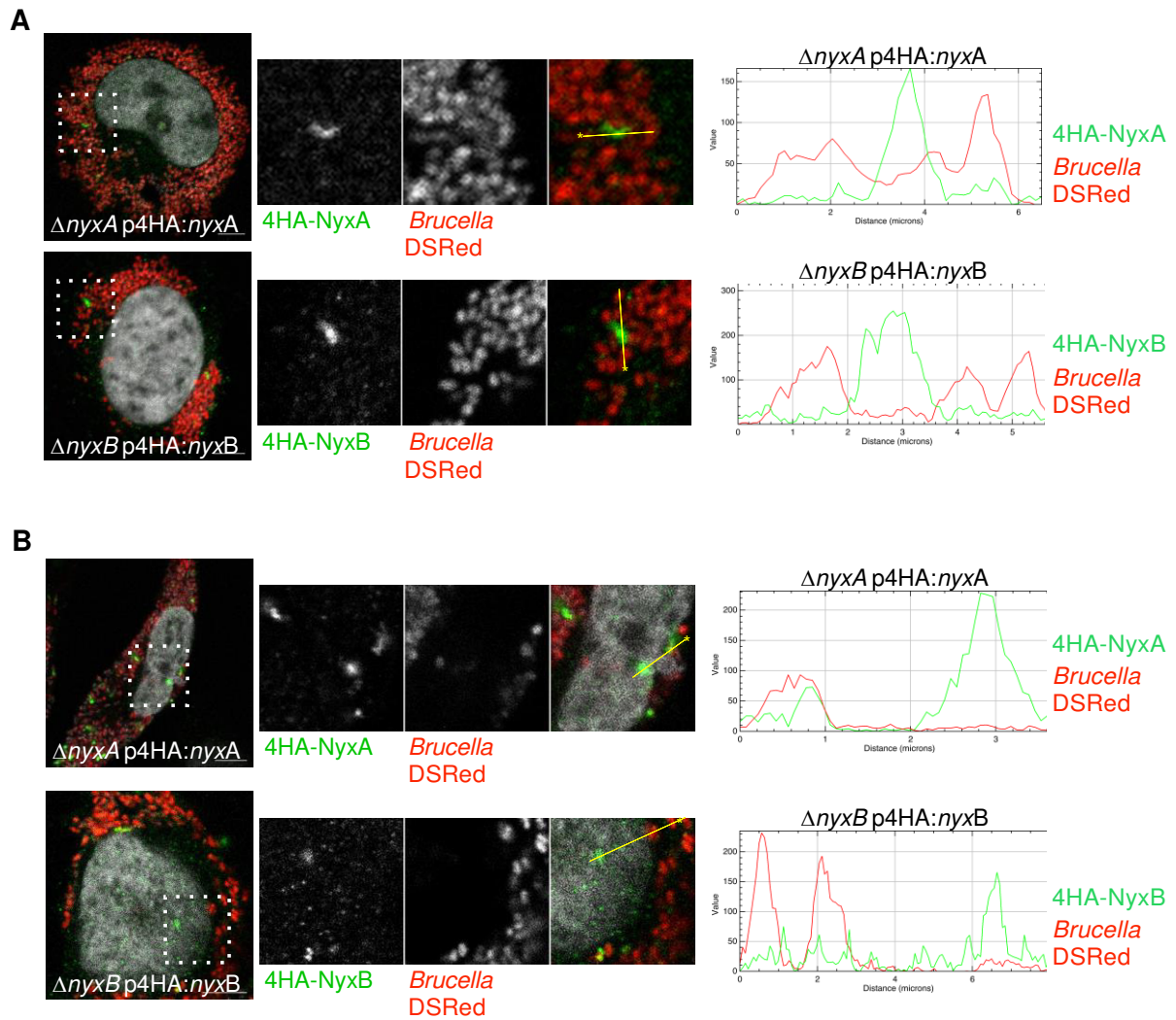


**Figure 22. NyxA and NyxB accumulate in cytosolic and nuclear structures. (A)** Accumulation of 4HA-tagged NyxA (top) or 4HA-tagged NyxB (bottom) in cytosolic punctate or filament-like structures or **(B)** in the nucleus, in HeLa cells infected for 48h with  $\Delta nyxA$  or  $\Delta nyxB$  strains expressing DSRed and the corresponding 4HA-tagged effector. The cell nucleus is visible with DAPI. A fluorescence intensity profile along a defined straight line across the 4HA-positive structures is included for each image, with the HA signal represented in green and bacterial signal in red.



For both effectors, punctate and filament-like structures were observed (Figure 23A). Equivalent NyxA structures were observed with an N-terminal 3Flag (Figure 23B), suggesting these are not an artefact due to the 4HA tag.

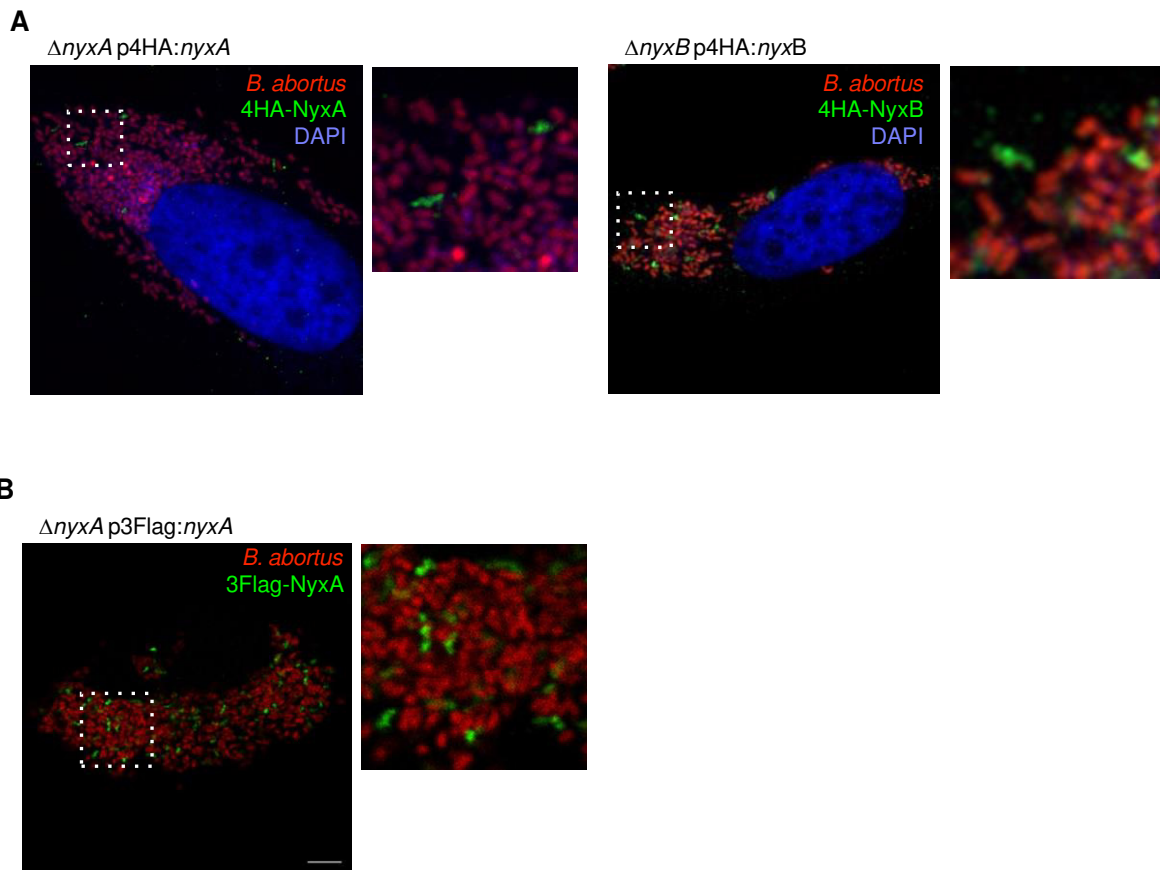


**Figure 23. Punctate and filament-like structures positive for NyxA and NyxB.** (A) Representative images to exemplify the filament-like structures visible with both 4HA-tagged NyxA (left) or NyxB (right). HeLa cells were infected for 48h with  $\Delta nyxA$  or  $\Delta nyxB$  strains expressing DSRed and carrying p4HA:nyxA or p4HA:nyxB. The cell nucleus is visible with DAPI (blue). (B) Representative confocal microscopy images showing accumulation of 3Flag-NyxA (green) punctate structures in HeLa cells infected for 48h with  $\Delta nyxA$  expressing DSRed and 3Flag-NyxA.

## 2. NyxA and NyxB interact with each other and target the same cellular compartments

Imaging of translocated NyxA and NyxB suggested that these effectors may have an identical subcellular localisation. To investigate this possibility, we ectopically expressed NyxA and NyxB with different tags. We found that HA-tagged NyxA and NyxB predominantly accumulated in

nuclear aggregates (Figure 24A, top panels and Figure 24B), with a few cytosolic vesicular structures visible in most cells. Interestingly, 4HA-tagged NyxA and NyxB were mostly found in the cytosol in structures resembling what we observed during infection (Figure 24A, bottom panels and Figure 24B). This suggests that the presence of the 4HA strongly reduces the nuclear import of NyxA and NyxB, revealing its initial cytosolic location. The co-transfection of HA-NyxA and myc-NyxB showed substantial co-localization levels, suggesting that these two proteins target the same cellular compartments (Figure 24C). As NyxB does not have a CAAX motif, but retains the same localization as NyxA, we can conclude that the potential CAAX motif of NyxA does not contribute to its intracellular localization.

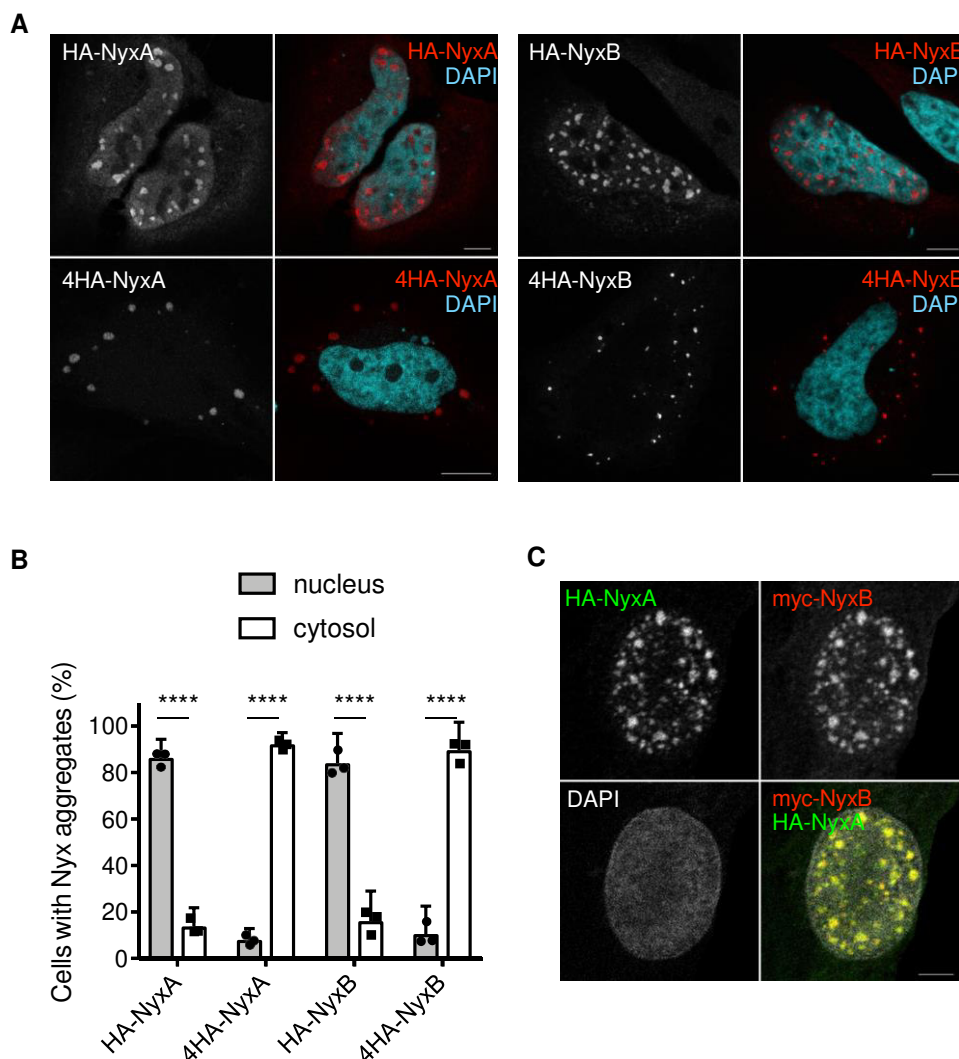


**Figure 24. Ectopically expressed NyxA and NyxB localize in cytosolic or nuclear structures. (A)** Representative confocal microscopy images of HA- or 4HA-tagged NyxA and NyxB (red) ectopically expressed in HeLa cells. The nucleus of the cells is labelled with DAPI. Scale bars are 5  $\mu$ m. **(B)** Quantification of the percentage of cells with majority of tagged effector accumulating in cytosolic or

nuclear structures. Data correspond to means  $\pm$  95% confidence intervals from 3 independent experiments, in which at least X cells were counter per condition. **(C)** Confocal imaging showing co-localization of HA-NyxA (green) and myc-NyxB (red) aggregates in the nucleus (white).

To determine if these two effectors could interact, we purified them both and carried out pull-down experiments *in vitro*. We found that His-NyxA could pull-down purified NyxB (Figure 25A). Furthermore, microscale thermophoresis confirmed this interaction and determined a Kd of  $482 \pm 126$  nM (Figure 25B). Similar results were obtained using His-NyxB against NyxA (Figure 26A and B). Together, these results show NyxA and NyxB interact and can accumulate in cytosolic structures as well as the nucleus, suggesting they are likely cycling between these two cellular compartments.

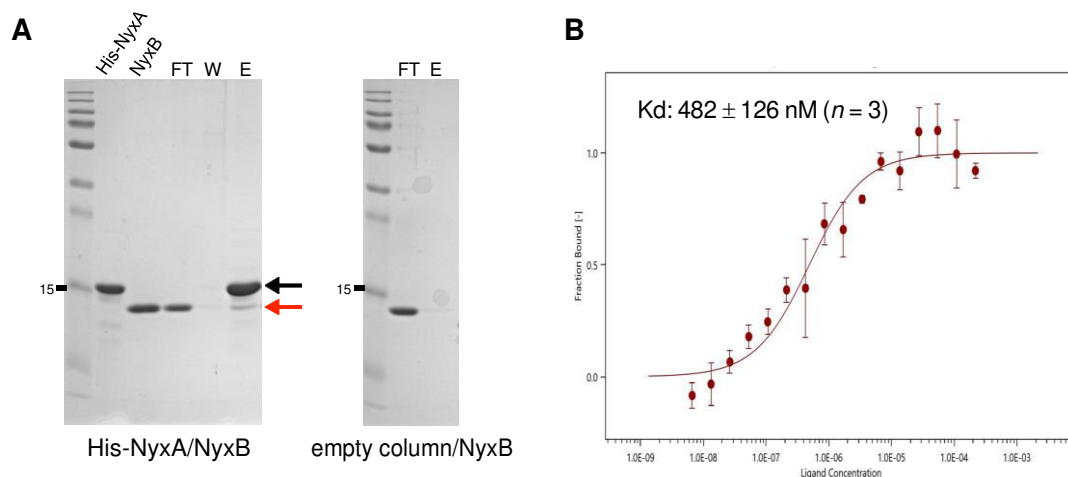
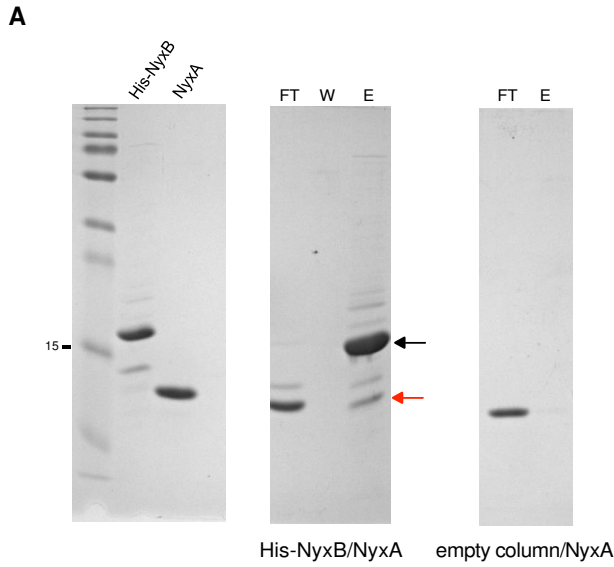


**Figure 25. NyxA and NyxB directly interact. (A)** Pull-down experiment using purified NyxB against His-NyxA immobilized on a Ni NTA resin. An empty column was used as a control for non-specific binding. Interactions were visualized with coomassie blue stained gels. The flowthrough (FT), wash (W) and elution (E) fractions are shown for each sample and the molecular weights indicated (kDa). Eluted His-NyxA and NyxB are indicated with black and red arrows, respectively. **(B)** Microscale thermophoresis measuring the fraction of 20 nM of purified NyxA labelled with kit protein labelling RED-NHS binding to increasing concentrations of NyxB (6,67nM-219 $\mu$ M). Data correspond to means  $\pm$  standard deviations of 3 independent experiment. The obtained Kd is indicated.



**B**

Samples 18_0106-0107 - Gel from 16/c 2/2018												
Ref. PSF	Ref. Labo	LCMSMS Analysis (Q Exactive HF)					Database			Enzyme	Results File PD 2.1	
18_0107	NyxA	180302-0107-01.raw					uniprot-brucella-abortion_1803 + séquences HisBnpB et BnpA			Chymotrypsin	180302-0106-01.pdResult	
Checked	Master	Accession	Description	Sum PEP Score	Coverage	# Peptides	# PSMs	nique PeptideProtein Groups	MW [kDa]	Score Sequest HT	# Peptides Sequest HT	
TRUE	Master Protel NyxA	ALOUCHE_1802		86,6	79,3	14	99	7	1	15,2	14	
TRUE	Master Protel HisNyxB	ALOUCHE_1802		26,2	38,9	9	60	2	1	18,8	9	

NyxA coverage:											
GIDPF	TMNAH	TNISGSAAFD	PNAWHHSQMT	IREAIDLSQS	GGHPYSSPNV	PRGENTVVG	FFDCYD	WVPA	AYD	DDEGNAM	
KDREL	IQYEE	WCAKY	ARKLG	LEVKEVEAPA	ALKVRGIMTL	KAYPEAL	LEI	RCLEL			

HisNyxB coverage:											
MHHHHH	HGKP	IPNLL	LGLDS	TENLYF	QGID	PFTMNT	QATI	DTAAV	APLNF	DPNAWHHSQ	M
VPRGF	NTVVG	R	FFDTYD	WYP	AAV	DDEGNA	MKDRE	IQYE	DWCAKY	ARTL	GLEVKEVEAP
RLIEM											AALKVRGIMA
											LKAYPEALLE

**Figure 26. NyxA and NyxB directly interact. (A)** Pull-down experiment using purified NyxA against His-NyxB immobilized on a Ni NTA resin. Empty column was used as a control for non-specific binding. Interactions were visualized with coomassie blue stained gels. The flowthrough (FT), wash (W) and elution (E) fractions are shown for each sample and the molecular weights indicated (kDa). Eluted NyxA and His-NyxB are indicated with black and red arrows, respectively. **(B)** Confirmation of the identity of the two major eluted bands by mass spectrometry. The identified peptides are highlighted in green.

3. NyxA and NyxB enriched nuclear structures are in close association with PML-nuclear bodies

To determine the nature of these nuclear aggregates formed upon ectopic expression of NyxA and NyxB we labelled cells with antibodies recognizing different nuclear bodies (Figure 27A and B). We found the highest level of colocalization (measured by the Pearson Coefficient Correlation PCC) between NyxA and NyxB. Both effectors also extensively co-localize with

PMLs unlike nuclear speckles, suggesting closer association with PML-nuclear bodies. As many proteins that accumulate or transit through these nuclear compartments often interact directly with the PML itself, we next carried out a pull-down experiment with either purified His-NyxA or NyxB and incubated with a cellular extract (Figure 27C). No interaction with PML was detected suggesting these *Brucella* effectors do not interact with PML in the conditions tested.

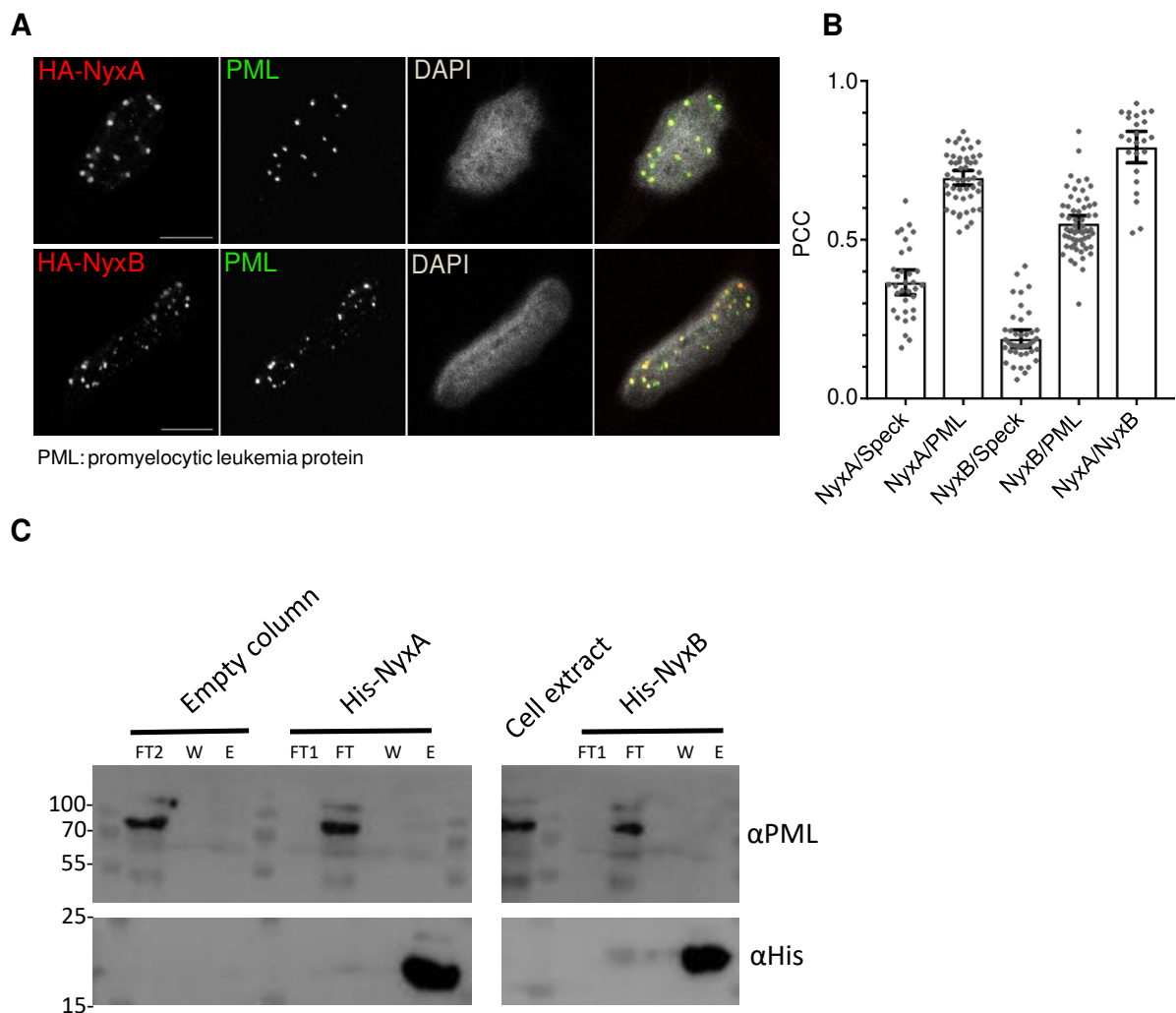


**Figure 27. Nuclear Nyx-positive structures are closely associated with PML-nuclear bodies.** (A) HeLa cells were transfected for 12h with either HA-NyxA or NyxB (red) and labelled with an anti-PML antibody (green). (B) The level of co-localization measured with the Pearson's coefficient (PCC) between each effector and either PML or speckles. Co-transfection of the two effectors was used as a positive control. (C) Pull-down assay with His-NyxA or His-NyxB immobilized on Ni NTA resins that were incubated with a HeLa cell extract. Empty column was used as a control for non-specific binding.

Interactions with endogenous PML were visualized by western blotting (upper blot), and column binding with anti-His (lower blot). Non-bound fractions (F1 and F2), last wash (W) and elution (E) are shown for each sample and the molecular weights indicated (kDa). The cell extract is also shown.

#### 4. NyxA and NyxB do not interact with SUMO *in vitro*

As all proteins that associate with PML-nuclear bodies are SUMOylated we wondered if this was the case for NyxA and NyxB. We therefore investigated if NyxA and NyxB could be covalently conjugated by SUMO *in vitro*. These experiments were done by Mariam Taktek, a Canadian student that I supervised. We purified both NyxA and NyxB, as well as SUMO2 and UBC9, the SUMO ligase and carried out an *in vitro* SUMOylation assay. As a positive control GST-RanGAP1 was used. A single band was detected in the absence of ATP, indicated with a red asterisk at 46.5 KDa, whereas in the presence of ATP a second band was visible (red square) corresponding to the SUMOylated protein (Figure 28). In contrast, no SUMOylated NyxA nor NyxB were detected, which would have an approximative molecular weight of 25 KDa (Figure 28). Only the non-SUMOylated forms are observed in the presence of ATP (blue asterisk).

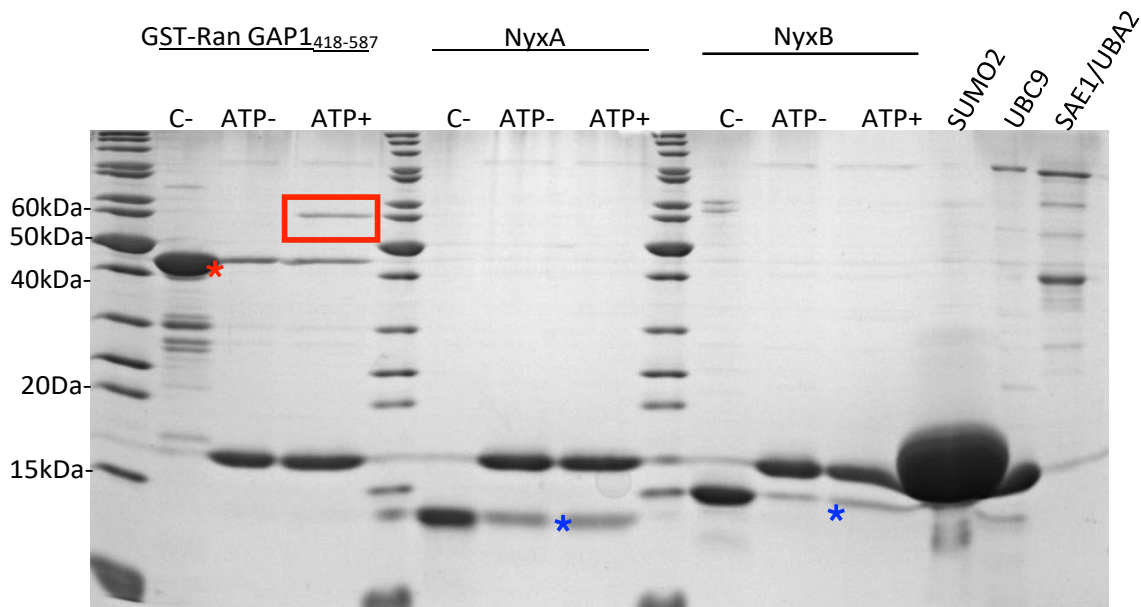


**Figure 28. NyxA and NyxB are not SUMOylated *in vitro*.** Purified GST-Ran GAP1, NyxA or NyxB were incubated with SUMO2, Ubc9 and SAE1/UBA2 in the presence or absence of ATP. GST-RanGAP<sub>418-587</sub> It is used as a positive control, in the presence of ATP a band appears in the red frame corresponding

to the sumoylated form of RanGAP1. In the case of NyxA, middle wells and NyxB, wells on the right side of the figure we do not observe a sumoylated form.

5. The Nyx effectors interact with SENP3, which is necessary for efficient *B. abortus* intracellular multiplication

To identify potential host-interacting partners of the *Brucella* Nyx effectors, our collaborator Jean-Paul Borg (CRCM, Marseille) performed a yeast two-hybrid screen. One of the main proteins identified was SENP3, and taking into account the nuclear localization of the Nyx effectors, we focused on this potential target. However, we cannot exclude that the other candidates identified are not relevant (Table 4).

**Table 4. Eukaryotic proteins interacting with NyxA identified with the yeast two-hybrid (Y2H) screen.**

Baits from Y2H for NyxA interaction partner	Number of hits
Homo sapiens SUMO1/sentrin/SMT3 specific peptidase 3 (SENP3)	5
Homo sapiens complement component 1, r subcomponent (C1R)	8
Homo sapiens canopy 4 homolog (zebrafish) (CNPY4)	2
TAF6 TAF6 RNA polymerase II, TATA box binding protein (TBP)-associated factor	1
CEBPZ CCAAT/enhancer binding protein (C/EBP), zeta [ Homo sapiens ]	3
ARL6IP4 ADP-ribosylation-like factor 6 interacting protein 4	3
Glutathione S-transferase kappa 1	1
Homo sapiens chromosome 11 genomic scaffold, alternate assembly HuRef SCAF_1103279188392	1
Homo sapiens chromosome 11 genomic scaffold, alternate assembly CHM1_1.0	
Homo sapiens chromosome 11 genomic contig, GRCh37.p10 Primary Assembly	
Heparan sulfate proteoglycan 2 (HSPG2)	1
Homo sapiens RNA binding motif, single stranded interacting protein 3 (RBMS3)	1
Homo sapiens alkaline phosphatase, intestinal (ALPI), mRNA	1
Homo sapiens alkaline phosphatase, placental-like 2 (ALPPL2), mRNA	
Homo sapiens alkaline phosphatase, placental (ALPP), mRNA	

SENP3 belongs to a family of cysteine proteases that share a conserved catalytic domain, characterized by a papain-like fold [231]. The variable N-terminal region often contributes to intracellular targeting of the protease. In the case of SENP3, the N-terminal region is implicated in nucleolar targeting, encoding a nucleolar localization sequence (NoLS) and



phosphorylation site for mTOR, necessary for subsequent interaction with NPM1 and nucleolar targeting [268] (Figure 29A).

To confirm the interaction between SENP3 and the Nyx effectors, we attempted to purify the whole SENP3. We were not successful and instead focused on the purification of the N-terminal region of SENP3 that comprised all the yeast two-hybrid hits (SENP3<sub>7-159</sub>). His-V5-tagged NyxA or NyxB were able to pull-down SENP3<sub>7-159</sub>, confirming a direct interaction of these effectors with the N-terminus domain of SENP3 (Figure 29B). No unspecific binding to the column was detected (right panel, Figure 29B). We cannot exclude the involvement of other regions of SENP3, but our data show SENP3<sub>7-159</sub> is sufficient for this interaction.

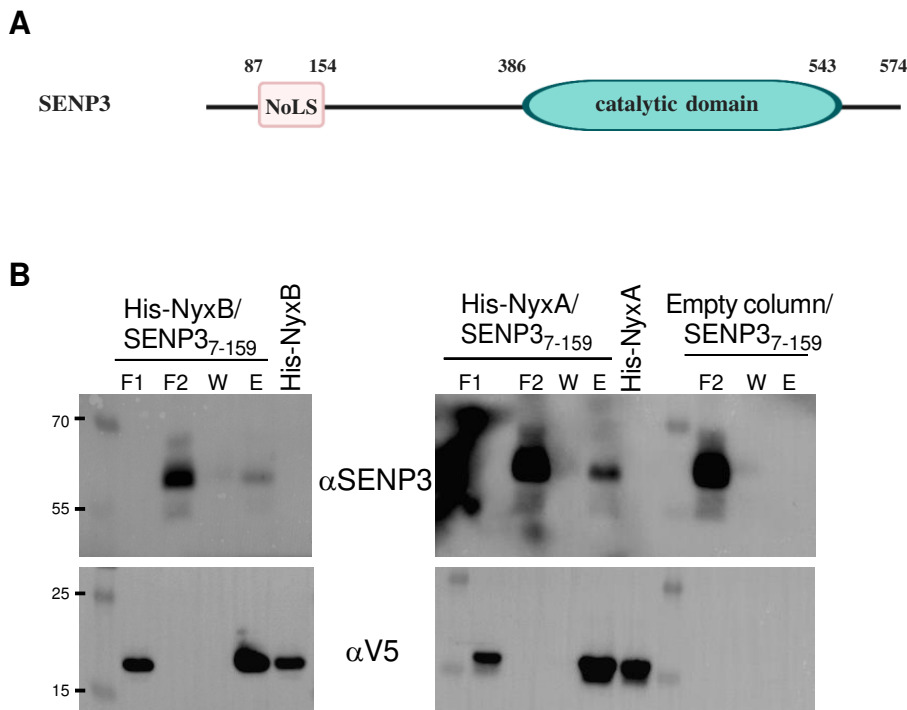


**Figure 29. The Nyx effectors interact with host protease SENP3. (A)** Schematic representation of SENP3, highlighting its catalytic domain and its N-terminal nucleolar localization sequences (NoLS). **(B)** Pull-down assay with the N-terminal region of SENP3 from amino acid 7 until 159 (SENP3<sub>7-159</sub>) against His-V5-NyxA or His-V5-NyxB immobilized on Ni NTA resins. An empty column was used as a control for non-specific binding and purified His-NyxA and His-Nyx-B inputs are shown. Interactions were visualized by western blotting using anti-SENP3 antibody, and column binding with anti-V5 (lower blot). Non-bound fractions (F1 and F2), last wash (W) and elution (E) are shown for each sample and the molecular weights indicated (kDa).



As SENP3 seems to be the host target of NyxA and NyxB, we next sought to determine its relevance during infection. Amandine Blanco in the lab carried out these experiments. The depletion of SENP3 was efficiently achieved only after 72h treatment with siRNA (Figure 30A and B), after which cells were infected with wild-type *B. abortus*. We observed a decrease in CFU counts at 48h post-infection following the depletion of SENP3 (Figure 30C). These results were confirmed by microscopy counts, which showed a reduction in the percentage of cells with more than ten bacteria at 48h post-infection when SENP3 was depleted (Figure 30D) but not at earlier stages (not shown). Therefore, in the late stages of the infection, SENP3 was required for *B. abortus* to multiply efficiently inside cells.

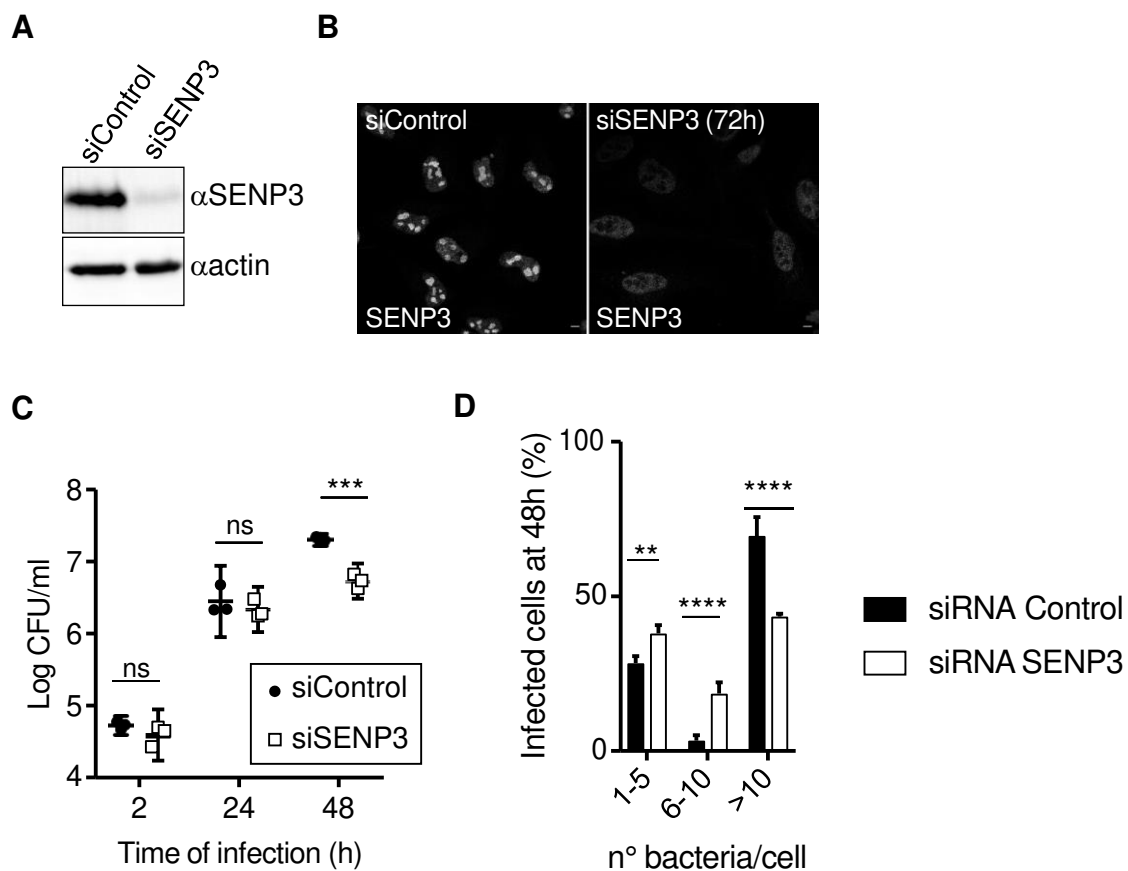


**Figure 30. SENP3 is important for efficient *B. abortus* intracellular multiplication. (A)** Western blot of HeLa cell lysate treated with siRNA control (siControl) or siRNA SENP3 (siSENP3) for 72h. Membrane was probed with an anti-SENP3 antibody followed by anti-actin for loading control. **(B)** Depletion was also verified by microscopy, showing a predominant nucleolar localization of SENP3 in control cells which is strongly reduced in siSENP3 treated cells. Scale bar is 5  $\mu$ m. **(C)** Bacterial colony forming units (CFU) counts of wild-type *B. abortus* following 2, 24 or 48h of infection of HeLa cells pre-treated with either siControl or siSENP3 for 72h. Data correspond to means  $\pm$  95% confidence intervals from 3 independent experiments. A two-way ANOVA with Bonferroni correction was used to compare siControl and siSENP3 at each time-point. **(D)** HeLa cells depleted for SENP3 or treated with the control

siRNA for 72h were infected with wild-type *B. abortus* expressing DSRed and the percentage of cells with either 1 to 5, 6 to 10 or more than 10 bacteria per cell was quantified by microscopy at 48h post-infection. Data correspond to means  $\pm$  95% confidence intervals from 3 independent experiments, with more than 500 cells being counted for each siRNA treatment. A two-way ANOVA with Bonferroni correction was used to compare the bacterial counts obtained in siControl treated cells with siSENP3 depleted cells, for each subgroup (1-5, 6-10 or >10 bacteria/cell).

## 6. The NyxB structure defines a novel family of effectors

To gain further insight into the function of NyxA and NyxB and their interaction with SENP3, Laurent Terradot and Virginie Gueguen-Chaignon (PSF) solved the crystal structure of NyxB at 2.5Å (Figure 31). The asymmetric unit of the crystal contains twelve monomers of NyxB but no significant differences were found between them and thus only the structure of subunit A is described hereafter.

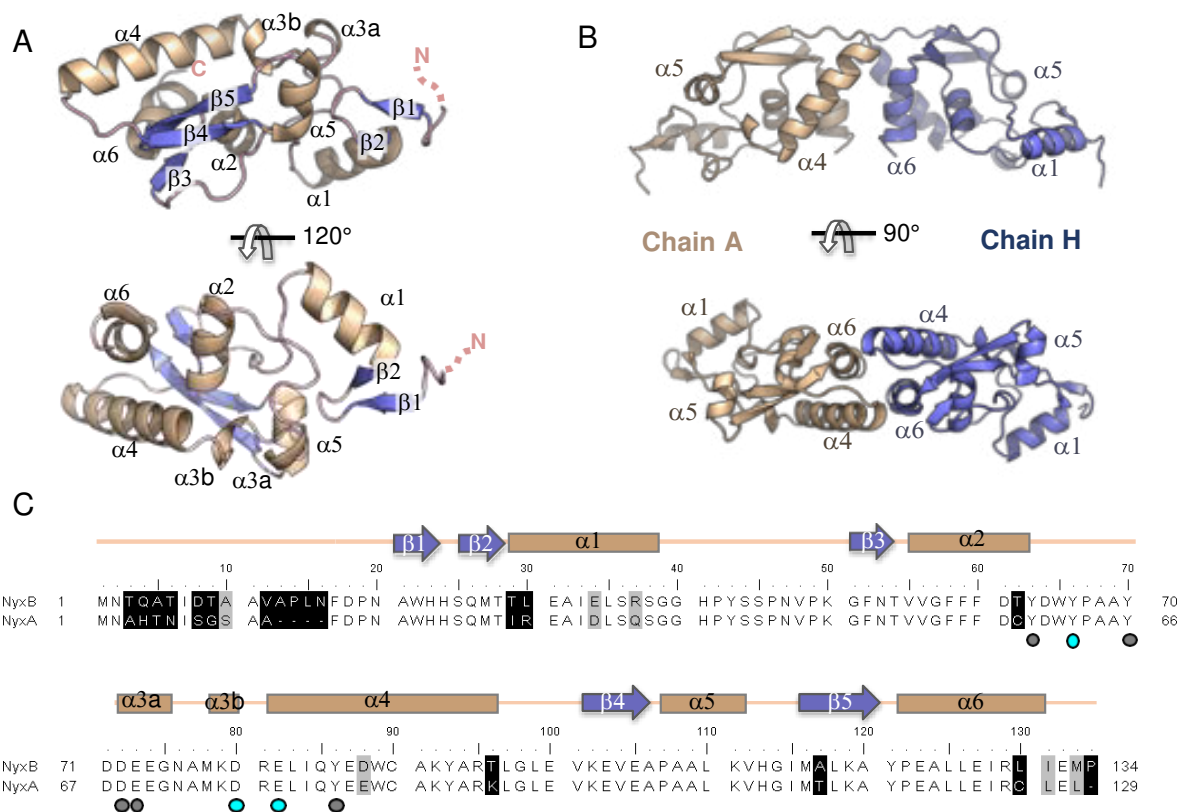


**Figure 31. The NyxB structure defines a novel family of effectors and allowed identification of the SENP3 interacting groove. (A)** Two views of the NyxB monomer depicted in ribbon with helices coloured in wheat, strands in blue and loops in pink. **(B)** Two views of the NyxB dimer. **(C)** Structure-based sequence alignment of NyxB and NyxA. Secondary structure elements are indicated above the sequences. Identical residues are not shaded, residues shaded in black and grey are non-conserved

and conserved, respectively. Dots indicate residues identified in the acidic patch and cyan dots indicate acidic groove mutants (MAG).

The NyxB model encompasses residues 17 to C-terminal residue 134. Lack of density for residues 1 to 16 suggest that this part is flexible. NyxB has a mixed  $\alpha$ - $\beta$  fold with five  $\beta$  strands and six  $\alpha$ -helices with a core made of helices  $\alpha$ 2 to  $\alpha$ 4 and a small curved  $\beta$ -sheet formed by  $\beta$ 3,  $\beta$ 4 and  $\beta$ 5. The longest helix  $\alpha$ 4 interacts with  $\alpha$ 2 and  $\alpha$ 6 and is connected to the core via a loop containing two short  $3_{10}$  helices designated  $\alpha$ 3a and  $\alpha$ 3b (Figure 31A). Helix  $\alpha$ 1 is loosely associated with the rest of the protein core and is positioned by the preceding and following loops. In particular, a  $\beta$ -hairpin formed by  $\beta$ 1 and  $\beta$ 2 packs against  $\alpha$ 5 and anchors  $\alpha$ 1 to the protein core. Search for structural homologues did not reveal any significant homology and thus make of NyxB structure a prototype for this protein family.

Size exclusion chromatography coupled to multi-angle light scattering (MALS) experiments indicate that both NyxA and NyxB form dimers (Figure 32). Two putative dimers (dimer 1 and dimer 2) were identified in the asymmetric unit (Figure 32). The association of dimer 1 (chain A and H) buries a total of 530  $\text{\AA}^2$  (Figure 32B) while dimer 2 (chain A and J) relies on fewer interactions burying a total 400  $\text{\AA}^2$  (Figure 32B). To determine which dimer(s) existed in solution we used size exclusion coupled to small angle X-ray scattering (SEC-SAXS) done by Célia Bergé in Laurent Terradot's lab on NyxB and NyxA proteins. Data indicates that the Rg of NyxB and NyxA are 2.9 and 2.7 nm, with  $D_{\text{max}}$  values of 10.2 nm and 9.6 nm, respectively. These data are in agreement with a dimeric form of the proteins given that theoretical Rgs for dimer 1 and 2 are 2.4 nm and 2 nm, respectively while Rg of a monomer of NyxB is 1.4 nm. The higher Rg observed in solution might be due to the disordered region present at the N-terminal portion of each NyxB monomer (residues 1-16) and NyxA (residues 1-12). Comparison of NyxB experimental SAXS data with theoretical curves obtained with NyxB dimer 1 or dimer 2 indicates that the best fit is obtained with dimer 1 ( $\chi^2= 1.3$ ) compared to dimer 2 ( $\chi^2= 3.3$ ) (Figure 32C and D). Ab initio modelling using SAXS data confirmed that the envelope obtained fits better the NyxB dimer1. Similar results were obtained using NyxA (Figure 32C). Collectively, X-ray, MALS and SEC SAXS data clearly establish that dimer 1 (Figure 31A) is the conformation of NyxB and NyxA in solution. This NyxB dimer relies on reciprocal

hydrophobic and electrostatic interactions between  $\alpha 4$  of one subunit and  $\alpha 6$  of the other subunit and between the two  $\alpha 4$ - $\beta 4$  loops, burying a total of  $530 \text{ \AA}^2$ .

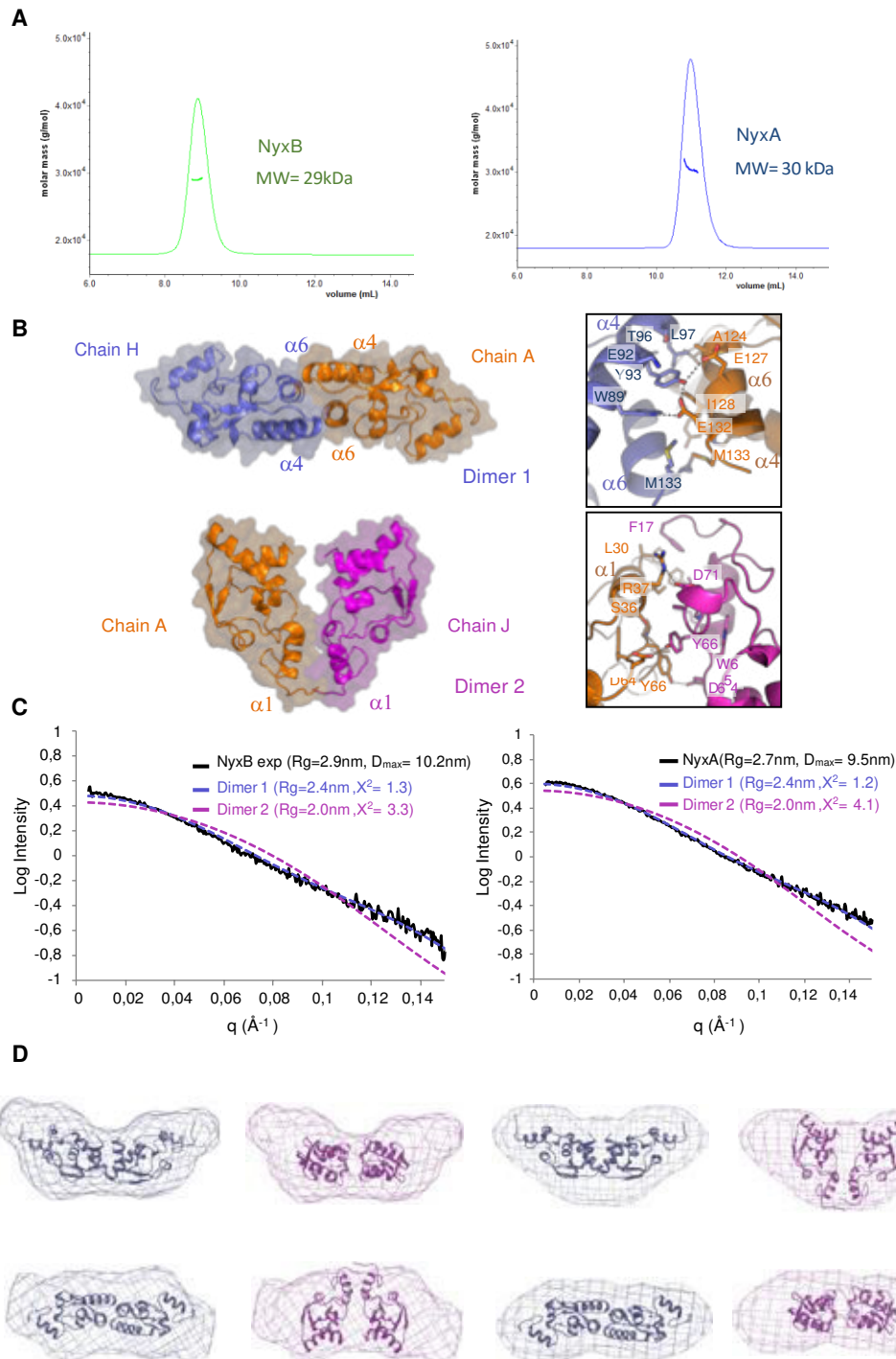


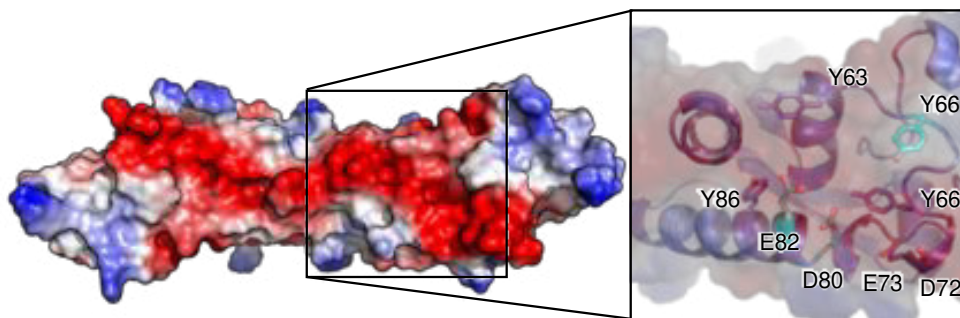
**Figure 32. NyxA and NyxB dimer formation.** (A) Chromatograms ( $A_{280}$ , plain) and mass measurements (dots) by Multi Angle Light Scattering of NyxB (left, green) and NyxA (right, blue). The average molecular weight determined is indicated. (B) Surface representation of dimer A (chains A and H) and

dimer 2 (chains A and J) with detailed view of each interface side chains involved represented as ball-and-sticks. **(C)** Comparison of the theoretical small-angle X-ray scattering profiles of NyxB dimers with experimental data (black curves) obtained for NyxB (left) and NyxA (right). Fitting values ( $c_2$ ) obtained using FoXS server are indicated. **(D)** Fitting of NyxB dimers into ab initio SAXS envelopes obtained with GASBOR using NyxB data (left) and NyxA (right) showing that dimer 1 fits much better each of the experimental curves.

## 7. Identification of the Nyx-SENP3 interacting groove

Taking advantage of the structural information of NyxB, we looked for potential interacting sites. Analysis of the NyxB surface revealed an acidic pocket delineated by residues Y66, D80 and E82 within an acidic patch consisting of amino acids D72, E73, Y70, Y86 and Y63, residues that are strictly conserved in NyxA (Figure 33A). In the context of the dimer, these surfaces are juxtaposed to form an extended concave negatively charged area of around 2000 Å<sup>2</sup> (Figure 33A).

**A**



**B**

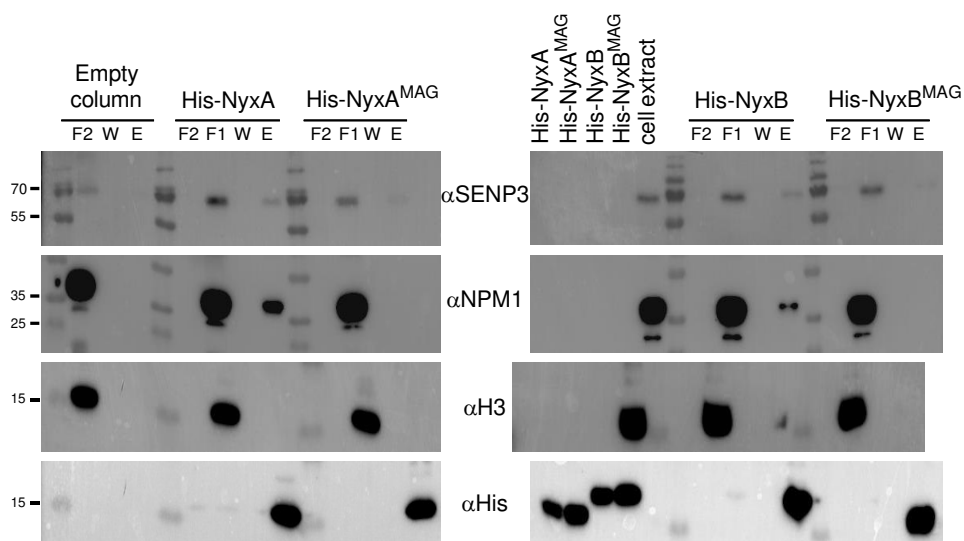


**Figure 33. Identification of the SENP3 interacting groove.** (A) Surface representation of NyxB dimer coloured according to electrostatic potential (red negative, blue positive) showing the extended acidic patch. The inset shows a close-up view of the area with residues' side chains displayed as ball-and-sticks and mutated residues (E82, Y66 and D80) coloured in cyan. (B) Pull-down assay with His-NyxA, His-NyxB or the specific catalytic mutants (His-NyxA<sup>MAG</sup> or His-NyxB<sup>MAG</sup>) immobilized on Ni NTA resins that were incubated with a HeLa cell extract. Empty column was used as a control for non-specific binding. Interactions with endogenous SENP3, NPM1 or Histone 3 (H3) were visualized by western blotting using the corresponding antibody, and column binding with anti-His (lower blot). Non-bound fractions (F1 and F2), last wash (W) and elution (E) are shown for each sample and the molecular weights indicated (kDa). The cell extract and the different purified Nyx inputs are also shown.

We mutated Y66, D80 and E82 to obtain His-NyxB<sup>MAG</sup>, where “MAG” stands for mutated acidic groove and Y62, D76 and E78 to obtain His-NyxA<sup>MAG</sup>. Purified NyxA or NyxB was indeed able to pull-down endogenous SENP3 from a HeLa cell extract confirming their interactions (Figure 33B). A decreased ability for both His-NyxA<sup>MAG</sup> and His-NyxB<sup>MAG</sup> to interact with SENP3 was observed (Figure 33B). However, we could only detect a small amount of endogenous SENP3 in the cell extract with our antibody. As it is well established that when SENP3 is pulled-down from a cell extract, its major cellular partner NPM1 can be easily detected by western blotting, we next probed the same membrane with an antibody against NPM1. NPM1 was not pulled-down by His-NyxA<sup>MAG</sup> and His-NyxB<sup>MAG</sup>, confirming that this mutation strongly impaired in their ability to bind the complex SENP3-NPM1 (Figure 33B). As a negative control, the membrane was also probed for Histone 3, an abundant nuclear protein that did not bind to NyxA nor NyxB (Figure 33B).

Together these results identify SENP3 as a target of the *Brucella* Nyx effectors and identify the acidic groove responsible for this interaction *in vitro*.

#### 8. The *Brucella* Nyx effectors induce delocalisation of SENP3

After showing that NyxA and NyxB interact directly with SENP3, a eukaryotic protein mainly found in the nucleoli, we were intrigued by what impact these effectors could have on SENP3 (Figure 5A, top panel). Ectopic expression of HA-tagged NyxA resulted in a marked reduction of endogenous nucleolar SENP3, which instead formed aggregates in the nucleoplasm (Figure 34A and B). As SENP3 redistribution from nucleoli to the nucleoplasm could be due to starvation or mild oxidative stress [268] [257], we ectopically expressed the mutant HA-

NyxA<sup>MAG</sup>, that we know is less able to interact with SENP3. The mutation of the acidic interaction groove impaired delocalisation of SENP3 by NyxA, confirming this effect was due to NyxA's direct interaction with SENP3. Consistently, analysis of the same images for co-localization of SENP3 with HA-NyxA revealed important recruitment, dependent on the acidic groove (Figure 34C). All the cells quantified are shown, with each colour corresponding to an independent experiment and its corresponding mean ( $N = 4$ ). NyxB was also able to delocalise SENP3 from the nucleoli and recruit SENP3 *via* direct interaction, implicating both effectors in this phenotype (Figure 34B, C and D).

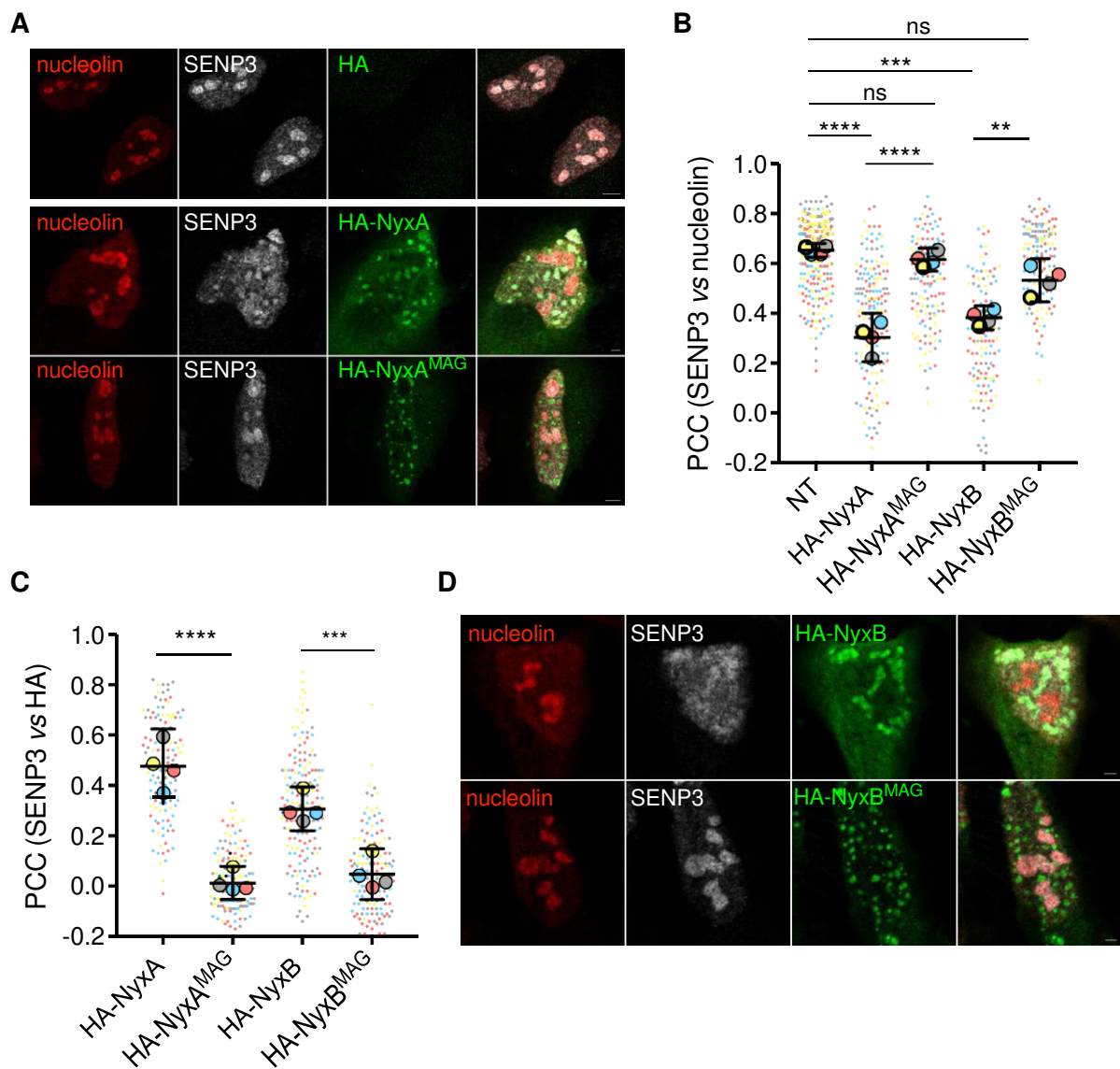


**Figure 34. The *Brucella* Nyx effectors directly reduce the SENP3 nucleolar localization in host cells. (A)** Representative confocal microscopy images of HeLa cells expressing the HA empty vector (top),



HA-NyxA (middle) and HA-NyxA<sup>MAG</sup> (bottom). Nucleolin (red), SENP3 (white) and HA (green) were revealed with specific antibodies. **(B)** Quantification of the Pearson's coefficient of SENP3 versus nucleolin (see methods for plugin description). Data are represented as means  $\pm$  95% confidence intervals from 4 independent experiments. Each experiment is colour coded and all events counted are shown. Data were analysed using one way ANOVA by including all comparisons with Tukey's correction. Not all comparisons are shown. **(C)** The same data set was used for quantification of the Pearson's coefficient of SENP3 versus HA to assess recruitment.

Next, we investigated the prevalence of these phenotypes during infection. We infected HeLa cells with either the wild-type *B. abortus* strain, the mutant lacking *nyxA*, or a complemented strain, expressing *nyxA* from the chromosome under the control of its promoter. Analysis of the level of SENP3 retained in the nucleoli during infection showed a significant lack of nucleoli localization of SENP3 in cells infected with the wild-type *B. abortus* strain in contrast with the  $\Delta$ *nyxA* strain (Figure 35A and B). The wild-type phenotype was partially restored with the complemented strain but not with a  $\Delta$ *nyxA* strain expressing *nyxA*<sup>MAG</sup>. This mutation impairs interaction with SENP3 *in vitro* but does not affect effector translocation during infection (Figure 36). This result shows that NyxA's interaction with SENP3 during infection prevents its accumulation in the nucleoli.

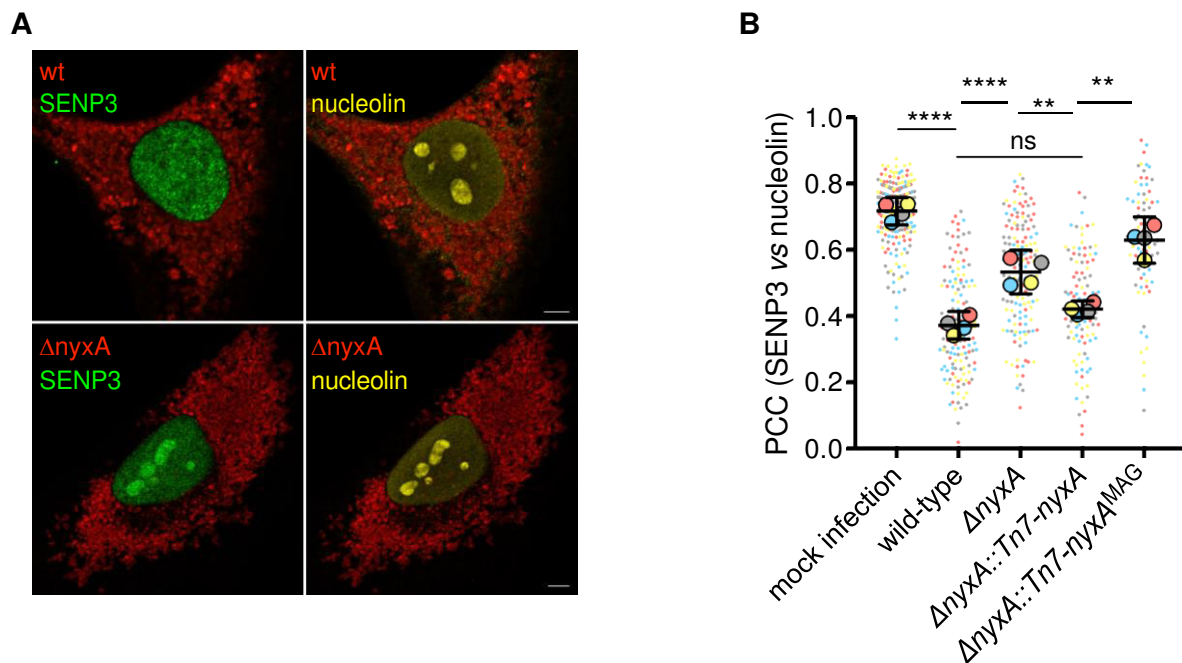


**Figure 35. The *Brucella* NyxA effector directly reduces the SENP3 nucleolar localization in host cells.** **(A)** Representative confocal microscopy images of cells expressing HA-NyxB (top) and HA-NyxB<sup>MAG</sup> (bottom), with nucleolin (red), SENP3 (white) and HA (green). **(B)** Quantification of the Pearson's coefficient of SENP3 versus nucleolin in HeLa cells infected for 48h with either *B. abortus* wild-type or



$\Delta nyxA$ , its complemented strain  $\Delta nyxA::Tn7-nyxA$  or a complementing strain expressing the mutated acidic groove responsible for interaction with SENP3 ( $\Delta nyxA::Tn7-nyxA^{MAG}$ ). Data are represented and were analysed as in (B). Not all comparisons are shown. All microscopy images displayed have scale bars corresponding to 5  $\mu\text{m}$ .

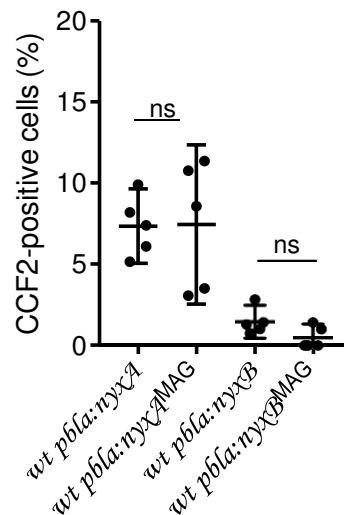


**Figure 36. The *Brucella* Nyx effectors with mutated acidic grooves are still translocated during infection.** RAW macrophage-like cells was infected for 24h with *B. abortus* wild-type expressing TEM1 (encoded by the *bla* gene) fused with NyxA, NyxA<sup>MAG</sup>, NyxB or NyxB<sup>MAG</sup>. The percentage of cells with coumarin emission, which is indicative of translocation, was quantified after incubation with the CCF2-AM substrate. Data represent means  $\pm$  95% confidence intervals from 5 independent experiments.

In the case of NyxB, we could also observe a statistically significant increase of SENP3 in the nucleoli in cells infected with the  $\Delta nyxB$  strain compared to cells infected with wild-type *B. abortus*, although to a lesser extent than what we observed for  $\Delta nyxA$ . However, we could not fully complement this phenotype, possibly due to the low sensitivity of this microscopy approach combined with a weaker phenotype (Figure 37A). As expected, a strain lacking both genes encoding for NyxA and NyxB could not mislocalise SENP3 as the wild-type strain. Representative images of all strains are shown in the (Figure 37B). These phenotypes could not be evaluated in macrophages, as we could not detect SENP3 in bone marrow-derived macrophages with any of the commercial antibodies available.

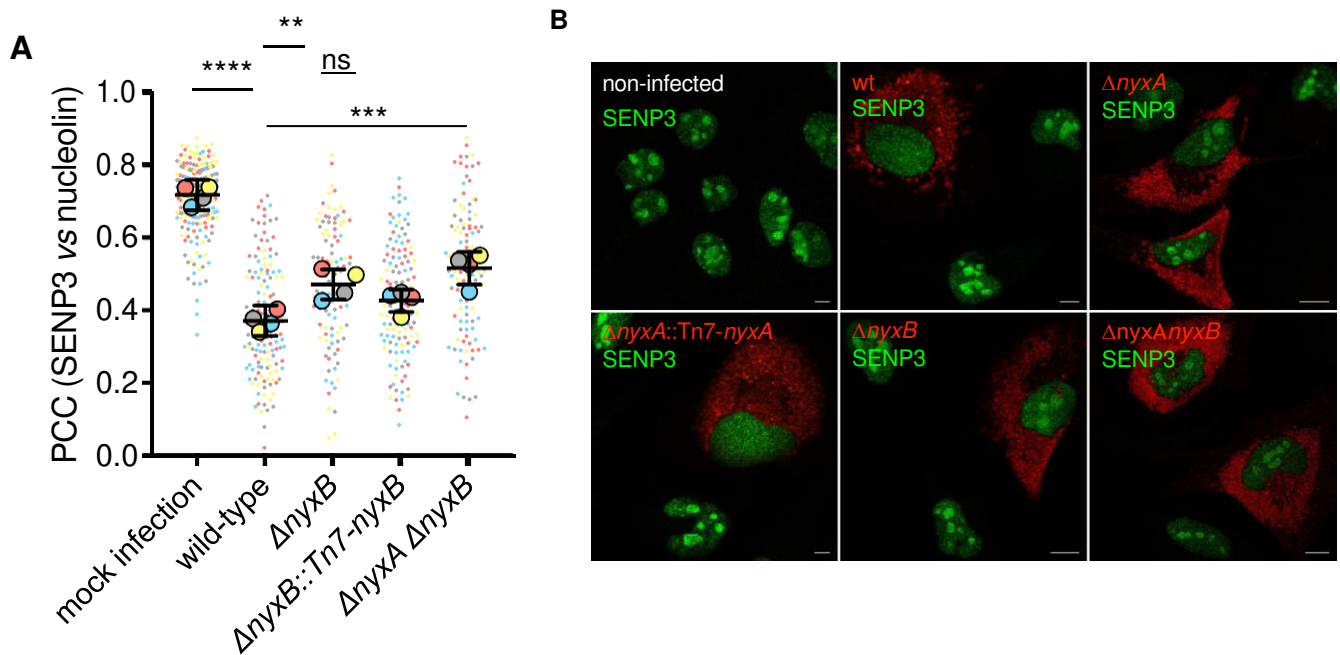


**Figure 37. The *Brucella* NyxB effector also potentially contributes to SENP3 mislocalization during infection. (A)** Quantification of the Pearson's coefficient of SENP3 versus nucleolin in HeLa cells infected for 48h with either *B. abortus* wild-type or  $\Delta nyxB$ , its complemented strain  $\Delta nyxB::Tn7-nyxB$  or double deletion mutant  $\Delta nyxA \Delta nyxB$ . Data are represented as means  $\pm$  95% confidence intervals from 4 independent experiments. **(B)** Representative confocal microscopy images of HeLa cells infected with the different strains expressing DSRed and labelled for SENP3 (green), in comparison to mock infected control cells (non-infected first panel).

### 9. Nyx effectors and SENP3 depletion induce cytosolic accumulation of the nucleolar proteins NVL

The observation that SENP3 was unable to accumulate in the nucleoli during *B. abortus* infection prompt us to investigate if NyxA and NyxB could impact other nucleoli proteins associated with SENP3 functions. One of the principal roles of SENP3 in the nucleoli is to regulate ribosomal biogenesis, specifically of the 60S ribosomal subunit. Briefly, mammalian 80S ribosomes result from assembly of a large 60S subunit, composed of 5S, 5.8S and 28S rRNAs, and a small 40S subunit comprised of the 18S rRNA. A high number of ribosomal proteins are associated with each subunit. SENP3 is implicated in the 28S rRNA maturation, by de-SUMOylating several nucleoli proteins, including NPM1. Therefore, we investigated the impact of *B. abortus* infection on the localization of different nucleoli proteins implicated in ribosomal biogenesis. We did not observe any effect of the nucleolar accumulation of

Pescadillo (PES1) (Figure 38A), involved in the maturation of the 28S and 5.8S rRNAs and, similarly to SENP3, requires interaction with NPM1 for nucleolar targeting [268]. A slight effect on NPM1 was observed in some *B. abortus* infected cells (Figure 20B), but to a lower extent than SENP3, suggesting that the bulk of nucleolar NPM1 remains unaffected.

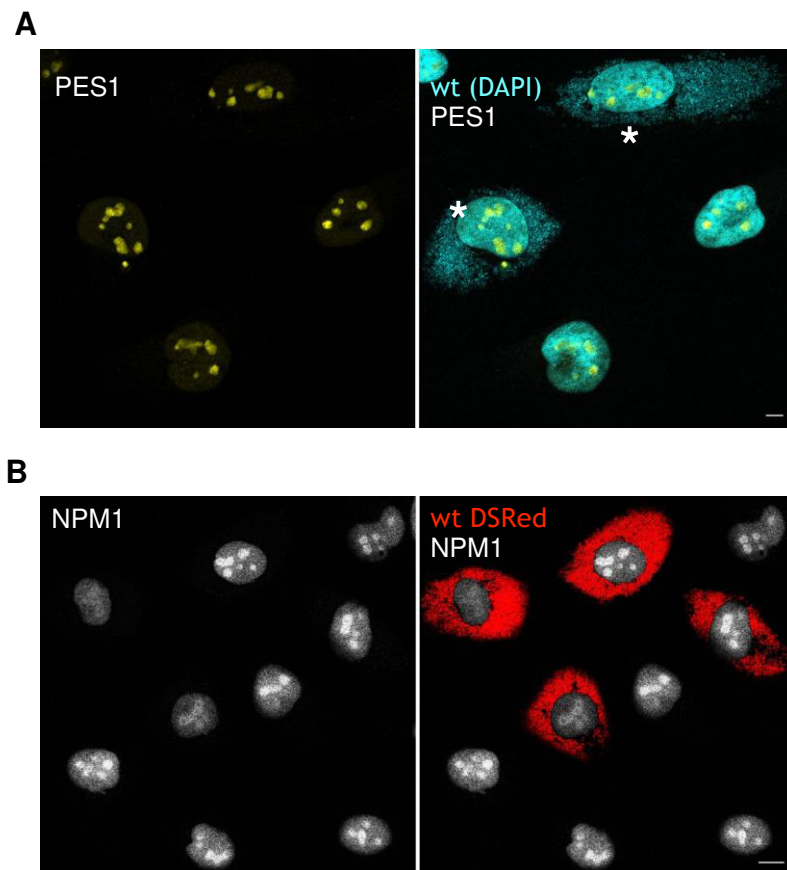


**Figure 38. *B. abortus* does not induce significant delocalization of PES1 and NPM1 from the host nucleoli. (A)** Representative confocal images of HeLa cells infected for 48h with wild-type *B. abortus* and labelled for DNA to visualize bacteria and cell nuclei (cyan) and PES1 (yellow). Infected cells are indicated with an asterisk. **(B)** HeLa cells infected for 48h with DSRRed-expressing wild-type *B. abortus* and labelled for NPM1 (white). All scale bars correspond to 5  $\mu$ m.

We next analysed the nucleolar accumulation of the VCP-like AAA-ATPase (NVL), also part of the complex of proteins involved in the maturation of the 28S and 5.8S rRNAs [282]. Unexpectedly, we observed a striking cytoplasmic accumulation of NVL in punctate structures in all *B. abortus* infected cells rarely visible in non-infected cells (Figure 39A). It is important to note that significant NVL staining was still observed in the nucleoli of infected cells.

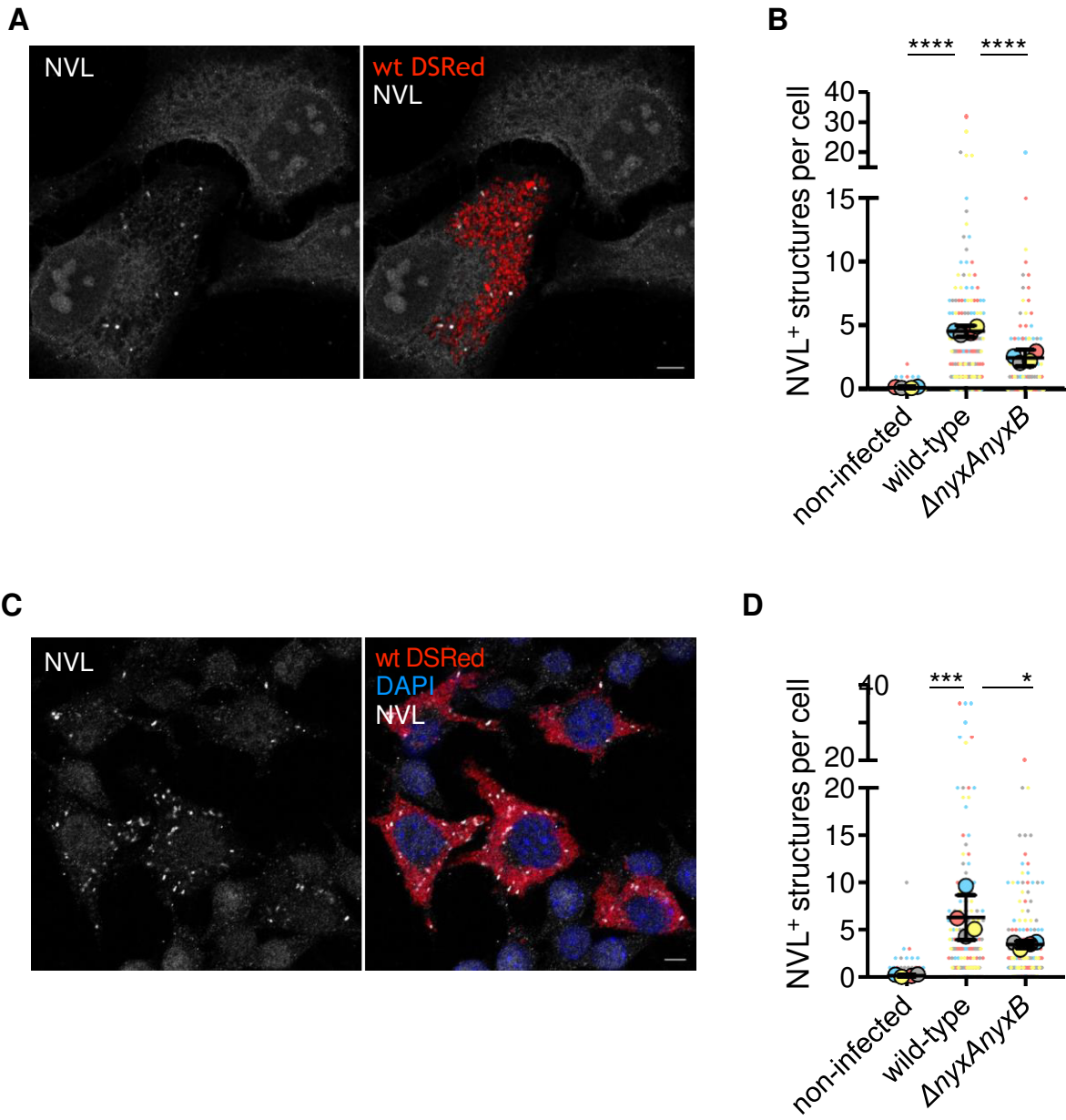


**Figure 39. *B. abortus* induces cytoplasmic punctate accumulation of NVL in a manner partially dependent of the Nyx effectors. (A)** Confocal microscopy image of wild-type *B. abortus* (expressing DSRRed) infected HeLa cells labeled with an anti-NVL antibody (white). **(B)** Quantification of the number of NVL-positive cytosolic structures in mock infected control cells in comparison to wild-type or a mutant strain lacking both *nyxA* and *nyxB*. Data are represented as means ± 95% confidence intervals

from 4 independent experiments. Data were analysed using one way ANOVA by including all comparisons with Tukey's correction. Not all comparisons are shown. **(C)** Confocal microscopy image of wild-type *B. abortus* (expressing DSRed) infected immortalized bone-marrow derived macrophages (iBMDM) labeled with an anti-NVL antibody (white) and DAPI (blue). **(D)** Quantification of the number of NVL-positive cytosolic structures in mock infected control iBMDM in comparison to wild-type or a mutant strain lacking both *nyxA* and *nyxB*. Data are represented and were analysed as in (B).

To determine if the *Brucella* Nyx effectors induced the formation of these NVL-positive cytoplasmic structures, Amandine Blanco quantified their number in HeLa cells infected either wild-type or a mutant lacking both NyxA and NyxB. She found that cells infected with  $\Delta nyxA nyxB$  had fewer NVL-positive structures (Figure 39B), suggesting the Nyx effectors contribute to their induction. This difference was not due to different intracellular bacterial numbers as *nyx* mutant strains replicate as efficiently as the wild-type in HeLa cells (Figure 40). Strong induction of NVL cytoplasmic punctate accumulation was also observed in immortalized bone marrow-derived macrophages infected with wild-type *B. abortus* (Figure 39C), in a Nyx-dependent manner (Figure 39D).

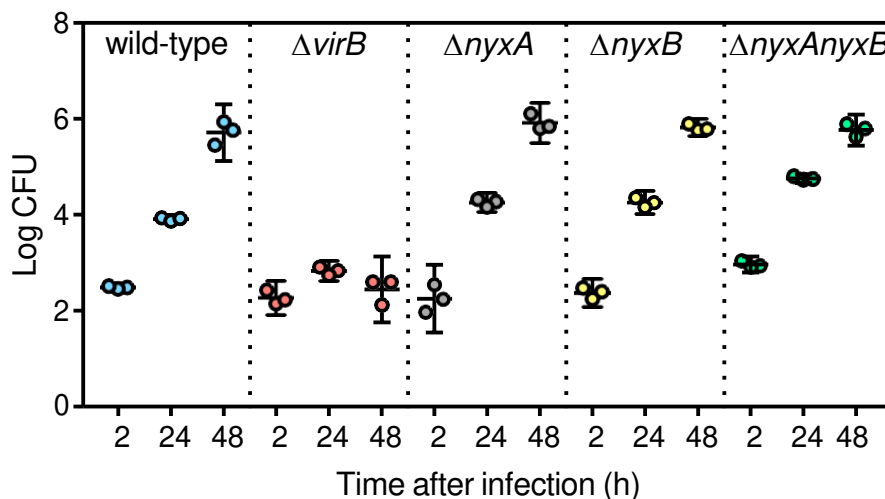


**Figure 40. Deletion of NyxA and NyxB does not impact intracellular multiplication of *B. abortus*.** Enumeration of bacterial colony forming units (CFU) of wild-type *B. abortus*,  $\Delta virB9$ ,  $\Delta nyxA$ ,  $\Delta nyxB$  or  $\Delta nyxA nyxB$  following 2, 24 or 48h of infection of HeLa cells. Data correspond to means  $\pm$  95% confidence intervals from 3 independent experiments.

NyxA and NyxB interaction with SENP3 and subsequent nuclear mislocalization is likely to lead to decreased activity of SENP3 within the nucleoli, where it usually is part of the 60S maturation and assembly complexes, along with many other proteins including NVL. To determine if the absence of SENP3 activity could account for the induction of NVL cytoplasmic structures, we depleted SENP3 for 72h and infected cells with wild-type *B. abortus* for a further 48h. The depletion of SENP3 resulted in a substantial rise in cytosolic NVL vesicles being formed (Figure 41A and B). These results were also observed as early as 24h post-infection, at which time-point an increase of cytosolic NVL was already observable in wild-type infected cells (data not shown).

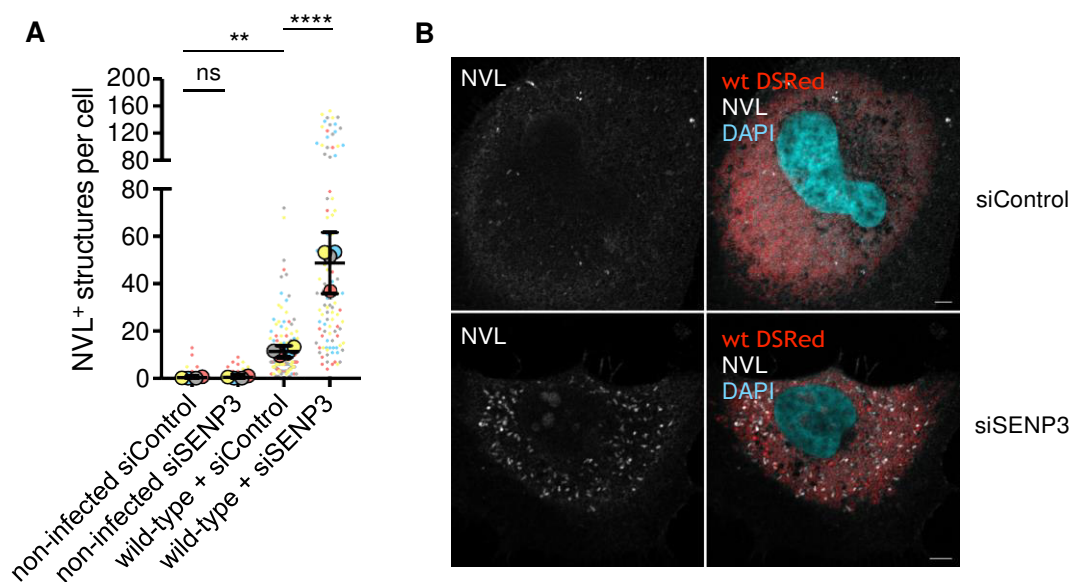


**Figure 41. SENP3 depletion induces accumulation of NVL in cytosolic punctate structures during infection.** (A) Quantification of the number of NVL-positive cytosolic structures in HeLa cells pre-treated for 72h with control siRNA or siSENP3 and infected for an additional 48h with wild-type *B. abortus*. Mock infected cells are included as controls. Data are represented as means  $\pm$  95% confidence intervals from 4 independent experiments. (B) Representative images of NVL cytosolic punctate accumulation (white) in HeLa cells treated with control siRNA (top) or depleted for SENP3 (bottom) for 72h, followed by infection for 48h with *B. abortus* expressing DSRed. All scale bars correspond to 5  $\mu$ m.

These results indicate that induction of NVL accumulation in cytosolic punctate structures during *Brucella* infection is dependent on SENP3. We must now complement the mutant phenotypes to confirm these results.



It is important to note that depletion of SENP3 alone was not sufficient to induce NVL cytosolic accumulation, suggesting this phenotype is triggered by the infection. Therefore, we wondered it could constitute a generalized cellular response to intracellular bacteria. We selected another intracellular pathogen, *Legionella pneumophila*, that multiplies in an ER-derived vacuole inducing ER stress as observed for *B. abortus* [283]. Experiments done by Monica Rolando in the team of Carmen Buchrieser (Inst. Pasteur) showed tha infection with *L. pneumophila* did not result in NVL cytosolic accumulation (Figure 42), suggesting this phenomenon is specifically induced during *B. abortus* infection.

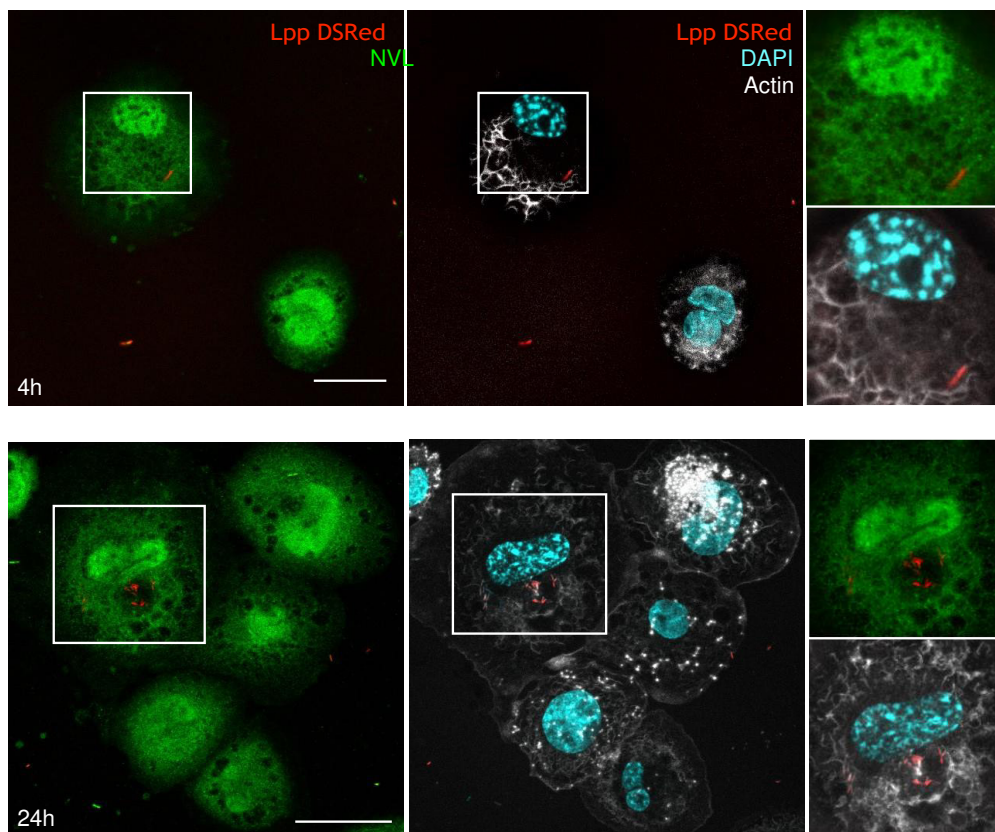


**Figure 42. *Legionella* infection does not induce NVL cytosolic accumulation.** Immunofluorescence analysis of THP-1 cells infected 4 and 24 hours with wild type *L. pneumophila* strain Paris, carrying a DsRed expressing plasmid. Cells were stained with an anti-NVL antibody (green) and analyzed by confocal microscopy. DAPI, light blue; Phalloidin, grey. Scale bars correspond to 10  $\mu$ m.

#### 10. *B. abortus* induces NVL cytosolic structures enriched in RPL5 and the ribophagy receptor NUFIP1

Next, we aimed to identify the nature of the cytosolic NVL-positive structures formed during *B. abortus* infection. NVL interacts with the ribosomal protein 5 (RPL5), a component of the

60S ribosomal subunit, responsible for transporting NVL to the nucleus and nucleoli [275]. We wondered if RPL5 could also be retained in the cytosol, we analysed RPL5 distribution in cells infected with wild-type *B. abortus*. We observed the same striking accumulation of RPL5 in cytosolic structures in all infected HeLa cells (Figure 43A) and bone marrow-derived macrophages (Figure 43B).

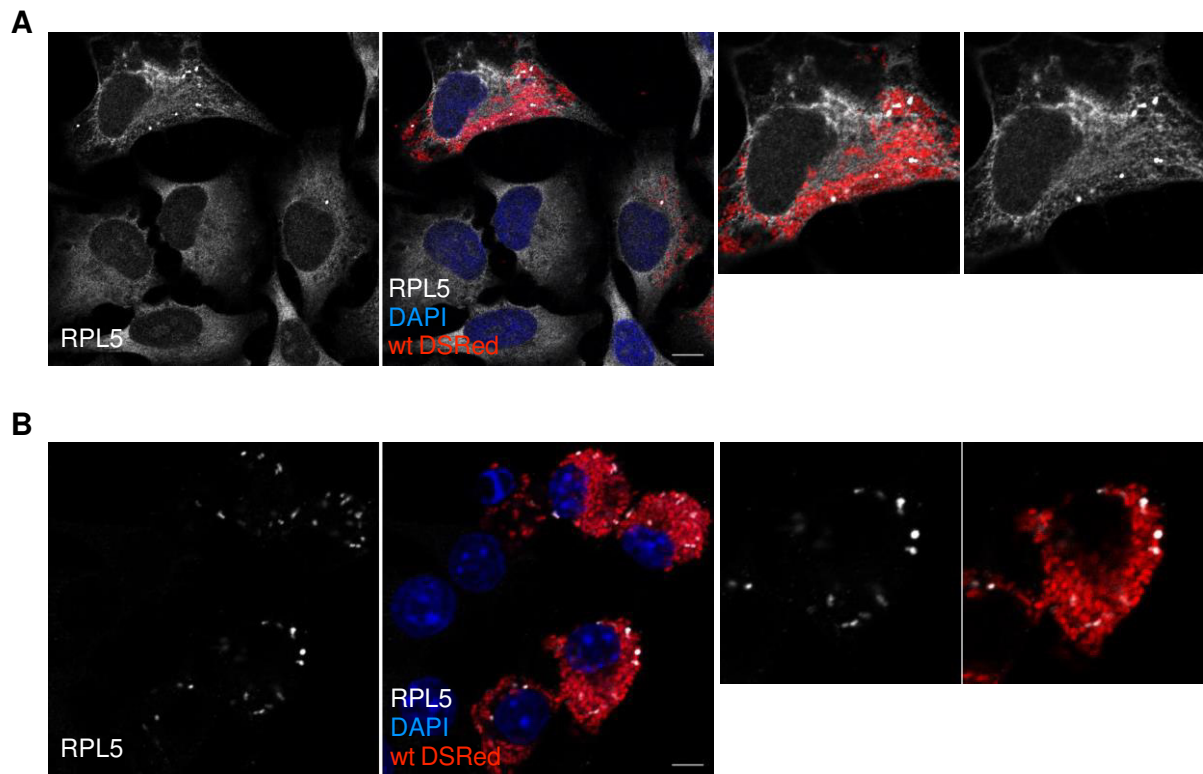


**Figure 43. *B. abortus* induces cytosolic accumulation of RPL5.** Representative confocal microscopy images of (A) HeLa cells or (B) iBMDM infected with wild-type DSRRed-expressing *B. abortus* for 48h and labelled for RPL5 (white) and DAPI (blue). Zoomed cells are included on the right.

As these structures were reminiscent of the localization of 4HA-NyxA and NyxB during infection, we infected cells with strains expressing 4HA-tagged effectors and co-stained for NVL and RPL5. Indeed, NVL-positive punctate structures induced upon *Brucella* infection contained NyxA and NyxB in both HeLa cells and macrophages (Figure 44A and B). The same was observed with RPL5 labelling (Figure 45) and also when using 3Flag-tagged NyxA (Figure 46). These data overwhelmingly support the idea that these cytosolic *Brucella*-induced structures contain NVL, RPL5, and both Nyx effectors, at least transiently.



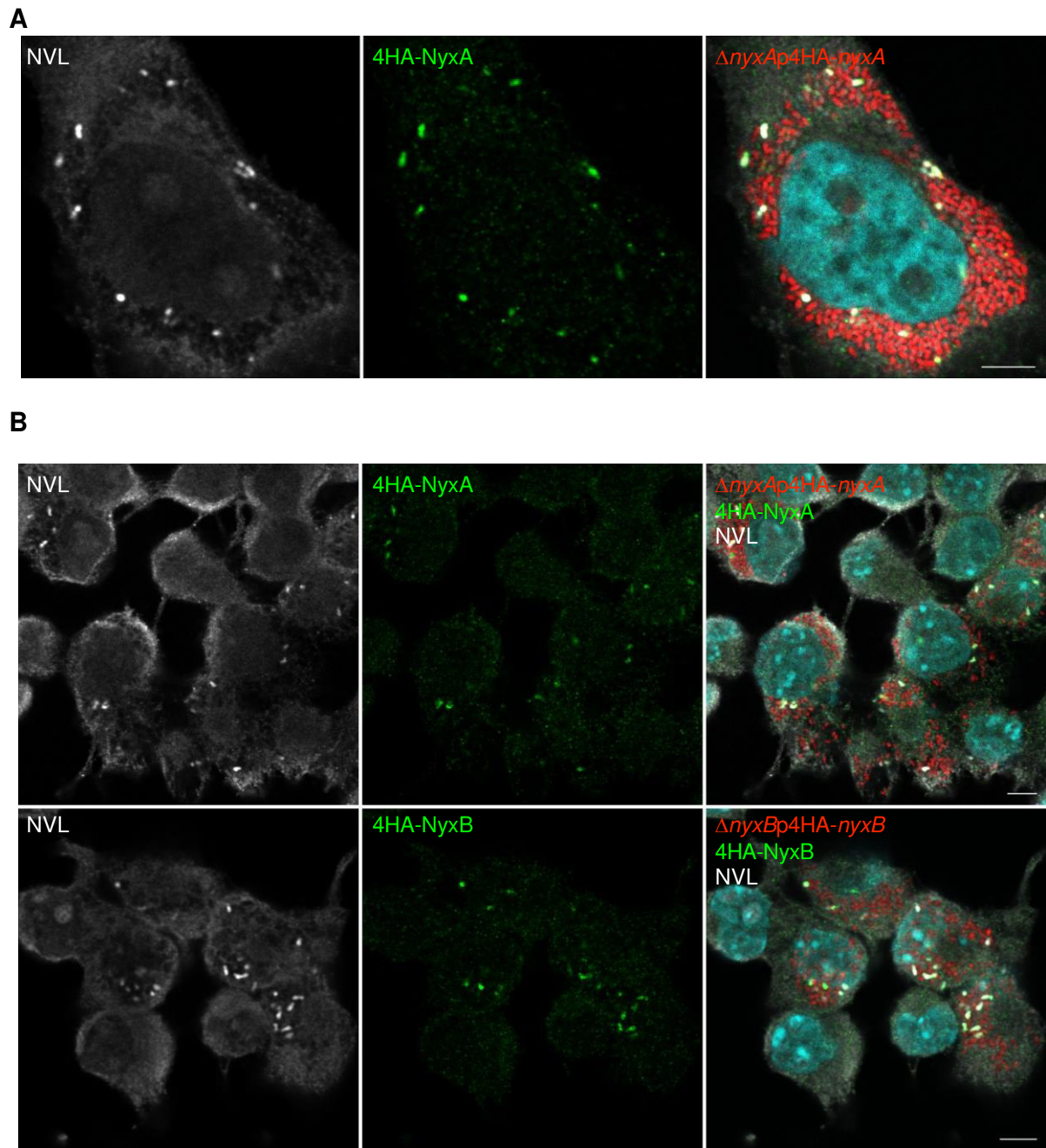


**Figure 44. *B. abortus* NVL-punctate cytosolic structures are enriched in Nyx effectors.** Representative confocal microscopy images of **(A)** HeLa cells or **(B)** iBMDM infected with *B. abortus* strains expressing either 4HA-NyxA or NyxB (green) for 48h and labelled for NVL (white) and DAPI (blue). Scale bars correspond to 5  $\mu$ m.

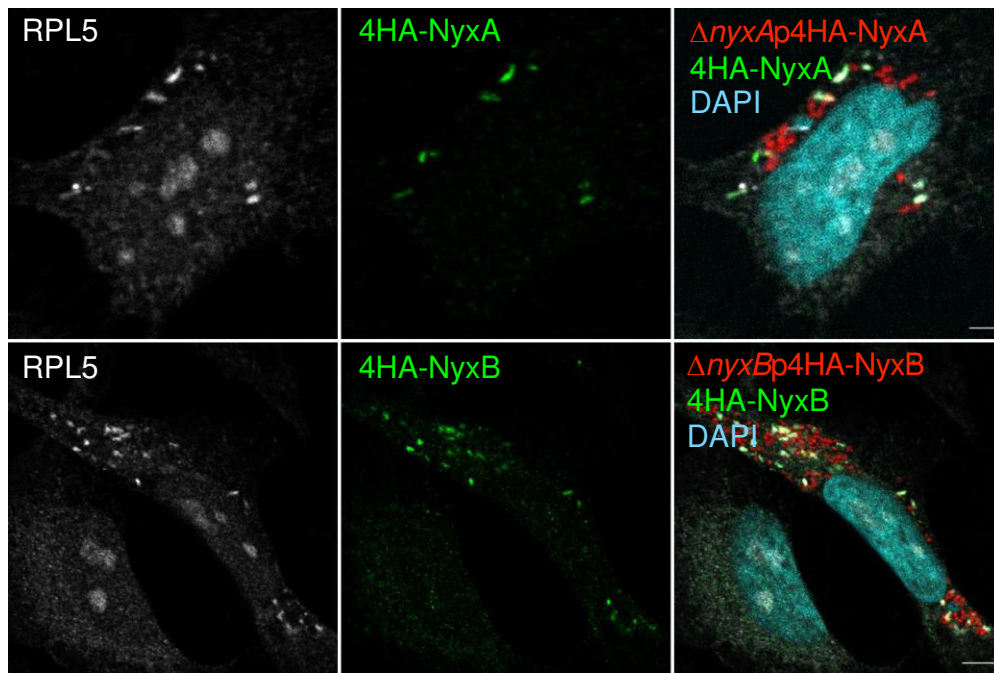
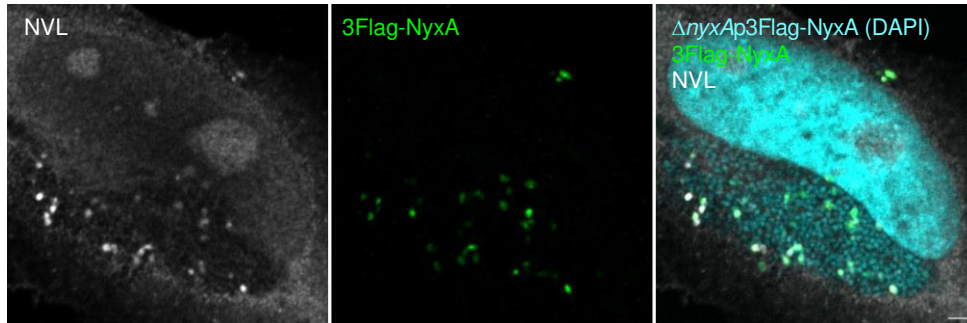


**Figure 45.** *B. abortus* RPL5-punctate cytosolic structures are enriched in Nyx effectors. Representative confocal microscopy images of **(A)** HeLa cells infected with *B. abortus* strains expressing either 4HA-NyxA or NyxB (green) for 48h and labelled for RPL5 (white) and DAPI (blue). Scale bars correspond to 5  $\mu$ m.

**A**



**B**

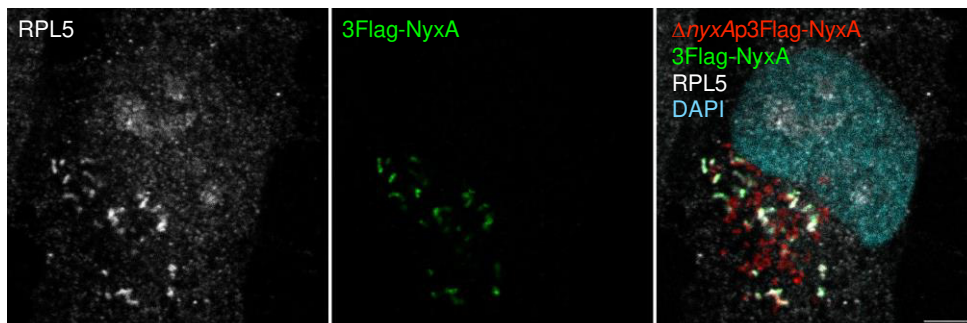


**Figure 46.** *B. abortus* induces cytosolic accumulation of NVL and RPL5 that colocalizes with translocated 3Flag-tagged NyxA. **(A)** HeLa were infected with  $\Delta$ *nyxA* expressing 3Flag-NyxA (green) for 48h and labelled for NVL (white) and DAPI (cyan). **(B)** HeLa cells were infected with  $\Delta$ *nyxA*

expressing DSRed and 3Flag-NyxA (green) for 48h and labelled for RPL5 (white) and DAPI (cyan). All scale bars correspond to 5µm.

Formation of cytosolic aggregates has been described in several bacterial infections, including stress granules [284], P-bodies [285] and U-bodies[286]. None of these were observed at 48h post-infection by Amandine Blanco (data not shown) when NVL and RPL5 structures are normally present. Labelling with the FK2 antibody did reveal the presence of aggregates of mono- and poly-ubiquitinated proteins in some *B. abortus* infected cells, but these did not co-localize with NVL (data not shown).

We then focused on other cellular processes resulting in cytoplasmic accumulation of nucleolar proteins. Recent reports have described NUFIP1 (nuclear fragile X mental retardation-interacting protein 1) as a nucleo-cytoplasmic shuttling protein that accumulates in the cytoplasm upon starvation [287]. In this context, NUFIP1 acts as a receptor for ribophagy, a specialized autophagy process dedicated to the degradation of ribosomes to generate nutrients and enhance cell survival [288]. We therefore wondered if NUFIP1 accumulation in the cytosol, a hallmark of ribophagy, could be enhanced in infected cells. Indeed, cells infected with wild-type *B. abortus* resulted in an increase in cytosolic NUFIP1 compared to non-infected cells (Figure 47A), with the appearance of vesicular structures. These were also enriched in NyxA (Figure 47B).

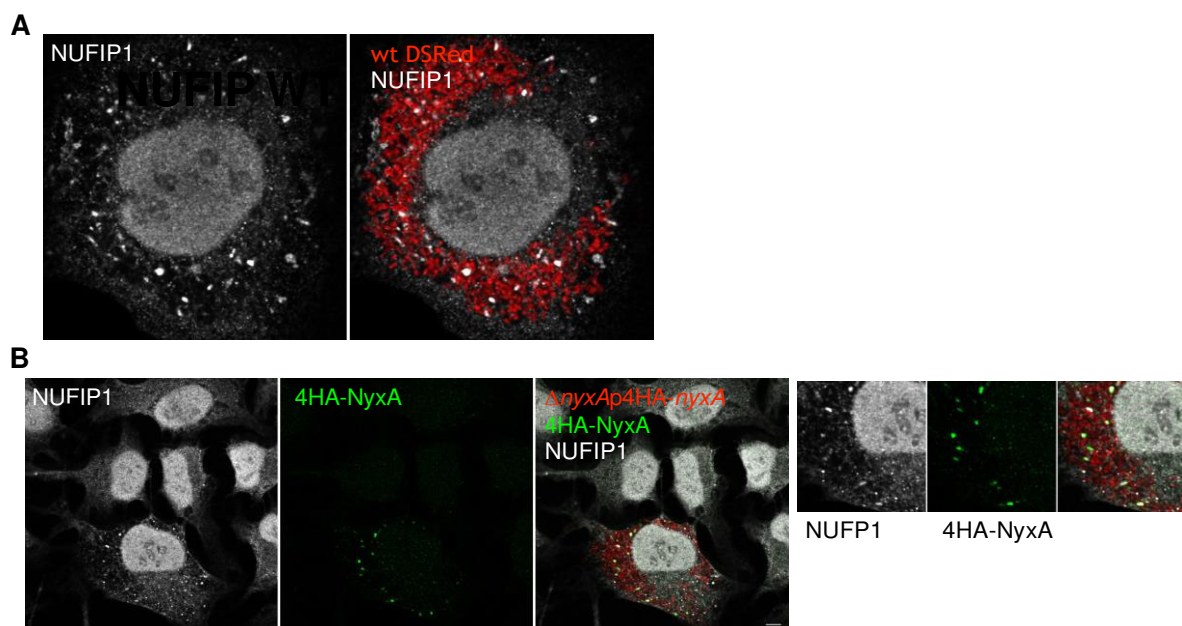


**Figure 47. NVL punctate cytosolic structures are enriched in Nyx effectors and the ribophagy receptor NUFIP1.** Representative confocal images of HeLa cells infected for 48h with (A) infected with wild-type



*B. abortus* DSRed and labeled with an anti-NUFIP1 antibody (white); **(B)** infected with  $\Delta nyxA$  DSRed expressing 4HA-NyxA (green) and immunolabeled with an anti-NUFIP1 antibody (white).

However, these structures were negative for LAMP1, suggesting blockage with lysosomes or that they constitute a different NUFIP1-positive compartment (Figure 48).

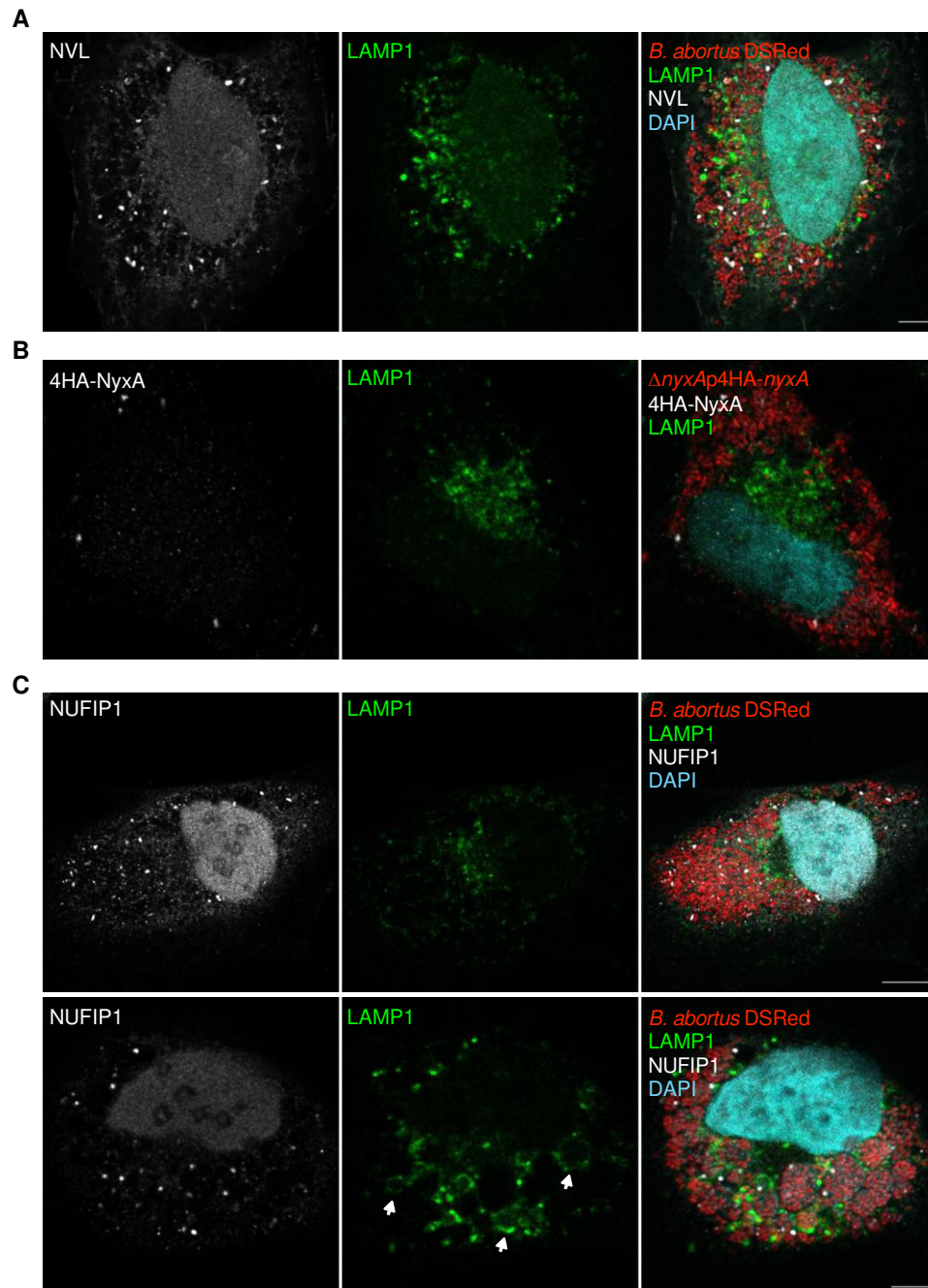


**Figure 48. NVL, Nyx and NUFIP1-positive cytosolic punctate structures are not lysosomal compartments.** Representative confocal microscopy images of HeLa cells infected for 48h with DSRed-expressing (A and C) wild-type *B. abortus* or (B)  $\Delta nyxA$  encoding 4HA-NyxA. Cells were labelled for DAPI (cyan), the lysosomal marker LAMP1 (green) and either (A) NVL, (B) HA or (C) NUFIP1 (white). In (C)

the top image corresponds to LAMP1-negative *Brucella*-containing vacuoles indicative of the replicative compartment whereas the bottom image corresponds to large LAMP1-positive vacuoles characteristic of autophagic *Brucella*-containing vacuoles that mediate bacterial egress from infected cells. All scale bars correspond to 5µm.

Finally, since the cytosolic punctate structures induced during infection were positive for NUFIP, but also NVL, we wondered if this could constitute a new marker for ribophagy, potentially induced during *B. abortus* infection. To address this, we analysed NVL labelling in cells undergoing starvation, known to induce ribophagy and cytosolic accumulation of NUFIP1. Indeed, we observed the formation of NVL enriched punctate structures in starved cells in contrast to normal cells (Figure 49). We are now confirming these are indeed NUFIP and LC3-positive ribophagosomes but, overall, our results suggest that NVL cytosolic structures induced by *B. abortus*, enhanced by the presence of NyxA and NyxB, result from increased ribophagy. Therefore, we propose that NyxA and NyxB act as suppressors of SENP3 activity to modulate ribophagy levels during infection.

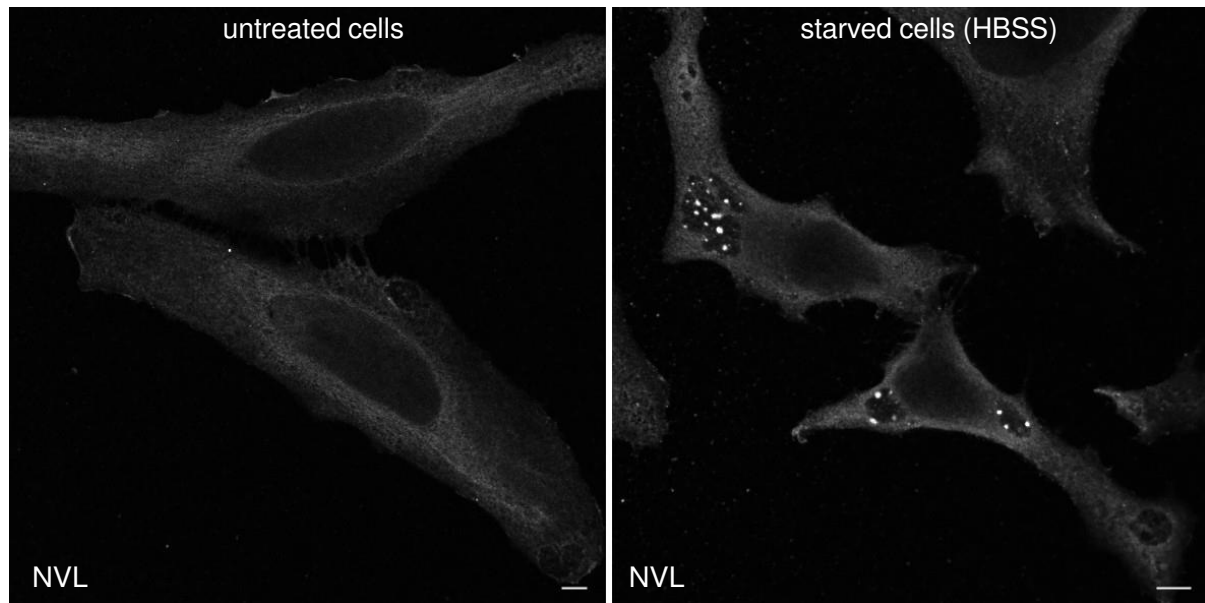


**Figure 49. NVL-positive cytosolic punctate structures are observed under starvation condition.** Representative confocal microscopy images of HeLa cells untreated or treated with HBSS (starved cells) for 4h and labelled with NVL (white). All scale bars correspond to 5µm.



### 3. Materials and Methods

#### 1. Cells and culture conditions

HeLa and RAW cell lines were obtained from ATCC and were grown in DMEM supplemented with 10% of fetal calf serum. Immortalized bone marrow-derived macrophages [289] from C57BL/6J mice were maintained in DMEM supplemented with 10% FCS and 10% spent medium from L929 cells that supplies MC-CSF. All cells were routinely tested and were mycoplasma free. When indicated cells were starved with HBSS for 8h.

#### 2. *Brucella* strains, cultures and infections

*B. abortus* 2308 was used in this study. Wild-type and derived strains were routinely cultured in liquid tryptic soy broth and agar. 50 µg/ml kanamycin was added for cultures of DSRed and 50 µg/ml ampicillin for strains expressing pBBR1MCS-2 (4HA and 3Flag constructs) or complemented strains (with pUCTminiTn7T\_Km). The list of all *Brucella* strains constructed is included in Supplementary Table 2.

For infections, eukaryotic cells were plated on glass coverslips 18h before infection and seeded at  $2 \times 10^4$  cell/well and  $1 \times 10^5$  cells/well for 24 and 6 well plates, respectively. Bacterial cultures were incubated for 16h from isolated colonies in TSB shaking overnight at 37 °C. Culture optical density was controlled at 600 nm. Bacterial cultures were diluted to obtain a multiplicity of infection (MOI) of 1:1000 in the appropriate cell culture medium. Inoculated cells were centrifuged at 400 x g for 10 min to initiate bacterial-cell contact followed by incubation for 1h at 37°C and 5% CO<sub>2</sub> for HeLa cells and 30 min for iBMDMs. Cells were then washed 3 times with DMEM and incubated a further hour with complete media supplemented with gentamycin (50 µg/mL) to kill extracellular bacteria. The gentamycin concentration was then reduced to 10 µg/mL by replacing the media. At the different time points coverslips were fixed for immunostaining. For enumeration of bacterial colony forming units (CFU), cells were lysed in 0.1% Triton for 5 min and a serial dilution plated in tryptic soy agar.

### 3. *Brucella* expressing vectors

DNA fragments coding for NyxA and NyxB were obtained by PCR amplification from the *B. abortus* 2308 genome, digested with XbaI and cloned into pFlagTEM1 [290] using Infusion (Takara Bio). After verification by sequencing, plasmids were introduced into *B. abortus* 2308 or  $\Delta virB9$  by electroporation.

*B. abortus* 2308 knockout mutant  $\Delta nyxA$  and  $\Delta nyxB$  were generated by allelic replacement. Briefly, upstream and downstream regions of about 750 bp flanking each gene were amplified by PCR (Q5 NEB) from the *B. abortus* 2308 genomic DNA. An overlapping PCR was used to associate the two PCR products and the  $\Delta nyxA$  or  $\Delta nyxB$  fragments were digested and cloned in a EcoRV digested suicide vector (pNPTS138) for NyxB. These vectors were then electroporated in *B. abortus* and transformants selected using the kanamycin resistance cassette of the pNPTS138 vector. The loss of the plasmid concomitant with either deletion or a return to the wild type phenotype was then selected on sucrose, using the *sacB* counter selection marker also present on the vector. Deletant ( $\Delta$ ) strain was confirmed by PCR and sequencing.

The complementing strain was constructed by amplifying either *nyxA* or *nyxB* and their corresponding promoter region (500 bp upstream) with the PrimeStar DNA polymerase (Takara). Insert and pUCTminiTn7T\_Km [83] were digested with BamHI and SpeI and ligated overnight. Transformants were selected on kanamycin 50  $\mu\text{g}/\text{mL}$  and verified by PCR and sequencing. To obtain the complementing strain the  $\Delta nyxA$  or  $\Delta nyxB$  mutants were electroporated with pmini-Tn7-*nyxA* or -*nyxB*, respectively, with the helper plasmid pTNS2. Electroporants were selected with kanamycin 50  $\mu\text{g}/\text{mL}$  and verified by PCR.

### 4. Eukaryotic expression vectors

The NyxA and NyxB constructs were obtained by cloning in the gateway pDONR<sup>TM</sup> (Life Technologies) and then cloned in the pENTRY Myc or HA. The NyxA<sup>MAG</sup> and NyxB<sup>MAG</sup> constructs were obtained by site-directed mutagenesis. The 4HA-NyxA and NyxB were clone into pBBR-MCS4. All the primers used are listed in Supplementary Table 2.



## 5. Bacterial expression vectors

NyxA and NyxB were amplified by PCR and inserted into the pET151D topo vector following the manufacturer's procedure (Invitrogen) to obtain His-NyxA and His-NyxB. An additional V5 tag is also present. His-NyxA<sup>MAG</sup> and His-NyxB<sup>MAG</sup> were obtained by site-directed mutagenesis. For expression and purification of SENP3<sup>7-159</sup>, a vector with *E. coli* codon-optimized SENP3 was obtained from ThermoFisher and used as a template. All the primers used are listed in Supplementary Table 2.

## 6. Immunofluorescence microscopy

At the indicated time points, coverslips were washed twice with PBS, fixed with PFA 3.2% (Electron Microscopy Sciences) for 20 minutes and then washed again 4 times with PBS. Best NVL staining was achieved with AntigenFix (Micromicrotech France). For SENP3, NVL, RPL5, PES1 and NUFIP1 immunostaining, permeabilization was carried out with a solution of PBS containing 0.3% triton for 30 minutes followed by blocking also for 30 minutes in a solution of PBS containing 2% bovine serum albumin (BSA), 10% horse serum, 0.3% triton. For HA and Flag to detect translocated effectors blocking and antibody solutions did not contain Triton (only the permeabilization step). For NPM1 staining Permeabilization was done with Tween 0.05% followed by antibody diluted in 2% BSA, 10% horse serum and 0.3M glycine. Coverslips were then incubated at 4 °C overnight with primary antibody diluted in the blocking solution. Subsequently, the coverslips were washed twice in PBS and incubated for 2h with secondary antibodies. When indicated DAPI was also included in the secondary antibody mix (1/1000). Finally, coverslips were washed twice in PBS, once in PBS and once in ultrapure water. Lastly, they were mounted on a slide with ProLongGold (Life Technologies). The coverslips were visualized with a Confocal Zeiss inverted laser-scanning microscope LSM800 and analyzed using ImageJ software. All dilution, sources for each antibody are indicated in Supplementary Table 1.

## 7. Transfections and siRNA

All cells were transiently transfected using Fugene<sup>®</sup> (Promega) overnight, according to manufacturer's instructions. HeLa cells were seeded 18h prior to experiments at  $2 \times 10^4$  cells/well for 24 well plates. siRNA experiments were done with Lipofectamine<sup>®</sup> RNAiMAX Reagent (Invitrogen) according the protocol of the manufacturers. Cells were seeded at  $1.4 \times 10^4$  cells/well. Importantly, siRNA depletion of SENP3 was done by treatment with 0.1 $\mu$ M siRNA every day for 72h. The following sequence was used AAACUCCGUACCAAGGGUUAU. A scrambled siControl was also used. Some cell detachment was observed following the 3 days siRNA treatment.

## 8. *Legionella* infection

*Legionella pneumophila* strain Paris was cultured in *N*-(2-acetamido)-2-aminoethanesulfonic acid (ACES)-buffered yeast extract broth or on ACES-buffered charcoal-yeast (BCYE) extract agar. Human monocyte cell line (THP-1) was cultured and infected as previously described [291]. For immunofluorescence analyses cells were fixed in 4 % paraformaldehyde, permeabilized with PBS-triton 0.5% and stained with 4-6-diamidino-2-phenylindole (DAPI), Phalloidin and and primary anti-NVL antibody (16970-1-AP). Immunosignals were analyzed with a Leica SP8 microscope at 63X. Images were processed using ImageJ software.

## 9. Pulldown assays

50  $\mu$ g of His tag recombinant protein was incubated with recombinant protein during 2 h at 4°C, then incubated within gravity flow column (Agilent) containing 80  $\mu$ l Ni-NTA agarose beads (Macherey-Nagel) during 1 h beforehand washed in water and pre-equilibrated in equilibrium buffer 20 mM Tris–HCl pH7.5, 250 mM NaCl. The column was washed successively three times in equilibrium buffer supplemented with 25 mM imidazole, three times in equilibrium buffer and eluted in equilibrium buffer supplemented with 500 mM imidazole. Proteins eluted were separated by SDS–PAGE, transferred to a PVDF membrane, incubated with specific primary antibodies for 1 h and detected with horseradish peroxidase (HRP)-conjugated secondary antibodies by using Clarity<sup>TM</sup> Western ECL Blotting Substrate (Bio-Rad).

Pulldown assays between cell extract and purified Nyx and MAG mutants, see annexe 3

## 10. Quantification of SENP3 localization

Colocalization analysis for the transfected HeLa cells were performed with a custom ImageJ<sup>ref1</sup>/Fiji<sup>ref2</sup>-based macro, that segmented the nuclei and the nucleoli of the cells in each image, classified the cells in two classes according to the intensity of HA-NyxA/NyxB, and then measured in the areas of each nucleus the Pearson correlation coefficients (by calling the plugin Coloc2 - [https://github.com/fiji/Colocalisation\\_Analysis](https://github.com/fiji/Colocalisation_Analysis)) between the signal of SENP3 and the nucleolin as well as between the signals of SENP3 and HA-NyxA/NyxB. For each nucleus, the ratio between the mean intensity of the SENP3 signal in the nucleoli and the mean intensity of the SENP3 signal outside the nucleoli is also calculated. The details can be found in the source code and the comments of the macro. In the same way, this software was used to quantify the colocalization between PML and HA-NyxA/NyxB.

For the *Brucella* infected HeLa cells, a pipeline in the software CellProfiler<sup>ref3</sup> was used to measure the Pearson correlation coefficient between the signal of SENP3 and the nucleolin, in the nuclei of the cells. The cells were also classified in two classes according to the intensity of the *Brucella* DSRed signal in the perinuclear area.

## 11. TEM1 translocation assay

RAW cells were seeded in a 96 well plates at  $1 \times 10^4$  cells/well overnight. Cells were then infected with an MOI of 500 by centrifugation at 4 °C, 400 g for 5 min and 1 at 37 °C 5% CO<sub>2</sub>. Cells were washed with HBSS containing 2.5 mM probenidicid. Then CCF2 mix (as described in the Life Technologies protocol) and probenidicid were added to each well, and incubated for 1.5 h at room temperature in the dark. Cells were finally washed with PBS, fixed using 3.2% PFA and analysed immediately by confocal microscopy (Zeiss LSM800).

## 12. Thermophoresis

The method is based on the movement of molecules in a micro gradient of temperature, an effect called "thermophoresis" which varies depending on whether the molecule is free or in interaction (Figure 21). In the initial state, the proteins do not move. Then the solution protein will be heated by an infrared laser. The laser will cause a gradient of temperature (2

to 3°C). The molecules in solution will then move from hot to cold. Their movement depends on their charge, their size and their hydration layer. The interaction between a molecule and its partner will modify at least one of these parameters. Once the laser is turned off, the proteins will return to their initial state. The phenomenon of thermophoresis is followed by fluorescence. In practice, one of the partners is labelled with a fluorescent molecule or is capable of fluorescing natively. It is put in contact with a ligand at 10-16 different concentrations and then placed in capillaries. This system makes it possible to measure the dissociation constant of the interaction between two molecules without immobilization of a partner. It is a technique requiring little biological material and allows the study of interactions from nanomolar to millimolar. The experiments were performed at 20°C on a Monolith NT.115 (Nanotemper) with Premium Coated (Nanotemper) capillaries. The tested interactions were performed in triplicate. The labelling of NyxA is performed by covalent coupling of the lysines of the protein to a fluorophore using the RED-NHS (Nanotemper) Protein Labeling Kit. Unlabeled NyxB is used at the following increasing concentrations: 6,67nM, 13,34nM, 26,68nM, 53,3nM, 106,72nM, 213,44nM, 426,88nM, 853,76nM, 1,7µM, 3,4µM, 6,8µM, 13,6µM, 27,2µM, 54,4µM, 108,8µM, 217,6µM.

### 13. SUMOylation assay

In 50µl of reaction solution (20mM HEPES pH9, 20mM NaCl, 0.5mM DTT) were added 1.5µg of purified recombinant protein SUMO2 with 1µg of recombinant protein NyxA/NyxB or RanGAP1 (Biomol international #UW9755), 0.2µg of the SAE1/UBA2 heterodimer (Boston Biochem #E-315), 1µg of the purified recombinant protein hUbc9 in the presence or absence of Mg-ATP solution (Boston Biochem #B-20) at 5mM. This reaction solution is incubated for one hour at 37°C and then the reaction is stopped by 10mM of EDTA. 15µL of the reaction solution is used for analysis by coomassie blue staining.

### 14. Protein expression and purification

*E. coli* BL21-DE3-pLysS bacteria were transformed with the expression vectors, grown in LB media (Sigma-Aldrich) to OD<sub>280</sub>=0.6 and expression was induced with 1mM IPTG at 37°C for 3 hours. Cells were After harvested by 15 min of centrifugation at 5,000 g and resuspended in lysis buffer 20mM Tris pH 8, 150mM NaCl, 5% Glycerol, 0,1% Triton. Disruption cell was

achieved with sonication after addition of antiprotease EDTA-Free cocktail (Roche) and 30U/ml benzonase (Sigma-Aldrich). Cell debris were removed by centrifugation 30 min at 20,000g at 4°C. Recombinant protein was purified by chromatography using a Nickel-loaded Hitrap Chelating HP column (GE Healthcare). Unbound material was extensively washed using Tris 20mM pH8, NaCl 300mM, 25 mM Imidazole, 5mM  $\beta$ -mercaptoethanol, 10% Glycerol. An additional washing step with 2 column volumes of 1M NaCl was done before elution of NyxB over a 25 to 500 mM gradient of imidazole over 8 column volumes. Peak fractions were pooled and the His tag was cleaved with TEV protease (500  $\mu$ g/20mg of eluted protein) in presence of 1 mM DTT and 0,5 mM EDTA in overnight dialysis buffer 20mM Tris pH 8, 150mM NaCl. NyxB was further purified by size exclusion chromatography (Superdex 200 HiLoad 16/600, GE Healthcare) equilibrated in 20mM Tris pH 8, 150mM NaCl, 5 % Glycerol. Purity of the sample was assessed by SDS-PAGE. Freshly purified NyxB was concentrated to 21 mg/ml on 3 KDa Amicon Ultra concentrators (Millipore). SeMet-NyxB was produced in M9 minimum medium and purified as above, to a final concentration of pure SeMet-NyxB of 24 mg/ml.

#### 15. Crystallization and data collection

Screening was conducted using a Mosquito workstation (TTP Labtech) on commercial crystallization solutions with the sitting-drop vapour diffusion technique, against a protein solution. All crystallization trials were performed at 19°C and visualized on RockImager 182 (Formulatrix). Crystals of native NyxB were obtained with 21 mg/ml NyxB in 25% PEG4000, 0,2M CaCl<sub>2</sub>, 100 mM Tris pH 8. Crystals were frozen in reservoir solution supplemented with 15% Gly. Diffraction data was collected at the European Synchrotron Radiation Facility (ESRF) Beamline line ID23EH1 and crystals diffracted up to 2.5 Å resolution in space group P6<sub>1</sub>22, with 12 molecules per asymmetric unit. Crystals of Se-Met NyxB were obtained using a reservoir solution containing 2.6 M NaFormate and crystals were cryoprotected in 2.8 M Naformate supplemented with 10% glycerol. Data were collected at SOLEIL on beamline Proxima-2 from a single crystal that diffracted up to 3.7 Å resolution and belonged to the space group P6<sub>2</sub>22, with 2 molecules per asymmetric unit. Diffraction data were processed using XDS [292] and with SCALA from the CCP4 program suite [293].

The structure was solved using the single anomalous dispersion method on Se-Met crystals using AutoSol [294] from the Phenix program suite [295]. An excellent experimental

electron density map enabled us to manually build an initial model. The resulting model was then used for molecular replacement with data from native NyxB crystal using Phaser [295]. Twelve monomers were positioned and the resulting electron density map was then subjected to the AutoBuild program, part of the Phenix program suite [295]. Model building were completed with sessions of manual model building using Coot combined with model refinement using Phenix (Adams et al., 2002). The final model was refined to a final  $R_{work}/R_{free}$  of 0.20/0.24 with excellent geometry. The coordinates and structure factors of NyxB have been deposited in the protein DataBank with the code 7AD4. Figures were generated with Pymol.

#### 16. Size exclusion Multi-angle light scattering

Size exclusion chromatography (SEC) experiments coupled to multi-angle laser light scattering (MALS) and refractometry (RI) were performed on a Superdex S200 10/300 GL increase (GE Healthcare) for NyxA and a Superdex S75 10/300 GL (GE Healthcare) for NyxB. Experiments were performed in buffer 20 mM Tris pH 8, 150 mM NaCl, 5 % Glycerol. 100  $\mu$ l of proteins were injected at a concentration of 10 mg.ml<sup>-1</sup>. On-line MALS detection was performed with a miniDAWN-TREOS detector (Wyatt Technology Corp., Santa Barbara, CA) using a laser emitting at 690 nm and by refractive index measurement using an Optilab T-rex system (Wyatt Technology Corp., Santa Barbara, CA). Weight averaged molar masses ( $M_w$ ) were calculated using the ASTRA software (Wyatt Technology Corp., Santa Barbara, CA).

#### 17. Small-angle X-ray scattering

SAXS data were collected for NyxA and NyxB on BioSAXS beamline BM29, ESRF using an online size-exclusion chromatography setup. 50  $\mu$ l of protein (10 mg.ml<sup>-1</sup>) were injected into a size-exclusion column (Agilent BioSec-3) equilibrated in 50 mM Tris, pH 8.0, 200 mM NaCl. Images were acquired every second for the duration of the size-exclusion run. Buffer subtraction was performed by averaging 20 frames either side of the peak. Data reduction and analysis was performed using the BsxCuBE data collection software and the ATSAS package [296]. The program AutoGNOM was used to generate the pair distribution function ( $P(r)$ ) and to determine  $D_{max}$  and  $R_g$  from the scattering curves ( $I(q)$  versus  $q$ ) in an automatic, unbiased

manner. Theoretical curves from the models were generated by FoXS [297]. Ab initio modelling was performed with GASBOR [298].

#### 18. Yeast two-hybrid

NyxA was cloned into pDBa vector, using the Gateway technology, transformed into MaV203 and used as a bait to screen a human embryonic brain cDNA library (Invitrogen). Media, transactivation test, screening assay and gap repair test were performed as described [299] [300] [301] [302].

#### 19. Stats

All data sets were tested for normality using Shapiro-Wilkinson test. When a normal distribution was confirmed we used a One-Way ANOVA test with a Tukey's correction for multiple comparisons. For two independent variables, a Two-Way ANOVA test was used. For data sets that did not show normality, a Kruskal-Wallis test was applied, with Dunn's correction. All analyses were done using Prism Graph Pad 6.

**Supplementary Table 1. Antibodies used in this study.**

Antibody	Species	Source	Reference	Dilution
SENP3	Rabbit	Cell Signalling	5591	1/400
NVL	Rabbit	Proteintech	16970-1-AP	1/25
RPL5	Rabbit	X		1/100
PES1	Rabbit	ATLAS antibodies	HPA040210	1/100
NPM1	Rabbit	Abcam	Ab37659	1/400
Nucleolin	Mouse	Invitrogen	39-6400	1/100
HA	Rat			1/100
Flag	Mouse	Sigma	F1804 (clone M2)	1/2000
Myc	Mouse	DSHB	(Clone E10)	1/1000
NUFIP1		Proteintech	12515-1-AP	1/50
LAMP1	Mouse	DSHB	(Clone H4A3)	1/200
FK2	Mouse	Enzo	BML-PW8810	1/1000
PML	Rabbit	Abcam	Ab53773	1/500
Western blot				
Actin	Mouse	Sigma	A4700	1/1000
His	Mouse	Sigma	H1029	1/3000
V5	Mouse	Invitrogen	R960-25	1/1000
SENP3	Rabbit	Cell Signalling	5591	1/1000
NPM1	Rabbit	Abcam	Ab37659	1/400
Histone 3	Rabbit	Abcam	Ab8895	1/500
PML	Rabbit	Abcam	Ab53773	1/500
Secondary antibodies				
Donkey anti-mouse AlexaFluor488/555/647		Invitrogen	A-21202/A-31570/A-31571	1/1000
Donkey anti-rabbit AlexaFluor488/555/647		Invitrogen	A-21206/A-31572/A-31573	1/1000
Donkey anti-rat AlexaFluor488/555/647		Invitrogen	A-21208/A-21434/A-21472	1/1000



**Supplementary Table 2. Primers used in this study.**

Purpose		Sequence 5'-3'
pNPTS138-NyxA	Fw1	GATAATGACGCTAGCTTTCA
	Rev1	GGCCACCCGACAAGCAGTTTGGAGGTTTACCTTTTGTGA
	Fw2	TCAACAAAAGGTAAACCTCCAAACTGCTTGTGGGTGGCC
	Rev2	GGGTGTCCTTGAACATCCA
pNPTS138-NyxB	Fw1	TTGGATCAATCCGGCGTGTG
	Rev1	GGGCTTCAACTTCTTTAACCGGCTATTCTTCTGTCAATT
	Fw2	AATTGACAGGAAGAATAGCCGGTTAAAGAAGTTGAAGCCC
	Rev2	CGTAAACGCTTCGGCAGGGA
pFlagTEM1-NyxA	fw	TAAGCATTGGTCTAGAATGAACGCTCACACAAACATAA
	rev	ACTGCAGTTATCTAGATCAAAGCTCCAAGCATCTAATT
pFlagTEM1-NyxB	fw	GAGATAGGTGCCTCACTGATTAAGCATTGGTCTAGAATGAACACGCAAGCAACAATA
	rev	GTGTGCTGGAATTCGCCCTACTGCAGTTATCTAGATCAAGGCATCTCGATAAG
pFlagTEM1-BAB1_0466	fw	TAAGCATTGGTCTAGAATGAAAATGTGGACCTTGC
	rev	ACTGCAGTTATCTAGATCACTGTTCTACGCAGCTTA
pTn7-nyxA	fw	GTGAAATCAATCAACAAAAGGTAAACCTCCatgaacgctcacacaaacataag
	rev	GGAATTCCTGCAGCCCGGGGATCCACTAGtcaagctccaagcatctaatttc
pTn7-nyxB	fw	ATTTAACCGAAATTGACAGGAAGAATAGCCatgaacacgcaagcaacaatag
	rev	GGAATTCCTGCAGCCCGGGGATCCACTAG tcaagcatctcgataaggc
pBBRMCS2 4HA-nyxA	fw	aaaaaaGAGCTCaaggagatatatacatatgTACC
	rev	aaaaaaACTAGTtcaagctccaagcatctaatttc
pBBRMCS2 3Flag-nyxA	fw	TATTCGGGGGATCCATGGGTAAGCCTATCCCTAACCTCTCCTCGGTCTCGATT CTACGAACGCTCACACAAACATAAG
	rev	TATAGGGCGAATTGGAGCTCAAGCTCCAAGCATCTAATTT
pBBRMCS2 4HA-nyxB	fw	aaaaaaGAGCTCaaggagatatatacatatgTACC
	rev	aaaaaaACTAGTtcaagcatctcgataaggc
pDONOR-NyxA	fw	<u>GGGGACAAGTTTGTACAAAAAAGCAGGCTTCAACGCTCACACAAACATAAG</u>
	rev	<u>GGGGACCACTTTGTACAAGAAAGCTGGGTCTAAAGCTCCAAGCATCTAATTTT</u>
pDONOR-NyxB	fw	<u>GGGGACAAGTTTGTACAAAAAAGCAGGCTTCAACACGCAAGCAACAATAGATA</u>
	rev	<u>GGGGACCACTTTGTACAAGAAAGCTGGGTCTAAGGCATCTCGATAAGGCGGATT</u>
Pet151His-NyxA	fw	<b>CACCATGAACGCTCACACAAAC</b>
	rev	TCAAAGCTCCAAGCATCT
Pet151His-NyxB	fw	<b>CACCATGAACACGCAAGCAAC</b>
	rev	CATTATGCTCCCCTGTTGT
NyxA <sup>MAG</sup>	fw	aaaaaaGAGCTCTAAGTGTCTGCCATAGCCGACG
	rev	aaaaaGGATCCtcaagctccaagcatctaatttc
NyxA Y62R	fw	CGATTGGcgaCCTGCCGCTATGATG
	rev	CGGCAGGtcgCCAATCGTAGCAGTCGAAG
NyxA D76R	fw	CCATGAAAcgaCGGGAAGTATCCAATACG
	rev	TTCCCGtctTTTCATGGCGTTGCCTTC
Nyx E78R	fw	CGACGGagaCTGATCCAATACGAAGAGTGGTG
	rev	GGATCAGtctCCGtctgTTTCATGGCG
NyxA <sup>MAG</sup>	fw	aaaaaaGAGCTCTTGGATCAATCCGGCGTGTGC
	rv	aaaaaGGATCCtcaagcatctcgataaggc
SEN3 <sup>7-159</sup>	Fw	CACCATGGCCGGCACCGGTAGCTGGGGTCCGGAACC
	rv	TTTGGATCCTTATTGCTATACAGCAGCATACGAAATGC

**Supplementary Table 2. *Brucella* strains used in this study.**

Strain name	Description/purpose	Genetic features	Resistance
<i>Brucella abortus</i> 2308	Wild-type (obtained from X. de Bolle)	-	Nalidixic acid natural resistance
<i>B. abortus</i> DSRed		pTn7-DSRed	Kanamycin
$\Delta virB9$	Deletion of <i>virB9</i>		
Wt <i>pbla:nyxA</i>	TEM1 translocation	pFlagTEM1-NyxA	Chloramphenicol
$\Delta virB9$ <i>pbla:nyxA</i>	TEM1 translocation	pFlagTEM1-NyxA	Chloramphenicol
Wt <i>pbla:nyxB</i>	TEM1 translocation	pFlagTEM1-NyxB	Chloramphenicol
$\Delta virB9$ <i>pbla:nyxB</i>	TEM1 translocation	pFlagTEM1-NyxB	Chloramphenicol
Wt <i>pbla:BAB1_0466</i>	TEM1 translocation	pFlagTEM1-BAB1_0466	Chloramphenicol
$\Delta nyxA$	Deletion of <i>BAB1_0296</i> ( <i>nyxA</i> )		
$\Delta nyxB$	Deletion of <i>BAB1_1101</i> ( <i>nyxB</i> )		
$\Delta nyxA nyxB$	Deletion of both		
$\Delta nyxA:Tn7-nyxA$	Complemented strain	pTn7- <i>nyxA</i>	Kanamycin
$\Delta nyxA:Tn7-nyxA^{MAG}$	Complemented strain with mutated acidic groove (MAG)	pTn7- <i>nyxA</i> <sup>MAG</sup>	Kanamycin
$\Delta nyxA:Tn7-nyxB$	Complemented strain	pTn7- <i>nyxB</i>	Kanamycin
$\Delta nyxAp4HA-NyxA$	Effector imaging	pBBRMCS2 4HA- <i>nyxA</i>	Ampicilin
$\Delta nyxAp3Flag-NyxA$	Effector imaging	pBBRMCS2 3Flag- <i>nyxA</i>	Ampicilin
$\Delta nyxBp4HA-NyxB$	Effector imaging	pBBRMCS2 4HA- <i>nyxB</i>	Ampicilin

## Chapter III: Discussion and conclusion

During this project, two new bacterial effectors were identified in *Brucella*. NyxA was identified through a bioinformatic screen of the *Brucella abortus* genome, looking for characteristic domains known to be involved in protein-protein interactions, motifs present in other known bacterial effectors or eukaryotic domains. Thus NyxA caught our attention since it exhibited a CAAX motif, however the results presented in this manuscript do not show the exploitation of host prenylation to anchor this effector in different host membranes suggesting that NyxA exhibits a non-functional CAAX motif. Indeed, preliminary data from the lab using HeLa cells were transfected with a plasmid encoding myc-NyxA or myc-NyxA $\Delta$ CLEL, showed no difference in localization between these proteins suggesting that this CAAX motif may not be functional (Figure 50). It remains possible thought that the CLEL motif present in NyxA plays a role in subcellular localization of this effector during infection.

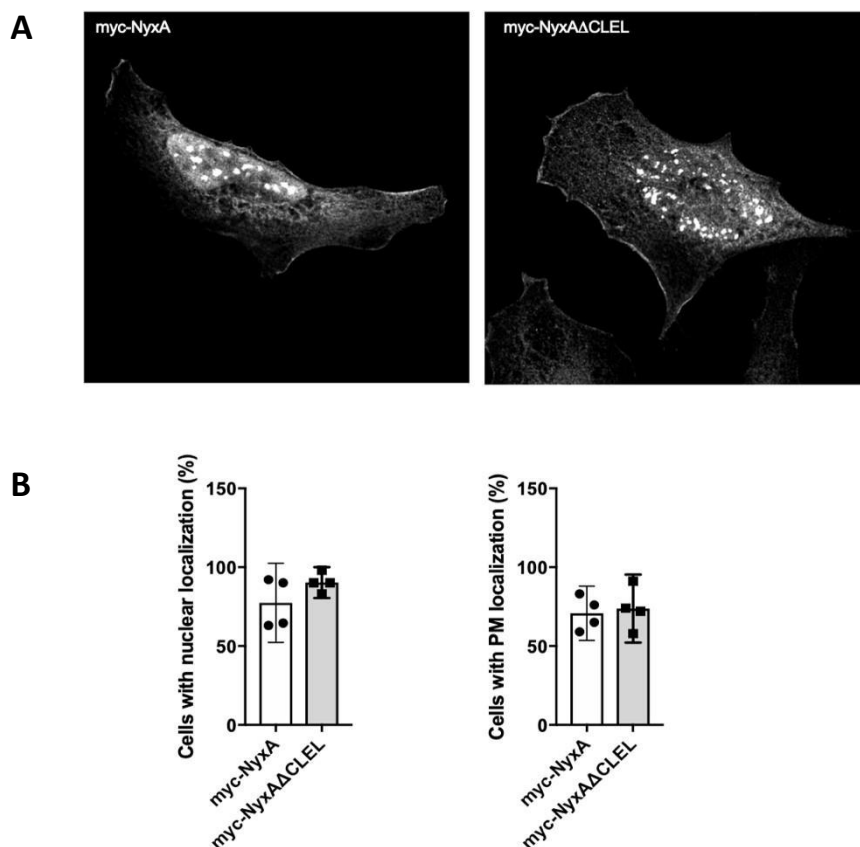


**Figure 50. CAAX motif is not essential for nucleus localization.** A) HeLa cells transiently expressing myc-NyxA or myc-NyxA $\Delta$ CLEL were stained with anti myc antibody to determine their localization. B) Quantification of the percentage of cells with nuclear localization and plasma membrane (PM) accumulation are shown.

Subsequently *nyxB* was identified in the *Brucella* genome encoding for a protein showing 82% identity with the sequence of NyxA. It is somewhat surprising that *Brucella* produces two highly similar effectors, yet this must be advantageous for the bacterium, otherwise during evolution *Brucella* would have lost one of the two genes.

The first step of our study was to confirm that these two potential effectors were translocated in the host cell during infection. For this, a reporter system, TEM1  $\beta$ -lactamase reporter, was used. We found that the translocation of NyxA is dependent on the T4SS present in *Brucella* but this does not seem to be the case for NyxB. This observation is rather surprising and raises many questions. The position of the reporter tag on the N-terminus of the effectors, may interfere with the translocation signal and perturb its association with the T4SS. It would be interesting to reproduce the experiment with constructions where the tag is at the C-terminal end. T4SS-mediated translocation does not present a consensus on the translocation signals in *Brucella*. The C-terminal region of VceC is required for its translocation [106] while the N-terminal region is required for the translocation of BPE123 [104]. The differences between NyxA and NyxB are mainly at the N-terminal end, suggesting that this area is involved in the T4SS support for translocation in the host cell. T4SS has been rendered inactive by mutating the gene coding for VirB9. However, in this background we observed that NyxB is still fully translocated and in fact NyxA is still capable of being translocated into the host cell, albeit to a much lesser extent. It is possible that the *virB9* mutation may not be sufficient to completely inactivate T4SS in *Brucella*. The *Brucella*'s T4SS is not yet fully characterized, and it is mostly based on homology with *Agrobacterium tumefaciens* T4SS. Other T4SS proteins known to lead to a non-functional VirB system such as VirB10 or VirB11 [104] could be mutated, or the entire VirB operon could be deleted. Consistent with our results, several *Brucella* effectors appear to be translocated independently of T4SS (for example, BspD, G, H, I, J, K) [83]. It therefore seems necessary to better characterize the molecular mechanisms involved in the translocation of effector protein in the host cell by the *Brucella* T4SS VirB to determine if an alternative secretion system is contributing. Perhaps NyxA and NyxB, highly similar but with clear translocation mechanisms, could provide an interesting tool to study these questions.

We next sought to observe directly the effectors translocated in the cell by immunofluorescence microscopy. We succeeded with a strain expressing 4HA-NyxA/B, an approach used many times for the observation of numerous effectors in particular in *Legionella* and *Coxiella* [303] [304] by increasing the fluorescence signal.

We observed a cytosolic and nuclear distribution of the effectors in transfection. Nevertheless, 4HA-Nyx as opposed to HA-Nyx is much less frequently found to accumulate in the nucleus suggesting that the 4HA tag disturbs this localization. It seems that this is not a direct consequence of the 4HA tag since 4HA-NopA, an effector of *Coxiella burnetii*, does not present a problem to localize in the nuclei of infected U2OS cells [304]. Consistently, we observed our Nyx effectors during infection using a 4HA tag sporadically localizing in the nucleus. Nonetheless, it is possible that due to its size a 4HA tag masks Nyx domains involved in the translocation from the cytosol to the nucleus. NLS have not been identified in Nyx, but Victor Cid's team have shown in yeast that the import of these effectors is active and dependent on the alpha-importin encoded by the SRP1 gene in yeast (figure 51), suggesting either that Nyx present NLS that are not identified to date or that they interact with proteins presenting functional NLS allowing them to reach the nucleus.

We believe that both observed localizations (cytosolic and nuclear) are relevant, suggesting that Nyx must either shuttle between cytosol and nucleus or it is a sequential mechanism with a first step in the cytosol before being imported into the nucleus. Further work will be needed to understand the mechanisms and kinetics for the nuclear import of these effectors.

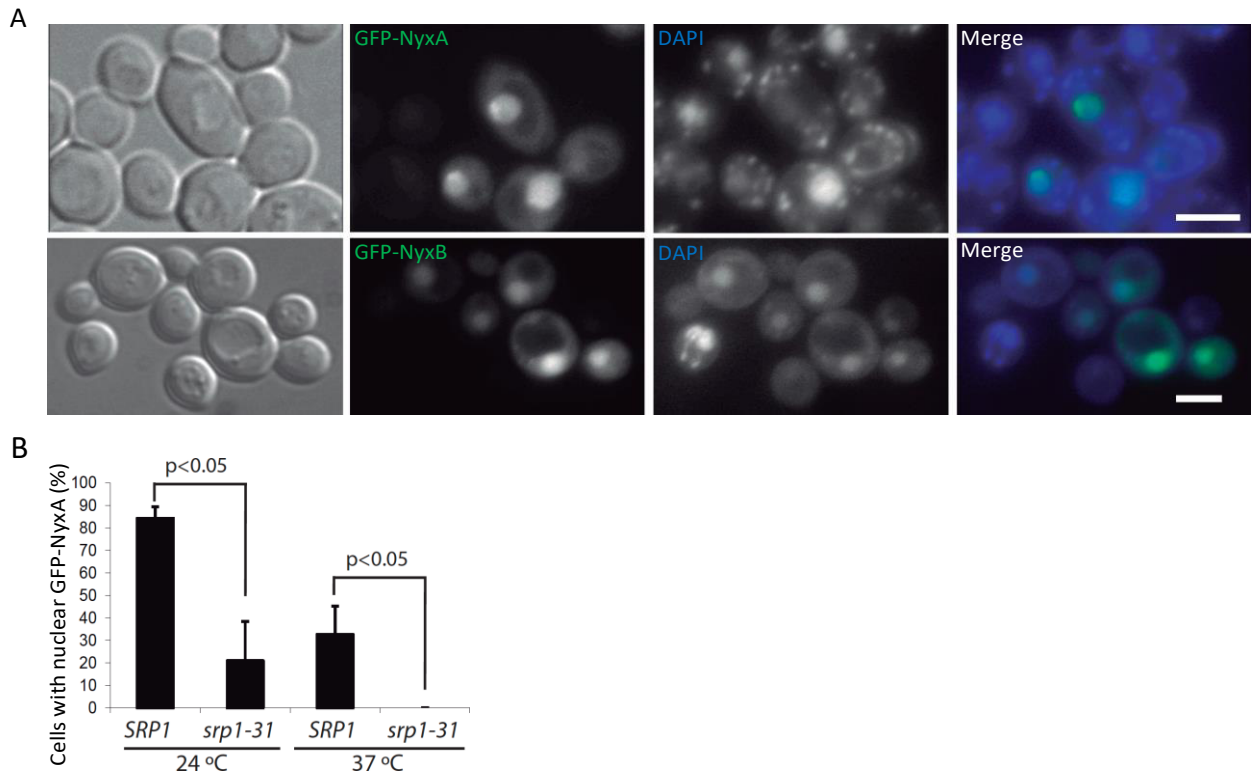


**Figure 51 : NyxA and NyxB are targeted to the yeast nucleus in an alpha importin-dependent manner.**

A) Transformants of YPH499 strain with either pYES2-GFP-NyxA or pYES2-GFP-NyxB, as indicated, were incubated in synthetic galactose medium for 6 h, stained with DAPI and observed. Cells expressing GFP-NyxA/B fusion proteins had a signal coincident with DAPI-stained nuclei. B) Srp1 function is required for nuclear localization of NyxA. Transformants of the W303 (SRP1) or thermosensitive isogenic JCY1410 (*srp1-31*) strains with pYES2-GFP-NyxA were incubated for 6h at 24 °C or shifted for 1 h to 37 °C after 5 h of incubation, as indicated. Cells with nuclear fluorescence in the population were counted (n > 100) and expressed as percentage. Data are the average of three individual transformant clones. Bars indicate the standard deviation. A student t-test was performed for statistical significance. Data from Victor Cid's lab.

Biochemistry experiments have shown that NyxA and NyxB are able to interact together and form dimers in solution. Nevertheless we could not establish the stoichiometry of this interaction. Is there formation of heterodimer or heterotetramer (figure 52)? Further

experiments in Isothermal Calorimetric Titration (ITC), MicroScale Thermophoresis (MST) and SEC-MALLS could give us indications on the formation of this complex.

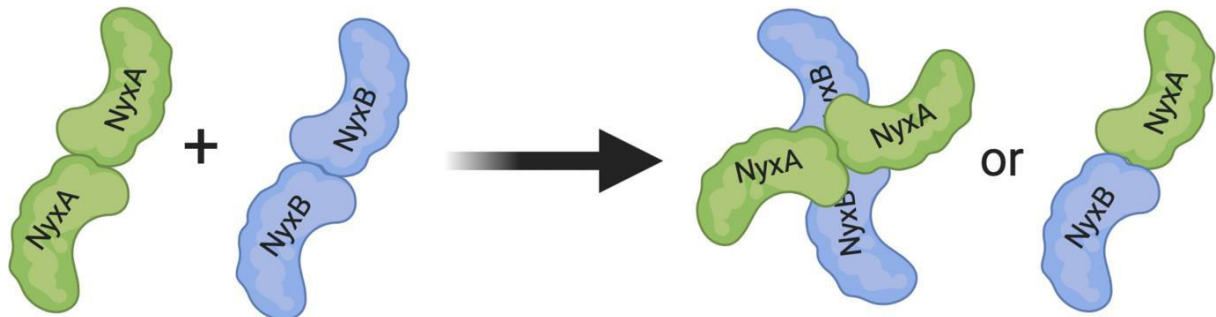


**Figure 52 : Illustration of the potential assembly between NyxA and NyxB**

Moreover, does the NyxA or NyxB dimer play a physiological role? For that, I have made a series of constructs intended to break this dimer by mutating the residues involved in dimerization (Y93A, E132K). Preliminary results of the visualization of these constructions by microscopy do not show an impact on the relocation of SENP3 in transfection. Nevertheless, it would be necessary to purify these constructs and perform SEC-MALLS experiments to confirm that the protein is no longer able to form dimers in solution.

We have seen that in transfection, the NyxA/B protein is localized at the level of the PML nuclear bodies. Work in our lab has found that other *Brucella* effectors also show this localization: SerB and BspJ (figure 53). It is known that PML nuclear bodies have a role in antiviral and antibacterial defense. Thus *Brucella*, by targeting PML nuclear bodies, could modulate the host's immune response and this is something we still need to investigate. Work is currently being undertaken in the laboratory by Amandine Blanco to understand the role of PMLs in *Brucella* infection. My co-precipitation experiments have shown that Nyx do not interact with PML under our laboratory conditions, which could have explained its localization. To date, all proteins present within PMLs have the characteristic of being SUMOylated. Our *in vitro* studies suggest Nyx are not covalently conjugated with SUMO2/3, however we cannot exclude that they are SUMOylated by SUMO1, SUMO4 or SUMO5. Moreover, NyxA and NyxB present several potential SIM motifs that could explain the recruitment of these effectors at



the level of PML nuclear bodies. We have recently obtained a SUMO2 expressing stable cell line that will allow us to determine by co-immunoprecipitation in ectopically expressed NyxA and NyxB are SUMOylated.

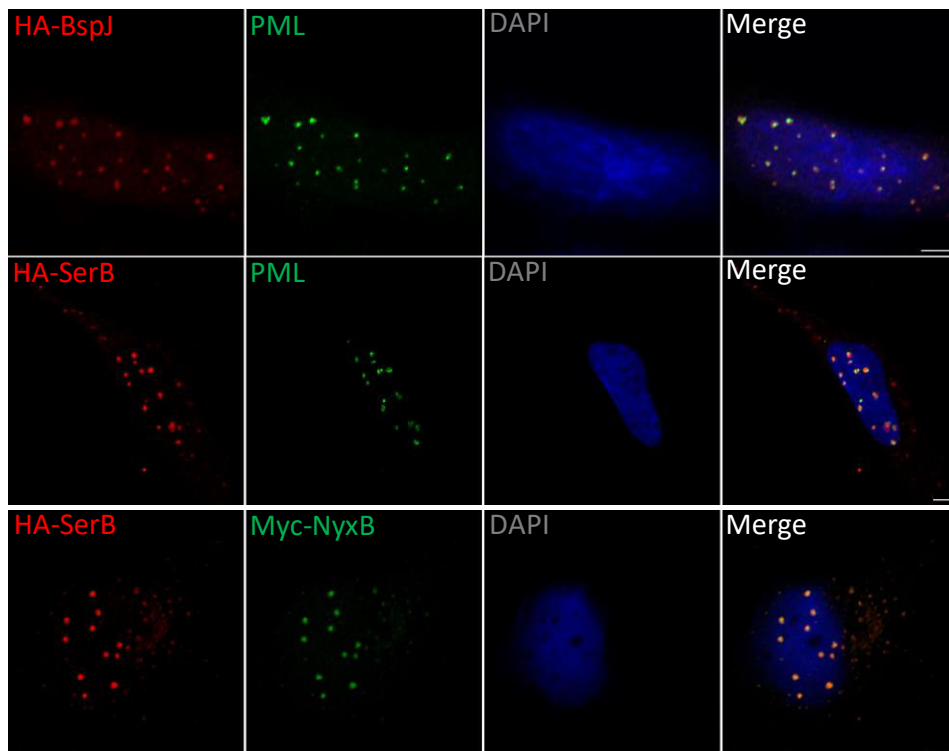


**Figure 53 : Ectopically expressed SerB and BspJ are associated with PML-nuclear bodies like Nyx.** HeLa cells were transfected 18h with either HA-BspJ, HA-SerB or co-transfected with HA-SerB and Myc-NyxB and labelled with anti-PML antibody (green). All microscopy images displayed have scale bars corresponding to 5  $\mu$ m. Images from Emilie Mills, Erasmus student in the lab.

We have identified SENP3 as the eukaryotic target of our two effectors. Moreover, the analysis of the crystallographic structure of NyxB allowed us to identify a pocket of interaction. Thus we confirmed this interaction by co-precipitation experiments with purified NyxA and NyxB against the N-terminal domain of SENP3. We were not able to purify the entire protein or the C-terminal domain, so we cannot exclude that the Nyx effectors do not interact with the C-terminal domain of SENP3. It would have been interesting to be able to carry out measurements of affinity constant between Nyx and SENP3 as well as Nyx mag and SENP3, in order to show a decrease or an abolition of the formation of this complex.

The pocket of interaction observed thanks to the crystallographic structure corresponds to a large acidic domain present on Nyx allowing the interaction with an arginine rich domain present on SENP3 at the level of the NoLS domain. It is at the level of this domain that mTOR phosphorylates SENP3, which allows it to translocate into the nucleoli and to interact with NPM1. It is interesting to note that this interaction between Nyx and SENP3 seems to be similar to that between SENP3 and NPM1. Indeed, NPM1 presents an acidic domain involved in the interaction with the arginine-rich motif of SENP3 [268]. Thus, the interaction between SENP3 and Nyx could mask the domain of interaction with NPM1 but this seems unlikely as we are able to pull-down NPM1 with purified Nyx effectors. It is even more likely that Nyx interactions would mask the mTOR phosphorylation residues of SENP3. Indeed, it seems that the phosphorylation of SENP3 is not necessary for the interaction with Nyx, since the interaction with the purified recombinant proteins of Nyx and the N-terminal domain of SENP3 is observed. Thus NyxA/B would interact with SENP3 upstream of mTOR phosphorylation thus preventing its nucleolar localization.

In order to understand the role of these effectors in the cell we expressed ectopically in HeLa cells the Nyx as well as Nyx mag in which the interaction pocket with SENP3 was mutated. We observe that Nyx are able to recruit SENP3, displacing it from its natural nucleoli localization, and recruitment is dependent on the acidic domain identified on the Nyx. The same observations could be made in infection, especially for NyxA.

To date we do not really understand the interest of *Brucella* to produce two highly similar proteins. We have observed that NyxA always shows a stronger impact on the phenotypes of SENP3 delocalization, in comparison to NyxB. Furthermore, the effects of NyxA and NyxB are not cumulative consistent with their observed interaction *in vitro*. One possibility is that NyxA by interacting with NyxB could increase its interaction with SENP3 and this would give NyxB a role of chaperone protein for NyxA.

To add to the complexity of these phenotypes, we observed that BspJ ectopically expressed in HeLa cells, was also able to delocalize SENP3, although less than Nyx, however BspJ does not recruit SENP3 (results not shown) unlike both Nyx effectors. In addition, we observed that

cells infected with a mutant strain lacking NyxA still have significant SENP3 displaced from nucleoli. These observations suggest that Nyx may act in concert with other *Brucella* effectors such as BspJ and SerB. Consistent with these results, deletion of NyxA and NyxB alone does not impact *Brucella* intracellular replication, however we saw that in cells in which we turned off the expression of SENP3 *Brucella* had a replication defect, highlighting the key role of SENP3 during infection. It would be interesting to observe the impact on the localization of SENP3 and *Brucella*'s ability to replicate when HeLa cells are infected with strains in which the genes encoding all four effectors, NyxA, NyxB, BspJ, and SerB are mutated.

In addition to the delocalization of SENP3 from nucleoli, our study also established that the cytosolic punctiform structures containing translocated Nyx effectors are enriched in NVL, RPL5 and NUFIP1. NVL is an AAA-ATPase that localizes in nucleoli following its interaction with RPL5 and participates in ribosome synthesis [54]. During infection of HeLa cells or BMDMs by *Brucella* we observed a relocation of NVL from the nucleus into punctiform structures of the cytosol, partially dependent on NyxA and NyxB. It seems that NyxA/B is not the only one responsible for this delocalization and that something else during the infection allows it, it would be interesting to observe if SerB and BspJ could also be involved in this phenotype. These quantifications of the cytosolic structures of NVL were made for the wild type strain and the mutant strain lacking the genes encoding *nyxA* and *nyxB*. Nevertheless, it would be very important to quantify the cytosolic structures of NVL when cells are infected with *nyxA* or *nyxB* mutant *Brucella* strains that have been complemented with either *nyxA/B* wild type or *nyxA/B* mag. This would allow us to confirm that this phenotype is directly dependent on Nyx interaction with SENP3.

During my thesis, we thought that this was the first time that NVL was observed in cytosolic structures. A study published in the summer of 2020 presented for the first time NVL outside the nucleus, in the cytosol. The authors established that NVL was involved in the absorption of albumin. Absorption of albumin involves a multi-ligand receptor complex called CUBAM containing cubulin (CBN) and amnionless (AMN). Although the mechanisms of albumin endocytosis are not fully characterized, the authors observed that NVL interacts with AMN.

They observed that the co-expression of NVL and AMN in cells led to the delocalization of NVL from nucleoli to a cytosolic compartment and that the abolition of NVL expression greatly altered albumin internalization, revealing a new function of NVL in endocytic regulation [305]. However, cytosolic NVL was only observed under when AMN was over-expressed and authors did not analyze endogenous NVL in these conditions. It would be interesting to observe whether this role of NVL in endocytic regulation is involved in *Brucella* infections.

We have also hypothesized that these cytosolic structures could correspond to autophagy. More generally, autophagy is a ubiquitous degradation mechanism orchestrated by more than 30 specific proteins called ATGs (autophagy-related genes) (Figure 54) [306]. It is a dynamic membrane process that begins with the *de novo* formation of vacuoles called autophagosomes encompassing cytoplasmic fractions. The degradation of the sequestered material also called the cargo occurs after fusion of the autophagosomes with the lysosomes, in vacuoles called autolysosomes. Autophagy has multiple functions within the cell. It removes damaged or non-functional components and recycles nutrients to maintain homeostasis. In particular, it is a fundamental process in the host's response to infection by pathogens, involved in both innate and adaptive immune responses. This defense mechanism can be countered or used by intracellular microorganisms for their own multiplication. First of all, membrane supply via autophagy is very often beneficial for both bacteria and viruses. Because of their inability to replicate in an acidic environment, these microorganisms block, at least partially, the maturation stage of autophagosomes. *Coxiella burnetii* for example, which can survive at acidic pH, uses autophagy for optimal development of its replicative vacuole. Several studies have implicated autophagy at different stages of *Brucella* trafficking. The YipA protein that localizes at the site where formation of rBCVs is initiated, is necessary for rBCV formation. This process is dependent on Atg9 and WIP1 [307]. In addition, multi-membrane BCVs capable of incorporation of monodansyl cadaverine, a marker of autophagosomes, have been described in epithelial cells [54] [55]. At the late stages of the trafficking, autophagic vacuoles are formed that mediate bacterial exit from infected cells. Current data converge towards a model where there is a very selective hijacking of autophagy components at different stages of BCV maturation, with dependency on Atg9 and WIP1 for rBCVs [307] and

ULK and Beclin-1 for aBCVs [90]. Consistently, inhibition of a large panel of components involved in autophagosome nucleation and elongation did not prevent rBCV formation [90].

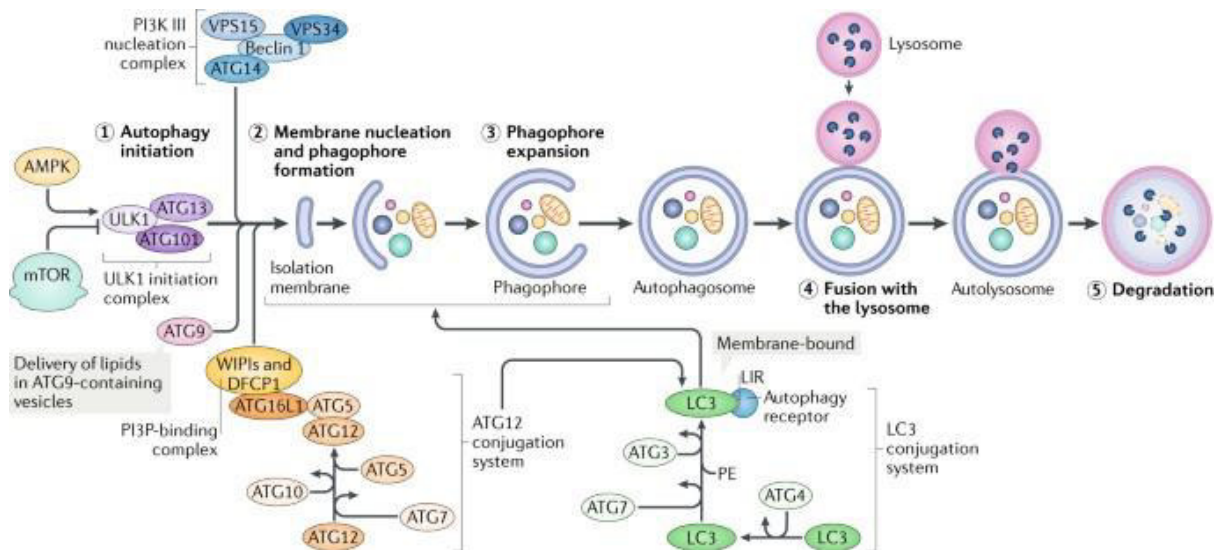


**Figure 54 : General schema of autophagy. [306]**

More recently, it has been shown that autophagy is a catabolic pathway conserved over time involved in the degradation of proteins, organelles or molecular complexes. Thus, the concept of selective autophagy has emerged, where we can find ribophagy leading to ribosome degradation, ER phagy leading to ER degradation or proteaphagy for the degradation of defective proteasomes ... [308]. Each of these selective autophagy processes will be initiated according to different stresses involving particular signals for the recognition of cargoes by different receptors.

Thus, our study revealed that *Brucella*-infected cells present NUFIP1 in cytosolic structures corresponding to NyxA/B, NVL and RPL5. NUFIP1 is a receptor for selective autophagy of ribosomes, a nuclear protein that is delocalized in the cytosol when ribophagy is induced. In humans, ribophagy leads to the degradation of the small and large ribosomal subunit. It is triggered by various stresses: starvation, inhibition of mTOR by Torin1, sodium arsenite, oxidative stress such as oxygen peroxide or reversin, an inhibitor of MPS1 that leads to protein imbalance due to poor chromosomal segregation [309]. In human cells the loss of NUFIP1 leads to an inability of the cell to degrade ribosomes following starvation. During the response

to starvation NUFIP1 changes location. In the cytoplasm, NUFIP1 will bind to the ribosome and deliver its cargo to the autophagic vesicle by binding to LC3B through its LC3 Interaction Region (LIR) [287].

The presence of the RPL5 ribosomal protein of the large subunit 60S in these cytosolic structures reinforces the idea that we are dealing with ribophagy. We could also label other ribosomal proteins such as RPS3 associated with the 40S subunit or RPL28 which is associated with the 60S subunit and observe by confocal microscopy whether they colocalize with NUFIP1, NyxA/B or NVL. On the other hand, the presence of NVL and NyxA/B are rather surprising since they are not associated with ribosomes. It is interesting to note that NVL has several potential LIR sequences and NyxA/B also has one. Furthermore, it would be interesting to select infected cells expressing 4HA-NyxA/B using a cell sorter and to perform co-immunoprecipitation using an anti-HA resin to purify these NyxA/B /RPL5/NVL/NUFIP1 structures and to perform mass spectrometry in order to identify other associated proteins.

Quantification of the number of NUFIP1 present in the cytosol of cells infected with wild *Brucella* and the NyxA/B mutated strain will strengthen our hypothesis that NyxA/B may be ribophagy regulators. However, we do know that NyxA/B are not ribophagy activators since HeLa cells expressing NyxA/B do not present cytosolic NUFIP1. It is possible that *Brucella* infection causes a kind of starvation that activates the ribophagy. It would be interesting to measure the nutrient status of cells infected with either wild-type or *nyxA/nyxB* mutants.

Starvation-induced ribophagy provokes nucleolar delocalization of SENP3. Recently a study showed that SENP3 regulates autophagy by desumoylating beclin1 (BECN1). Cells not expressing SENP3 show an accumulation of LC3B due to increased autophagosome formation. BECN1 is required for the initiation of autophagy. BECN1 forms a complex with PIK3C3 important for autophagosome formation. SUMOylation of BECN1 on K380 promotes interaction with PIK3C3 accelerating autophagosome formation. On the other hand, SENP3 deSUMOylate BECN1 which weakens the interaction with PIK3C3 leading to a decrease in the formation of autophagosomes. According to the authors, when starvation occurs, SENP3 accumulates in the cytosol, allowing it to interact with BECN1. As a result, SENP3 can

negatively regulate autophagy [310]. It seems that SENP3 is a kind of a guard to prevent the cell from digesting too much. So far, I have never been able to observe SENP3 in the cytosol. Perhaps by using their labeling protocol we will be able to observe if SENP3 is also present in the cytosol in the vicinity of NUFIP1 in a NyxA/B dependent manner. Nyx potentially sequester SENP3 in the nucleoplasm and thus prevent the negative regulation of SENP3 on the ribophagy. Thus, SENP3 could be a specific regulator of ribophagy. The fact that the observed structures are LAMP1 negative suggests that fusion with lysosomes does not occur or that the observation at 48h post infection is too early for these structures to be LAMP1 positive, it would be interesting to perform further kinetics. *Brucella* may also divert ribophagosomes to obtain nutrients and membrane. How can BCV recruit these structures? How can *Brucella* metabolize ribosomes? Currently we cannot totally exclude that potentially these NUFIP1 positive structures do not correspond to ribophagy, experiments are in progress to confirm this.

During my thesis, I also spent time setting up an iBMDM infection protocol with *Brucella*, in order to obtain a maximum of infected cells. The objective was then to perform a mass spectrometry SUMOscan to obtain the SUMOyloma of *Brucella* WT versus *Brucella nyxAnyxB* infected cells. Unfortunately, I did not have time to perform this experiment, one can imagine that BECN1 would have emerged from this screening, as well as many other proteins.

In conclusion, we have identified two novel *Brucella* effectors that target SENP3 and induce the relocation of this nucleolar protein during infection. We propose that the SENP3 interaction leads to the induction of ribophagy, visible with the appearance of cytosolic structures enriched in NUFIP1, NVL, RPL5, and the two Nyx *Brucella* effectors that may allow replicative *Brucella*-containing vacuoles to obtain nutrients or membranes while promoting cell survival. NyxA and NyxB can act as positive regulators of ribophagy by diverting SENP3, which normally acts as a negative regulator of ribophagy. In addition, our work suggests that NVL is potentially a novel ribophagy marker.





# ANNEXES

1. Annexe 1: The TIR Homologue Lies near Resistance Genes in *Staphylococcus aureus*, Coupling Modulation of Virulence and Antimicrobial Susceptibility

Patot et al PLoS Pathogens 2016

In this manuscript we highlighted a role of the *S. aureus* TIR protein TirS, present on a chromosomal cassette containing multiple antibiotic resistance genes, on the control of virulence. In addition, this was the first study to show upregulation of a TIR protein upon antibiotic treatment and an epidemiological link with enhanced success of bacterial spread. My contribution was on the evaluation of the intracellular localization of TirS in transfected cells and attempts to express and purify TirS in *E. coli* for *in vitro* assays.

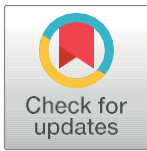
RESEARCH ARTICLE

# The TIR Homologue Lies near Resistance Genes in *Staphylococcus aureus*, Coupling Modulation of Virulence and Antimicrobial Susceptibility

Sabine Patot<sup>1</sup>, Paul RC Imbert<sup>2</sup>, Jessica Baude<sup>1</sup>, Patricia Martins Simões<sup>1</sup>, Jean-Baptiste Campergue<sup>3</sup>, Arthur Louche<sup>2</sup>, Reindert Nijland<sup>4,5</sup>, Michèle Bès<sup>1,3</sup>, Anne Tristan<sup>1,3</sup>, Frédéric Laurent<sup>1,3</sup>, Adrien Fischer<sup>6</sup>, Jacques Schrenzel<sup>6</sup>, François Vandenesch<sup>1,3</sup>, Suzana P Salcedo<sup>2</sup>, Patrice François<sup>6</sup>, Gérard Lina<sup>1,3\*</sup>

**1** CIRI, Centre International de Recherche en Infectiologie, Inserm U1111, Université Lyon 1, Ecole Normale Supérieure de Lyon, CNRS UMR 5308, Lyon, France, **2** Laboratory of Molecular Microbiology and Structural Biochemistry, University of Lyon, CNRS UMR5086, Lyon, France, **3** Centre National de Référence des Staphylocoques, Hospices Civils de Lyon, Lyon, France, **4** Medical Microbiology, University Medical Center Utrecht, Utrecht, The Netherlands, **5** Laboratory of Phytopathology, Wageningen University, Wageningen, The Netherlands, **6** Genomic Research Laboratory, University of Geneva Hospitals, Geneva, Switzerland

\* [gerard.lina@univ-lyon1.fr](mailto:gerard.lina@univ-lyon1.fr)



**OPEN ACCESS**

**Citation:** Patot S, RC Imbert P, Baude J, Martins Simões P, Campergue J-B, Louche A, et al. (2016) The TIR Homologue Lies near Resistance Genes in *Staphylococcus aureus*, Coupling Modulation of Virulence and Antimicrobial Susceptibility. PLoS Pathog 12(12): e1006092. doi:10.1371/journal.ppat.1006092

**Editor:** Alice Prince, Columbia University, UNITED STATES

**Received:** June 20, 2016

**Accepted:** November 28, 2016

**Published:** December 29, 2016

**Copyright:** © 2016 Patot et al. This is an open access article distributed under the terms of the [Creative Commons Attribution License](https://creativecommons.org/licenses/by/4.0/), which permits unrestricted use, distribution, and reproduction in any medium, provided the original author and source are credited.

**Data Availability Statement:** ENA database project study accession number PRJEB12840; sample accessions ERS1070204 to ERS1070207 and ERS1434451, ERS1434452.

**Funding:** This work was supported by the LABEX ECOFECT (ANR-11-LABX-0048) of Université de Lyon, within the program "Investissements d'Avenir" (ANR-11-IDEX-0007) operated by the French National Research Agency (ANR) and a FINOVI Young Researcher Grant and by the Swiss

## Abstract

Toll/interleukin-1 receptor (TIR) domains in Toll-like receptors are essential for initiating and propagating the eukaryotic innate immune signaling cascade. Here, we investigate TirS, a *Staphylococcus aureus* TIR mimic that is part of a novel bacterial invasion mechanism. Its ectopic expression in eukaryotic cells inhibited TLR signaling, downregulating the NF-κB pathway through inhibition of TLR2, TLR4, TLR5, and TLR9. Skin lesions induced by the *S. aureus* knockout *tirS* mutant increased in a mouse model compared with wild-type and restored strains even though the *tirS*-mutant and wild-type strains did not differ in bacterial load. TirS also was associated with lower neutrophil and macrophage activity, confirming a central role in virulence attenuation through local inflammatory responses. TirS invariably localizes within the staphylococcal chromosomal cassettes (SCC) containing the *fusC* gene for fusidic acid resistance but not always carrying the *mecA* gene. Of note, sub-inhibitory concentration of fusidic acid increased *tirS* expression. Epidemiological studies identified no link between this effector and clinical presentation but showed a selective advantage with a SCC*mec* element with SCC *fusC/tirS*. Thus, two key traits determining the success and spread of bacterial infections are linked.

## Author Summary

Pathogenic microbes have evolved elaborate strategies to manipulate host defenses to establish and spread in the host population. One such mechanism involves disruption of the immune signaling cascade orchestrated by the Toll-like receptors (TLRs), which sense

National Science Foundation grant 31003A\_153474. SP was supported by the Innovative Medicines Initiative Joint Undertaking under the Combatting Bacterial Resistance in Europe (COMBACTE) grant agreement no. 115523. The funders had no role in study design, data collection and analysis, decision to publish, or preparation of the manuscript.

**Competing Interests:** The authors have declared that no competing interests exist.

microbial attack. TLR signaling elicits a proinflammatory response that controls immune cell recruitment to infected tissues. Here, we show that *Staphylococcus aureus*, an opportunistic human pathogen, expresses a host defense-like protein, TirS, that actively perturbs the initial TLR activation stage. Results with isolated human cells and mouse models show that TirS is a broad innate immune inhibitor of TLR-dependent signaling and modulates bacterial virulence, attenuating local inflammation. Moreover, the *tirS* gene lies near antimicrobial resistance genes for an antibiotic that enhances TirS production, shifting the balance to favor the pathogen and promote disease. Understanding mechanisms by which *S. aureus* modulates the immune response may lead to novel approaches for preventing and treating infection.

## Introduction

The innate immune system constitutes the first line of host defense against invading microbial pathogens in multicellular organisms. Key components of the innate immune response are pattern recognition receptors, which recognize a wide range of conserved bacterial structures, collectively called pathogen-associated molecular pattern and initiate an intracellular signaling immune cascade [1]. The Toll-like receptor/interleukin (IL)-1 receptor (TLR/IL-1R) superfamily, which comprises Toll-like receptors (TLRs) and interleukin-1 receptors (IL-1Rs), is required for many host innate immune responses and characterized by the presence of Toll/interleukin-1 receptor (TIR) domains cytoplasmically located on each TLR [2]. The TIR domain is critical for protein-protein interactions between TLRs with the corresponding TIR-containing adaptors. These interactions activate specific transcription factors such as nuclear factor- $\kappa$ B (NF- $\kappa$ B), which regulates the expression of various inflammatory mediators [3,4]. The TIR domain therefore plays a pivotal role in signaling from these receptors, and their importance in immune regulation has made them the subject of intense study.

The TLR signaling pathway is a key target of pathogen mechanisms of host immune system evasion [4]. Indeed, microbes can target various levels of the TLR signaling pathway, from modification of pathogen-associated molecular patterns to modifications in the immune signaling cascade. A potential host evasion mechanism involving TLRs came to light with the identification of bacterial TIR homologues. The majority of studies on bacterial TIR proteins have focused on their potential role as virulence factors that directly subvert host TLR signaling. For example, TIR-like protein A (TlpA) from *Salmonella enterica* serovar Enteritidis reduces NF- $\kappa$ B activation by a TLR4, IL-1R, and MyD88-dependent pathway and modulates IL-1 $\beta$  secretion during infection [5]. TcpC in the uropathogenic *Escherichia coli* CFT073 and Btp1/BtpA/TcpB in *Brucella* species suppress TLR2- and TLR4-mediated activation of NF- $\kappa$ B by targeting MyD88 [6,7]. A second TIR-containing protein in *Brucella* ssp. (BtpB) was reported to be a potent inhibitor of TLR signaling, probably via MyD88 as well [8].

The presence of a putative TIR-domain-containing protein in *Staphylococcus aureus* was suggested through a data search analysis [5] before being recently confirmed [9]. *S. aureus* is an important human pathogen that causes a wide variety of community and healthcare-associated infections [10]. This bacterium has a proven ability to adapt to the selective pressure of antibiotics. *S. aureus* was initially methicillin-sensitive (MSSA) but isolates resistant to this antibiotic were identified soon after its introduction (MRSA, or methicillin-resistant *S. aureus*) [11]. *S. aureus* becomes resistant to methicillin mainly by the acquisition of the methicillin-resistant gene *mecA*, which occurred first in hospital settings and now takes place in the community and in livestock [12,13]. The *mecA* gene is carried on a particular class of mobile

genetic elements prevalent in staphylococci, the staphylococcal chromosomal cassette (SCC), designated as *SCCmec* [14]. Askarian et al. [9] characterized the TIR domain protein TirS in the *SCC<sub>476</sub>* element of the methicillin-susceptible *S. aureus* strain MSSA476. *SCC<sub>476</sub>* is integrated at the same site on the chromosome as *SCCmec* elements in MRSA [15]. TirS interferes with the TLR2-induced MAPK and NF- $\kappa$ B signaling pathway and enhances bacterial survival within the host [9].

In the present work, we report that TirS is spread among 12% of MRSA and MSSA strains. In an attempt to describe the genetic context of *tirS* (for staphylococcal TIR gene) in *S. aureus*, we fully sequenced the SCC element of representative bacterial strains. In all MRSA and MSSA lineages, the *tirS* gene was invariably located within this mobile genetic element and co-located with the *fusC* and *mecA* (for the MRSA strains) antibiotic resistance genes. Interestingly, our results show that sub-inhibitory concentration of fusidic acid induced overexpression of *tirS*. We also confirm previous findings that *tirS* expression induces a negative regulation of the TLR signaling pathway. Our results with a mouse model of skin infection support that TirS modulates bacterial virulence through attenuation of host inflammatory responses during infection. This work is the first description of a TIR homolog protein carried by a mobile genetic element conferring resistance to antibiotics, suggesting a potential selective advantage. Indeed, these features may contribute to the ability of *S. aureus* to survive and establish a critical population size.

## Results

### *tirS* distribution and molecular epidemiology in *S. aureus* lineages

To assess the prevalence of *tirS* in various MRSA and MSSA lineages, a series of 226 well-characterized clinical isolates from more than 27 clonal complexes (CCs) or sequence types were subjected to *tirS*-specific PCR. Among the 226 strains examined, 28 (12.4%) yielded positive *tirS* amplification (Table 1). *tirS* was detected in MRSA and MSSA strains belonging to only 3 CCs: CC1, CC5, and CC8. In detail, the *tirS* gene was detected in 18/18 MRSA strains, CC5 Geraldine clone; 1/6 MRSA strains, CC5 pediatric clone; 1/2 MRSA strains, CC1; 6/9 MSSA strains, CC1; and 2/10 MSSA strains, CC8. Of further interest was our finding of a perfect association between *tirS* gene amplification and the MRSA Geraldine clone.

We next examined the molecular epidemiology of *tirS* in human staphylococcal infections. *S. aureus* strains were isolated from clinical specimens of individuals presenting skin and soft tissue infections, community-acquired pneumonia, bacteremia, infective endocarditis, or nasal colonization (asymptomatic bacterial carriage). No significant association was detected between specific disease and the presence of *tirS*. Among the 28 *tirS*-positive clinical samples, 10 were isolated from healthy patients (asymptomatic portage; 36%), 8 from patients with cutaneous infection (29%), 5 from patients with pneumonia (18%), 3 from patients with osteomyelitis (11%), 1 from a patient with bacteremia (4%), and 1 from a patient with infective endocarditis (4%).

### Genomic context of the *tirS* gene in MRSA and MSSA

Because the *tirS* gene was previously described on a staphylococcal chromosomal cassette *SCC<sub>476</sub>* [9], we performed whole-genome shotgun sequencing of six representative MRSA and MSSA strains positive for the presence of the *tirS* gene. These included four MRSA lineages: the prototype Geraldine clone strain HT20030749 (CC5; *SCCmec* I), strain ST20120331 (CC5, *SCCmec* IV), and strains ST20121850 and ST20130096 (CC1; *SCCmec* V *fusC*+) (ENA database project study accession number PRJEB12840; sample accessions ERS1070204 to ERS1070207). Two MSSA strains *tirS*-positive were also added to the study: strain ST20110167 (CC1) and

**Table 1. Distribution of *tirS* gene among MSSA and MRSA clinical strains.**

CC/ST <sup>ab</sup>	SCCmec <sup>bc</sup>	Clone name <sup>b</sup>	No. of strains tested	No. of positive PCR tests for <i>tirS</i> /no. of strains tested (%) <sup>d</sup>	
CC1	-	NA	9	6/9 (67)	
	IV	USA400	2	0/2 (0)	
	IV	WA MRSA-1/57	2	0/2 (0)	
	V	Bengal Bay/WA MRSA-60	2	0/2 (0)	
	V	Other	2	1/2 (50) *	
CC5	-	NA	9	0/9 (0)	
	<b>I</b>	<b>Geraldine</b>	<b>18</b>	<b>18/18 (100) *</b>	
	IV	Pediatric	6	1/6 (16) *	
	VI	New pediatric	2	0/2 (0)	
	V	WA MRSA-11/80	2	0/2 (0)	
	II	New York Japan	1	0/1 (0)	
	II	EMRSA-3/Rhine-Hesse	3	0/3 (0)	
CC8	-	NA	6	2/6 (40)	
	I	North German/Iberian	3	0/3 (0)	
	I	Ancestral	2	0/2 (0)	
	III	Vienna/Hungarian/Brazilian	2	0/2 (0)	
	IV	Lyon /EMRSA-2	6	0/6 (0)	
	IV	EMRSA-14/WA MRSA-5	2	0/2 (0)	
	IV	USA300	4	0/4 (0)	
	IV	Other	2	0/2 (0)	
	IV	MRSA-44	2	0/2 (0)	
	IV	USA700	2	0/2 (0)	
	V	MRSA-91	1	0/1 (0)	
	CC6	IV	WA MRSA 51	2	0/2 (0)
	CC9	-	NA	1	0/1 (0)
CC10	-	NA	1	0/1 (0)	
CC12	-	NA	3	0/3 (0)	
CC15	-	NA	5	0/5 (0)	
CC20	-	NA	2	0/2 (0)	
CC22	-	NA	8	0/8 (0)	
	IV	EMRSA-15/Barnim/Middle Eastern	5	0/5 (0)	
CC30	-	NA	20	0/20 (0)	
	IV	Southwest pacific	3	0/3 (0)	
ST34	-	NA	4	0/4 (0)	
ST36	II	EMRSA-16	2	0/2 (0)	
CC45	-	NA	8	0/8 (0)	
	IV	Berlin	2	0/2 (0)	
	IV	Other	2	0/2 (0)	
CC59	-	NA	3	0/3 (0)	
	IV	USA1000	2	0/2 (0)	
	V	Taiwan	2	0/2 (0)	
	V	Other	1	0/1 (0)	
CC80	IV	European	4	0/4 (0)	
CC88	IV	WA MRSA-2	2	0/2 (0)	
	V	Other	2	0/2 (0)	
ST93	IV	Queensland Clone	2	0/2 (0)	
CC97	-	NA	5	0/5 (0)	

(Continued)

Table 1. (Continued)

CC/ST <sup>ab</sup>	SCCmec <sup>bc</sup>	Clone name <sup>b</sup>	No. of strains tested	No. of positive PCR tests for <i>tirS</i> /no. of strains tested (%) <sup>d</sup>
CC121	-	NA	5	0/5 (0)
CC130	XI	MRSA-XI	2	0/2 (0)
CC152	-	NA	5	0/5 (0)
CC182	-	NA	3	0/3 (0)
ST188	-	NA	2	0/2 (0)
ST398	-	NA	9	0/9 (0)
	IV	LA-MRSA	4	0/4 (0)
ST1755	-	<i>mecC</i> +	2	0/2 (0)
Other	-	NA	13	0/13 (0)

<sup>a</sup> CC: clonal complex; ST: sequence type

<sup>b</sup> CC/ST, SCCmec, and MRSA clone name were identified using the identibac *S. aureus* Genotyping Kit.

<sup>c</sup> —: absence of SCCmec

<sup>d</sup> *tirS* gene detected by specific PCR as described in the Material and Methods

\* SCCmec element sequencing

doi:10.1371/journal.ppat.1006092.t001

strain ST20121341 (CC8) (sample accessions ERS1434451 and ERS1434452). As reference to the comparison with our sequenced strains, we used the genome of strain MSSA476, in which *tirS* was recently described [9]. Whole-genome alignment and search for the site-specific insertion sequences (ISS) typical of SCC-like cassette insertions showed that *tirS* is invariably present within the SCC element of all six MRSA and MSSA genomes analyzed (Fig 1). Moreover, this gene is found in a highly conserved region within the J1 region (between the *ccr* complex and the 5' ISS(L)), consisting of five open reading frames (ORFs) that include the *tirS* gene but also the *fusC* gene, responsible for resistance to fusidic acid. This region is present as well in MRSA as in the MSSA strains analyzed (Fig 1).

Furthermore, BLASTn searches using the *tirS* and its surrounding four ORFs (“*tirS* region”), as annotated in the strain MSSA476 genome (GenBank: BX571857.1), against the GenBank nucleotide collection (nr/nt) revealed the presence of the *tirS* region in 14 MRSA, 2 other MSSAs, and a methicillin-sensitive *Staphylococcus hominis* strain. Unexpectedly, in all 17 staphylococci, the *tirS* region was conserved and located in SCC elements in the vicinity of the site-specific recombinase of type *ccrAB*. For 15 of the *S. aureus* strains in which the *tirS* region was detected, a whole-genome shotgun sequence was available, and we observed that they belonged to four distinct clonal complexes: CC1 (2 MRSA and 1 MSSA), CC5 (7 MRSA), CC8 (1 MSSA), and CC22 (4 MRSA).

### TirS production

To investigate TirS production by *S. aureus*, *tirS* expression was examined by quantitative real-time reverse transcription PCR (RT-qPCR) during bacterial growth in one MRSA (clone Geraldine, CC5) and one MSSA (CC1) *tirS*-positive strains. The analysis of the *tirS* expression kinetics showed stable expression of *tirS* during growth with a marginal increase at the end of the exponential phase (Fig 2A). The difference in *tirS* expression and the standardization gene *hu* was generally around seven cycles.

Because *tirS* is located in the SCC element, we investigated the effect on *tirS* expression of adding a sub-minimum inhibitory concentration (sub-MIC) of oxacillin (1/2 MIC) and fusidic acid (1/4 MIC) during the exponential phase of *S. aureus* growth in 9 strains. Addition of fusidic acid appeared to significantly modulate *tirS* expression both in MSSA and MRSA strains

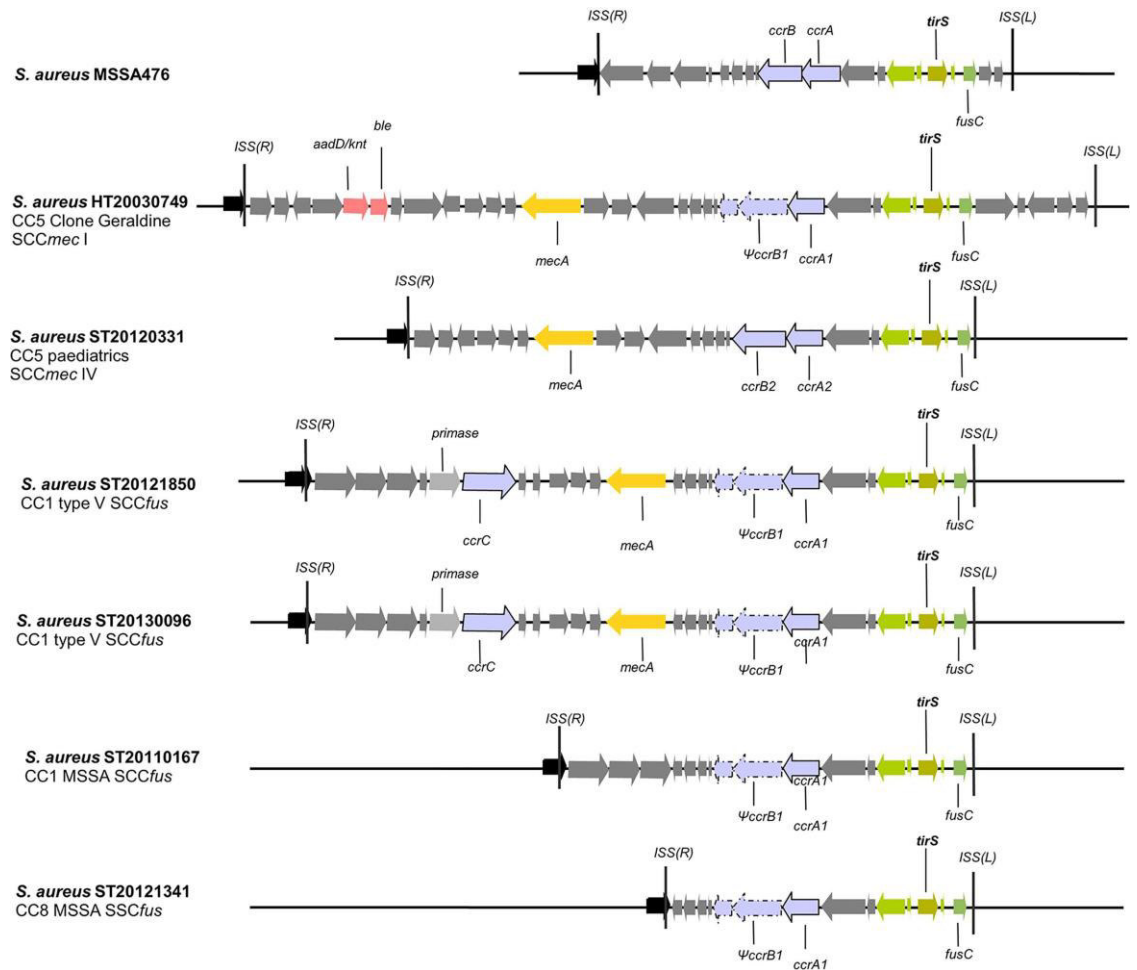


**Fig 1. Characterization of the genomic context of the *tirS* region in *S. aureus* MRSA and MSSA strains.** Localization of the *tirS* gene and surrounding context in 4 *tirS*-positive MRSA strains and 2 *tirS*-positive MSSA strains. For all 6 strains, the *tirS* gene was found within the SCC element. Schematic diagrams represent the genomic comparison of the 6 SCC regions of both MRSA and MSSA strains used in our study and the SCC<sub>476</sub> element of strain MSSA476 for which the *tirS* gene was first described [9]. Predicted ORFs are marked in the direction of transcription as arrows. The highly conserved *tirS* region, consisting of the *tirS* gene and 4 surrounding genes among which we find the *fusC* gene (fusidic acid resistance), is represented by green arrows. Light rose arrows represent genes coding for antibiotic resistance, orange arrows represent the *mecA* gene conferring resistance to beta-lactams and blue-gray arrows represent the site specific recombinases (*ccrAB* or *ccrC*) of SCC elements. The SCC elements ISS(L) and ISS(L) are also represented as black vertical bars. Abbreviations: *ccrAB* = cassette chromosome recombinase A and B; *fusC* = fusidic acid resistance gene; *mecA* = methicillin resistance gene; *ccrC*: cassette chromosome recombinase C; *ble* = bleomycin resistance gene; *aadD/knt* = kanamycin nucleotidyltransferase (resistance gene).

doi:10.1371/journal.ppat.1006092.g001

(Fig 2B). *tirS* was upregulated up to six-fold with fusidic acid compared to its expression without antibiotic stress and level of induction by fusidic acid was strain dependent. In contrast, no difference in levels of expression of *tirS* was observed with exposure to sub-MIC of oxacillin.

### TirS interferes with TLR signaling

TirS belongs to the family of bacterial TLRs [9]. We therefore investigated the ability of TirS to specifically interfere with TLR signaling using an *in vitro* NF-κB-dependent luciferase reporter system. Although a variety of TLR receptors have been described, in humans the most relevant for recognition of bacterial molecules are TLR2, TLR4, TLR5, and TLR9. Ectopic expression of



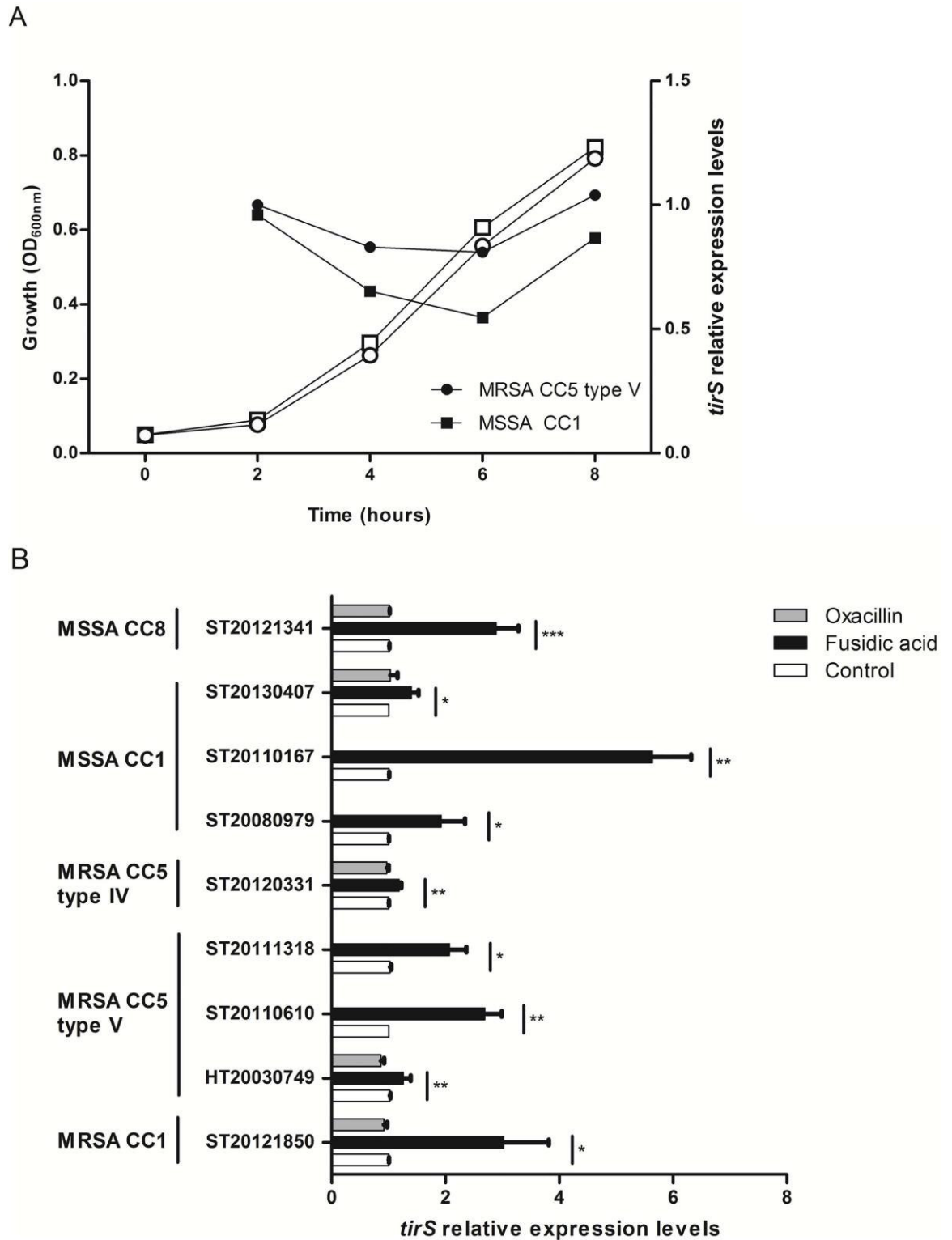


**Fig 2. Impact of bacterial growth and antibiotic on *tirS* expression.** (A) The expression of *tirS* was quantified by RT-qPCR and normalized to the level of *hu* expression from total RNA extracts prepared from bacterial cultures at 2, 4, 6, and 8 h. MHB medium condition at 2 h was used as a reference. The figure shows an average of 2 independent experiments. White symbols represent bacterial growth, black symbols represent *tirS* expression. (B) Expression of *tirS* on 2-h bacterial cultures and 30 min

of antibiotic treatment. Bacterial strains without stress were used as reference (relative quantity = 1) to estimate the relative quantity of *tirS* mRNA. White bars correspond to negative control (no antibiotic), grey bars to bacteria exposed to oxacillin, and black bars to bacteria exposed to fusidic acid. Data represent mean  $\pm$  SEM of three to six independent assays. \*  $p < 0.05$ ; \*\*  $p < 0.01$ ; \*\*\*  $p < 0.001$ .

doi:10.1371/journal.ppat.1006092.g002

*tirS* in HEK293T cells transfected with the luciferase reporter vector and various TLRs resulted in reduced TLR2 activation and to a lesser extent, reduced activation of TLR9, TLR4, and TLR5 (Fig 3A). As a control, we confirmed that this inhibitory effect of TirS on murine TLR2 was dose-dependent by carrying out the transfections with increasing amounts of the expression vector encoding TirS (Fig 3B). Inhibition of human TLR2 and TLR4 pathways following addition of the appropriate ligands was also observed (Fig 3C). These results suggest that TirS may, at least partly, target a common molecule between these pathways such as the adaptor molecule MyD88. Consistently, reduction of IL-1R following IL-1 $\beta$  stimulation was also observed in the presence of TirS (Fig 3D). In contrast, although much lower levels of activation can be obtained for TLR3, which is independent of MyD88, we did not observe any significant effect of TirS on this pathway (Fig 3E). This was also the case for endogenous TNF receptor (TNFR) (Fig 3D). Overall, these results are in agreement with data from Askarian et al. [9] that previously described TirS inhibition of TLR2, MyD88 and TIRAP dependent pathways *in vitro*.

In addition to its ability to interfere with TLR signaling, the bacterial TIR effector protein from *Brucella* BtpA targets and modulates microtubules [16] through a WxxxE motif [17] as well as the recently identified TIR protein from *Bacillus anthracis* referred to as BaTcp [18]. Since the WxxxE is also present in TirS, we investigated the intracellular localization of ectopically expressed TirS by confocal microscopy on HeLa cells transfected with myc-TirS and indirect immuno-fluorescence staining with anti-myc antibodies. We found that myc-tagged TirS accumulated in filament-like structures of irregular shapes within the host cytosol (Fig 3F). Similar results were observed for GFP-TirS, suggesting that this localization was not dependent on the tag (S1 Fig). In addition, TirS showed no co-localization with cytoskeleton components as observed after labeling with either phalloidin for actin, tubulin for microtubules, or vimentin for intermediate filaments (Fig 3F), suggesting a different targeting than previously described for BtpA and BaTdp.

### TirS modulates *S. aureus* virulence

To further investigate the role of TirS during infection, we carried out *in vivo* studies in mice. Because *S. aureus* is the leading cause of skin infection, we developed a subcutaneous model of infection in mice with the inoculation of *S. aureus* clone Geraldine-wild type (WT) strain, a deleted for the *tirS* gene ( $\Delta tirS$ ) strain, or a  $\Delta tirS$  strain restored for *tirS* gene in a chromosomal position ( $\Delta tirS + tirS$ ). First, we confirmed that bacterial growth was not affected by genetic manipulation of TirS by assessing growth in two different media (brain–heart infusion (BHI), tryptic soy broth (TSB)) (S2 Fig). Then, wild-type (WT) C57Bl/6 mice were inoculated with the three strains. Cutaneous infection resulted in the development of visible lesions by day 1 that healed by day 14 regardless of the strain (Fig 4A and 4B). As control, injection of sterile phosphate buffered saline (PBS) did not induce any skin lesions in mice. Infection with  $\Delta tirS$  strain resulted in larger lesions (~2.5-fold) compared with the WT strain ( $p < 0.01$ ). These differences appeared around day 6 and persisted for about 4 days before being resolved at the same time for both strains. Similar lesion sizes were observed in mice infected with the *S. aureus* restored strain compared with the WT strain ( $p = 0.9$ ), confirming the role of TirS on the observed results.

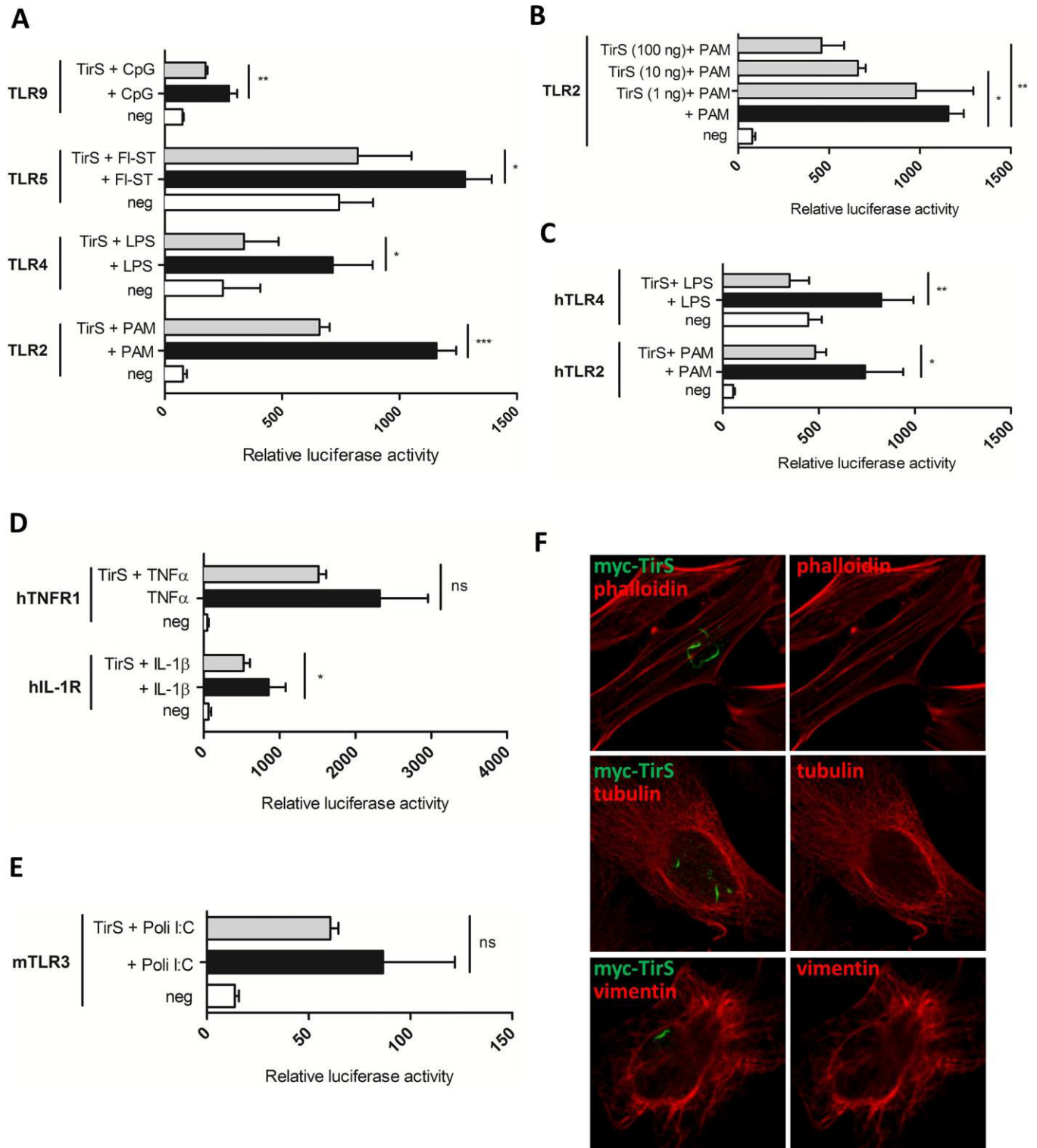


**Fig 3. TirS interferes with TLR and IL-1R signaling.** (A) HEK293T cells were transiently transfected for 24 h with the luciferase reporter vector and murine TLR2, TLR4, TLR5, or TLR9 in the presence or absence of TirS (50 ng). Cells were then stimulated with the appropriate ligand (PAM, LPS, Fl-ST, and CpG) for 6 h before measurement of luciferase activity. White bars correspond to negative control, black bars to cells stimulated with the appropriate ligand, and gray bars to cells transfected with TirS and stimulated with the ligand. Data represent the means  $\pm$  SEM of the relative luciferase activity and were obtained from duplicates of 3 independent experiments. (B) Luciferase activity of murine TLR2 following transfection with

increasing amounts of vector encoding *tirS* (1, 50, 100 ng) in order to obtain different levels of expression and for (C) human TLR2 and TLR4. (D) Effect of TirS on TNFR and IL-1R activation following TNF- $\alpha$  or IL-1 $\beta$  stimulation, respectively and (E) TLR3 following stimulation with poli:IC. (F) HeLa cells were transfected with myc-TirS for 10 h and labeled for myc (green) and different components of the cytoskeleton: actin (top panels, phalloidin), microtubules (medium panels, tubulin), or intermediate filaments (bottom panels, vimentin). ns: not significant, \*  $p < 0.05$ , \*\*  $p < 0.01$ , and \*\*\*  $p < 0.001$ .

doi:10.1371/journal.ppat.1006092.g003

To better understand the factors that might be important in determining the size of skin lesions in the mouse model, animals were sacrificed between 5 and 9 days after infection induced by MRSA clone Geraldine WT and  $\Delta$ *tirS* strains to the sample lesion. First, we enumerated the bacterial load in the skin lesion. No significant differences in colony-forming unit (CFU) counts between the strains were observed (Fig 5A). Moreover, lesion size was not correlated with bacterial burden in either the WT or  $\Delta$ -*tirS* strain (*S. aureus* WT:  $r^2 = 0.39$ ;  $p = 0.2$ , *S. aureus*  $\Delta$ *tirS*:  $r^2 = 0.35$ ;  $p = 0.2$ ) (Fig 5B). This finding raised the possibility that the inflammatory response was more important in determining lesion severity, as assessed by lesion size, than bacterial burden in the lesions.

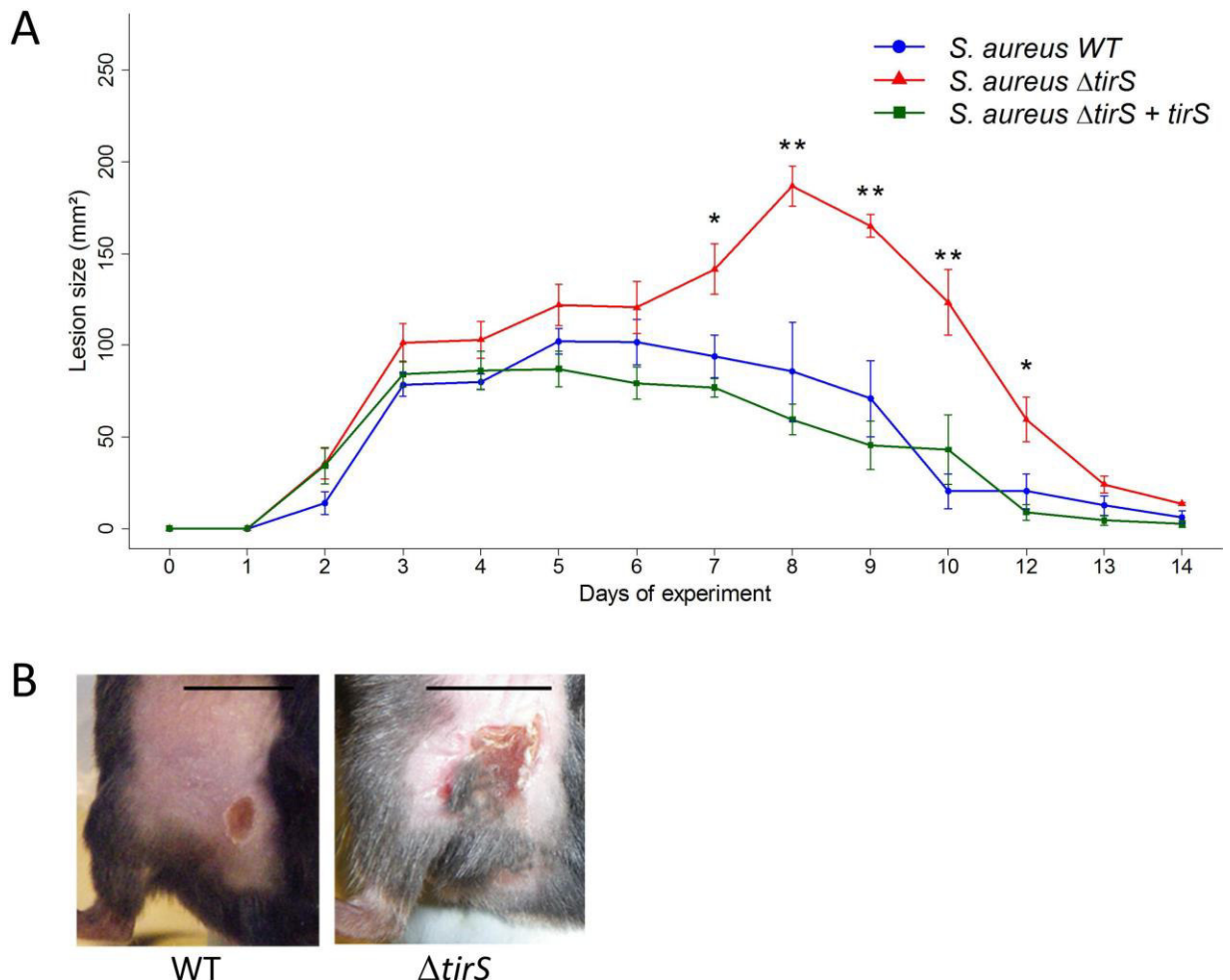


**Fig 4. *S. aureus* deleted for *tirS* induced larger skin lesions in WT C57Bl/6 mice.** (A) Data are presented as mean total lesion size (mm<sup>2</sup>)  $\pm$  SEM and are representative of 3 independent experiments with at least 4 mice/group. \*  $p < 0.05$ ; \*\*  $p < 0.01$  (B) Photographs of representative lesions at day 7 after staphylococcal infection. Black bars indicate 10 mm. Abbreviations: WT = wild-type;  $\Delta$ *tirS* = deleted for the *tirS* gene;  $\Delta$ *tirS* + *tirS* =  $\Delta$ *tirS* strain chromosomally restored for *tirS* gene.

doi:10.1371/journal.ppat.1006092.g004

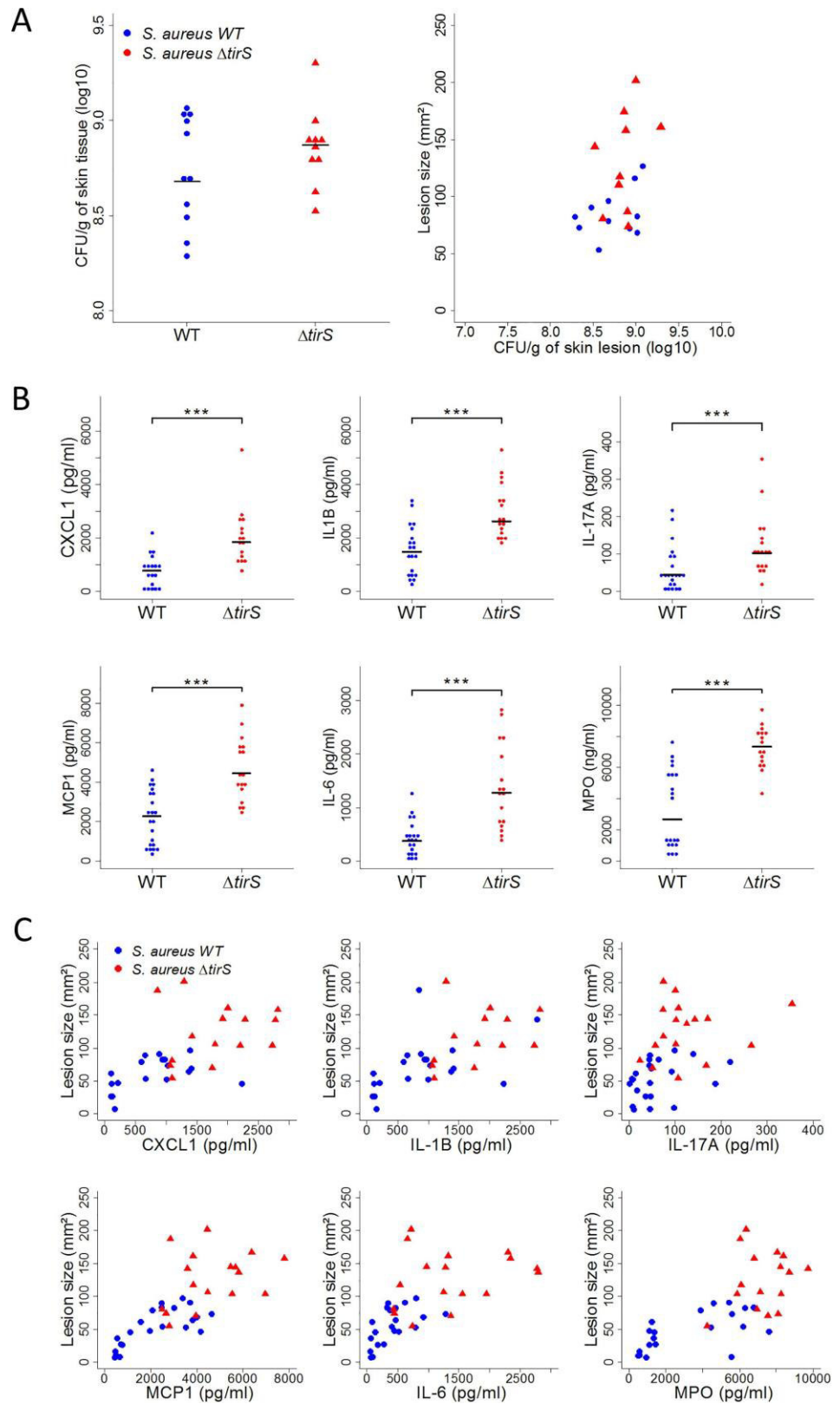


**Fig 5. TIR induces reduced inflammation despite similar bacterial counts in skin lesions.** (A) Bacterial burden in skin lesions of mice infected with *S. aureus* WT (n = 11) or *S. aureus*  $\Delta tirS$  (n = 10) and correlation between bacterial burden and lesion size. Data were obtained 5 and 7 days after inoculation from 2



independent experiments. (B) Levels of IL-1 $\beta$ , IL-6, IL-17, CXCL1, MCP1 (pg/ml), and myeloperoxidase (MPO) activity (ng/ml) from lesional skin at 7, 8, and 9 days after inoculation. Data were obtained from 16 to 22 mice infected with *S. aureus* WT or *S. aureus*  $\Delta$ *tirS* from 4 independent experiments (all data shown). (C) Correlation between levels of IL-1 $\beta$ , IL-6, IL-17, CXCL1, MCP1, MPO, and lesion size from lesional skin at 7, 8, and 9 days after inoculation. Data were obtained from 16 to 22 mice infected with *S. aureus* WT or *S. aureus*  $\Delta$ *tirS* from 4 independent experiments (all data shown). Each symbol represents an animal and the median values are marked by horizontal bold lines. Abbreviations: WT = wild-type;  $\Delta$ *tirS* = deleted for the *tirS* gene. \*\*\*  $p < 0.001$ .

doi:10.1371/journal.ppat.1006092.g005

To follow up on these observations, we sought to measure neutrophil and macrophage activity with the quantification of levels of myeloperoxidase (MPO) and a panel of inflammatory cytokines in the skin lesions of mice infected with MRSA clone Geraldine WT and  $\Delta$ *tirS* strains. Interestingly, the levels of MPO and IL-1 $\beta$ , IL-6, IL-17, CXCL1, and MCP1 were significantly lower in the murine skin lesions developed after the WT strain inoculation compared with the  $\Delta$ *tirS* strain (Fig 5B). Correlation between skin lesion size and the levels of MPO, IL-1 $\beta$ , IL-6, IL-17, CXCL1, and MCP1 was statistically confirmed for each of these inflammatory markers (MPO:  $r^2 = 0.71$ ,  $p < 0.001$ ; CXCL1:  $r^2 = 0.55$ ,  $p < 0.001$ ; IL-1 $\beta$ :  $r^2 = 0.61$ ,  $p < 0.001$ ; IL-17A:  $r^2 = 0.45$ ,  $p < 0.01$ ; MCP1:  $r^2 = 0.74$ ,  $p < 0.001$ ; IL-6:  $r^2 = 0.64$ ,  $p < 0.001$ ) (Fig 5C). Therefore, the smaller lesions observed after experimental inoculation with the bacterial WT strain were associated with lower levels of chemokines and less inflammation but not with decreased bacterial burden. These data support the notion that the local inflammatory response is a key determinant of lesion size. These results are consistent with a role for TirS in the control of the inflammatory response during *S. aureus* infection *in vivo*.

Finally, to evaluate the contribution of the TIR-containing adaptor protein MyD88, a key component of the TLR signaling pathway implicated in proinflammatory mechanisms [19], MyD88-deficient mice from the C57BL/6 genetic background were subcutaneously inoculated with MRSA clone Geraldine WT and  $\Delta$ *tirS* strains. An identical infection protocol and bacterial concentration were used as in WT mice. As control, injection of sterile PBS did not induce any skin lesions in mice. Interestingly, there was no significant difference in lesion size between MyD88-deficient mice infected with the WT or  $\Delta$ *tirS* *S. aureus* strain (Fig 6), suggesting that MyD88 might play a role in virulence of the MRSA clone Geraldine used. These results confirm *in vitro* previously reported data showing that TirS inhibits signaling in a MyD88-dependent manner [9].

## Discussion

Bacterial strategies for innate immune evasion involve manipulation of the TLR signaling by TIR homologues such as TirS for *S. aureus* [20]. In this work we report the localization of the *tirS* in different SCC elements and its role in the control of the inflammatory response during *S. aureus* infection. Using a mouse model of *S. aureus* skin infection, we evaluated the role of TirS on *S. aureus* virulence. We show that *S. aureus* Geraldine deleted for the *tirS* gene exhibited superior virulence compared to the WT strain, as attested by the size of the skin lesion. Of note, bacterial counts in the skin lesions did not differ between the mutant and the WT strains and did not correlate with clinical severity (*i.e.*, lesion size). This finding suggests that bacterial burden may not be the primary driver of lesion severity and argues that lesion severity may be due, at least in part, to the associated inflammatory response. In support of this hypothesis, we found a correlation between lesion size and levels of the proinflammatory cytokines, as well as neutrophil activity (as assessed by MPO levels). These findings are consistent with previous studies, which underscores that the severity of skin infection is often driven by

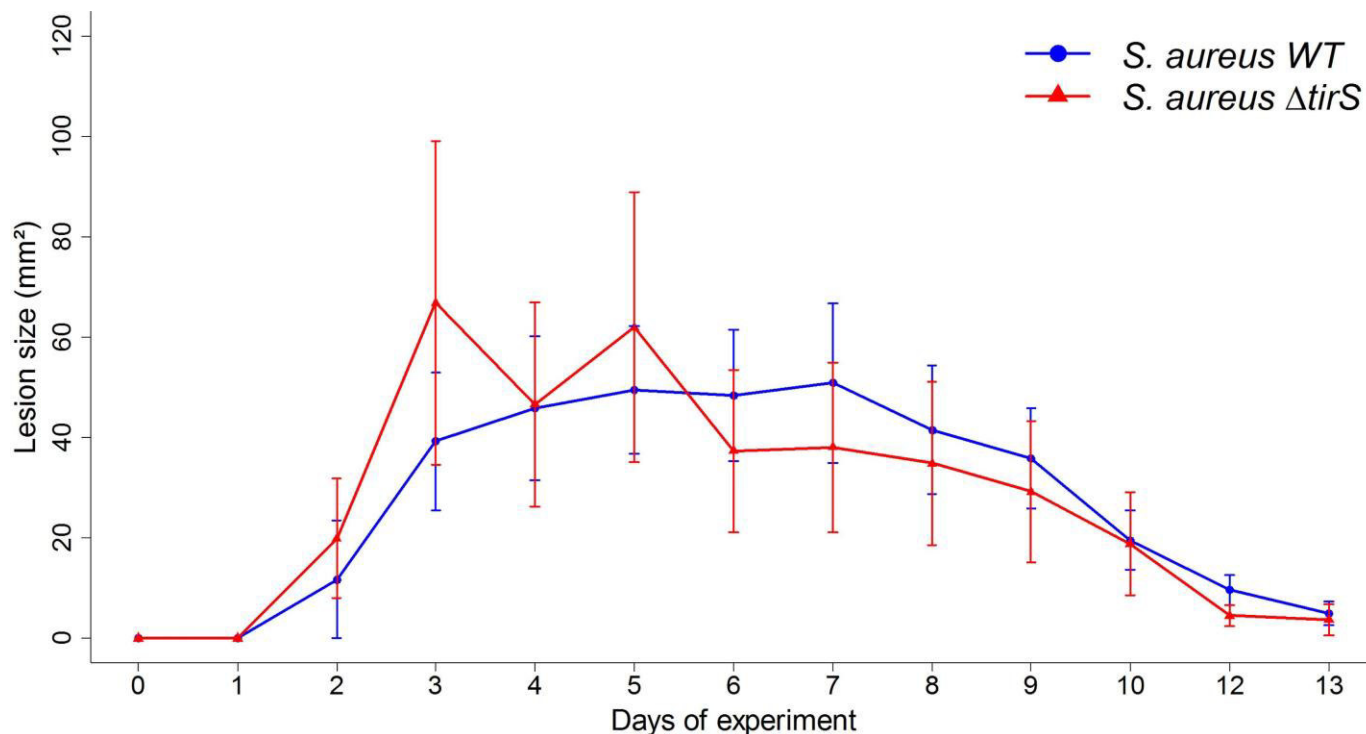


**Fig 6. *S. aureus* deleted for *tirS* induced similar skin lesion size in MyD88-deficient mice.** Data are presented as mean total lesion size (mm<sup>2</sup>) ± SEM and are representative of 2 independent experiments with at least 4 mice/group. Abbreviations: WT = wild-type;  $\Delta tirS$  = deleted for the *tirS* gene.

doi:10.1371/journal.ppat.1006092.g006

the inflammatory response to the invading pathogen as much or more than by the direct effects of the pathogen itself [21–23]. This inference suggests that the attenuation of skin inflammation observed with *S. aureus* WT strain, compared to its *tirS* mutant, was driven by modulation of the inflammation resulting from TirS action. Such a conclusion is concordant with the fact that the ectopic expression of TirS in eukaryotic cells appeared to temper stimuli-induced TLR2-, TLR4-, TLR5-, and TLR9-mediated NF- $\kappa$ B activation. Accordingly, a previous and independent work has reported a negative interference of TirS with the TLR2 signaling pathway [9]. These results can be directly linked to our *in vivo* observations in mice, explaining the modulation of virulence during *S. aureus* infection by *tirS* [4,20]. Here the bacterial TIR effector has been shown to induce attenuation of virulence during infection because of the downregulation of the innate immune pathway.

In addition to control of inflammatory responses, some TIR domain-containing proteins such as BtpA or BaTcp have been shown to target and modulate microtubules [18,24] through a WxxxE motif that is also present in TirS and involved in cross-talk between the TLR and GTPase signaling pathways [16]. We found that ectopically expressed TirS accumulated in filament-like structures of irregular shapes within the host cytosol but that do not co-localize with typical cytoskeleton components (microtubules, actin or intermediate filaments). This observation is different from those previously described for other bacterial TIR proteins from *Bru-cella* [8,16] and BaTdp from *B. anthracis* [18]. The role of TirS accumulation in filament-like structures in the modulation of *S. aureus* pathogenicity remains to be explored.

The host interacting partner of TirS has yet to be identified. MyD88 is a general adaptor protein that plays an important role in Toll/IL-1 receptor family signaling. *In vitro* results of Askarian et al. [9] showed that TirS interferes with TLR2 and both MyD88 and TIRAP

pathways *in vitro*. Here we report that *in vitro*, TirS is a potent inhibitor of not only TLR2 but also TLR4, TLR5, and TLR9. All of these proteins are dependent on MyD88, a general adaptor protein that plays an important role in the Toll/IL-1 receptor family signaling, which argues for an interaction of TirS with MyD88. Consistently, we found that *S. aureus* carrying *tirS* induced no increased virulence in a MyD88 knockout mice model. Taken together, these results suggest that TirS modulates an inflammatory response at the site of the infection through the MyD88 adaptor protein. Preliminary work from our lab has not been able to purify TirS, which is highly insoluble and failed to detect an interaction by co-immunoprecipitation assays. Further work is now required to understand the molecular mechanism by which TirS interacts and/or competes with MyD88.

As yet, there is no clear consensus on the mechanism by which TIR proteins enter host cells and localize to the host cell cytoplasm. From deduced amino acid sequences, no recognizable signal sequence for secretion was detected in TIR proteins, including TirS. In the case of TlpA from *Salmonella enterica*, for which no direct evidence of secretion has been reported, the suggested mechanism is a role for type III or type IV secretion systems (T3SS or T4SS) that can directly inject TIR effectors into the host cells [5]. TcpC of *E. coli* has been reported to be secreted into the media of cultured bacterial cells and subsequently taken up into host macrophages to interfere with TLR-mediated tumor necrosis factor induction [17]. In the case of *Brucella*, BtpA and BtpB are translocated into host cells in a manner partially dependent on the T4SS [8]. As observed with other TIR protein genes, the *tirS* gene is not co-located with genes encoding for a secretion system in *S. aureus*. However, TirS has been reported to be secreted into the media through an unknown mechanism [9]. Further studies are needed to clarify this issue, perhaps by performing real-time imaging and co-localization studies.

A comparison of different SCC elements in various *S. aureus* genetic backgrounds highlights the invariable presence of *tirS* within the SCC *fusC/tirS* mobile genetic element, sometimes included in the SCC*mec* elements in the J1 region. As proposed previously [9, 25], the finding that *tirS* region was invariably present within an SCC element suggests that similar to *mecA* and *fusC* transmission, SCC-mediated horizontal transfer is the major mechanism of *tirS* dissemination. Moreover, horizontal transfer of the *tirS* region is also suggested with the nearby presence of site-specific recombinases of the *ccrAB* type in all SCC elements carrying the *tirS* gene [25]. Of further interest, all published sequences of SCC *fusC/tirS* have identified four conserved additional genes. Future work should attempt to assign functional roles of these putative proteins and evaluate their involvement in the regulation or modulation of *tirS* and *fusC* transcription.

The co-location of *mecA* and *fusC* genes in this genetic element suggested that, in addition to antibiotic resistance genes, the presence of *tirS* may also confer a selective advantage for *S. aureus*. However, our observation indicated that a sub-inhibitory concentration of fusidic acid but not oxacillin induced overexpression of *tirS* in all strains tested. These results were unexpected because we observed the opposite outcome for Panton Valentine leukocidine and alpha-toxin expression with the same antibiotics: overexpression by oxacillin and inhibition by fusidic acid [26]. The acquisition by *S. aureus* of a gene encoding for factors that modulate virulence in the SCC*mec* element is not exceptional. The *pls* gene encoding for a large surface protein with an LPXTG peptidoglycan-anchoring sequence is a part of the type I SCC*mec* element [27]. This protein reduces *S. aureus* adherence and invasiveness [28]. Pls was also described in SCC*mec* III [29] but never in MSSA. Conversely, genes encoding for phenol soluble modulins alpha 1 to 3 (PSM- $\alpha$ 1–3; small peptides with an amphipathic  $\alpha$ -helical structure and strong surfactant-like properties that induce the production of proinflammatory cytokines and recruit, activate and lyse neutrophils) were first described in MSSA [30] before being found to be part of SCC*mec*II, SCC*mec*III, and SCC*mec*VIII (PSM- $\alpha$ -*mec*) [31,32]. To our knowledge, is



it not yet known whether antibiotics whose resistance is encoded by these SCC elements modulate the expression of Pls and/or PSM-*mec*.

A number of bacteria expressing TIR-containing proteins have been described, but as far as we know, only one study references their prevalence throughout a bacterial species [24]. In this work, we report the presence of *tirS* gene in 12.4% of a clinical MSSA and MRSA *S. aureus* strain collection. The TirS effector was not shown to be associated with a specific clinical human presentation by molecular epidemiology studies. For the Geraldine clone that always holds the *tirS* gene, previous observation did not identify a particular association with disease severity [33,34]. By contrast, the first nosocomial outbreak due to the Geraldine clone was recently reported, emphasizing its efficiency in being transmitted and easily spread within health care settings [35]. Indeed, this clone has been reported to be both a community-acquired and hospital-acquired MRSA. Thus, the clone Geraldine SCC*mec* element may provide a selective advantage in both settings: in the hospital because of a higher antimicrobial resistance compared to drug-susceptible WT *S. aureus* strains, and in the community because of its enhanced inhibition of the innate immune response. Similarly, different groups recently described the emergence in the community and in the hospital of ST1, ST45, and ST149 MRSA *fusC* positive strains in England and of *fusC* positive ST5 MRSA in New Zealand that also are *tirS* positive [36,37]. These epidemiological observations highlight the selective advantage of *S. aureus* in carrying the SCC*mec* element with SCC *fusC/tirS*.

In summary, we identify for the first time a bacterial TIR homolog protein genetically linked to an antimicrobial agent resistance determinant in the genetic mobile element SCC, thus providing a molecular connection between two key traits determining the successful outcome and spread of bacterial infections. Moreover, TIR homolog protein production was modulated by one antibiotic, fusidic acid, for which the resistance is encoded in a conserved region, which includes the *tirS* gene, and located within these SCC*mec* and non-*mec* SCC elements. This result expands knowledge about bacterial TIR homologs that constitute an ingenious strategy of pathogenic bacteria to evade the host immune system. The current state of knowledge strongly suggests that TIR effectors should be considered as potential key effectors of host defense, which emphasizes that further research is required to elucidate the precise mechanism of action of these interesting molecules. From the clinical point of view, the identification of the critical role of TirS signaling for modulating the immune response to a site of infection raises the possibility that this pathway could be locally targeted to engage the host's own immune responses in the treatment of a microbial infection.

## Materials and Methods

### Ethical statements

Isolates were obtained as part of routine diagnostic testing and were analyzed anonymously. All data were collected in accordance with the European Parliament and Council decision for the epidemiological surveillance and control of communicable disease in the European community [38,39]. Ethical approval and informed consent were not required.

All mouse protocols were carried out in strict accordance with the Directive 2010/63/EU revising Directive 86/609/EEC on the protection of animals used for scientific purposes. This directive was translated in the French regulation as the Décret N°2013–118 of February 2013 under the jurisdiction of the Ministry of Education, Research and Technology. The initial research project had been approved by the local Animal Ethic Evaluation Committee CEC-CAPP (Comité d'Evaluation Commun au Centre Léon Bérard, à l'Animalerie de transit de l'ENS, au PBES et au laboratoire P4) with the references ENS\_2014\_025 and ENS\_2014\_052 and subsequently authorized by the French Ministry of Education, Research and Technology.

## Bacterial strain characterization

A subset of 226 strains from the collection of the Centre National de Référence des Staphylocoques (Lyon, France), composed of 103 strains of the main community and hospital-acquired MRSA clones, and 123 strains of MSSA were used in this study. They were sent to the laboratory for detection of toxin production in the context of nasal colonization, skin and soft tissue infection, pneumonia, bacteremia, or endocarditis. The *S. aureus* HT20030749 strain belonging to the clone Geraldine was isolated from blood culture of patient with bone–joint infection.

All strains were genotyped as previously described. Briefly, bacterial DNA was extracted according to the manufacturer’s recommended protocol using commercial extraction kits (Qiagen). The diagnostic DNA microarrays, identibac *S. aureus* Genotyping (Alere) used for this study, as well as related procedures and protocols, have been previously described in detail [40]. This microarray covers 332 different target sequences corresponding to approximately 185 distinct genes and their allelic variants. The assigning of isolates to CCs was determined by the comparison of hybridization profiles with those previously characterized by using multilocus sequence typing reference strains [40].

**Illumina Sequencing.** Genomic DNA were extracted from each isolate using a QIAcube extraction kit (Qiagen). The Nextera XT DNA preparation kit (Illumina) was used to generate sequencing libraries from 1 ng of DNA. Whole-genome sequencing was finally done with an Illumina HiSeq (Illumina, San Diego, CA, USA) to generate 150-bp paired-end reads.

**De novo assembly.** For each isolate, the raw paired-end reads were assembled using a modified version of the A5-miseq open-source pipeline [41]. This pipeline implements a complete sequencing data processing workflow from raw read cleaning to *de novo* assembly. The first task of the read cleaning involves removing the regions of the raw reads that are contaminated by the adapters during the Nextera XT protocol using the Trimmomatic program [42]. Then, the reads are filtered and trimmed according to quality and length criteria using Trimmomatic and the preprocess function of String Graph assembler (SGA) [43]. Finally, the correct function of SGA is used to correct errors in the reads by a k-mer frequency-based method. After being quality filtered and error corrected, the reads were assembled by the IDBA-UD500 program, which implements an iterative De Bruijn graph built with several values of k-mer lengths, from low to high values, instead of a single value as for most *de novo* assemblers [44]. The reads are then mapped against the assembly using BWA-MEM [45] to polish the contigs at every position where basecalls differ between the mapping and the assembly. The scaffolding implemented at the end of the original A5-miseq pipeline was not performed because it provides no gain in the subsequent analysis of marker detection.

**Characterization of SCCmec V and *tirS* regions.** First, the three MRSA genomes were aligned against the strain MSSA476 genome using progressiveMauve with default parameters [46]. Then, identification of SCC was done by searching for the ISS of these elements [47,48], both at the end of the ORF X / *rlmH* gene and further downstream. The newly detected SCCmec elements were annotated using the RAST Server (<http://rast.nmpdr.org/>), and blastn searches were performed (<http://blast.ncbi.nlm.nih.gov/>) against the nucleotide collection (nr/nt) using the megablastn algorithm and the organism filter for *S. aureus* (taxid:1280).

## *tirS* amplification

Oligonucleotide primers *tirS*-For-CTTCAAAAAGAGCAGTCTAGG and *tirS*-Rev-CTTCAA CACTCACTTTATGCC were designed according to *tirS* sequence. After amplification for 30 cycles (30 s of denaturation at 94°C, 30 s of annealing at 53°C, and 30 s of extension at 72°C), the PCR products were resolved by electrophoresis through 1.5% agarose gels (Sigma, Saint

Quentin Fallavier, France). This step was followed by SYBR Safe DNA (Life Technologies) staining and analysis. To assess the specificity of *tirS* amplification, PCR products were subjected to DNA sequencing (Biofidal, Lyon, France). *S. aureus* HT20030749 and RN4220 strains were used as positive and negative amplification controls, respectively.

### Transcription of *tirS*

*tirS* expression was analyzed using RT-qPCR. MRSA ST20121850 (CC1), MSSA ST20130407, ST20110167, ST20080979 (CC1), MSSA ST20121341 (CC8), MRSA ST20120331 (CC5, type IV), MRSA ST20111318, ST20110610, HT20030749 (CC5, type V) were grown in fresh MHB at 37°C, after a 1:100 dilution of overnight cultures. For kinetics analysis, total RNA of two representative strains (MRSA HT20030749, CC5 and MSSA ST20130407, CC1) was purified at 2, 4, 6, and 8 h of growth as previously described [49]. Total RNA was extracted with the RNeasy Plus (Qiagen) kit including a gDNA eliminator column and an additional DNase treatment (Qiagen). RNA quality and quantity were determined by Bioanalyzer (Agilent) using the RNA Nano chips and quantified using the ND-8000 (NanoDrop Technologies). Absence of DNA contamination was checked by using *tirS*-specific primers and probe at optimal concentrations (assessed as previously described [50] without the reverse-transcription step). The final concentrations were 0.2  $\mu$ M for primers and probe (*tirS*-F-CTATTTGGCATAAAGTGAGTGTT GAAG, *tirS*-R-AAATCACTTGTATTCAATGCATACTTATCT, and *tirS*-P-CGTGCATAC AACCCATAT labeled with NED at the 5' and 3'-minor groove binder), and reactions were performed in a one-step RT-PCR enzymatic mixture (Agilent Technologies, Brilliant II QRT-PCR Master Mix Kit) in a final volume of 20  $\mu$ l in the CFX96 system (Bio-Rad) and following manufacturer's instructions. Differences in Ct values between tested transcripts and *hu* signals were used for normalization purposes and based on the MHB medium condition at 2 h as a reference. The fold change was expressed as the inverse exponential of the difference between MHB Ct (reference) and the stress condition Ct. This assay was also used on 2-h cultures to assess gene expression values of *tirS* in various stress conditions such as the presence of 1/2 MIC of oxacillin for MSSA and 5  $\mu$ g/ml for MRSA or 1/4 MIC of fusidic acid for MSSA and MRSA [49] on total RNA purified after 30 min of exposition. MICs were determined using CLSI recommendations [50], and the stress experiments were performed with drug concentrations showing minor impact on growth rate following control experiments (S3 Fig).

### Construction of the *tirS*-deleted mutant

*S. aureus* RN4220 (lab strain collection) was used for plasmid amplification and genetic manipulations because it is a nitroso-guanidine-induced mutant capable of accepting *E. coli* DNA [51]. To delete the *tirS* gene, we performed allelic replacement using double crossover recombination as previously described [52]. Using the primers and restriction enzymes listed in S1 Table, we generated two fragments of 930 bp 5' and 1029 bp 3' of *tirS*. These fragments were ligated in 5' and 3' of the chloramphenicol acetyl transferase gene [53] and inserted into pMAD [54]. Plasmid and inserts were checked by PCR and sequencing using the primers listed in S1 Table. Plasmid was introduced by electroporation in RN4220 and then in HT20030749 (Geraldine strain). We performed double crossover recombination yielding to deletion of *tirS* in HT20030749 (Geraldine strain). The mutant strain obtained was called  $\Delta$ *tirS*. Gene deletion was checked by PCR and sequencing using specific primer hybridizing with internal and external positions of the deleted region (S1 Table). Insert presence was checked with primers IngDNA\_F and vG\_CDS\_1\_R or IngDNA\_F and vG\_cat\_1\_R, yielding a negative PCR and a 2017-bp amplicon for the correct construct.

## Construction of the *tirS* restored strain

Total DNA and plasmid DNA were prepared with Qiagen kits (QIAamp DNA Mini Kit and QIAprep Spin Miniprep Kit) after lysostaphin lyses for *S. aureus*. When necessary, transformation of *E. coli* DH5 $\alpha$  (Promega, Madison, USA) was performed by treatment with CaCl<sub>2</sub>, and *S. aureus* strains were transformed by electroporation (Bio-Rad gene pulser). The *tirS*-deleted strain was complemented by inserting the *tirS* gene sequence downstream from the leukocidin promoter *P-lukS* in the bacterial chromosome using sequences homologous to sequence NWMN\_0029 and NWMN\_0030 of Newman strain (GenBank: AP009351.1) for chromosomal recombination. The region of NWMN\_0029 and NWMN\_0030 was amplified using primers New29-523 and New30-2371, restricted by EcoRI and Sall and cloned on a pBlue-script vector (Stratagene) to obtain plasmid pLUG37. The *tirS* gene sequence was amplified and cloned between the *P-lukS* promoter region and *lukF*-PV transcriptional terminator of the Pantan-Valentine leukocidin genes (respectively amplified using primers phi259/phi748 and phi2648/phi2819) on pBluescript. The whole DNA fragment obtained by SmaI was cloned in pLUG37 in the natural EcoRV restriction site between the NWMN39 and NWMN30 sequences. From the resulting plasmid, the DNA fragment corresponding to NWMN30-PlukS-*tirS*-term *lukF*-NWMN29 obtained by EcoRI-Sall restriction was cloned in the pMAD vector (pLUG1158). The resulting chromosomal restored strain was called  $\Delta$ *tirS* + *tirS*. Expression of *tirS* in the restored strain was confirmed by RT-PCR. Oligonucleotides primers for PCR and DNA cloned subfragments are detailed in [S2 Table](#).

## Luciferase activity assay

HEK293T cells (American Type Culture Collection (ATCC), USA) were transiently transfected using Fugene (Roche) for 24 h, according to the manufacturer's instructions, for a total of 0.4  $\mu$ g of DNA consisting of 50 ng TLR plasmids, 200 ng of pBIIXLuc, a reporter plasmid containing luciferase under the control of two IgK-KB sites [55], 5 ng of control Renilla luciferase (pRL-null, Promega), and 50 ng of myc-TirS expression vector, unless stated otherwise. In the case of TLR4, MD2 was co-transfected for efficient detection of LPS. When indicated, an increasing amount of vector (ng) was used for the transfections to obtain different levels of expression of TirS. In all cases, the total amount of DNA was kept constant by adding empty vector. Negative control corresponds to empty vector alone (pCDNA3.1). Where indicated, cells were treated with *E. coli* LPS (1  $\mu$ g/ml), Pam<sub>2</sub>CSK4 (100 ng/ml), CpG ODN1826 (1  $\mu$ M), and Flagellin Fl-ST (1  $\mu$ g/ml), all obtained from Invivogen, for 6 h, and then cells were lysed and luciferase activity measured using the Dual-Glo Luciferase Assay System (Promega). In the case of IL-1R and TNFR, endogenous detection was monitored following 6 h of stimulation with IL-1 $\beta$  (100 ng/ml) or TNF- $\alpha$  (100 ng/ml). The *tirS* construct was obtained with the following primers *tirS*-fw-GGGGACAAGTTTGTACAAAAAAGCAGGCTTCTCAGTATTA GAACTAAATTAATAAAG and *tirS*-rev-GGGGACCACTTTGTACAAGAAAGCTGGGTCC TAATTCTTAGAATTAACGATTACTTG and then cloned in the gateway (Life Technologies) entry vector and subsequently in the pDEST-Myc (Life Technologies) to create an N-terminal myc tag fusion with TirS.

## Immunofluorescence microscopy

HeLa cells (ATCC, USA) were transfected with *myc-tirS* using Fugene (following manufacturer's instructions) for 10 h. Cells were either fixed in 3% paraformaldehyde, pH 7.4, at room temperature for 15 min or placed in ice-cold methanol for 5 min. Cells were then permeabilized for 10 min with 0.1% saponin in PBS, followed by blocking for 1 h with 2% bovine serum albumin and 10% horse serum in PBS with 0.1% saponin. Primary antibodies were incubated

for 1 h followed by three washes in PBS, 1 h incubation for secondary antibodies, two washes in PBS, and one wash in water before being mounted with Prolong Gold. Primary antibodies used were rabbit anti-myc (Abcam) at 1/1000, with either mouse anti-beta tubulin (TUB 2.1) at 1/250 or mouse anti-vimentin (V9) at 1/100 (both Sigma). Secondary antibodies used: donkey anti-rabbit Alexa 488, donkey anti-mouse Alexa 555 (Life Technologies) at 1/1000. The actin cytoskeleton was labeled with phalloidin 568 (Life Technologies). Samples were examined on a Zeiss 710 laser scanning confocal microscope for image acquisition. Images of 1024 × 1024 pixels were then assembled using ImageJ and Adobe Photoshop 7.0.

### Growth curves of *S. aureus* strains

*S. aureus* Geraldine WT and  $\Delta tirS$  strains were grown in fresh BHI medium or TSB medium at 35°C, after dilution of overnight cultures to OD<sub>600</sub> = 0.03. A thermostated microplate reader (TECAN M200 Infinite Pro) was used to follow bacterial growth by measuring OD<sub>600</sub> every 15 min for 24 h. As controls, specific wells were inoculated with medium only. Experiments were done in triplicate.

### Murine model of *S. aureus* subcutaneous infection

**Bacterial isolates and growth.** *S. aureus* Geraldine WT,  $\Delta tirS$ , and  $\Delta tirS + tirS$  strains were used in a murine model of skin infection. For preparation of the inoculum used for subcutaneous inoculation, the bacteria were grown into BHI medium at 37°C for 8 h with constant shaking (200 rpm). They were washed twice and resuspended in sterile PBS, aliquoted to a final concentration of 1.10<sup>7</sup> bacteria/ml, and stored at -80°C until used. For determination of bacterial titers, samples were serially diluted, plated on agar, and incubated overnight at 37°C. Viability of the inocula was confirmed by colony counts with each experiment. Moreover, to ensure that the results of experiments were consistent, hemolysis phenotype was checked using blood agar plates (Trypcase soy agar + 5% sheep blood, bioMérieux, France).

**Mouse strains.** Mice on a C57BL/6 genetic background were used in all experiments. Six-week-old WT female mice were purchased from Charles River, France. Male and female MyD88-deficient mice were kindly provided by L. Genestier (from S. Akira's lab; [56]). All mice were maintained in pathogen-free conditions in a biosafety level 2 facility at the Plateau de Biologie Expérimentale de la Souris (PBES, Ecole Normale Supérieure de Lyon, Lyon, France).

**Skin lesion model.** One day prior to infection, mice were prepared for inoculation. Animals first were anesthetized with 2% isoflurane, and a flank was shaved with electric clipper and hair remover cream (Nair, Church & Dwight Co. Inc., Princeton, NJ) on the shaved flank. On the day of infection, mice were infected subcutaneously with 100 μl of the bacterial suspension (1.10<sup>6</sup> CFUs) in the shaved area. This inoculum was determined in preliminary studies to produce consistent skin lesions. Mice were returned to their cages and observed to awaken. All mice had free access to food and water throughout the duration of the experiments. Animals were weighed at 24 h intervals for 14 days. The area of lesions was measured daily using an electronic caliper and calculated with the formula  $A = \pi \times (L/2) \times (W/2)$  (mm<sup>2</sup>). PBS injection was used for controls.

**Bacterial recovery and cytokine quantification in skin lesions.** To determine the number of CFUs at the site of infection, a second set of mice was inoculated as described above. On days 5 to 9 after infection, mice were euthanized by cervical dislocation; the lesion and the surrounding tissues were removed and transferred in sterile tubes. Tissue samples were weighed, homogenized in 1 ml of PBS (gentleMACS Dissociator, Miltenyi Biotec, Germany), diluted in sterile PBS, and plated on selective agar (ChromID *S. aureus*, bioMérieux, France).

Enumeration of CFUs was performed 24 h later. For determination of cytokine and MPO levels, lesion homogenates were centrifuged and the supernatant removed and immediately stored at  $-80^{\circ}\text{C}$ . Cytokine levels were determined using Luminex assays (Bio-Techne) according to the manufacturer's instructions. The amount of MPO in the skin lesions was quantified using a commercially available ELISA kit (Bio-Techne).

## Statistical analysis

The data were analyzed using R software (<http://www.r-project.org>). Student's t test, Wilcoxon test, or one-way ANOVA followed by multiple comparisons tests (Tukey) were used to compare *tirS* expression, luciferase activity, lesion size, cytokine levels, and bacterial CFUs between the groups. Correlations were assessed by Spearman's correlation. In all experiments, values of  $^{\circ} p < 0.05$ ,  $^{\circ\circ} p < 0.01$ , and  $^{\circ\circ\circ} p < 0.001$  were considered statistically significant.

## Supporting Information

**S1 Table. Primers and restriction enzymes used for construction of the *tirS*-deleted strain.** (PDF)

**S2 Table. Primers and restriction enzymes used for construction of the *tirS*-restored strain.** (PDF)

**S1 Fig. Intracellular localization of ectopically expressed GFP-TirS in HeLa cells.** (TIF)

**S2 Fig. Growth curves of *S. aureus* Geraldine WT and  $\Delta$ *tirS* in BHI medium or TSB medium.** (TIF)

**S3 Fig. Growth curves of *S. aureus* strains in presence of oxacillin or fusidic acid.** (TIF)

## Acknowledgments

We gratefully acknowledge Vale'rie Vogel and David Hernandez for help concerning bioinformatics analysis, and Myriam Girard, Christophe Ginevra and H'el'ene Meunier for technical assistance. We thank Christopher Montgomery and Lloyd Miller for mouse model consultation. We also thank Jacqueline Marvel for helpful discussions. We are grateful to Laurent Genestier for helpful discussions and for providing MyD88-deficient mice and to the staff members at PBES, with a particular thanks to Nadine Aguilera for their support in the animal facility.

## Author Contributions

**Conceived and designed the experiments:** SP RN JS FV SPS PF GL.

**Performed the experiments:** SP PRCI JB JBC AL AF.

**Analyzed the data:** SP JB PMS MB AT FL SPS PF GL.

**Wrote the paper:** SP PMS FV SPS PF GL.



## References

1. Akira S, Uematsu S, Takeuchi O. Pathogen recognition by innate immunity. *Cell*. 2006; 124: 783–801. doi: [10.1016/j.cell.2006.02.015](https://doi.org/10.1016/j.cell.2006.02.015) PMID: [16497588](https://pubmed.ncbi.nlm.nih.gov/16497588/)
2. Gay NJ, Gangloff M. Structure and function of Toll receptors and their ligands. *Annu Rev Biochem*. 2007; 76:141–65. doi: [10.1146/annurev.biochem.76.060305.151318](https://doi.org/10.1146/annurev.biochem.76.060305.151318) PMID: [17362201](https://pubmed.ncbi.nlm.nih.gov/17362201/)
3. Narayanan KB, Park HH. Toll/interleukin-1 receptor (TIR) domain-mediated cellular signaling pathways. *Apoptosis*. 2015; 20:196–209. doi: [10.1007/s10495-014-1073-1](https://doi.org/10.1007/s10495-014-1073-1) PMID: [25563856](https://pubmed.ncbi.nlm.nih.gov/25563856/)
4. Rana RR, Zhang M, Spear AM, Atkins HS, Byrne B. Bacterial TIR-containing proteins and host innate immune system evasion. *Med Microbiol Immunol*. 2013; 202(1):1–10. doi: [10.1007/s00430-012-0253-2](https://doi.org/10.1007/s00430-012-0253-2) PMID: [22772799](https://pubmed.ncbi.nlm.nih.gov/22772799/)
5. Newman R, Salunkhe P, Godzik A, Reed JC. Identification and characterization of a novel bacterial virulence factor that shares homology with mammalian Toll/interleukin-1 receptor family proteins. *Infect Immun*. 2006; 74(1):594–601. doi: [10.1128/IAI.74.1.594-601.2006](https://doi.org/10.1128/IAI.74.1.594-601.2006) PMID: [16369016](https://pubmed.ncbi.nlm.nih.gov/16369016/)
6. Salcedo SP, Marchesini MI, Lelouard H, Fugier E, Jolly G, Balor S, et al. *Brucella* control of dendritic cell maturation is dependent on the TIR-containing protein Btp1. *PLOS Pathog*. 2008; 4(2).
7. Cirl C, Miethke T. Microbial Toll/interleukin 1 receptor proteins: A new class of virulence factors. *Int J Med Microbiol*. 2010; 300:396–401. doi: [10.1016/j.ijmm.2010.04.001](https://doi.org/10.1016/j.ijmm.2010.04.001) PMID: [20451449](https://pubmed.ncbi.nlm.nih.gov/20451449/)
8. Salcedo SP, Marchesini MI, Degos C, Terwagne M, Von Bargen K, Lepidi H, et al. BtpB, a novel *Brucella* TIR-containing effector protein with immune modulatory functions. *Front Cell Infect Microbiol*. 2013; 3(July):28. doi: [10.3389/fcimb.2013.00028](https://doi.org/10.3389/fcimb.2013.00028) PMID: [23847770](https://pubmed.ncbi.nlm.nih.gov/23847770/)
9. Askarian F, Van Sorge NM, Sangvik M, Beasley FC, Henriksen JR, Sollid JUE, et al. A *Staphylococcus aureus* TIR domain protein virulence factor blocks TLR2-mediated NF- $\kappa$ B signaling. *J Innate Immun*. 2014; 6(4):485–98. doi: [10.1159/000357618](https://doi.org/10.1159/000357618) PMID: [24481289](https://pubmed.ncbi.nlm.nih.gov/24481289/)
10. Lowy FD. *Staphylococcus aureus* Infections. *N Engl J Med*. 1998; 339:520–32. doi: [10.1056/NEJM199808203390806](https://doi.org/10.1056/NEJM199808203390806) PMID: [9709046](https://pubmed.ncbi.nlm.nih.gov/9709046/)
11. Jevons MP. 'Celbenin'-Resistant Staphylococci. *Br Med J*. 1961; 1:124–5.
12. Wulf MWH, Sørnum M, Van Nes A, Skov R, Melchers WJG, Klaassen CHW, et al. Prevalence of methicillin-resistant *Staphylococcus aureus* among veterinarians: an international study. *Clin Microbiol Infect*. 2008; 14(1):29–34. doi: [10.1111/j.1469-0691.2007.01873.x](https://doi.org/10.1111/j.1469-0691.2007.01873.x) PMID: [17986212](https://pubmed.ncbi.nlm.nih.gov/17986212/)
13. Vandenesch F, Naimi T, Enright MC, Lina G, Nimmo GR, Heffernan H, et al. Community-acquired methicillin-resistant *Staphylococcus aureus* carrying panton-valentine leukocidin genes: Worldwide emergence. *Emerg Infect Dis*. 2003; 9(8):978–84. doi: [10.3201/eid0908.030089](https://doi.org/10.3201/eid0908.030089) PMID: [12967497](https://pubmed.ncbi.nlm.nih.gov/12967497/)
14. Katayama Y, Ito T, Hiramatsu K. A new class of genetic element, staphylococcus cassette chromosome *mec*, encodes methicillin resistance in *Staphylococcus aureus*. *Antimicrob Agents Chemother*. 2000 Jun; 44(6):1549–55. PMID: [10817707](https://pubmed.ncbi.nlm.nih.gov/10817707/)
15. Holden MTG, Feil EJ, Lindsay JA, Peacock SJ, Day NPJ, Enright MC, et al. Complete genomes of two clinical *Staphylococcus aureus* strains: evidence for the rapid evolution of virulence and drug resistance. *Proc Natl Acad Sci U S A*. 2004; 101(26):9786–91. doi: [10.1073/pnas.0402521101](https://doi.org/10.1073/pnas.0402521101) PMID: [15213324](https://pubmed.ncbi.nlm.nih.gov/15213324/)
16. Felix C, Kaplan Türköz B, Ranaldi S, Koelblen T, Terradot L, O'Callaghan D, et al. The *Brucella* TIR domain containing proteins BtpA and BtpB have a structural WxxxE motif important for protection against microtubule depolymerisation. *Cell Commun Signal*. 2014; 12:53. doi: [10.1186/s12964-014-0053-y](https://doi.org/10.1186/s12964-014-0053-y) PMID: [25304327](https://pubmed.ncbi.nlm.nih.gov/25304327/)
17. Cirl C, Wieser A, Yadav M, Duerr S, Schubert S, Fischer H, et al. Subversion of Toll-like receptor signaling by a unique family of bacterial Toll/interleukin-1 receptor domain-containing proteins. *Nat Med*. 2008; 14(4):399–406. doi: [10.1038/nm1734](https://doi.org/10.1038/nm1734) PMID: [18327267](https://pubmed.ncbi.nlm.nih.gov/18327267/)
18. Carlsson E, Thwaite JE, Jenner DC, Spear AM, Flick-Smith H, Atkins HS, et al. *Bacillus anthracis* TIR Domain-Containing Protein Localises to Cellular Microtubule Structures and Induces Autophagy. *PLoS One*. 2016; <http://dx.doi.org/10.1371/journal.pone.0158575>.
19. Coste I, Le Corf K, Kfoury A, Hmitou I, Druillenec S, Hainaut P, et al. Dual function of MyD88 in RAS signaling and inflammation, leading to mouse and human cell transformation. *J Clin Invest*. 2010; 120(10):3663–7. doi: [10.1172/JCI42771](https://doi.org/10.1172/JCI42771) PMID: [20941850](https://pubmed.ncbi.nlm.nih.gov/20941850/)
20. McGuire VA, Arthur JSC. Subverting Toll-Like Receptor Signaling by Bacterial Pathogens. *Front Immunol*. 2015; 6:607. doi: [10.3389/fimmu.2015.00607](https://doi.org/10.3389/fimmu.2015.00607) PMID: [26648936](https://pubmed.ncbi.nlm.nih.gov/26648936/)
21. Casadevall A, Pirofski LA. The damage-response framework of microbial pathogenesis and infectious diseases. *Nat Rev Microbiol*. 2003; 1(October):17–24. doi: [10.1007/978-0-387-09550-9\\_11](https://doi.org/10.1007/978-0-387-09550-9_11) PMID: [18841709](https://pubmed.ncbi.nlm.nih.gov/18841709/)

22. Montgomery CP, Daniels MD, Zhao F, Spellberg B, Chong AS, Daum RS. Local Inflammation Exacerbates the Severity of *Staphylococcus aureus* Skin Infection. *PLoS One*. 2013; 8(7):1–6.
23. Lin L, Tan B, Pantapalangkoor P, Ho T, Baquir B, Tomaras A, et al. Inhibition of LpxC protects mice from resistant *Acinetobacter baumannii* by modulating inflammation and enhancing phagocytosis. *MBio*. 2012; 3(5).
24. Radhakrishnan GK, Harms JS, Splitter GA. Modulation of microtubule dynamics by a TIR domain protein from the intracellular pathogen *Brucella melitensis*. *Biochem J*. 2011; 439(1):79–83. doi: [10.1042/BJ20110577](https://doi.org/10.1042/BJ20110577) PMID: [21692747](https://pubmed.ncbi.nlm.nih.gov/21692747/)
25. Zhang Q, Zmasek CM, Cai X, Godzik A. TIR domain-containing adaptor SARM is a late addition to the ongoing microbe-host dialog. *Dev Comp Immunol*. Elsevier Ltd; 2011; 35(4):461–8.
26. Dumitrescu O, Badiou C, Bes M, Reverdy M, Vandenesch F, Etienne J, et al. Effect of antibiotics, alone and in combination, on Panton–Valentine leukocidin production by a *Staphylococcus aureus* reference strain. *Clin Microbiol Infect*. 2004; 14(4):384–8.
27. Juuti K, Ibrahim S, Virolainen-Julkunen A, Vuopio-Varkila J, Kuusela P. The *pls* Gene Found in Methicillin-Resistant *Staphylococcus aureus* Strains Is Common in Clinical Isolates of *Staphylococcus sciuri*. *J Clin Microbiol*. 2005; 43(3):1415–9. doi: [10.1128/JCM.43.3.1415-1419.2005](https://doi.org/10.1128/JCM.43.3.1415-1419.2005) PMID: [15750121](https://pubmed.ncbi.nlm.nih.gov/15750121/)
28. Hussain M, Schäfer D, Juuti KM, Peters G, Haslinger-Löffler B, Kuusela PI, et al. Expression of Pls (plasmin sensitive) in *Staphylococcus aureus* negative for *pls* reduces adherence and cellular invasion and acts by steric hindrance. *J Infect Dis*. 2009; 200:107–17. doi: [10.1086/599359](https://doi.org/10.1086/599359) PMID: [19473097](https://pubmed.ncbi.nlm.nih.gov/19473097/)
29. Deurenberg RH, Vink C, Oudhuis GJ, Mooij JE, Driessen C, Coppens G, et al. Different Clonal Complexes of Methicillin-Resistant *Staphylococcus aureus* Are Disseminated in the Euregio Meuse-Rhine Region. *Antimicrob Agents Chemother*. 2005; 49(10):4263–71. doi: [10.1128/AAC.49.10.4263-4271.2005](https://doi.org/10.1128/AAC.49.10.4263-4271.2005) PMID: [16189107](https://pubmed.ncbi.nlm.nih.gov/16189107/)
30. Queck SY, Jameson-Lee M, Villaruz AE, Bach THL, Khan BA, Sturdevant DE, et al. RNAIII-Independent Target Gene Control by the agr Quorum-Sensing System: Insight into the Evolution of Virulence Regulation in *Staphylococcus aureus*. *Mol Cell*. 2008; 32(1):150–8. doi: [10.1016/j.molcel.2008.08.005](https://doi.org/10.1016/j.molcel.2008.08.005) PMID: [18851841](https://pubmed.ncbi.nlm.nih.gov/18851841/)
31. Queck SY, Khan BA, Wang R, Bach THL, Kretschmer D, Chen L, et al. Mobile genetic element-encoded cytolysin connects virulence to methicillin resistance in MRSA. *PLOS Pathog*. 2009; 5(7):1–12.
32. Monecke S, Engelmann I, Archambault M, Coleman DC, Coombs GW, Cortez De Jäckel S, et al. Distribution of SCC*mec*-associated phenol-soluble modulin in staphylococci. *Mol Cell Probes*. 2012; 26:99–103. doi: [10.1016/j.mcp.2012.01.001](https://doi.org/10.1016/j.mcp.2012.01.001) PMID: [22251619](https://pubmed.ncbi.nlm.nih.gov/22251619/)
33. Durand G, Bes M, Meugnier H. New methicillin-resistant *Staphylococcus aureus* clones containing the toxic shock syndrome toxin 1 gene responsible for hospital-and community-acquired infections. *J Clin Microbiol*. 2006; 44(3):847–53.
34. Dauwalder O, Lina G, Durand G, Bes M, Meugnier H, Jarlier V, et al. Epidemiology of invasive methicillin-resistant *Staphylococcus aureus* clones collected in France in 2006 and 2007. *J Clin Microbiol*. 2008; 46(10):3454–8. doi: [10.1128/JCM.01050-08](https://doi.org/10.1128/JCM.01050-08) PMID: [18667599](https://pubmed.ncbi.nlm.nih.gov/18667599/)
35. Leroyer C, Lehours P, Tristan A, Boyer F, Marie V, Elleau C, et al. Outbreak in newborns of methicillin-resistant *Staphylococcus aureus* related to the sequence type 5 Geraldine clone. *Am J Infect Control*. Elsevier Inc; 2016; 44(2):10–2.
36. Baines SL, Howden BP, Heffernan H, Stinear TP, Carter GP, Seemann T, et al. Rapid emergence and evolution of *Staphylococcus aureus* clones harbouring *fusC*-containing Staphylococcal Cassette Chromosome elements. *Antimicrob Agents Chemother*. 2016; 60(4):2359–65. doi: [10.1128/AAC.03020-15](https://doi.org/10.1128/AAC.03020-15) PMID: [26856837](https://pubmed.ncbi.nlm.nih.gov/26856837/)
37. Ellington MJ, Reuter S, Harris SR, Holden MTG, Cartwright EJ, Greaves D, et al. Emergent and evolving antimicrobial resistance cassettes in community-associated fusidic acid and methicillin-resistant *Staphylococcus aureus*. *Int J Antimicrob Agents*. 2015; 45:477–84. doi: [10.1016/j.ijantimicag.2015.01.009](https://doi.org/10.1016/j.ijantimicag.2015.01.009) PMID: [25769787](https://pubmed.ncbi.nlm.nih.gov/25769787/)
38. The Commission of the European Communities. Commission decision of 22 December 1999 on the communicable diseases to be progressively covered by the community network under decision number 2119/98/EC of the European Parliament and of the Council. *Off J Eur Communities*. 2000;(L28/50).
39. The European Parliament and the Council of the UE. Decision number 2119/98/EC of the European Parliament and of the Council of 24 September 1998: setting up a network for the epidemiological surveillance and control of communicable diseases in the community. *Off J Eur Communities*. 1998;(L 268/1).
40. Monecke S, Luedicke C, Slickers P, Ehrlich R. Molecular epidemiology of *Staphylococcus aureus* in asymptomatic carriers. *Eur J Clin Microbiol Infect Dis*. 2009; 28:1159–65. doi: [10.1007/s10096-009-0752-2](https://doi.org/10.1007/s10096-009-0752-2) PMID: [19434432](https://pubmed.ncbi.nlm.nih.gov/19434432/)



41. Coil D, Jospin G, Darling AE. A5-miseq: An updated pipeline to assemble microbial genomes from Illumina MiSeq data. *Bioinformatics*. 2015; 31(4):587–9. doi: [10.1093/bioinformatics/btu661](https://doi.org/10.1093/bioinformatics/btu661) PMID: [25338718](https://pubmed.ncbi.nlm.nih.gov/25338718/)
42. Lohse M, Bolger AM, Nagel A, Fernie AR, Lunn JE, Stitt M, et al. RobiNA: a user-friendly, integrated software solution for RNA-Seq-based transcriptomics. *Nucleic Acids Res*. 2012; 40(Web Server issue):W622–7. doi: [10.1093/nar/gks540](https://doi.org/10.1093/nar/gks540) PMID: [22684630](https://pubmed.ncbi.nlm.nih.gov/22684630/)
43. Simpson JT, Durbin R. Efficient de novo assembly of large genomes using compressed data structures. *Genome Res*. 2012; 22(3):549–56. doi: [10.1101/gr.126953.111](https://doi.org/10.1101/gr.126953.111) PMID: [22156294](https://pubmed.ncbi.nlm.nih.gov/22156294/)
44. Peng Y, Leung HCM, Yiu SM, Lv MJ, Zhu XG, Chin FYL. IDBA-tran: A more robust de novo de Bruijn graph assembler for transcriptomes with uneven expression levels. In: *Bioinformatics*. 2013. 29(13):i326–34. doi: [10.1093/bioinformatics/btt219](https://doi.org/10.1093/bioinformatics/btt219) PMID: [23813001](https://pubmed.ncbi.nlm.nih.gov/23813001/)
45. Li H, Durbin R. Fast and accurate short read alignment with Burrows–Wheeler transform. *Bioinformatics*. 2009; 25(14):1754–1760. doi: [10.1093/bioinformatics/btp324](https://doi.org/10.1093/bioinformatics/btp324) PMID: [19451168](https://pubmed.ncbi.nlm.nih.gov/19451168/)
46. Darling AE, Mau B, Perna NT. Progressivemauve: Multiple genome alignment with gene gain, loss and rearrangement. *PLoS One*. 2010; 5(6).
47. Ito T, Takeuchi F, Okuma K, Yuzawa H, Hiramatsu K. Novel Type V Staphylococcal Cassette Chromosome. *Antimicrob Agents Chemother*. 2004; 48(7):2637–51. doi: [10.1128/AAC.48.7.2637-2651.2004](https://doi.org/10.1128/AAC.48.7.2637-2651.2004) PMID: [15215121](https://pubmed.ncbi.nlm.nih.gov/15215121/)
48. Noto MJ, Archer GL. A Subset of *Staphylococcus aureus* Strains Harboring Staphylococcal Cassette Chromosome *mec* (SCC*mec*) Type IV Is Deficient in *ccrAB*-Mediated SCC*mec* Excision. *Antimicrob Agents Chemother*. 2006; 50(8):2782–8. doi: [10.1128/AAC.00032-06](https://doi.org/10.1128/AAC.00032-06) PMID: [16870772](https://pubmed.ncbi.nlm.nih.gov/16870772/)
49. Beaume M, Hernandez D, Farinelli L, Cile Deluen C, Linder P, Gaspin C, et al. Cartography of Methicillin-Resistant *S. aureus* Transcripts: Detection, Orientation and Temporal Expression during Growth Phase and Stress Conditions. *PLoS One*. 2010; 5(5).
50. Clinical and Laboratory Standards Institute (CLSI). Performance standards for antimicrobial susceptibility testing. Natl Comm Clin Lab Stand Wayne, PA. 2003 (CLSI Document M100–S13).
51. Kreiswirth B, Löfdahl S, Betley M, O'Reilly M, Schlievert P, Bergdoll M, et al. The toxic shock syndrome exotoxin structural gene is not detectably transmitted by a prophage. *Nature*. 1983; 305:709–12. PMID: [6226876](https://pubmed.ncbi.nlm.nih.gov/6226876/)
52. Fischer A, Kambara K, Meyer H, Stenz L, Bonetti E-J, Girard M, et al. GdpS contributes to *Staphylococcus aureus* biofilm formation by regulation of eDNA release. *Int J Med Microbiol*. 2014; 304:284–99. doi: [10.1016/j.ijmm.2013.10.010](https://doi.org/10.1016/j.ijmm.2013.10.010) PMID: [24275081](https://pubmed.ncbi.nlm.nih.gov/24275081/)
53. Charpentier E, Anton AI, Barry P, Alfonso B, Fang Y, Novick RP. Novel Cassette-Based Shuttle Vector System for Gram-Positive Bacteria. *Appl Environ Microbiol*. 2004; 70(10):6076–85. doi: [10.1128/AEM.70.10.6076-6085.2004](https://doi.org/10.1128/AEM.70.10.6076-6085.2004) PMID: [15466553](https://pubmed.ncbi.nlm.nih.gov/15466553/)
54. Arnaud M, Chastanet A, Débarbouillé M. New Vector for Efficient Allelic Replacement in Naturally Non-transformable, Low-GC-Content, Gram-Positive Bacteria. *Appl Environ Microbiol*. 2004; 70(11):6887–91. doi: [10.1128/AEM.70.11.6887-6891.2004](https://doi.org/10.1128/AEM.70.11.6887-6891.2004) PMID: [15528558](https://pubmed.ncbi.nlm.nih.gov/15528558/)
55. Kopp E, Ghosh S. Inhibition of NF- $\kappa$ B by sodium salicylate and aspirin. *Science*. 1994; 265:956–9. PMID: [8052854](https://pubmed.ncbi.nlm.nih.gov/8052854/)
56. Adachi O, Kawai T, Takeda K, Matsumoto M, Tsutsui H, Sakagami M, et al. Targeted disruption of the MyD88 gene results in loss of IL-1- and IL-18-mediated function. *Immunity*. 1998; 9(143–150). PMID: [9697844](https://pubmed.ncbi.nlm.nih.gov/9697844/)





2. Annexe 2 : A *Pseudomonas aeruginosa* TIR effector mediates immune evasion by targeting UBAP1 and TLR adaptors

Imbert et al. EMBO Journal 2017

This work identified PumA, a TIR protein of an atypical *P. aeruginosa* strain, as a key virulence determinant capable of interfering with both TLR and TNF receptor signalling. This work also implicated for the first time a role for the endosomal-sorting complex required for transport I (ESCRT-I) in modulation of intracellular trafficking of TLR adaptors. I carried out all the *in vitro* interaction assays with purified PumA and PumA<sub>1-136</sub> either using eukaryotic cell extracts expressing TIRAP and Myd88 or by co-expression in *E. coli* and realized lipid binding experiments.

# A *Pseudomonas aeruginosa* TIR effector mediates immune evasion by targeting UBAP1 and TLR adaptors

Paul RC Imbert<sup>1</sup>, Arthur Louche<sup>1</sup>, Jean-Baptiste Luizet<sup>1</sup>, Teddy Grandjean<sup>2</sup>, Sarah Bigot<sup>1</sup>, Thomas E Wood<sup>3</sup>, Stéphanie Gagné<sup>1</sup>, Amandine Blanco<sup>1</sup>, Lydia Wunderley<sup>4</sup>, Laurent Terradot<sup>1</sup>, Philip Woodman<sup>4</sup>, Steve Garvis<sup>5</sup>, Alain Filloux<sup>3</sup> , Benoit Guery<sup>2</sup> & Suzana P Salcedo<sup>1,\*</sup> 

## Abstract

Bacterial pathogens often subvert the innate immune system to establish a successful infection. The direct inhibition of downstream components of innate immune pathways is particularly well documented but how bacteria interfere with receptor proximal events is far less well understood. Here, we describe a Toll/interleukin 1 receptor (TIR) domain-containing protein (PumA) of the multi-drug resistant *Pseudomonas aeruginosa* PA7 strain. We found that PumA is essential for virulence and inhibits NF- $\kappa$ B, a property transferable to non-PumA strain PA14, suggesting no additional factors are needed for PumA function. The TIR domain is able to interact with the Toll-like receptor (TLR) adaptors TIRAP and MyD88, as well as the ubiquitin-associated protein 1 (UBAP1), a component of the endosomal-sorting complex required for transport I (ESCRT-I). These interactions are not spatially exclusive as we show UBAP1 can associate with MyD88, enhancing its plasma membrane localization. Combined targeting of UBAP1 and TLR adaptors by PumA impedes both cytokine and TLR receptor signalling, highlighting a novel strategy for innate immune evasion.

**Keywords** *Pseudomonas*; TIR domain; TLR adaptors; UBAP1; virulence  
**Subject Categories** Microbiology, Virology & Host Pathogen Interaction  
DOI 10.15252/embj.201695343 | Received 27 July 2016 | Revised 29 March 2017 | Accepted 5 April 2017 | Published online 8 May 2017  
The EMBO Journal (2017) 36: 1869–1887

## Introduction

Microbial pathogen recognition by innate immune receptors initiates a progression of molecular interactions and signalling events assuring host defence. In bacterial infections, detection of surface

components, such as peptidoglycan, lipopolysaccharides and flagellin by Toll-like receptors (TLR) 2, 4 and 5, respectively, is essential for induction of pro-inflammatory cytokines and type I interferon (IFN) responses. Specific sorting and signalling adaptor proteins bridge activated receptors with downstream kinases to initiate signalling cascades via Toll/interleukin 1 receptor (TIR) domains present on both the adaptors and the cytosolic face of TLRs (Brubaker *et al*, 2015). Upon TLR2 or TLR4 activation, the TIR-containing adaptor protein (TIRAP) recruits myeloid differentiation primary response 88 (MyD88) that interacts with the TLR via its TIR domain (Fitzgerald *et al*, 2001; Horng *et al*, 2001; Kagan & Medzhitov, 2006). MyD88 oligomerization and recruitment of specific kinases leads to the formation of myddosomes, signalling platforms that induce NF- $\kappa$ B translocation into the nucleus and subsequent transcription of pro-inflammatory associated genes (Nagpal *et al*, 2011; Bonham *et al*, 2014). TLR4 activation also results in induction of a type I IFN via another set of adaptors, TRAM and TRIF (Fitzgerald *et al*, 2001; Yamamoto *et al*, 2002; Kagan *et al*, 2008). In the case of the MyD88-dependent TLR5, the identity of a sorting adaptor remains undefined and the role of TIRAP unclear although it has been implicated in proper TLR5 signalling in epithelial cells (Choi *et al*, 2013).

Microbial pathogens have been shown to counter these host defence pathways. Most bacterial immune-modulatory proteins described to date rely on inhibition of downstream signalling components, such as MAP kinases and transcription factors (reviewed in Rosadini & Kagan, 2015). In contrast, few examples of direct blocking at the level of initial receptor–adaptor complexes are known. Some bacterial pathogens rely on TIR domain-containing proteins to perturb TIR-dependent interactions (Newman *et al*, 2006; Cirl *et al*, 2008; Salcedo *et al*, 2008, 2013), essential in innate immune signalling. The growing number of bacterial TIR proteins recently identified in both Gram-negative and Gram-positive human

<sup>1</sup> Laboratory of Molecular Microbiology and Structural Biochemistry, Centre National de la Recherche Scientifique, University of Lyon, Lyon, France

<sup>2</sup> EA 7366 Recherche Translationnelle Relations Hôte-Pathogènes, Faculté de Médecine Pôle Recherche, Université Lille 2, Lille, France

<sup>3</sup> MRC Centre for Molecular Bacteriology and Infection, Imperial College London, London, UK

<sup>4</sup> School of Biological Sciences, Faculty of Biology Medicine and Health, University of Manchester, Manchester Academic Health Science Centre, Manchester, UK<sup>†</sup>

<sup>5</sup> Laboratoire de Biologie et Modélisation, Ecole Normal Supérieur, UMR5239, Lyon, France

\*Corresponding author. Tel: +33 437652915; E-mail: [suzana.salcedo@ibcp.fr](mailto:suzana.salcedo@ibcp.fr)

<sup>†</sup>Correction added on 3 July 2017, after first online publication: affiliation 4 has been corrected

pathogens (Spear *et al*, 2012; Askarian *et al*, 2014; Zou *et al*, 2014) highlights the importance of this immune evasion strategy in disease. However, the molecular mechanisms underlying most TIR-dependent virulence strategies remain to be defined.

We focused on a previously uncharacterized TIR domain-containing protein of the multi-drug resistant pathogen *Pseudomonas aeruginosa* PA7, that we called PumA. *P. aeruginosa* PA7 lacks genes encoding the type III secretion system (T3SS) and its cognate effector proteins that are normally associated with strong induction of cell death, a hallmark of acute *P. aeruginosa* infections (reviewed by Filloux, 2011). In addition, PA7 does not show high lytic capacity towards epithelial cells due to exolysin A (ExlA) as described for the haemorrhagic pneumonia-causing strain of the same family (Elsen *et al*, 2014; Reboud *et al*, 2016). We thus took advantage of the absence of traditional virulence factors in this *P. aeruginosa* strain to study the molecular interactions involved in TIR-mediated bacterial targeting of events proximal to receptor–adaptor signalling complexes and to dissect PumA function. We found that the PumA *Pseudomonas* TIR domain-containing protein is essential for PA7 virulence conferring a previously unrecognized ability to *Pseudomonas* to down-modulate innate immune responses during infection. We show that PumA directly interacts with both TIRAP and MyD88 to control TLR signalling. Uniquely, it also targets the ubiquitin-associated protein 1 (UBAP1), a recently discovered component of the endosomal-sorting complex required for transport I (ESCRT-I; Stefani *et al*, 2011). UBAP1 is known to play a key role in selective sorting of ubiquitinated endosomal cargo on multi-vesicular bodies (MVB), via its interaction with VPS37A and other components of ESCRT-I namely TSG101 (Wunderley *et al*, 2014), as well as with the ESCRT regulator, His domain protein tyrosine phosphatase (HDPTP; Stefani *et al*, 2011). UBAP1 has been shown to control endosomal sorting of ubiquitinated EGFR (Stefani *et al*, 2011) as well as ubiquitin-dependent degradation of antiviral surface proteins (Agromayor *et al*, 2012) and integrins (Kharitidi *et al*, 2015). More recently, UBAP1 was shown to modulate steady-state trafficking of cytokine receptors in non-stimulated cells (Mamińska *et al*, 2016). UBAP1 is expressed in a wide range of tissues, but when deleted in mice, it is lethal for embryos (Agromayor *et al*, 2012).

We propose that this novel *Pseudomonas* effector modulates UBAP1 function, hence the name PumA (for *Pseudomonas* UBAP1 modulator A), which confers to this TIR domain-containing protein the distinctive ability to also interfere with cytokine receptor signalling. Targeting of both TLR adaptors and UBAP1 by PumA is not spatially restricted as we found UBAP1 can associate with MyD88 in host cells. Our results thus highlight a novel role of bacterial TIR domains and place UBAP1 sorting in the context of TLR signalling.

## Results

### PumA is required for *Pseudomonas aeruginosa* PA7 virulence *in vivo*

In *Pseudomonas*, TIR domain-containing proteins were first identified in an *in silico* study in *P. aeruginosa* and the plant pathogen *P. syringae* (Zhang *et al*, 2011). Analysis of currently available genomes shows that several plant strains encode such proteins as

well as additional human pathogenic strains of *P. stutzeri* and *P. aeruginosa*. The closest orthologue is found in the plant pathogen *P. viridiflava*. The TIR domain of PumA spans the first 136 amino acids of PumA (Appendix Fig S1A and B), with no significant sequence/structure homologies detected for the C-terminal domain (amino acid 137–303) and no signal peptide. Analysis of the PA7 genome shows *pumA* (PSPA7\_2375) is within the genomic island RGP56, which displays a G+C content of 58.5% in contrast to the average 66.5% in the remaining genome. Interestingly, using Geneious (Kearse *et al*, 2012), we found the *pumA* gene itself has an even larger reduction in G+C content (46.6%) (Appendix Fig S1C), suggesting that it is not a conserved gene within its immediate genetic context.

We assessed the potential role of PumA in virulence by infecting the nematode *Caenorhabditis elegans*, a well-established model for *P. aeruginosa* allowing for rapid assessment of virulence (Garvis *et al*, 2009). Infection with the highly virulent strain *P. aeruginosa* PA14 which contains virulence factors such as the T3SS but no TIR protein resulted in 50% lethality at day 5. The PA7 wild-type strain caused 50% lethality 7 days after inoculation. In contrast, we found that the PA7  $\Delta pumA$  mutant showed a slight but significant attenuation in virulence in *C. elegans* (Fig 1A). These differences were not due to an *in vitro* growth defect of the mutant (Appendix Fig S2A) nor to a problem in expression of PumA in the wild-type *P. aeruginosa* PA7 strain (Appendix Fig S2B).

We then used an acute *in vivo* infection model to evaluate the involvement of *pumA* in *P. aeruginosa* induced lung injury. Mice infected with *DpumA* showed a clear increased survival compared to wild-type strain (Fig 1B). A dose of  $4.10^7$  CFU of PA7 induced 100% lethality after 52 h against 62.5% survival after 96 h for the *DpumA* mutant. Bacterial clearance and cellular recruitment were then analysed with a lower inoculum of  $3.10^7$  CFU. PA7*DpumA* infected mice showed decreased cell recruitment (Fig 1C) and an enhanced lung bacterial clearance in bronchoalveolar lavages (BAL) compared to the wild-type strain (Fig 1D). The bacterial dissemination measured with the spleen bacterial load was equivalent between the two groups (Fig 1E). Together these results show that PumA is required for *P. aeruginosa* PA7 infection.

### PumA inhibits NF- $\kappa$ B translocation into the nucleus during infection *in vitro*

As bacterial TIR proteins down-modulate NF- $\kappa$ B activation (Newman *et al*, 2006; Cirl *et al*, 2008; Salcedo *et al*, 2008, 2013; Spear *et al*, 2012; Askarian *et al*, 2014; Zou *et al*, 2014), we infected the lung carcinoma epithelial cell line A549, a well-established cellular model for *Pseudomonas* infection and analysed NF- $\kappa$ B translocation into the nucleus after one hour of infection by confocal microscopy. We developed an automated analysis of p65/RelA fluorescence in relation to DAPI labelling using a specific ImageJ plugin from images obtained by confocal microscopy (Fig EV1A) which allowed us to clearly differentiate between TNF $\alpha$ -treated and mock-infected cells (Figs 2A and EV1B). Infection with the three heat-killed *P. aeruginosa* strains, wild-type PA7, isogenic mutant *DpumA* or wild-type PA14 resulted in significant induction of NF- $\kappa$ B translocation into the nucleus, although to a lower level than TNF $\alpha$ -treated cells (Fig 2A). When cells were infected with PA7, there was no significant induction of

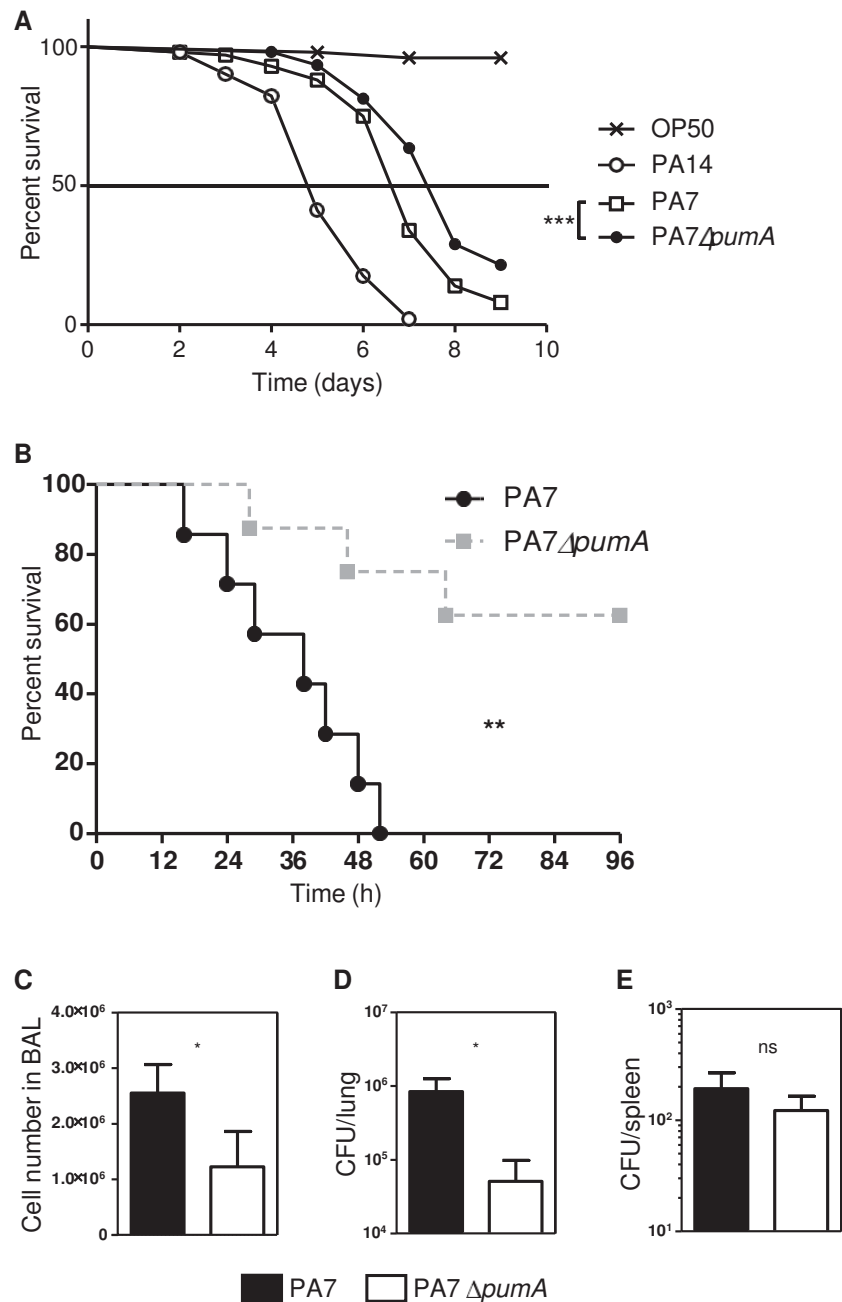


Figure 1. PumA is required for *Pseudomonas aeruginosa* PA7 virulence *in vivo*.

A *Caenorhabditis elegans* survival curve. Fifty *C. elegans* were infected with *E. coli* OP50 and with highly virulent strain *P. aeruginosa* PA14. One hundred *C. elegans* were infected with *P. aeruginosa* PA7 and PA7  $\Delta$ pumA. Test of Mantel–Cox was used with \*\*\* $P$  = 0.0002.

B To establish an *in vivo* model of acute infection, mice were intranasally infected with  $4 \times 10^7$  CFU *P. aeruginosa* PA7 or PA7 $\Delta$ pumA strains ( $n$  = 7/group). Lethality was monitored for 96 h, and a test of Mantel–Cox was used, with \*\* $P$  = 0.0035.

C–E Mice were intranasally infected with  $3 \times 10^7$  CFU *P. aeruginosa* PA7 or PA7 $\Delta$ pumA strains ( $n$  = 7/group). Cells from bronchoalveolar lavage (BAL) were counted (C). Bacterial load in the lungs (D) and dissemination (E) were assessed through cultured lung or spleen homogenate. Non-parametric two-tailed Mann–Whitney test was carried out with (C) \* $P$  = 0.0173, (D) \* $P$  = 0.0364 and (E)  $P$  = 0.3629. All data correspond to mean  $\pm$  standard error.

NF- $\kappa$ B when compared with the mock-infected negative control (Fig 2B), suggesting PA7 blocks NF- $\kappa$ B translocation into the nucleus. In contrast, *DpumA* infection promoted NF- $\kappa$ B nuclear translocation, attaining activation levels similar to those observed with heat-killed bacteria. The inability of *pumA* mutants to block

NF- $\kappa$ B nuclear transport was complemented by chromosomal expression of this gene under an arabinose-inducible promoter (Fig 2C). Importantly, when *pumA* expression was repressed with glucose, no complementation of NF- $\kappa$ B inhibition was observed (Fig 2B). Addition of arabinose had no effect on NF- $\kappa$ B

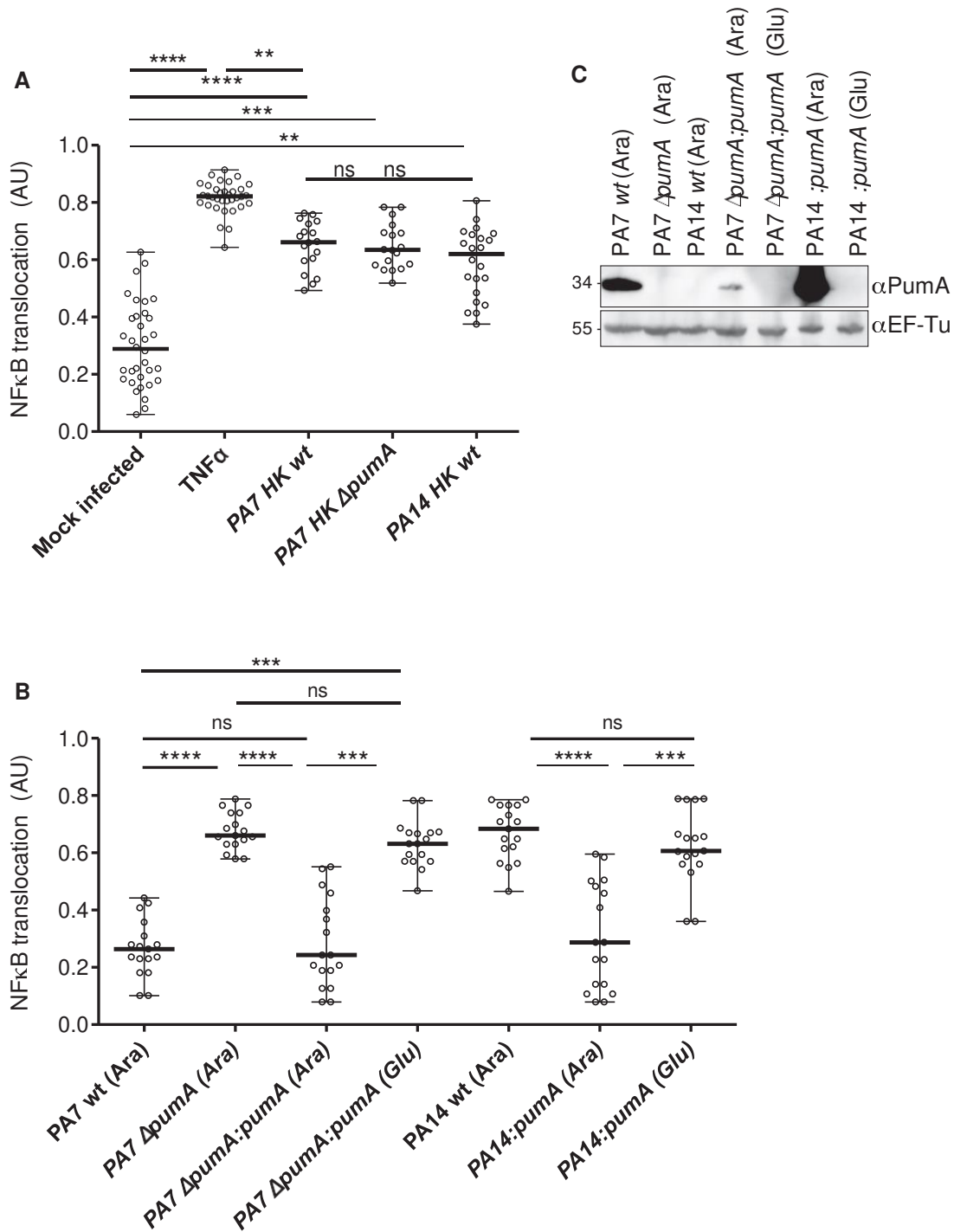


Figure 2. PumA is essential for control of NF- $\kappa$ B translocation into the nucleus during *Pseudomonas aeruginosa* infection of human A549 lung epithelial cells.

A Quantification of fluorescence ratio between nuclear NF- $\kappa$ B (p65) and nuclear DAPI staining. Negative control corresponds to uninfected cells that underwent all steps of the experiment. Positive control corresponds to full NF- $\kappa$ B activation with TNF $\alpha$  (1  $\mu$ g/ml). A549 cells were incubated for 1 h with heat-killed (HK) bacteria to establish maximum activation induced by *Pseudomonas* infection.

B Cells were infected for 1 h with either *P. aeruginosa* PA7 wt,  $\Delta$ pumA,  $\Delta$ pumA:pumA (Ara) induced with 1% arabinose and  $\Delta$ pumA:pumA (Glu) repressed with 0.5% glucose, PA14 wt, PA14:pumA (Ara) induced with 1% arabinose and PA14:pumA (Glu) repressed with 0.5% glucose. For consistency, arabinose was also included for the infections with wild-type and deletion mutant strains.

C Western blots from representative inocula used for the infection experiments, showing expression of PumA (34 kDa) in the different *P. aeruginosa* strains visualized using a polyclonal rabbit anti-PumA with control blot against the standard cytoplasmic protein EF-Tu (45 kDa) below.

Data information: For (A) and (B), between 200 and 400 cells per condition were counted and data correspond to median  $\pm$  standard error from three independent experiments. Non-parametric one-way ANOVA Kruskal–Wallis test, with Dunn's multiple comparisons test was performed; \*\*\*\* $P$  < 0.0001, \*\*\* $P$  < 0.001, \*\* $P$  < 0.01.



translocation (Fig 2B versus EV1B). Furthermore, absence of NF- $\kappa$ B nuclear translocation was not due to reduced immune detection of the mutant strain as incubation of host cells with heat-killed *DpumA* resulted in equivalent levels of NF- $\kappa$ B activation to the wild-type PA7 (Fig 2A). To further support that the differences observed relate to PumaA and are not indirect, we verified that all strains showed equivalent levels of membrane permeability (Fig EV2A), the global protein composition of the cell envelope was not altered in a *pumA* mutant (Fig EV2B), and no differences were observed in cytotoxicity (Fig EV2C and D) nor host cell adhesion (Fig EV2E) between wild-type PA7 and isogenic *DpumA* mutant. Together these results show that PumaA is responsible for *P. aeruginosa* PA7 inhibition of NF- $\kappa$ B nuclear translocation during infection.

We then investigated whether expression of PumaA alone could confer the ability to block NF- $\kappa$ B translocation to a different *Pseudomonas* strain. We chose PA14, which does not contain *pumA* and is known to be more virulent due to the presence of several virulence factors, namely those secreted by the T3SS. As expected, cells infected with wild-type PA14 showed high levels of NF- $\kappa$ B translocation into the nucleus (Fig 2B). Induction of *pumA* from the PA14 chromosome, which did not impact membrane permeability (Fig EV2A), was sufficient to enable this highly virulent strain to block NF- $\kappa$ B accumulation in the nucleus of infected cells (Fig 2B). These data indicate that PumaA expression in *P. aeruginosa* is necessary and sufficient for NF- $\kappa$ B inhibition, highlighting its central role in immune evasion.

#### PumaA translocation into host cells during infection *in vitro*

We next sought to determine whether PumaA could be secreted by *Pseudomonas*. Fractionation of bacterial cells grown in liquid culture indicates that PumaA is mostly cytoplasmic and to a lesser extent associated with the inner membrane (Appendix Fig S3A). The protein was not detected in the outer membrane fractions nor could it be found in the supernatant indicating absence of secretion into the extracellular milieu *in vitro*. To determine whether PumaA could be found inside host cells during infection, we fused chromosomal PumaA with the TEM1  $\beta$ -lactamase. Although the presence of other  $\beta$ -lactamases in PA7 and/or potential bacterial lysis resulted in non-specific cleavage of the CCF2 substrate within host cells infected with the wild-type strain, significant levels of coumarin fluorescing cells following infection with a strain containing PumaA-TEM1 (Appendix Fig S3B) suggest that PumaA is translocated into host cells during infection.

#### PumaA is associated with both TIRAP and MyD88 at the plasma membrane and intracellular compartments

To determine the mechanism by which PumaA interferes with NF- $\kappa$ B activity, PumaA was expressed in mammalian cells. We found PumaA localized mostly at the plasma membrane, with some intracellular distribution, independently of the tag and in both immortal HeLa cells (Fig EV3A, top panel) and primary mouse embryonic fibroblasts (MEFs, Fig EV3B). As this localization was reminiscent of that of the TLR adaptor TIRAP (Fig EV3A and B), we co-transfected cells with PumaA and TIRAP. We found extensive co-localization, in particular at the plasma membrane in both HeLa and MEFs (Fig 3A

and B). We observed these results with any combination of tags (HA, Myc or GFP) for both proteins.

In contrast with TIRAP, MyD88 is mostly localized in intracellular structures that do not label the plasma membrane. We therefore co-expressed MyD88 with PumaA. Surprisingly, we found enrichment of PumaA in a proportion of MyD88-positive structures in both cell types although to a lesser extent than that observed with TIRAP (Fig 3A and B). These results were confirmed by structured illumination microscopy (SIM) to enable imaging at higher resolution (Fig 3C and D). PumaA enrichment was observed with PumaA tagged with Myc or HA and MyD88 fused to either HA, FLAG or Myc. Curiously, this phenotype was exacerbated when GFP-PumaA, normally at the cell surface (Fig EV3) was co-expressed with MyD88, resulting in the majority of GFP-PumaA being recruited to MyD88-positive compartments (Fig EV3C).

#### The TIR domain of PumaA is responsible for interaction with both TIRAP and MyD88

We then investigated whether the TIR domain present in the first 136 amino acids of PumaA was responsible for membrane targeting. PumaA<sub>1-136</sub> was also efficiently targeted to the plasma membrane (Fig 4A). However, unlike TIRAP and another bacterial TIR protein BtpA/TcpB which are known to interact with specific phospholipids of the plasma membrane (Kagan & Medzhitov, 2006; Radhakrishnan *et al*, 2009), PumaA and PumaA<sub>1-136</sub> did not show any lipid binding properties when incubated with phosphoinositide phosphate strips (Fig 4B). We then tested whether PumaA could interact with TIRAP, which could explain its membrane localization. We found that TIRAP-GFP and Myc-PumaA co-immunoprecipitated (co-IP) suggesting TIRAP and PumaA could be part of the same complex (Fig 4C). This association was confirmed using purified His-tagged PumaA or PumaA<sub>1-136</sub> immobilized on Ni-NTA resin, which both retained HA-TIRAP (Fig 4D).

As we had also observed enrichment of PumaA in MyD88-positive compartments, we investigated whether PumaA could interact with this adaptor protein. Although we did not observe an interaction between GFP-MyD88 and Myc-PumaA (Fig 4C) nor HA-PumaA and Myc-MyD88 (Appendix Fig S4A), using co-IP assays, His-PumaA or PumaA<sub>1-136</sub> were able to retain HA-MyD88 (Fig 5A), suggesting PumaA is also able to interact with MyD88. To confirm these results, we took advantage of the strong enrichment in MyD88-positive compartments when Myd88 is co-expressed with the GFP-tagged version of PumaA (Fig EV3C) and carried out co-IP in these conditions. Indeed, GFP-PumaA and Myc-Myd88 could be co-immunoprecipitated as well as GFP-PumaA and Myc-TIRAP (Fig 5B), suggesting that PumaA can interact with MyD88. As a control for non-specific TIR-TIR interactions, we tested the ability of PumaA to interact with TLR2, also by co-IP. Indeed, GFP-PumaA could interact with FLAG-TIRAP but not FLAG-TLR2, suggesting some level of specificity in PumaA targeting (Appendix Fig S4B and C).

Finally, we co-expressed in *E. coli* His-PumaA<sub>1-136</sub> with His-MBP (Fig 5C), His-MBP-TIRAP (Fig 5D) or His-MBP-MyD88 (Fig 5E) and we could clearly see co-elution of both TIRAP and MyD88 in contrast to the His-MBP control (also see Appendix Fig S4D).

We next sought to determine whether the C-terminus of PumaA<sub>137-303</sub> could also participate in these interactions. Lack of expression of His-PumaA<sub>137-303</sub> in *E. coli* prevented us from purifying



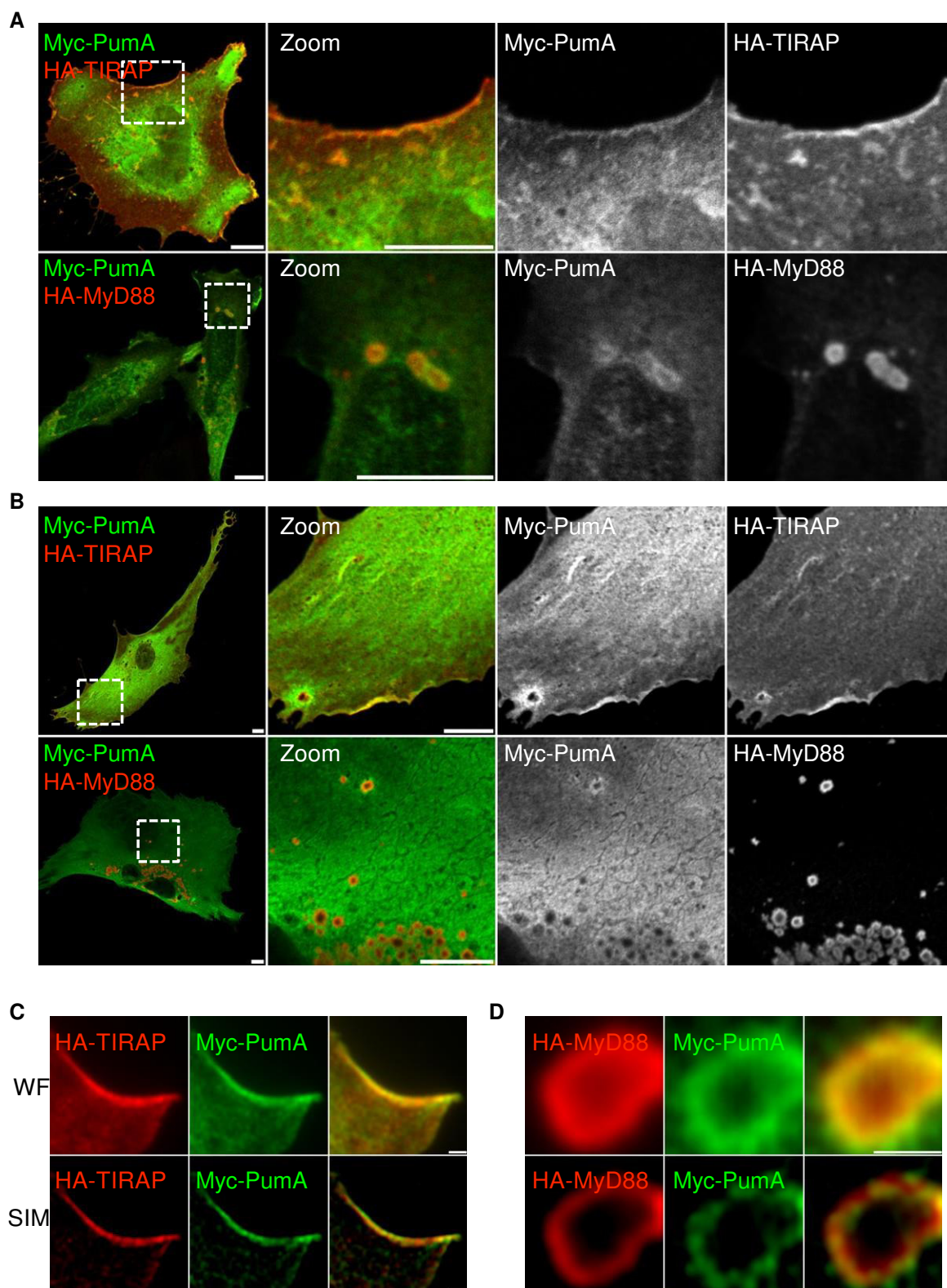


Figure 3. Puma co-localizes with TIRAP at the plasma membrane and to a lesser extent with intracellular MyD88, when ectopically expressed in host cells.

A, B Confocal microscopy of HeLa cells (A) and mouse embryonic fibroblast (MEFs) (B) co-expressing Myc-PumA and adaptor proteins HA-TIRAP (top panel) and HA-MyD88 (bottom panel). Cells were fixed after 10 h of transfection. Scale bars correspond to 10  $\mu$ m.

C, D Representative micrographs obtained by super resolution structure illumination microscopy (SIM) of MEFs co-expressing (C) Myc-PumA and TIRAP and (D) Myc-PumA and HA-MyD88. Wide field (WF) is shown in top panels and structured illumination of wide field (SIM) in bottom panels. Scale bars correspond to 1  $\mu$ m.

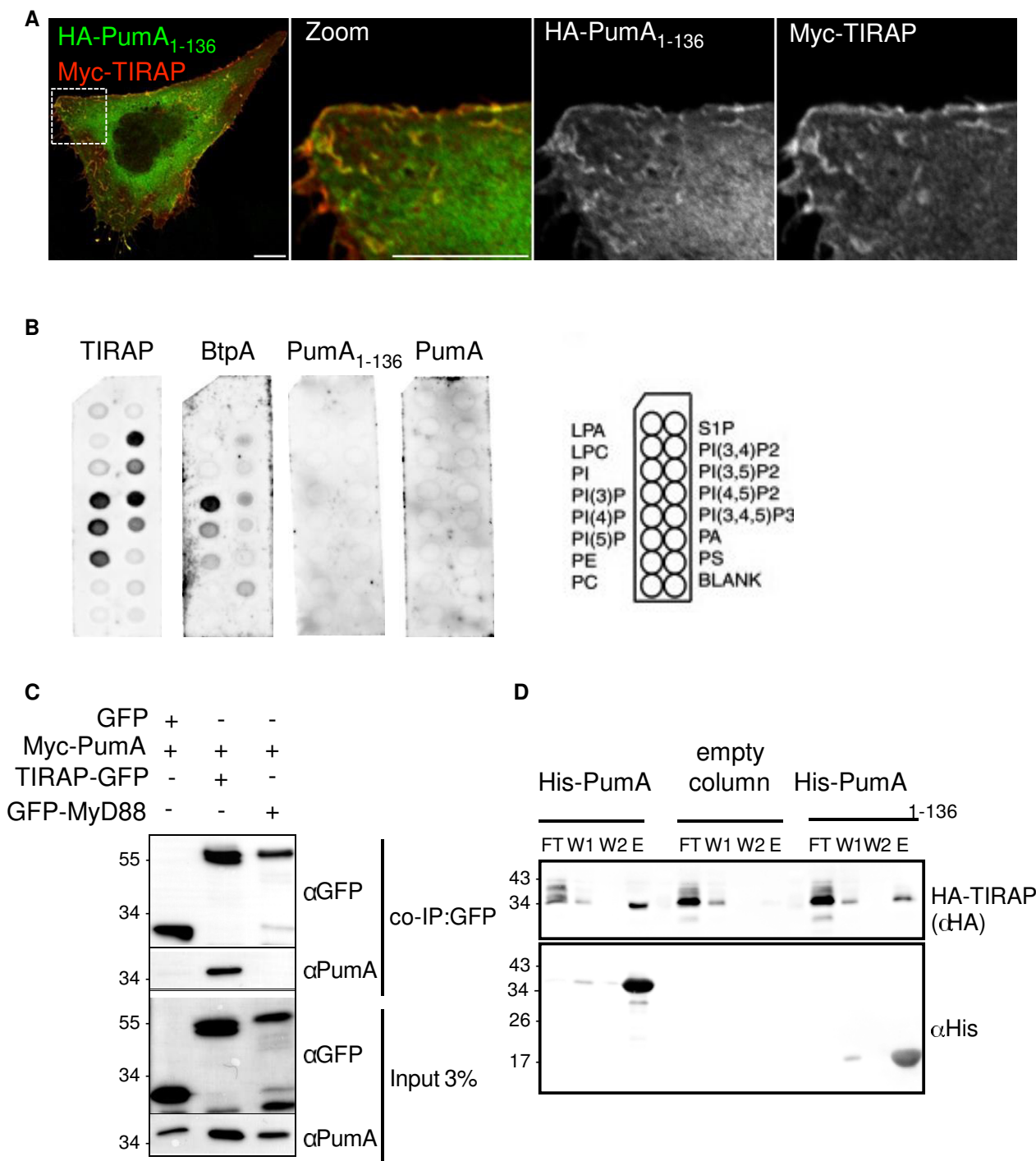


Figure 4. The TIR domain of PumA is required for plasma membrane targeting and interaction with TIRAP.

A Confocal microscopy of HeLa cells co-expressing HA-PumA<sub>1-136</sub> (TIR domain) and Myc-TIRAP labelled with anti-HA (green) and anti-Myc (red) antibodies. Cells were fixed after 10 h of transfection. Scale bars correspond to 10 μm.

B PIP strip binding of purified TIRAP, BtpA (*Brucella* TIR protein A), PumA<sub>1-136</sub> or full-length PumA. Scheme on the right indicates the identity of each phospholipid on the PIP strips.

C Co-immunoprecipitation (co-IP) assay from cells co-expressing Myc-PumA and GFP (control) or Myc-PumA with either TIRAP-GFP or GFP-MyD88. The co-IP was revealed using an anti-PumA antibody, binding to beads using an anti-GFP antibody and the inputs (shown below) using both anti-GFP and anti-PumA antibodies.

D Pull-down assay using extracts from cells expressing HA-TIRAP against His-PumA or His-PumA<sub>1-136</sub> immobilized on a Ni-NTA resin. Empty column was used as a control for non-specific binding. Interactions were visualized by Western blotting using anti-HA antibody, and column binding with anti-His (lower blot). Flow-through (FT), two washes (W1 and W2) and elution (E) are shown for each sample.

Source data are available online for this figure.

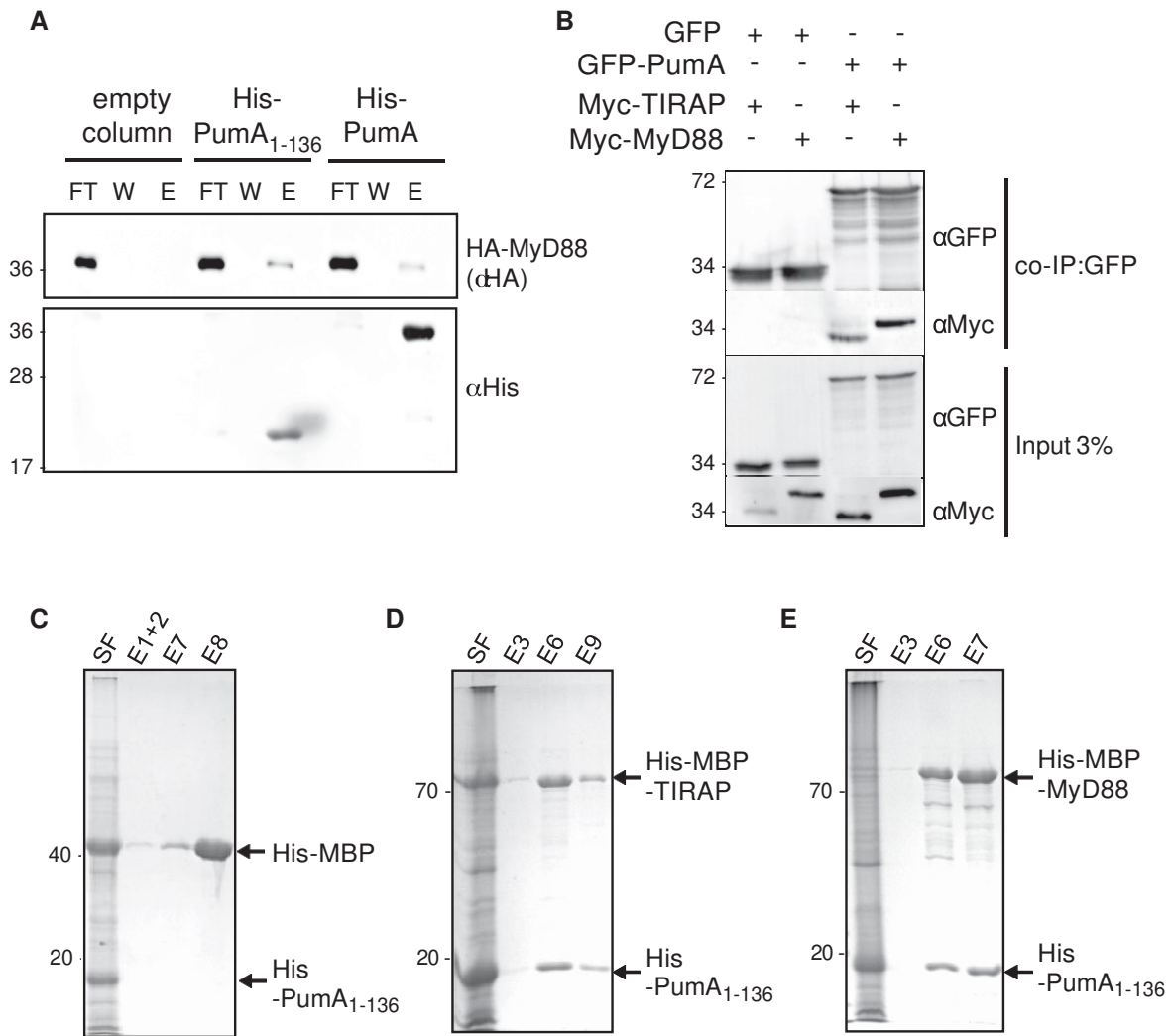


Figure 5. PumA is also capable of interacting with MyD88.

**A** Pull-down assay using extracts from cells expressing HA-MyD88 against His-PumA or His-PumA<sub>1-136</sub> immobilized on a Ni-NTA resin. Empty column was used as a control for non-specific binding. Interactions were visualized by Western blotting using anti-HA antibody, and column binding with anti-His (lower blot). Non-bound fraction (FT), last wash (W) and elution (E) are shown for each sample and the molecular weights indicated (kDa).

**B** Co-immunoprecipitation (co-IP) assay from cells expressing GFP-PumA and either Myc-TIRAP or Myc-MyD88. GFP was used as a control for non-specific binding. The co-IP was revealed using an anti-Myc antibody, the fraction bound to GFP-trapping beads using an anti-GFP antibody and the inputs (shown on the bottom two images) using both anti-Myc and anti-GFP antibodies.

**C-E** Co-purification of His-PumA<sub>1-136</sub> co-expressed in *E. coli* BL21 with either (C) His-MBP (control), (D) His-MBP-TIRAP or (E) His-MBP-MyD88. Interactions were visualized with coomassie blue stained gels. Soluble fraction (SF) and selected elutions (E) are shown for each sample and the molecular weights indicated (kDa).

Source data are available online for this figure.

this domain. We therefore carried out co-IP experiments with GFP-PumA<sub>137-303</sub> expressed in host cells. We could not detect any interaction between PumA<sub>137-303</sub> and TIRAP (Fig EV4A) nor between PumA<sub>137-303</sub> and MyD88 (Fig EV4B). However, it is important to note that expression of PumA<sub>137-303</sub> results in loss of plasma membrane localization. Instead, we observed formation of cellular aggregates that are positive for FK2 labelling (Fig EV4C), which recognizes mono- and poly-ubiquitinated proteins and could correspond to misfolded protein. For this reason, we cannot completely exclude a role of the C-terminus of PumA in these interactions. Nonetheless, our data identify TIRAP and MyD88 as host cell targets

of PumA, which mediates interaction with these adaptor proteins via its TIR domain.

#### PumA interacts with the ESCRT-I component UBAP1

As PumA was able to interact with both TIRAP and MyD88, two key adaptors in TLR signalling, we hypothesized PumA's function was to block all immune pathways dependent on these adaptors. Using an *in vitro* luciferase assay, we tested key immune receptors implicated in *Pseudomonas* infection. Surprisingly, we found PumA could not only block TLR4, TLR5 and IL-1b but also the TNF receptor,

which is not dependent on TIR–TIR interactions (Fig EV5A). TNFR1 inhibition was specific to PumA as expression of the *Brucella* TIR domain-containing protein BtpA/TcpB did not have any significant effect (Fig EV5B). We therefore carried a yeast two-hybrid screen to identify an alternative target of PumA and found UBAP1, a key component of the ESCRT-I mediating trafficking and sorting of ubiquitinated cargo proteins on MVBs (Stefani *et al*, 2011; Agromayor *et al*, 2012). This interaction was confirmed by co-IP from cells co-expressing PumA and UBAP1 (Fig 6A and B) as well as by pull-down using purified PumA or PumA<sub>1–136</sub> and cell extracts with either streptavidin-tagged UBAP1 (Fig 6C) or Myc-UBAP1 (Appendix Fig S5A). These results were specific to PumA as the *Brucella* TIR protein BtpA/TcpB did not show any interaction (Fig 6C). Furthermore, PumA<sub>137–303</sub> could not co-IP UBAP1 (Fig EV4D) supporting a role of the TIR domain in targeting UBAP1. Not surprisingly, microscopy analysis of cells expressing both PumA and UBAP1 showed significant co-localization at the plasma membrane and intracellular compartments (Appendix Fig S5C).

We next investigated whether PumA is interacting with UBAP1 in the context of the ESCRT-I machinery. As over-expression of UBAP1 could result in its mislocalization, we carried out endogenous co-IP from cells expressing HA-PumA. Full-length PumA not only interacted very efficiently with endogenous UBAP1 but more importantly also co-immunoprecipitated TSG101 (Fig 6D), confirming PumA is targeting the ESCRT-I machinery. As expected, PumA also interacted with endogenous TIRAP (Fig 6D). The TIR domain of PumA only weakly interacted with endogenous UBAP1 and TIRAP (Fig 6E), whereas the C-terminus of PumA showed no interactions (Fig 6F).

While we were conducting this work, another study reported UBAP1 participates in control of TNFR1 and other cytokine receptor trafficking (Mamińska *et al*, 2016). Our data along with this recently published study thus suggest that PumA interaction with UBAP1 results in inhibition of the TNF receptor-mediated pathway. To determine whether PumA was targeting two different types of cellular compartments, one with UBAP1 controlling the TNFR pathway and another containing TLR adaptors, we analysed whether UBAP1 was excluded from TIRAP and MyD88 containing compartments. We first analysed their intracellular localization following transfection as we were not able to detect endogenous UBAP1 with currently available antibodies. Extensive co-localization was observed at the plasma membrane and intracellular structures when co-expressing UBAP1 and TIRAP (Fig 7A), with no visible impact on the normal distribution of TIRAP. However, in the case of MyD88, co-expression with UBAP1 resulted in accumulation of this adaptor at the plasma membrane, not seen in cells expressing MyD88 alone (Fig 7A, bottom panel and B). Quantification of membrane enrichment of MyD88 in cells expressing UBAP1 showed MyD88 membrane association was even more striking in the presence of UBAP1 (Fig 7C) than that observed when co-expressing TIRAP with MyD88 (Kagan & Medzhitov, 2006), suggesting UBAP1 could be participating in MyD88 intracellular sorting.

To determine whether UBAP1 could be interacting with these TLR adaptors, we carried out biochemical analysis of cells co-expressing UBAP1 and either TIRAP or MyD88. We could efficiently detect an interaction between UBAP1 and MyD88 by co-IP (Appendix Fig S5D and E) but not UBAP1 and membrin (Appendix Fig S5E), used as a control eukaryotic protein with the same tag. In the case of TIRAP, the co-IP was much less efficient

(Appendix Fig S5D). These results suggest that UBAP1 may be associated with MyD88-containing compartments and to a lesser extent TIRAP, consistent with our microscopy observations. To confirm these results and ensure these interactions were taking place with UBAP1 in the context of the ESCRT-I, we determined whether MyD88 and TIRAP could interact with endogenous UBAP1 and TSG101. We found that HA-MyD88 co-immunoprecipitated both components of the ESCRT-I as well as endogenous TIRAP (Fig 7D), as expected. However, we did not observe an interaction between HA-TIRAP and endogenous UBAP1 nor TSG101 (Fig 7E), suggesting that only MyD88 can be found associated with the ESCRT-I.

Overall, these data suggest that PumA mediates interactions with UBAP1 in the context of ESCRT-I, which can itself associate with the TLR adaptor MyD88, also targeted by this *P. aeruginosa* effector protein.

#### *Pseudomonas aeruginosa* PA7 induces a decrease of TNFR1 in a PumA-dependent manner during infection *in vitro*

It is well described in the literature that inhibition of UBAP1 induces intracellular accumulation of EGFR, LTBR and TNFR1 (Stefani *et al*, 2011; Mamińska *et al*, 2016). To establish a link between PumA interaction with UBAP1 and the ability of PumA to reduce TNF-dependent signalling (Fig EV5A), we analysed the levels of TNFR1 during infection. In wild-type PA7 infected A549 cells, we observed a decrease of TNFR1 compared to the negative control (Fig 7F). In contrast, the mutant lacking PumA was not able to reduce the levels of TNFR1 in infected cells and this phenotype could be fully restored by expression of PumA in the complemented strain. This is consistent with PumA targeting of UBAP1 and enhancing its activity during infection *in vitro*. Interestingly, we did not see any impact on the overall levels of TIRAP during infection (Fig 7F) suggesting that PumA is not inducing TIRAP degradation as was previously reported for BtpA (Sengupta *et al*, 2010).

## Discussion

Many pathogens have developed sophisticated strategies to evade or modify host immune responses to their advantage. We have found that the TIR domain-containing protein PumA plays a major role in the virulence of multi-drug resistant *P. aeruginosa* PA7 strain. PumA ensures efficient inhibition of innate immune responses by interacting with MyD88 and TIRAP, key adaptor proteins for IL-1R and the main relevant TLRs in *Pseudomonas* infection (TLR4 and TLR5), as well as UBAP1 which regulates cytokine receptor pathways. These results identify UBAP1 as a novel cellular target for bacterial pathogens.

*Pseudomonas aeruginosa* is an important human pathogen associated with high level of mortality in nosocomial infections and cystic fibrosis patients. Most *P. aeruginosa* strains rely on a multitude of virulence factors to control host cellular pathways, including effectors delivered by the T3SS. However, in a cystic fibrosis context, colonizing strains modulate levels of expression of some of these virulence factors (Hauser *et al*, 2011), namely down-regulation of the T3SS (Jain *et al*, 2004) and undergo a remarkable accumulation of pathoadaptive mutations (Marvig *et al*, 2014). The



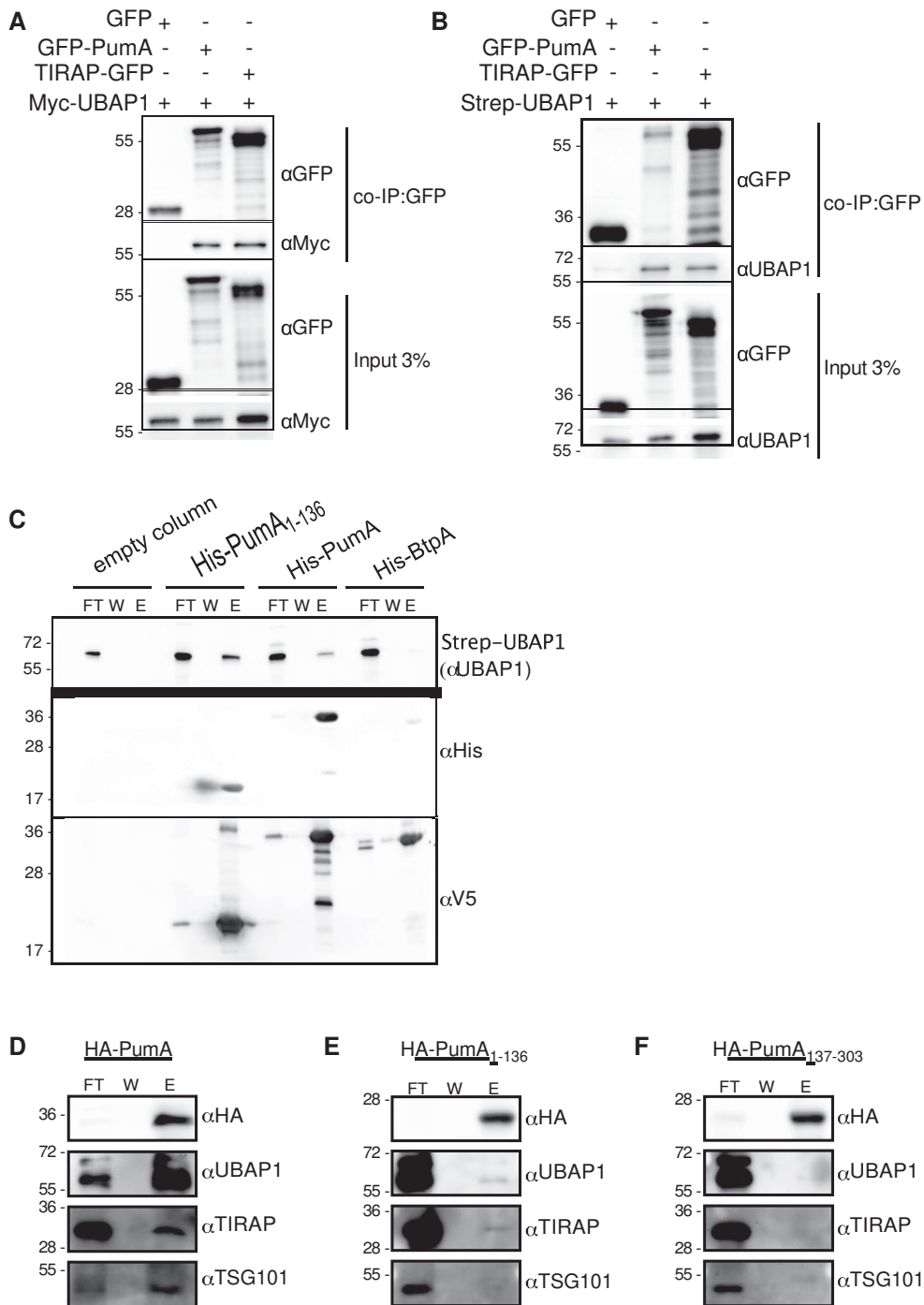


Figure 6. Identification of UBAP1 as a novel host protein targeted by the bacterial TIR domain of Puma.

A, B Co-immunoprecipitation (co-IP) assay from cells expressing Myc-UBAP1 (A) or Strep-UBAP1 (B) with either GFP, GFP-PumA or TIRAP-GFP. The co-IPs were revealed using an anti-Myc (A) or anti-UBAP1 (B) antibodies, the fractions bound to GFP-trapping beads using an anti-GFP antibody and the inputs using anti-Myc, anti-GFP or anti-UBAP1 antibodies as indicated.

C Pull-down assay using extracts from cells expressing Strep-UBAP1 against His-PumA or His-PumA<sub>1-136</sub> immobilized on a Ni-NTA resin. Empty column was used as a control for non-specific binding. Interactions were visualized by Western blotting using anti-UBAP1 antibody, and column binding with anti-His (middle blot), followed by anti-V5 (lower blot), necessary for detection of BtpA, which for reasons we do not understand cannot be easily detected with the anti-His antibody (Appendix Fig S5B).

D-F Endogenous co-IP from cells expressing (D) HA-PumA, (E) HA-PumA<sub>1-136</sub> and (F) HA-PumA<sub>137-303</sub>. The fractions bound to HA-trapping beads were probed with anti-HA, anti-UBAP1, anti-TIRAP and anti-TSG101 antibodies. Non-bound fraction (FT), last wash (W) and elution (E) are shown for each sample and the molecular weights indicated (kDa).

Source data are available online for this figure.

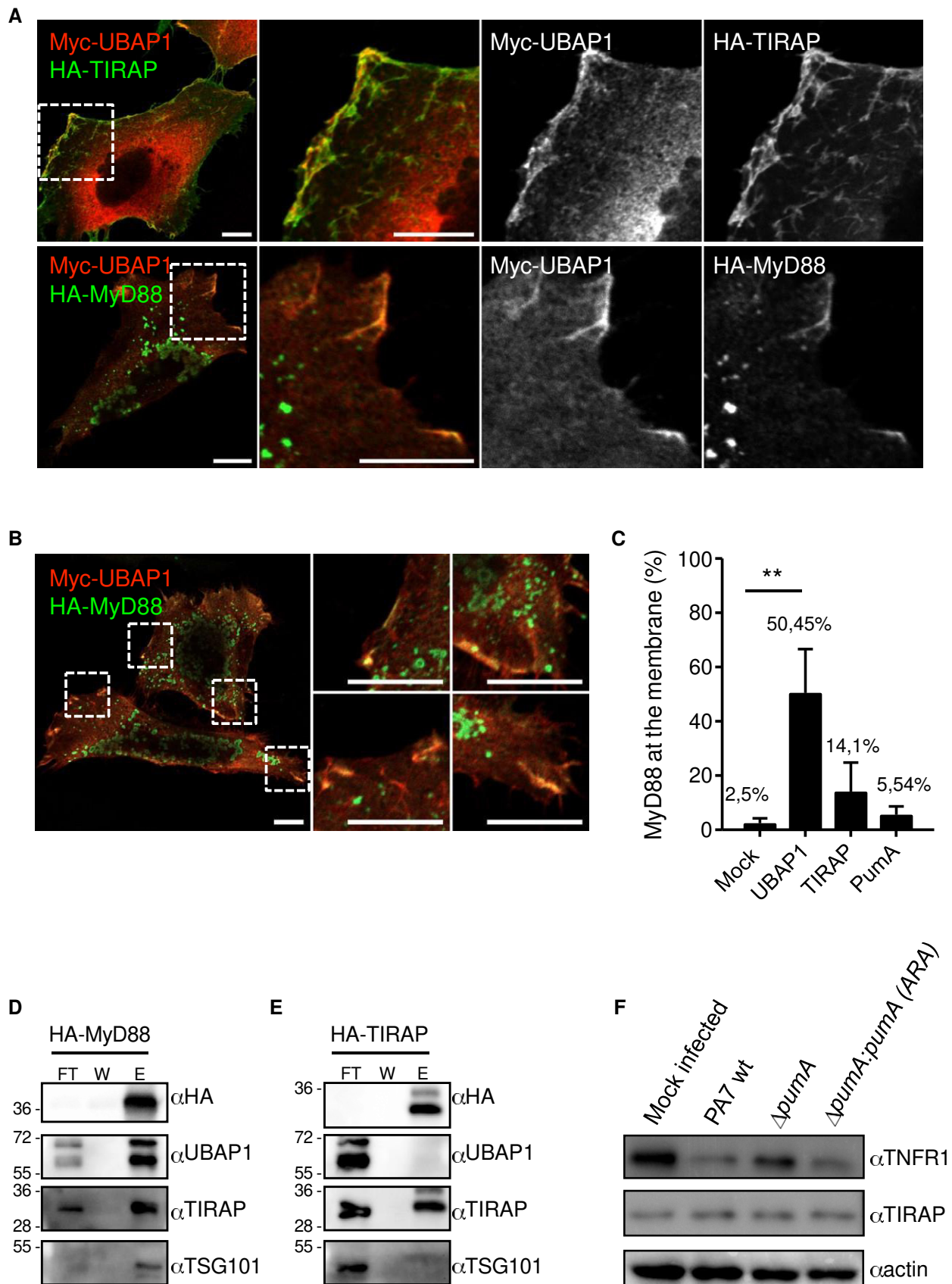


Figure 7.

E

Figure 7. Analysis of the impact of UBAP1 on TIRAP and MyD88.

- A Representative micrographs obtained by confocal microscopy of HeLa cells co-expressing Myc-UBAP1 (red) and adaptor proteins HA-TIRAP (green, top panel) or HA-MyD88 (green, bottom panel). Cells were fixed after 10 h of transfection. Scale bars correspond to 10  $\mu$ m.
- B Different zoomed images showing HA-MyD88 (green) recruitment to the plasma membrane in the presence of Myc-UBAP1 (red). Scale bars correspond to 10  $\mu$ m.
- C Quantification of plasma membrane localization of MyD88 in cells expressing MyD88 alone or with either UBAP1, TIRAP or PumA. At least 200 cells were enumerated in three independent experiments, and membrane localization was defined under the strict criteria of clear line at the plasma membrane. Cells with MyD88-positive vesicles in close proximity to the plasma membrane were not counted as positive. Non-parametric one-way ANOVA Kruskal–Wallis test was performed, with Dunn's multiple comparisons test. \*\* $P < 0.01$ .
- D, E Endogenous co-IP from cells expressing (D) HA-MyD88 and (E) HA-TIRAP. The fractions bound to HA-trapping beads were probed with anti-HA, anti-UBAP1, anti-TIRAP and anti-TSG101 antibodies. Non-bound fraction (FT), last wash (W) and elution (E) are shown for each sample and the molecular weights indicated (kDa).
- F Western blot of TNFR1 in A549 cells infected for 1 h with either *P. aeruginosa* PA7 wt,  $\Delta$ pumA or  $\Delta$ pumA:pumA (Ara) induced with 1% arabinose. A mock-infected sample was included as a negative control. The same blot was also probed for TIRAP and actin to control loading.

Source data are available online for this figure.

PA7-related *P. aeruginosa* strains lack the 20-Kb-long genomic region encoding the T3SS core components and all genes encoding secreted effectors but contains several additional genomic islands and potential novel virulence factors (Pirnay et al, 2009; Roy et al, 2010; Cadoret et al, 2014; Freschi et al, 2015). In some of these strains, such as CLJ1, an exolysin secreted by a two-partner secretion system is responsible for hypervirulence (Elsen et al, 2014). However, in PA7, this exolysin is detected at only low levels in the secretome and is not responsible for cytotoxicity (Reboud et al, 2016), suggesting an alternative pathogenicity mechanism. In this context, we hypothesize that PumA might be underlying an alternative pathogenicity mechanism to allow PA7 persistence within a host. Consistently, we observed a clear attenuation in virulence for a PA7 strain lacking pumA in both *C. elegans* and in a mouse lung infection model. Interestingly, no impact in the ability of the pumA mutant to disseminate systemically was observed suggesting a role in control of local pathology. This type of *P. aeruginosa* infection based on persistence and colonization rather than rapid cytotoxicity could be relevant in specific clinical contexts such as infection of wound and burn patients, aggravated by the high level of multi-drug resistance. It is interesting to note that other *Pseudomonas* contain a TIR domain protein, namely several strains pathogenic in plants. In this context, it will be interesting to analyse the role of the orthologous TIR protein in the plant pathogens *P. syringae* or *P. viridiflava* with over 90% identity to PumA in amino acid sequence for the TIR domain, regarding control of plant responses as these functions may be relevant across taxonomic kingdoms.

*Pseudomonas* is not the only bacterial pathogen to take advantage of the TIR domain to engage TIR–TIR interactions which are essential components of innate immune signalling. Bacterial targeting of TLRs has been best described for uropathogenic *E. coli* TcpC (Cirl et al, 2008) and *Brucella* BtpA, also known as TcpB (Cirl et al, 2008; Salcedo et al, 2008), even though their molecular mode of action remains elusive. *Brucella* relies on an additional TIR protein, BtpB to down-modulate inflammation during infection (Salcedo et al, 2013). TcpC was shown to interfere with MyD88-dependent and independent pathways to down-modulate TLR signalling and contribute to kidney pathology (Cirl et al, 2008; Yadav et al, 2010). In the case of *Brucella*, BtpA/TcpB has been described as a mimic of TIRAP, since it can directly bind specific phosphoinositides of the plasma membrane (Radhakrishnan et al, 2009). This is clearly distinct from PumA that shows no significant lipid binding properties. In addition, BtpA/TcpB was also shown to bind TIRAP, which results in its increased ubiquitination and degradation during

infection (Sengupta et al, 2010), which also differs from PumA which despite TIRAP binding does not induce its degradation. Several studies have followed disputing the precise target of BtpA/TcpB with some proposing preferential binding to MyD88 (Chaudhary et al, 2011). One key question that remains unanswered is how these bacterial TIR proteins are entering host cells and where do they localize during infection? No direct imaging of bacterial TIR proteins has been described. In the case of TcpC, internalization into host cells was observed but the export mechanism was not identified (Cirl et al, 2008), whereas no data are available regarding *Salmonella*, *Yersinia*, *Staphylococcus* and *Enterococcus*. In the case of *Brucella*, depending on the fusion tags, translocation into host cells of BtpA/TcpB or BtpB was dependent or independent of the T4SS (Salcedo et al, 2013) whereas a separate group has proposed that BtpA/TcpB is cell permeable and may enter host cells in a passive manner (Radhakrishnan & Splitter, 2010). Unfortunately, PumA fusion with CyaA resulted in its cleavage preventing us from using this system. Using different fluorescent tags and the specific anti-PumA antibody, we were not able to confidently visualize it inside host cells during infection. We were however able to detect intracellular PumA using a TEM1 fusion. Further work needs to be carried out to confirm translocation of PumA into host cells and define the intracellular location of PumA during infection. PumA was also not found in the bacterial culture supernatant *in vitro*, suggesting that contact-dependent delivery is involved. How PumA is entering host cells will have to be further investigated, but since the T3SS is not present in PumA-encoding strains, it suggests that host cell delivery would need an alternative secretion pathway.

It is important to note that TIR domains are widespread in multicellular organisms, such as in plants (role in disease resistance) and amoebas (dual role in ingestion of bacteria and immune-like functions) as well as in numerous bacterial genera that include cyanobacteria and other non-pathogenic bacteria (Zhang et al, 2011). This suggests these domains have evolved as an essential protein–protein interaction platform that could have additional functions. Indeed, recently the TIR domain of TcpC has been shown to directly interact with the NACHT leucine-rich repeat PYD protein 3 (NLRP3) inflammasome and caspase-1, besides MyD88, to perturb inflammasome activation (Waldhuber et al, 2016). There are also additional potential targets yet to be identified for BtpA/TcpB since it interferes with microtubule dynamics (Radhakrishnan et al, 2011; Felix et al, 2014) and induces unfolded protein response (Smith et al, 2013).

This notion that bacterial TIR domains provide a broad interaction platform is supported by our observations. We found that in addition to directly interacting with TIRAP and MyD88, Puma also targets the ESCRT-I machinery by binding to UBAP1 as Puma could co-immunoprecipitate endogenous UBAP1 and TSG101. All these interactions seem to be mediated by the TIR domain of Puma, but endogenous co-IP experiments showed that the full-length Puma is required for efficient interactions to occur. It is likely that TIR–TIR interactions are taking place with TIRAP and MyD88. In the case of UBAP1, the Puma interacting domain remains to be identified. All yeast two-hybrid preys identified in our screen encoded for a region containing amino acid 45–164, present between two key functional domains: the N-terminal UBAP1-MVB12-associated (UMA) domain (residues 17–63) that binds the central stalk of ESCRT-I Vps37 and the central domain (residues 159–308), containing the recently identified key binding site for HDPTP which can act as a cargo adaptor (Gahloth *et al*, 2016). The C-terminal portion of UBAP1 includes a SOUBA domain (residues 381–502) known to bind ubiquitin (Agromayor *et al*, 2012). UBAP1 is a key component of ESCRT-I that enables sorting of ubiquitinated cargo on MVBs. Puma may be binding an intermediate region of UBAP1 that could partially overlap with that interacting with HDPTP. Further work is now necessary to confirm this hypothesis. In view of the recent work implicating UBAP1 in restriction of constitutive NF- $\kappa$ B signalling (Mamińska *et al*, 2016), Puma could be impacting the activation of TNFR pathway through UBAP1. Depletion of UBAP1 was shown to induce intracellular accumulation of the cytokine receptors in endosomal compartments (Mamińska *et al*, 2016), which leads to increase in constitutive levels of NF- $\kappa$ B, since UBAP1 cannot ensure proper steady-state cytokine receptor (such as LT $\beta$ R and TNFR1) sorting and subsequent degradation. Since *in vitro* experiments suggest Puma is blocking TNF receptor-mediated pathway, Puma could be enhancing activity of UBAP1. This phenotype is specific of Puma since we observed no effect of another bacterial TIR domain-containing protein BtpA/TcpB which does not interact with UBAP1 and its ectopic expression does not result in inhibition of the TNF-induced pathway. Consistent with our hypothesis, wild-type PA7 decreases the levels of TNFR1 in A549 cells in a Puma-dependent manner suggesting targeting of UBAP1 is occurring during infection and could enhance its activity.

In an attempt to determine whether distinct intracellular locations were targeted by Puma to enable interaction with TLR adaptors and the ESCRT-I component UBAP1, we analysed whether UBAP1 was excluded from TIRAP or MyD88-enriched compartments. Surprisingly, co-IP experiments revealed endogenous UBAP1 itself and TSG101 could be found associated with MyD88 but not TIRAP, suggesting that the ESCRT-I machinery may be interacting with specific TLR adaptors. We therefore propose that additional crosstalk between these pathways may exist. MyD88 has been shown to interact with TLRs and with TIRAP via its TIR domain or the death domain. It remains to be demonstrated whether UBAP1 interacts directly with MyD88 but our data strongly suggest they can be found in the same complex, namely at the plasma membrane. Interestingly, co-expression of MyD88 and UBAP1 resulted in MyD88 enhanced plasma membrane targeting, to higher levels than that previously described for TIRAP (Kagan & Medzhitov, 2006). Further work is required to determine if UBAP1 interaction with MyD88 promotes

activation of TLR signalling and whether Puma could disrupt this interaction. A few studies have suggested the implication of ESCRT-I or MVBs in the control of TLR pathways. In *Drosophila*, ESCRT-0 components modulate endosomal sorting of Toll (Husebye *et al*, 2006; Huang *et al*, 2010). ESCRT have been also shown to negatively regulate TLR7 and 9 to enable recycling of these receptors following ubiquitination (Chiang *et al*, 2012). More interestingly, inhibition of endosomal sorting via ESCRT-I increases LPS-induced signalling (Husebye *et al*, 2006), suggesting it is playing a role in sorting and degradation of activated receptor complexes.

In conclusion, our study describes a *P. aeruginosa* effector Puma that targets UBAP1 in the context of ESCRT-I and plays a major role in virulence. In addition, our data associate UBAP1 to MyD88, highlighting a potential larger role of endosomal sorting by ESCRT-I in regulation of TLR signalling.

## Materials and Methods

### Strains

*Pseudomonas aeruginosa* strains used in this study were wild-type PA7, PA14 or derived strains and were routinely cultured in liquid Luria Bertani (LB) medium. Antibiotics were added to *P. aeruginosa* cultures, when appropriate, at the following concentrations: 150  $\mu$ g/ml tetracycline and 750  $\mu$ g/ml carbenicillin. When indicated, arabinose at 1% or glucose at 0.5% was added to cultures. For *Escherichia coli* cultures, antibiotics were added when necessary at the following concentrations: 50  $\mu$ g/ml kanamycin and 50  $\mu$ g/ml ampicillin.

### Construction of *Pseudomonas Dpuma* mutant and complemented strains

The 500 base pairs upstream and 500 base pairs downstream of *puma* gene (*PSPA7\_2375*; NC\_009656.1.) were amplified from *P. aeruginosa* PA7 genomic DNA to do overlapping PCR, using primers 5'-TTTGGGCCCCAAGACGATCAGCGGCACC-3', 5'-ATCGGCTCTGCCCTATGCCATCTTTTAACTCCATCCTTGTAAATCC-3', 5'-GGATGGAGTTAAAAAGATGGCATAGGGCAGAGCCGAT-3' and 5'-TTTGATCACAACACTACCCGATGCGTT-3', respectively. Then, the PCR product was sub-cloned into pGEM<sup>®</sup>-T Easy Vector (PROMEGA) and ligated into pKNG208 (Cadoret *et al*, 2014) following digestion with *SpeI* and *ApaI* to generate pKNG208- $\Delta$ *puma*. This plasmid was introduced into *P. aeruginosa* PA7 by conjugation where it is incapable of autonomous replication. Homologous recombination events were primary selected using tetracycline resistance (150  $\mu$ g/ml) in *Pseudomonas* isolation agar (PIA) plates and secondary selected using sucrose 6% sensitivity in LB agar plates during 2–3 days at room temperature. PCR and sequencing analyses confirmed the *puma* wild-type gene was deleted and Western blotting showed absence of Puma production of the PA7  $\Delta$ *puma* strain (Appendix Fig S2B).

The mini-CTX-*P<sub>BAD</sub>* plasmid was constructed by cloning the *Sall*-*AraC*-*P<sub>BAD</sub>*-*SacI* fragment from pJN105 vector (Newman & Fuqua, 1999) into the 6711 bp *Sall*/*SacI* DNA fragment from miniCTX-lacZ vector (Hoang *et al*, 1998). *PSPA7\_2375* gene was amplified with an artificial Shine-Dalgarno (AAGAAG) and cloned into mini-CTX-*P<sub>BAD</sub>* digested by *SpeI*/*SacI* using the SLIC method (Jeong *et al*, 2012).



Primers used were 5<sup>0</sup>-AGCCCGGGGATCCACTAGTAGGAGGTGA GATATAACAATGGCGGTCTTCATTAGTTA-3<sup>0</sup> and 5<sup>0</sup>-ACCATCCAGT GCAGGAGCTCCTATGCGCGCGGCCACGGG-3<sup>0</sup>.

#### Construction of PA7 *pumA::bla1* strain

The 500 base pairs upstream and downstream of *pumA* stop codon from *P. aeruginosa* PA7 genomic DNA and *blaM* gene from pJC121 plasmid (Myeni et al, 2013) were PCR amplified using primers 5<sup>0</sup>-ATTACGCGTTAACCCGGGCCAGGATGTTGACGGCTATC-3<sup>0</sup>, 5<sup>0</sup>-CAGCGTTTCTGGTGC GCGCGGCCACGG-3<sup>0</sup>, 5<sup>0</sup>-CTGATTAAGTAGGG CAGAGCCGATCAGCTC-3<sup>0</sup>, 5<sup>0</sup>-ACTGCGCGCCGTTACTAGTGCTG GACTGGCGCAACTA-3<sup>0</sup>, 5<sup>0</sup>-TGGCCGCGCACCCAGAAACGCTGGT GAAA-3<sup>0</sup> and 5<sup>0</sup>-ATCGGCTCTGCCTACTTAATCAGTGAGGCACC T-3<sup>0</sup> and used in overlapping PCR. DNA product was then cloned by the SLIC method (Jeong et al, 2012) into pKNG208 (Cadoret et al, 2014) digested by *Apal/SpeI* to generate pKNG208-*pumA::bla1* vector.

#### Construction of eukaryotic expression vectors

The PumA constructs were obtained by cloning in the gateway pDONR™ (Life Technologies) and then cloned in the pENTRY Myc, HA or GFP vectors. The following primers were used 5<sup>0</sup>-GGGGA CAAGTTGTACAAAAAGCAGGCTTCGCGGTCTTCATTAGTTATT CCCACG-3<sup>0</sup> and 5<sup>0</sup>-GGGGACCACTTTGTACAAGAAAGCTGGGTCC TATGCGCGCGGCCACGGGTAGC-3<sup>0</sup>. PumA<sub>1-136</sub> was constructed with the following primers: 5<sup>0</sup>-GGGG ACAAGTTGTACAAAAA GCAGGCTTCATGGCGGTCTTCATTAGTTATTCC -3<sup>0</sup>; 5<sup>0</sup>-GGGGACCA CTTTGTACAAGAAAGCTGGGTCTTACGGGACTGATCAGGATTAG AG-3<sup>0</sup>. PumA<sub>137-303</sub> with 5<sup>0</sup>-GGGGACAAGTTTGTACAAAAAAGCA GGCTTC ATTGAGGATGTTGACGGCTA-3<sup>0</sup>; 5<sup>0</sup>-GGGGACCACTTTG TACAAGAAAGCTGGGTCTTATGCGCGCGGCCACGGGGTAGC -3<sup>0</sup>.

#### Construction of prokaryotic expression vectors

The full-length *P. aeruginosa* PA7 *pumA* and its TIR domain (residues 1–136) were cloned into pET151/D-Topo (Invitrogen)—which carries the T7 promoter, N-terminal 6xHis and V5 tags, protease recognition site for tobacco etch virus (TEV) protease and ampicillin resistance gene. The following primers were used: 5<sup>0</sup>-CAC CATGGCGGTCTTCATTAGTTATTCC-3<sup>0</sup> and 5<sup>0</sup>-TGATCGGCTCT GCCCTATGC-3<sup>0</sup> for *pumA*; the same forward primer and 5<sup>0</sup>-CTAACGGGACTGATCAGGATTAGAG-3<sup>0</sup> for *pumA* TIR domain. BtpA was cloned in this same vector. The HA-TIRAP and HA-Myd88 vector was used as a template to clone TIRAP and Myd88, respectively, into pRSF-MBP vector. This vector corresponds to pRSFDuet-1 (Novagen) but modified to insert 6xHis-MBP from pETM-41 vector (EMBL) behind the cloning multiple site.

#### Cell culture and transfections

HeLa, HEK 293T and A549 cells (all obtained from ATCC) were grown in DMEM supplemented with 10% of foetal calf serum (FCS). Mouse embryonic fibroblasts were prepared as described previously (Conner, 2001) and maintained in DMEM supplemented with 10% (FCS). All cells were transiently transfected using Fugene (Roche) for 24 h, according to manufacturer's instructions.

#### *Pseudomonas* infection of A549 cells

For adhesion assays and microscopy analysis of NF- $\kappa$ B, cells were first seeded into 24-well tissue culture plates at  $2 \times 10^5$  cells/well (to obtain a monolayer) or  $5 \times 10^4$  cells/well, respectively. Cells were infected with overnight cultures at a MOI of 10 or 100 of *P. aeruginosa* in 500  $\mu$ l of complete medium per well. Plates were centrifuged at  $400 \times g$  for 5 min and then incubated for 1 h at 37°C with 5% CO<sub>2</sub> atmosphere. Cells were then washed five times with DMEM and either lysed or fixed. In the case of the cytotoxicity assays, cells were incubated for longer periods with complete media. When indicated, arabinose at 1% or glucose at 0.5% was added.

For NF- $\kappa$ B experiments, exponential phase cultures were also used, but no differences were detected. After 1 h, medium was removed and cells were washed two times with ice-cold PBS. Control samples were always performed by incubating cells with mock inocula and following the exact same procedure as for the infection.

For adhesion assays, cells were lysed with 500  $\mu$ l of 0.1% Triton solution and pipetted vigorously several times. Lysed samples were harvest, and serial 10-fold dilutions in PBS were plated on LB agar to enumerate CFUs.

For Western blot analysis of TNFR1, cells were seeded in six-well plates at  $2 \times 10^5$  cells/well and infected as described above. At 1 h post-infection, cells were washed with ice-cold PBS 2 times, were collected and lysed directly with loading buffer. For each sample, six wells were pooled.

Cell cytotoxicity exerted by bacteria was quantified with the cytotoxicity detection kit-LDH (Roche), which measures the activity of cellular lactate dehydrogenase released into the supernatants. The assays were performed according to the instructions of the manufacturer.

For propidium iodide staining, A549 cells were maintained in DMEM media supplemented with 10% FCS. Cells were seeded at  $1 \times 10^5$  cells/ml in 96-well plate to achieve confluent monolayers. Cells were then infected with overnight cultures of *P. aeruginosa* or mutants supplemented with arabinose to a final concentration of 2% (as indicated) at a MOI of 100. The plates were centrifuged at  $400 \times g$  for 5 min and incubated for 1 h at 37°C. After 1 h of infection, cells were washed three times with PBS then incubated with complete media (without red phenol) containing propidium iodide and labelling measured during 6 h every 15 min with a Tecan Infinite M1000.

#### Immunofluorescence labelling and microscopy

Cells were fixed in Antigenfix (DiaPath), at room temperature for 10 min. Cells were then labelled at RT with primary antibody mix diluted in 0.1% saponin in PBS with 1% BSA and 10% horse serum for blocking. Primary antibody was incubated for 1 h followed by two washes in 0.1% saponin in PBS. Secondary antibodies were then mixed and incubated for a further 30 min, followed by two washes in 0.1% saponin in PBS, one wash in PBS and one wash in distilled water before mounting with Prolong Gold. Samples were examined on a Zeiss LSM710 or Zeiss LSM800 laser scanning confocal microscopes for image acquisition. Images of  $1,024 \times 1,024$  pixels were then assembled using plugin FigureJ from ImageJ.

For immunofluorescence microscopy analysis of NF- $\kappa$ B, cells were permeabilized for 6 min with 0.1% Triton in PBS, followed by a blocking for 1 h with 2% BSA in PBS. Primary antibodies were

incubated for 1 h followed by two washes in 2% BSA in PBS, 30-min incubation for secondary antibodies, two washes in 2% BSA in PBS, one wash in PBS and one wash in water before mounting with Prolong Gold (Life Technologies). Samples were examined on a Zeiss LSM710 laser scanning confocal microscope for image acquisition. Images of 2,648 × 2,648 pixels were then passed through a specific plugin of ImageJ developed by L. Plantevin, based on a previous study (Noursadeghi *et al*, 2008); raw images were treated with a median filter and threshold moments, afterwards total NF- $\kappa$ B was subtracted from the Dapi channel to obtain cytoplasmic NF- $\kappa$ B. Total NF- $\kappa$ B was then subtracted from cytoplasmic NF- $\kappa$ B to obtain nuclear NF- $\kappa$ B (Fig EV1A). Quantification was always done by counting at least 200 cells per condition in minimum three independent experiments, for a total of at least 600 host cells analysed per condition.

#### Antibodies and reagents

Primary antibodies used were rabbit anti-p65 from Santa Cruz (clone C-20, ref. sc-372) at 1/250, mouse anti-myc9E10 (developed by Bishop, J.M. was obtained from the Developmental Studies Hybridoma Bank, created by the NICHD of the NIH and maintained at the University of Iowa), mouse anti-HA (Eurogentec, clone 16B12, ref. MMS-101R), rabbit anti-HA (Sigma, ref. H6908), rabbit anti-GFP (Amsbio, ref. TP401), rabbit anti-UBAP1 (Proteintech, ref. 12385-1-AP), mouse anti-His (Sigma, clone HIS-1, ref. H1029), mouse anti-FLAG (Sigma, clone M2, ref. F1804) all at 1/1000 and mouse anti-TNFR1 (Santa Cruz, clone H-5, ref. sc-8436) and rabbit anti-TSG101 (Atlas Antibodies, ref. HPA006161) both at 1/200. Rabbit polyclonal anti-PumA serum was obtained by repeated immunization of rabbits with purified PumA (Eurogentec) and was used at 1/1,000 for Western blot and for immunofluorescence microscopy. Purified BtpA was used to obtain chicken anti-BtpA (Eurogentec). Anti-EF-Tu antibody (kind gift from R. Voulhoux) was used at 1/10,000.

Secondary antibodies used were anti-rabbit, mouse, chicken or rat conjugated with Alexas-488, -555 or -647 all from Jackson ImmunoResearch. When necessary, phalloidin-568 (1/1,000) was used to label the actin cytoskeleton and DAPI nuclear dye (1/1,000) for the host cell nucleus. For Western blots, anti-mouse or rabbit-HRP antibodies were used at 1/5,000.

#### TEM translocation assay

HeLa cells were seeded in a 96-well plates at  $1 \times 10^4$  cells/well overnight. Cells were then infected with an MOI of 100 by centrifugation at 4°C, 400 g for 5 min and 1 at 37°C 5% CO<sub>2</sub>. Cells were washed with HBSS containing 2.5 mM probenecid. Then, 6 l of CFF2 mix (as described by Life Technologies protocol) and 2.5 mM probenecid were added to each well, and incubated for 1.5 h at room temperature in the dark. Cells were finally washed with PBS, fixed using Antigenfix and analysed immediately by confocal microscopy (Zeiss LSM800) or flow cytometry (MACSQuant10 analyser).

#### Luciferase activity assay

HEK 293T cells were seeded in a 96-well plates at  $2 \times 10^4$  cells/well overnight, and cells were transiently transfected with FuGENE® 6

(Promega) for 24 h for a total of 0.4  $\mu$ g of DNA consisting of 50 ng TLR plasmids, 200 ng of pBIIxLuc reporter plasmid, 5 ng of control Renilla luciferase (pRL-null, Promega) and 50 ng of myc-PumA expression vector. The total amount of DNA was kept constant by adding empty vector. Where indicated, cells were treated with *E. coli* LPS (1  $\mu$ g/ml) and Flagellin FLA-ST (1  $\mu$ g/ml), all obtained from InvivoGen, for 6 h. In the case of IL-1 $\beta$  and TNFR, endogenous receptors were stimulated with IL-1 $\beta$  (100 ng/ml) and TNFA (100 ng/ml), respectively. Cells were then lysed and luciferase activity measured using Dual-Glo Luciferase Assay System (Promega).

#### Yeast two-hybrid screen

Full-length *pumA* cloned in pB27 (N-LexA-bait-C fusion) was used in a ULTimate screen against a human normal lung-RP1 library (Hybrigenics).

#### Protein expression and purification

*Escherichia coli* BL21 star (DE3) cells carrying pET151D topo-*pumA*, pET151D topo-*pumA*<sub>1-136</sub>, or pRSFDuet-TIRAP or MyD88 plasmids were grown in 1 L Luria Bertani (LB) media containing ampicillin or kanamycin according to the plasmid at 37°C until an OD<sub>600</sub> value of 0.5–0.8 was reached. Isopropyl- $\beta$ -D-thiogalactopyranoside (IPTG) was added to final concentration of 1 mM, and culture was further grown overnight at 20°C. Cells were harvested by centrifugation at 6,000 × g for 20 min at 4°C.

Bacterial pellets were lysed by sonication in cold lysis buffer (40 mM Tris-HCl pH8, 250 mM NaCl, 10% (v/v) glycerol, 1% (v/v) Triton X-100) supplemented with DNase-I, lysozyme and protease inhibitor tablets (Roche). Extracts were cleared at 16,000 × g for 20 min at 4°C and loaded onto a 5 ml His-Trap column or 5 ml MBP-Trap column (GE Healthcare) pre-equilibrated with buffer A (40 mM Tris [pH8], 250 mM NaCl, 5% glycerol). The column was washed successively with buffer A, 10% v/v buffer B (buffer A with 500 mM imidazole), 1M NaCl and eluted in a gradient of buffer B (His-Trap) or wash in buffer A and eluted in buffer A containing 20 mM maltose (MBP-Trap).

Proteins used for lipid binding assay were incubated with TEV protease, 1mM DTT and 0.5 mM EDTA, dialysed against buffer A at 4°C overnight. The untagged recombinant protein was purified through a second His-trap column. Pure fractions were pooled, concentrated and applied to size exclusion chromatography (Superdex 75 10/300; GE Healthcare).

Fractions were analysed by SDS-PAGE.

#### Pull-downs from cell extracts

Human embryonic kidney (HEK) 293T cells were seeded at  $5 \times 10^5$  in 10-cm cell culture dish in Dulbecco's modified Eagle's medium (Life Technologies) supplemented with 10% foetal bovine serum. Cells were incubated overnight in a 37°C humidified atmosphere of 5% CO<sub>2</sub>. Cells were transiently transfected with different plasmids (8  $\mu$ g) using FuGENE 6 (Promega). 22 h after infection, cells were washed in ice-cold PBS, harvested and resuspended in 200 l of RIPA buffer (Sigma) supplemented with phenylmethylsulfonyl fluoride (Sigma) and protease inhibitor

cocktail (Roche). Extracts were then centrifuged at 17,000 *g* at 4°C for 20 min. The supernatant was incubated with 50  $\mu$ g of His tag recombinant protein during 2 h at 4°C, then incubated within gravity flow column (Agilent) containing 80  $\mu$ l Ni-NTA agarose beads (Macherey-Nagel) during 1 h beforehand washed in water and pre-equilibrated in equilibrium buffer 20 mM Tris–HCl pH7.5, 250 mM NaCl. The column was washed successively three times in equilibrium buffer supplemented with 25 mM imidazole, three times in equilibrium buffer and eluted in equilibrium buffer supplemented with 500 mM imidazole. Proteins eluted were separated by SDS–PAGE, transferred to a PVDF membrane, incubated with specific primary antibodies for 1 h and detected with horseradish peroxidase (HRP)-conjugated secondary antibodies by using Clarity™ Western ECL Blotting Substrate (Bio-Rad).

#### Co-immunoprecipitations

HEK 293T cells were cultured in 100 mm  $\times$  20 mm cell culture dishes at  $4 \times 10^5$  cells/dish overnight. Cells were transiently transfected with 14.7  $\mu$ l of Torpedo<sup>DNA</sup> (Ibidi) for 24 h for a total of 5  $\mu$ g of DNA/plate. On ice, after two washes with cold PBS, cells were collected by with a cell scraper and centrifuged at 80 *g* at 4°C during 5 min. Cell lysis and processing for co-immunoprecipitation were done as described by either GFP-Trap<sup>®</sup>\_A kit (Chromotek) or with the Pierce™ HA Epitope Antibody Agarose conjugate (Thermo scientific).

For endogenous co-IP, HeLa cells were cultured in 100 mm  $\times$  20 mm cell culture dishes at  $1 \times 10^6$  cells/dish overnight. Cells were transiently transfected and collected as described above. Cell lysis and processing for co-immunoprecipitation were done following the manufacturers' instructions (Pierce™ HA Epitope Antibody Agarose conjugate, Thermo scientific) but using 100  $\mu$ l of beads and increasing the number of washes to 5.

#### Co-expression analysis

*Escherichia coli* BL21 star (DE3) cells harbouring both pET151D topopumA<sub>1–136</sub> and pRSF-Duet vector-TIRAP (or Myd88 or empty vector) plasmids were grown in LB media containing ampicillin and kanamycin at 37°C until an OD<sub>600</sub> value of 0.5–0.8 and induced with 2 mM isopropyl- $\beta$ -D-thiogalactopyranoside overnight at 20°C.

Cells were lysed and loaded onto a 5 ml MBP column as described in the protein expression and purification section. Fractions were analysed by SDS–PAGE.

#### Lipid binding assays

Lipid binding assays were performed as described previously (Marek & Kagan, 2012). Briefly, phosphoinositide phosphate (PIP) strips (Echelon Biosciences) were saturated in blocking buffer (10 mM Tris [pH8], 150 mM NaCl, 0.1% Tween 20, 0.1% Ovalbumin) for 1 h at room temperature under shaking. Strips were probed for 2 h at room temperature with each recombinant protein (2.5  $\mu$ g) in the presence of the specific anti-protein antibody. PIP strips were then washed in blocking buffer three times for 10 min each and probed with an HRP-conjugated anti-rabbit IgG or anti-Hen IgY for

30 min in blocking buffer. Bound protein was detected using Clarity™ Western ECL Blotting Substrate.

#### *Caenorhabditis elegans* infection

The slow killing assay was performed as described previously (Garvis et al, 2009). Each independent assay consisted of three replicates. Briefly, five 60 mm NGM plates were inoculated with 60  $\mu$ l of overnight culture of each bacterial strain and incubated at 37°C overnight. Plates were seeded with L4 stage hermaphrodite fer-15 worms (10 per plate). Plates were then incubated at 25°C and scored each day for live worms. A worm was considered dead when it no longer responded to touch. *Escherichia coli* was used as a control. Animal survival was plotted using GraphPad Prism version 6.0 for Mac, GraphPad Software, La Jolla, California, USA. Survival curves are considered significantly different from the control when *P*-values are < 0.05. Prism calculates survival fractions using the product limit (Kaplan–Meier) method. Prism compares survival curves by two methods: the log-rank test (also called the Mantel–Cox test) and the Gehan–Breslow–Wilcoxon test.

#### Mouse model of *Pseudomonas* acute infection

Wild-type C57BL6/J male mice, 8–10 weeks old, were purchased from Janvier laboratories. Mice were randomized before the experiments and infection were performed blindly. Following a light anaesthesia with isoflurane (Baxter), a pulmonary infection model was induced by intranasal instillation with  $3 \times 10^7$  CFU of *P. aeruginosa* PA7 or PA7Dpuma strains (except for survival studies conducted with lethal inocula of  $4 \times 10^7$  CFU/mouse). All mice were sacrificed at 24 h or survival was monitored for 96 h.

To establish bacterial burden, mouse lungs and spleens were homogenized in sterile tubes with PBS. Lung and spleen homogenates were sequentially diluted and cultured on Lysogeny Broth agar plates for 24 h at 37°C to assess bacterial load. Bronchoalveolar lavage (BAL) was done as follows: lungs from each experimental group were washed with a total of 1.5 ml sterile phosphate-buffered saline (PBS). The recovered lavage fluid was centrifuged (200 *g* for 10 min), and red blood cells from the cellular pellet were lysed with 300  $\mu$ l of ACK Lysis Buffer (Gibco). Cell counts were performed directly by optical microscopy.

#### Ethics statement

All experiments involving animals were carried out in compliance with French and European regulations on the care and protection of laboratory animals (European Commission Directive 86/609 and the French Act #2001–486, issued on June 6, 2001) and performed by certified personnel. The study and all experimental protocols associated were registered and approved by the French authorities (Ministère de l'Enseignement Supérieur et de la Recherche—Direction Générale pour la Recherche et l'Innovation—Secrétariat Autorisation de projet, registration number 00481.01). Animals were housed at the Lille University Animal Research Facility (Département Hospitalo-Universitaire de Recherche Expérimentale de Lille, France) accredited by the French Ministry of Agriculture for animal care and use in research (#B59–350009).

### Fractionation of *Pseudomonas aeruginosa*

*Pseudomonas aeruginosa* strains were grown in LB for 4 h and adjusted to OD<sub>600</sub> 20 in 1 ml cold 50 mM Tris–HCl pH 8.0 with 1 mM EDTA and protease inhibitors (Roche). All subsequent steps were conducted at 4°C. The cell samples were sonicated three times at 30-s intervals, with the resulting cellular debris pelleted by centrifugation three times at 4,000 *g* for 5 min, taking the uppermost supernatant for each spin. The total membrane fraction was separated from the soluble fraction by ultracentrifugation at 100,000 *g* for 1 h. After washing the membrane pellet thoroughly in sonication buffer, the inner membrane fraction was solubilized in 200 l 50 mM Tris–HCl pH 7.6 with 2% (v/v) sodium lauroyl sarcosinate for 1 h with gentle agitation. The outer membrane fraction was pelleted by ultracentrifugation at 100,000 *g* for 1 h, washed and resuspended in sonication buffer. The preparation of supernatant samples separation by sodium dodecyl sulphate-polyacrylamide gel electrophoresis and subsequent immunoblotting has been described previously (Hachani *et al*, 2011). Immunodetection was conducted using monoclonal antibodies against RNA polymerase (NeoClone) and polyclonal antibodies against PilQ, XcpY (Michel *et al*, 1998) and LasB.

Expanded View for this article is available online.

### Acknowledgements

This work was funded by the FINOVI foundation under a Young Researcher Starting Grant and the Cystic Fibrosis French Foundation Vaincre la Mucoviscidose (VLM), grant RF20130500897. SS and SB are supported by INSERM and CNRS staff scientist contracts, respectively. SG and JBL are funded by the Région Rhône-Alpes ARC1 Santé fellowships. PI and AL by the VLM and FINOVI grants. TW is supported by a Wellcome Trust PhD fellowship. We thank the following people: L. Plantevin for programming of ImageJ plugin; V. Gueguen-Chaignon and the Protein Science Facility (SFR Biosciences, France) for protein purification and plasma resonance experiments; R. Voulhoux (CNRS UMR7255, Aix-Marseille University, France) for anti-EF-Tu and LasB antibodies, PA7 strain and vectors pKNG208; G. Ball (CNRS UMR7255, Aix-Marseille University, France) for advice on genetics of PA7; S. Lory (Harvard Medical School, USA) for anti-PilQ antibody; pCMV-HA-MyD88 was a gift from B. Beutler (UT Southwestern Medical Center, USA; Addgene plasmid # 12287), FLAG-TLR5 from R. Medzhitov (Yale University, USA; Addgene plasmid # 13088), TIRAP-GFP and GFP-MyD88 from J. Kagan (Harvard Medical School, USA); HA-TIRAP from L. O'Neil (Trinity College Dublin, Ireland); Myc-TIRAP from A. Weber; L. Alexopolou (CIML, France) FLAG-TLR2 and FLAG-TLR4. We also thank the PLATIM of the SFR Biosciences for help with microscopy, T. Henry (CIRI, Lyon) for discussion and J. Kagan (Harvard Medical School, USA) for discussion and critical reading of the manuscript.

### Author contributions

PRCI performed the majority of the experiments. AL carried out all purifications, pull-down and co-expression experiments. J-BL, TG, SB, SG, TEW, LW, SG, AB and SPS also performed experiments. PRCI, AL, SB, LT, AF, BG, PW, SPS conceived and designed experiments. All authors analysed data. SPS wrote the manuscript. All authors contributed to and corrected the manuscript.

### Conflict of interest

The authors declare that they have no conflict of interest.

## References

- Agromayor M, Soler N, Caballe A, Kueck T, Freund SM, Allen MD, Bycroft M, Perisic O, Ye Y, McDonald B, Scheel H, Hofmann K, Neil SJD, Martin-Serrano J, Williams RL (2012) The UBAP1 subunit of ESCRT-I interacts with ubiquitin via a SOUBA domain. *Structure* 20: 414–428
- Askarian F, van Sorge NM, Sangvik M, Beasley FC, Henriksen JR, Sollid JUE, van Strijp JAG, Nizet V, Johannessen M (2014) A *Staphylococcus aureus* TIR domain protein virulence factor blocks TLR2-mediated NF- $\kappa$ B signaling. *J Innate Immun* 6: 485–498
- Bonham KS, Orzalli MH, Hayashi K, Wolf AI, Glanemann C, Weninger W, Iwasaki A, Knipe DM, Kagan JC (2014) A promiscuous lipid-binding protein diversifies the subcellular sites of toll-like receptor signal transduction. *Cell* 156: 705–716
- Brubaker SW, Bonham KS, Zanoni I, Kagan JC (2015) Innate immune pattern recognition: a cell biological perspective. *Annu Rev Immunol* 33: 257–290
- Cadoret F, Ball G, Douzi B, Voulhoux R (2014) Txc, a new type II secretion system of *Pseudomonas aeruginosa* strain PA7, is regulated by the TtsS/TtsR two-component system and directs specific secretion of the CbpE chitin-binding protein. *J Bacteriol* 196: 2376–2386
- Chaudhary A, Ganguly K, Cabantous S, Waldo GS, Micheva-Viteva SN, Nag K, Hlavacek WS, Tung C-S (2011) The *Brucella* TIR-like protein TcpB interacts with the death domain of MyD88. *Biochem Biophys Res Commun* 417: 299–304
- Chiang C-Y, Engel A, Opaluch AM, Ramos I, Maestre AM, Secundino I, De Jesus PD, Nguyen QT, Welch G, Bonamy GMC, Miraglia LJ, Orth AP, Nizet V, Fernandez-Sesma A, Zhou Y, Barton GM, Chanda SK (2012) Cofactors required for TLR7- and TLR9-dependent innate immune responses. *Cell Host Microbe* 11: 306–318
- Choi YJ, Jung J, Chung HK, Im E, Rhee SH (2013) PTEN regulates TLR5-induced intestinal inflammation by controlling Mal/TIRAP recruitment. *FASEB J* 27: 243–254
- Cirl C, Yadav M, Fischer H, Wagner H, Svanborg C, Miethke T (2008) Subversion of Toll-like receptor signaling by a unique family of bacterial Toll/interleukin-1 receptor domain-containing proteins. *Nat Med* 14: 399–406
- Conner DA (2001) Mouse embryo fibroblast (MEF) feeder cell preparation. *Curr Protoc Mol Biol* Chapter 23: Unit 23.2–23.2.7
- Elsen S, Huber P, Bouillot S, Couté Y, Fournier P, Dubois Y, Timsit JF, Maurin M, Attrée I (2014) A type III secretion negative clinical strain of *Pseudomonas aeruginosa* employs a two-partner secreted exolysin to induce hemorrhagic pneumonia. *Cell Host Microbe* 15: 164–176
- Felix C, Kaplan-Türköz B, Ranaldi S, Koelblen T, Terradot L, O'callaghan D, Vergunst AC (2014) The *Brucella* TIR domain containing proteins BtpA and BtpB have a structural WxxxE motif important for protection against microtubule depolymerisation. *Cell Commun Signal* 12: 53.
- Filloux A (2011) Protein secretion systems in *Pseudomonas aeruginosa*: an essay on diversity, evolution, and function. *Front Microbiol* 2: 155
- Fitzgerald KA, Palsson-McDermott EM, Bowie AG, Jefferies CA, Mansell AS, Brady G, Brint E, Dunne A, Gray P, Harte MT, McMurray D, Smith DE, Sims JE, Bird TA, O'Neill LA (2001) Mal (MyD88-adaptor-like) is required for toll-like receptor-4 signal transduction. *Nature* 413: 78–83
- Freschi L, Jeukens J, Kukavica-Ibrulj I, Boyle B, Dupont M-J, Laroche J, Larose S, Maaroufi H, Fothergill JL, Moore M, Winsor GL, Aaron SD, Barbeau J, Bell SC, Burns JL, Cámara M, Cantin A, Charette SJ, Dewar K, Déziel É *et al* (2015) Clinical utilization of genomics data produced by the international *Pseudomonas aeruginosa* consortium. *Front Microbiol* 6: 1036



- Gahlth D, Levy C, Heaven G, Stefani F, Wunderley L, Mould P, Cliff MJ, Bella J, Fielding AJ, Woodman P, Taberner L (2016) Structural basis for selective interaction between the ESCRT regulator HD-PTP and UBAP1. *Structure* 24: 2115–2126
- Garvis S, Munder A, Ball G, De Bentzmann S, Wiehlmann L, Ewbank JJ, Tümmler B, Filloux A (2009) *Caenorhabditis elegans* semi-automated liquid screen reveals a specialized role for the chemotaxis Gene cheB2 in *Pseudomonas aeruginosa* virulence. *PLoS Pathog* 5: e1000540
- Hachani A, Lossi NS, Hamilton A, Jones C, Bleves S, Albesa-Jové D, Filloux A (2011) Type VI secretion system in *Pseudomonas aeruginosa*: secretion and multimerization of VgrG proteins. *J Biol Chem* 286: 12317–12327
- Hauser AR, Jain M, Bar-Meir M, McColley SA (2011) Clinical significance of microbial infection and adaptation in cystic fibrosis. *Clin Microbiol Rev* 24: 29–70
- Hoang TT, Karkhoff-Schweizer RR, Kutchma AJ, Schweizer HP (1998) A broad-host-range Flp-FRT recombination system for site-specific excision of chromosomally-located DNA sequences: application for isolation of unmarked *Pseudomonas aeruginosa* mutants. *Gene* 212: 77–86
- Hornig T, Barton GM, Medzhitov R (2001) TIRAP: an adapter molecule in the Toll signaling pathway. *Nat Immunol* 2: 835–841
- Huang HR, Chen ZJ, Kunes S, Chang GD, Maniatis T (2010) Endocytic pathway is required for *Drosophila* Toll innate immune signaling. *Proc Natl Acad Sci USA* 107: 8322–8327
- Husebye H, Halaas Ø, Stenmark H, Tunheim G, Sandanger Ø, Bogen B, Brech A, Latz E, Espevik T (2006) Endocytic pathways regulate Toll-like receptor 4 signaling and link innate and adaptive immunity. *EMBO J* 25: 683–692
- Jain M, Ramirez D, Seshadri R, Cullina JF, Powers CA, Schuler GS, Bar-Meir M, Sullivan CL, McColley SA, Hauser AR (2004) Type III secretion phenotypes of *Pseudomonas aeruginosa* strains change during infection of individuals with cystic fibrosis. *J Clin Microbiol* 42: 5229–5237
- Jeong J-Y, Yim H-S, Ryu J-Y, Lee HS, Lee J-H, Seen D-S, Kang SG (2012) One-step sequence- and ligation-independent cloning as a rapid and versatile cloning method for functional genomics studies. *Appl Environ Microbiol* 78: 5440–5443
- Kagan JC, Medzhitov R (2006) Phosphoinositide-mediated adaptor recruitment controls Toll-like receptor signaling. *Cell* 125: 943–955
- Kagan JC, Su T, Hornig T, Chow A, Akira S, Medzhitov R (2008) TRAM couples endocytosis of Toll-like receptor 4 to the induction of interferon-beta. *Nat Immunol* 9: 361–368
- Kearse M, Moir R, Wilson A, Stones-Havas S, Cheung M, Sturrock S, Buxton S, Cooper A, Markowitz S, Duran C, Thierer T, Ashton B, Meintjes P, Drummond A (2012) Geneious Basic: an integrated and extendable desktop software platform for the organization and analysis of sequence data. *Bioinformatics* 28: 1647–1649
- Kharitidi D, Apaja PM, Manteghi S, Suzuki K, Malitskaya E, Roldan A, Gingras M-C, Takagi J, Lukacs GL, Pause A (2015) Interplay of endosomal pH and ligand occupancy in integrin  $\alpha 5 \beta 1$  ubiquitination, endocytic sorting, and cell migration. *Cell Rep* 13: 599–609
- Mamińska A, Bartosik A, Banach-Orłowska M, Pilecka I, Jastrzębski K, Zdzalik-Bielecka D, Castanon I, Poulain M, Neyen C, Wolińska-Nizioł L, Toruń A, Szymańska E, Kowalczyk A, Piwocka K, Simonsen A, Stenmark H, Fürthauer M, Gonzalez-Gaitan M, Miaczynska M (2016) ESCRT proteins restrict constitutive NF- $\kappa$ B signaling by trafficking cytokine receptors. *Sci Signal* 9: ra8
- Marek LR, Kagan JC (2012) Phosphoinositide binding by the Toll adaptor dMyD88 controls antibacterial responses in *Drosophila*. *Immunity* 36: 612–622
- Marvig RL, Sommer LM, Molin S, Johansen HK (2014) Convergent evolution and adaptation of *Pseudomonas aeruginosa* within patients with cystic fibrosis. *Nat Genet* 47: 57–64
- Michel G, Bleves S, Ball G, Lazdunski A, Filloux A (1998) Mutual stabilization of the XcpZ and XcpY components of the secretory apparatus in *Pseudomonas aeruginosa*. *Microbiology* 144: 3379–3386
- Myeni S, Child R, Ng TW, Kupko JJ, Wehrly TD, Porcella SF, Knodler LA, Celli J (2013) *Brucella* modulates secretory trafficking via multiple type IV secretion effector proteins. *PLoS Pathog* 9: e1003556
- Nagpal K, Plantinga TS, Sirois CM, Monks BG, Latz E, Netea MG, Golenbock DT (2011) Natural loss-of-function mutation of myeloid differentiation protein 88 disrupts its ability to form myddosomes. *J Biol Chem* 286: 11875–11882
- Newman JR, Fuqua C (1999) Broad-host-range expression vectors that carry the L-arabinose-inducible *Escherichia coli* araBAD promoter and the araC regulator. *Gene* 227: 197–203
- Newman RM, Salunkhe P, Godzik A, Reed JC (2006) Identification and characterization of a novel bacterial virulence factor that shares homology with mammalian Toll/interleukin-1 receptor family proteins. *Infect Immun* 74: 594–601
- Noursadeghi M, Tsang J, Hausteint T, Miller RF, Chain BM, Katz DR (2008) Quantitative imaging assay for NF- $\kappa$ B nuclear translocation in primary human macrophages. *J Immunol Methods* 329: 194–200
- Pirnay J-P, Bilocq F, Pot B, Cornelis P, Zizi M, Van Eldere J, Deschaght P, Vanechoutte M, Jennes S, Pitt T, De Vos D (2009) *Pseudomonas aeruginosa* population structure revisited. *PLoS One* 4: e7740
- Radhakrishnan GK, Yu Q, Harms JS, Splitter GA (2009) *Brucella* TIR domain-containing protein mimics properties of the toll-like receptor adaptor protein TIRAP. *J Biol Chem* 284: 9892–9898
- Radhakrishnan GK, Splitter GA (2010) Biochemical and functional analysis of TIR domain containing protein from *Brucella melitensis*. *Biochem Biophys Res Commun* 397: 59–63
- Radhakrishnan GK, Harms JS, Splitter GA (2011) Modulation of microtubule dynamics by a TIR domain protein from the intracellular pathogen *Brucella melitensis*. *Biochem J* 439: 79–83
- Reboud E, Elsen S, Bouillot S, Golovkine G, Basso P, Jeannot K, Attrée I, Huber P (2016) Phenotype and toxicity of the recently discovered exlA-positive *Pseudomonas aeruginosa* strains collected worldwide. *Environ Microbiol* 18: 3425–3439
- Rosadini CV, Kagan JC (2015) Microbial strategies for antagonizing Toll-like-receptor signal transduction. *Curr Opin Immunol* 32: 61–70
- Roy PH, Tetu SG, Larouche A, Elbourne L, Tremblay S, Ren Q, Dodson R, Harkins D, Shay R, Watkins K, Mahamoud Y, Paulsen IT (2010) Complete genome sequence of the multiresistant taxonomic outlier *Pseudomonas aeruginosa* PA7. *PLoS One* 5: e8842
- Salcedo SP, Marchesini MI, Lelouard H, Fugier E, Jolly G, Balor S, Muller A, Lapaque N, Demaria O, Alexopoulou L, Comerci DJ, Ugalde RA, Pierre P, Gorvel J-P (2008) *Brucella* control of dendritic cell maturation is dependent on the TIR-containing protein Btp1. *PLoS Pathog* 4: e21
- Salcedo SP, Marchesini MI, Degos C, Terwagne M, Von Bargen K, Lepidi H, Herrmann CK, Santos Lacerda TL, Imbert PRC, Pierre P, Alexopoulou L, Letesson J-J, Comerci DJ, Gorvel J-P (2013) BtpB, a novel *Brucella* TIR-containing effector protein with immune modulatory functions. *Front Cell Infect Microbiol* 3: 28
- Sengupta D, Koblansky A, Gaines J, Brown T, West AP, Zhang D, Nishikawa T, Park S-G, Roop RM, Ghosh S (2010) Subversion of innate immune responses by *Brucella* through the targeted degradation of the TLR signaling adapter, MAL. *J Immunol* 184: 956–964

- Smith JA, Khan M, Magnani DD, Harms JS, Durward M, Radhakrishnan GK, Liu Y-P, Splitter GA (2013) Brucella induces an unfolded protein response via TcpB that supports intracellular replication in macrophages. *PLoS Pathog* 9: e1003785
- Spear AM, Rana RR, Jenner DC, Flick-Smith HC, Oyston PCF, Simpson P, Matthews SJ, Byrne B, Atkins HS (2012) A Toll/interleukin (IL)-1 receptor domain protein from *Yersinia pestis* interacts with mammalian IL-1/Toll-like receptor pathways but does not play a central role in the virulence of *Y. pestis* in a mouse model of bubonic plague. *Microbiology* 158: 1593–1606
- Stefani F, Zhang L, Taylor S, Donovan J, Rollinson S, Doyotte A, Brownhill K, Bennion J, Pickering-Brown S, Woodman P (2011) UBAP1 is a component of an endosome-specific ESCRT-I complex that is essential for MVB sorting. *Curr Biol* 21: 1245–1250
- Waldhuber A, Snyder G, Römmler F, Cirl C, Müller T, Xiao T, Svanborg C, Miethke T (2016) A comparative analysis of the mechanism of toll-like receptor-disruption by TIR-containing protein C from uropathogenic *Escherichia coli*. *Pathogens* 5: 25
- Wunderley L, Brownhill K, Stefani F, Taberner L, Woodman P (2014) The molecular basis for selective assembly of the UBAP1-containing endosome-specific ESCRT-I complex. *J Cell Sci* 127: 663–672
- Yadav M, Zhang J, Fischer H, Huang W, Lutay N, Cirl C, Lum J, Miethke T, Svanborg C (2010) Inhibition of TIR domain signaling by TcpC: MyD88-dependent and independent effects on *Escherichia coli* virulence. *PLoS Pathog* 6: e1001120
- Yamamoto M, Sato S, Mori K, Hoshino K, Takeuchi O, Takeda K, Akira S (2002) Cutting edge: a novel Toll/IL-1 receptor domain-containing adapter that preferentially activates the IFN-beta promoter in the Toll-like receptor signaling. *J Immunol* 169: 6668–6672
- Zhang Q, Zmasek CM, Cai X, Godzik A (2011) TIR domain-containing adaptor SARM is a late addition to the ongoing microbe-host dialog. *Dev Comp Immunol* 35: 461–468
- Zou J, Baghdayan AS, Payne SJ, Shankar N (2014) A TIR domain protein from *E. faecalis* attenuates MyD88-Mediated signaling and NF- $\kappa$ B activation. *PLoS One* 9: e112010



License: This is an open access article under the terms of the Creative Commons Attribution 4.0 License, which permits use, distribution and reproduction in any medium, provided the original work is properly cited.



### 3. Annexe 3 : Protein-Protein Interactions: Pull-Down Assays

Louche et al. *Methods in Molecular Biology* 2017

This methods paper was written based on the protocols I optimized for analyzing interactions between bacterial proteins and host eukaryotic partners.

---



## Protein–Protein Interactions: Pull-Down Assays

Arthur Louche, Suzana P. Salcedo, and Sarah Bigot

### Abstract

Determining protein partners is an essential step toward understanding protein function and identifying relevant biological pathways. Many methods exist for investigating protein–protein interactions. The pull-down assay is an *in vitro* technique used to detect physical interactions between two or more proteins and an invaluable tool for confirming a predicted protein–protein interaction or identifying novel interacting partners. This method typically involves the use of affinity purification with various wash and elution steps. In this chapter, we describe how an interaction between two purified bacterial proteins or between bacterial and eukaryotic proteins can be detected by pull-down experiments.

**Key words** Pull-down, Protein–protein interactions, Tagged protein, Affinity purification

---

### 1 Introduction

Pathogenic bacteria produce virulence factors that usually help the pathogen to survive in an environmental niche, to promote colonization and invasion of host tissues, or to modulate the immune system. Virulence factors are toxins or effector proteins that can be transported by diverse secretion machineries in bacteria [1, 2]. Once secreted, these proteins can be assembled on the bacterial cell surface, released in the extracellular space, or secreted directly into a host cell or a neighboring bacterium. Once in host cells, effectors often target key proteins to hijack the host cellular machinery to remodel signaling cascades. The yeast two-hybrid system is often used to screen a large number of host proteins that potentially interact with bacterial effectors [3]. Regarding the mechanism of the secretion systems, a bacterial two-hybrid system is frequently employed to identify interaction networks between components of the secretory apparatus, as well as interaction between effectors and proteins of the machinery [4]. However, protein–protein interactions that have been determined by two-hybrid assay must be confirmed by other methods [5].

Pull-down is an *in vitro* method widely used to detect or confirm interactions among multiple proteins. This assay is similar in methodology to co-immunoprecipitation experiments in its use of an affinity ligand to capture interacting proteins. The difference between these two methods is that while co-immunoprecipitation uses immobilized antibodies to capture protein complexes, the pull-down approach uses a purified and tagged protein as a “bait” to bind any interacting proteins. The method consists of first immobilizing the tagged protein (bait) on an affinity ligand specific to the tag, creating an affinity support to capture and purify other proteins (prey) that interact with the bait. The bait and prey proteins can be obtained from multiple sources, such as cell lysates, purified proteins, expression systems, and *in vitro* transcription/translation systems. Once the prey proteins have been incubated with an immobilized bait protein, interacting complexes are eluted using an eluting buffer depending on the affinity ligand. Each experiment needs proper controls to demonstrate that characterized interactions are not an artifact. For example, a positive control consisting of an immobilized bait protein alone is necessary to verify proper attachment of the tagged bait protein to the affinity support. To identify and eliminate false positives caused by nonspecific binding of prey proteins to the affinity support, cell lysates or purified proteins can be analyzed after being passed through a minus bait support. Following a pull-down experiment, protein fractions are resolved by sodium dodecyl sulfate-polyacrylamide gel electrophoresis (SDS-PAGE) and then visualized by gel staining or western-blotting detection.

In this chapter, we describe detailed pull-down assay procedures that allow the identification of interacting proteins. First, we focus on how to perform a pull-down experiment to identify an interaction between a bacterial bait protein and eukaryotic prey proteins expressed in host cells (Subheadings 3.1 and 3.2). Next, we present how the interaction between two purified proteins can be visualized by a pull-down assay (Subheading 3.3). In these procedures, pull-down experiments have been performed using specific bait proteins fused to a 6× histidine tag. As a consequence, we selected Ni-NTA agarose beads as the affinity support used to immobilize these recombinant proteins.

---

## 2 Materials

Prepare all solutions with distilled water at room temperature and keep them at the indicated temperatures.

### 2.1 Preparation of Cell Lysate

1. Eukaryotic cells.
2. Cell culture dish, treated for optimal cell attachment, with growth surface area around 55 cm<sup>2</sup>, sterile.

3. Plasmid containing the gene of interest fused to a specific tag (obtained from a EndoFree maxipreparation).
4. Transfection reagent.
5. Phosphate buffered saline (PBS): Prepare a 10× solution with bidistilled water (18.2 MΩ cm) containing 10.6 mM KH<sub>2</sub>PO<sub>4</sub>, 30 mM Na<sub>2</sub>HPO<sub>4</sub>·2H<sub>2</sub>O, and 1.54 M NaCl, and sterilize with a 0.2 μm filter. The 1× solution obtained following dilution with bidistilled water will have a pH of around 7.4.
6. Radioimmunoprecipitation assay (RIPA) buffer: Ready-to-use solution containing 150 mM NaCl, 1.0% IGEPAL® CA-630, 0.5% sodium deoxycholate, 0.1% SDS, 50 mM Tris, pH 8.0.
7. Antiprotease cocktail: Mix 1% (v/v) of protease inhibitor cocktail (Sigma-Aldrich), phosphatase inhibitor cocktail 2 (Sigma-Aldrich), phosphatase inhibitor cocktail 3 (Sigma-Aldrich), and phenylmethylsulfonyl fluoride (PMSF).

## 2.2 Pull-Down Assays

1. 1 M Tris-HCl, pH 7.5 stock solution. Weigh 121.1 g Tris base and transfer to a 1 L graduated cylinder. Add water to 800 mL, mix, adjust pH with HCl, and make up to 1 L with water. Store at room temperature (*see Note 1*).
2. 5 M NaCl stock solution. Weigh 292.2 g NaCl and transfer to a 1 L graduated cylinder. Add water to 800 mL, stir, and adjust volume to 1 L with water (*see Note 1*).
3. Equilibrium buffer (*see Note 2*): 20 mM Tris-HCl, pH 7.5, 250 mM NaCl. Mix 1 mL 1 M Tris-HCl, pH 7.5 stock solution with 2.5 mL 5 M NaCl stock solution in a 50 mL centrifuge tube, and add water to a volume of 50 mL. Keep at 4 °C (*see Note 3*).
4. Elution buffer (*see Note 2*): 20 mM Tris-HCl, pH 7.5, 250 mM NaCl, 500 mM imidazole. Weigh 1.7 g imidazole in 50 mL solution of equilibrium buffer. Keep at 4 °C (*see Note 3*).
5. Purified His-tagged protein (bait).
6. Ni-NTA agarose beads: 6% beaded agarose (cross-linked), pre-charged with Ni<sup>2+</sup> (Protino® Ni-NTA Agarose, Macherey Nagel, or equivalent). Store at 4 °C (*see Note 4*).
7. 0.8 mL empty columns for gravity flow (Pierce™ Centrifuge Columns, Thermo Fisher Scientific, or equivalent).
8. Refrigerated microcentrifuge.

## 2.3 Sodium Dodecyl Sulfate (SDS) Polyacrylamide Gel Components

1. Resolving gel: 1.5 M Tris-HCl, pH 8.8. Weigh 90.8 g, transfer to 500 mL graduated cylinder, and add 300 mL water. Adjust pH with HCl and fill with water to 500 mL. Store at room temperature.
2. Stacking gel buffer: 0.5 M Tris-HCl, pH 6.8. Weigh 30.275 g, transfer to 500 mL graduated cylinder, and add 300 mL water.

Adjust pH with HCl and fill with water to 500 mL. Store at room temperature.

3. 30% acrylamide/Bis solution (37.5:1 acrylamide:Bis). Store at 4 °C.
4. Ammonium persulfate (APS): 20% solution in water. Store at –20 °C (*see Note 5*).
5. *N,N,N',N'*-tétraméthyléthylènediamine (TEMED). Store at room temperature.
6. SDS-PAGE running buffer: 25 mM Tris-HCl, 192 mM glycine, 0.1% SDS. Prepare 10× running buffer solution: Weigh 30 g Tris base, 144 g glycine, and 10 g SDS and add distilled water to 1 L. Store at room temperature. Prepare fresh 1× solution before gel electrophoresis.
7. Laemmli lysis buffer [6], 4× concentrate: 62.5 mM Tris-HCl pH 6.8, 2% SDS, 10% glycerol, 0.01% bromophenol blue, 5% *p*-mercaptoethanol. Store at –20 °C (*see Note 6*).
8. Protein ladder.

---

## 3 Methods

### 3.1 Preparation of Cell Lysate

1. Seed eukaryotic cells at  $5 \cdot 10^5$  in 10 cm cell culture dish (*see Note 7*) and incubate overnight at 37 °C in CO<sub>2</sub>.
2. Transfect cells with plasmid containing gene of interest fused to a specific tag with appropriate transfection reagent for time necessary for optimal expression of protein (16–24 h is usually a good range).
3. Cool cells by placing plates on ice, wash cells with 1× PBS. Add 2 mL cold PBS and harvest cells using cell scraper.
4. Centrifuge 5 min at  $80 \times g$  at 4 °C.
5. Resuspend cells with 200 µL RIPA buffer supplemented with antiprotease cocktail.
6. Incubate on ice 20 min and mix gently every 5 min with a P200 micropipette.
7. Stock prepared cells at –80 °C (*see Note 8*).
8. Right before pull-down experiment, thaw prepared cell extract. Centrifuge at  $17,000 \times g$  at 4 °C for 20 min. Use the supernatant as prey by following **step 9** in Subheading 3.2 (*see Note 9*).

### 3.2 Pull-Down Assay Using Cell Lysate as Prey (See Notes 10 and 11)

1. Transfer 120 µL Ni-NTA agarose beads to gravity flow column (*see Note 12*).
2. Centrifuge column for 1 min at  $1000 \times g$  at 4 °C. Discard flow-through.

3. Add 400  $\mu\text{L}$  distilled water to column (*see Note 13*).
4. Centrifuge column for 1 min at  $1000 \times g$  at 4 °C. Discard flow-through.
5. Mix carefully 50  $\mu\text{g}$  His-tagged protein (bait) with 400  $\mu\text{L}$  equilibrium buffer and load onto column (*see Notes 14 and 15*).
6. Incubate 1 h (*see Note 16*) with agitation at 4 °C (*see Note 17*) and 10 min on ice without agitation (*see Note 18*).
7. Centrifuge column for 1 min at  $1000 \times g$  at 4 °C and keep flow-through.
8. Load flow-through to column, and centrifuge column for 1 min at  $1000 \times g$  at 4 °C (*see Note 19*). Keep flow-through at 4 °C for analysis.
9. Mix 200  $\mu\text{L}$  cell extract (*see Note 20*) with 200  $\mu\text{L}$  equilibrium buffer and load onto column (*see Note 21*).
10. Incubate 1 h at 4 °C under agitation (*see Note 22*) then 10 min on ice without agitation (*see Note 18*).
11. Centrifuge column for 1 min at  $1000 \times g$  at 4 °C. Keep flow-through for analysis.
12. Wash column by adding to column 400  $\mu\text{L}$  equilibrium buffer.
13. Centrifuge column for 1 min at  $1000 \times g$  at 4 °C. Discard flow-through.
14. Wash column by adding to column 400  $\mu\text{L}$  equilibrium buffer containing 50 mM imidazole. Keep the first washing for analysis.
15. Centrifuge column for 1 min at  $1000 \times g$  at 4 °C. Discard flow-through.
16. Repeat **steps 14 and 15** three times and go to **step 17**. Keep last washing fraction at 4 °C for analysis.
17. Elute by loading 80  $\mu\text{L}$  elution buffer to column and incubate 10 min at 4 °C (*see Note 18*).
18. Centrifuge column for 1 min at  $1000 \times g$  at 4 °C and keep eluted fraction.
19. Repeat **steps 17 and 18** with eluted fraction (*see Note 22*). Keep eluted fraction at 4 °C for analysis.

### 3.3 Pull-Down Assay Using Purified Protein as Prey (See Note 11)

1. Incubate 50  $\mu\text{g}$  His-tagged bait protein with 50  $\mu\text{g}$  purified prey protein in total volume of 400  $\mu\text{L}$  equilibrium buffer (*see Note 23*) 2 h 30 min at 4 °C under agitation (*see Notes 17 and 24*).
2. Add 80  $\mu\text{L}$  Ni-NTA agarose beads to gravity flow column and follow **steps 1–4** of Subheading 3.2.

3. Equilibrate column by adding 400  $\mu\text{L}$  equilibrium buffer supplemented with 20 mM imidazole.
4. Centrifuge column for 1 min at  $1000 \times g$  at 4 °C. Discard flow-through.
5. Load 400  $\mu\text{L}$  incubated bait and prey proteins onto column. Incubate 10 min on ice without agitation (*see Note 18*).
6. Centrifuge column for 1 min at  $1000 \times g$  at 4 °C. Keep flow-through at 4 °C for analysis.
7. Wash by adding to column 400  $\mu\text{L}$  equilibrium buffer supplemented with 20 mM imidazole.
8. Centrifuge column for 1 min at  $1000 \times g$  at 4 °C. Save first washing at 4 °C for analysis.
9. Repeat washing **steps 7 and 8** four times and keep last washing fraction at 4 °C for analysis.
10. Add 200  $\mu\text{L}$  elution buffer to column and incubate on ice 10 min.
11. Centrifuge column for 1 min at  $1000 \times g$  at 4 °C. Keep eluted fraction at 4 °C for analysis.

### 3.4 SDS-PAGE and Analysis of Protein Fractions

1. To 15  $\mu\text{L}$  protein fraction add 5  $\mu\text{L}$  Laemmli lysis buffer, 4 $\times$  concentrate. Heat for 3 min at 100 °C and centrifuge 30 s using a microcentrifuge to bring down condensate.
2. Load 10  $\mu\text{L}$  protein fraction and 5  $\mu\text{L}$  protein ladder on SDS-polyacrylamide gel.
3. Electrophorese proteins in running buffer at 100 V for 15 min then 180 V until dye front has reached bottom of gel.
4. Identify interacting proteins by immunodetection or blue coomassie coloration (*see Note 25*).

---

## 4 Notes

1. We prefer not to use the solutions after 6 months of storage.
2. A different buffer, such as HEPES (4-(2-hydroxyethyl)-1-piperazineethanesulfonic acid), MES (2-(*N*-morpholino) ethanesulfonic acid), or phosphate buffers, may be required for your specific protein–protein interaction. Additionally, different pH values may be tested as these are specific and dependent on the interaction between proteins.
3. We found that pull-down experiments work better with fresh equilibrium and elution buffers.
4. The bait proteins used in this protocol are tagged with 6 $\times$  His that bind the nickel agarose affinity support. The choice of the matrix-associated antibody depends on the fusion tag. The His



tag is composed of a peptide motif that consists of six histidine residues with a high affinity towards metals like nickel that composes the used Ni-NTA agarose but also the Ni-NDA, Ni-TED, or Ni-TALON resins. The 6× His tag is very small (~1 kDa), which renders it less immunogenic than other larger tags, is shown not to affect the native conformation of bait proteins, and maintains its partner binding activity. Few naturally occurring proteins also bind to Ni-NTA matrices, making this tag the most commonly used affinity tag. In pull-down assays, the choice of the matrix-associated antibody depends on the fusion tag. What follow are some examples of tags with their advantages and disadvantages. The FLAG tag is an octapeptide that is likely located on the surface of the fusion protein due to the hydrophilic nature of amino acid residues and has affinity to anti-FLAG resin. Like the His tag, the FLAG tag is small, but a disadvantage is that the monoclonal antibody matrix is not as stable as Ni-NTA. Glutathione S-transferase (GST) tag binds to glutathione-associated support with high affinity and specificity. This tag has the advantage that GST isoforms are not normally found in bacteria, so purified bacterial prey proteins normally do not have affinity with glutathione resin. However, GST tag is large (26 kDa), exists as a dimer, is prone to nonspecific interaction, is expensive, and affinity to its support depends on certain reagents. The maltose-binding protein (MBP) tag from an *Escherichia coli* periplasmic protein has affinity for matrix consisting of sugars or anti-MBP. This tag is used for the purposes of overcoming problems associated with the expression and purification of recombinant proteins [7]. However, the disadvantage of the MBP tag is its large size, its immunogenicity, and the mild elution of MBP-tagged proteins, which complicate pull-down experiments.

5. Make an aliquot of 1 mL before -20 °C storage. This will prevent the degradation caused by repeated thawing.
6. Make an aliquot of 500 μL before -20 °C storage. The used Laemmli lysis buffer can be kept at 4 °C for 1 month.
7. As negative control, prepare a cell lysate without expressing bait protein (negative cell lysate). This will eliminate false positives resulting from nonspecific interactions of cell lysate proteins with the Ni-NTA agarose beads. Additional negative controls can include an irrelevant protein with the same tag or expression of the tag alone, as in the case of the GFP.
8. Before stocking the cells, remove an aliquot and control by western blot the production of the prey protein.
9. Whole-cell lysate instead of the supernatant fraction can also be used to test whether the prey protein of interest localizes in the pellet fraction.

10. Pull-down experiments using cell lysates will not demonstrate that interaction between the bait and prey proteins is direct but only determine that they are part of the same complex. To prove a direct interaction, the prey protein must be purified and used in pull-down experiments as described in Subheading 3.3.
11. Try to work mostly on ice or at 4 °C to prevent the degradation or the denaturation of the proteins.
12. Break the end cap of the gravity flow column and place it on a 1.5 mL Eppendorf tube. Thoroughly resuspend the Ni-NTA resin by inverting the bottle several times to obtain a uniform suspension. Pipette tips must be cut to allow the Ni-NTA agarose beads to get into.
13. This step eliminates the left 30% ethanol present in the Ni-NTA resin.
14. Before loading the bait protein, plug the gravity flow column using a piece of parafilm before replacing it on a 2 mL Eppendorf tube.
15. Prepare a supplementary column by mixing 50  $\mu\text{g}$  of a known noninteracting bait fused to 6 $\times$  His tag with 400  $\mu\text{L}$  equilibrium buffer to an empty column. Additionally, prepare a column by adding 400  $\mu\text{L}$  equilibrium buffer to an empty column. These negative bait columns will be used in combination with cell lysates to eliminate false positives resulting from nonspecific interactions.
16. The incubation time can be increased from several hours to overnight at 4 °C under agitation depending on the strength of the interaction between bait and prey proteins.
17. Rotate on roller or rotating platform.
18. The column should stand straight on the ice. This step allows the resin to flow by gravity before centrifugation.
19. We found that loading two times the flow-through increases the capacity of the binding.
20. The volume is dependent on the protein concentration of the cell extract. As a guide, 125–150  $\mu\text{g}$  of protein of a cell extract is usually incubated per microgram of bait protein. Alternatively, cell extract samples can be normalized by visualization of transfected proteins to ensure equivalent expression of the prey and the relevant controls (*see Note 7*).
21. Several controls should be added at this step. Load 400  $\mu\text{L}$  equilibrium buffer without prey protein to analyze the efficiency of the immobilization of the bait protein. As negative controls, load onto the negative column (*see Note 12*) 200  $\mu\text{L}$  cell lysate containing the prey protein or the negative cell lysate (*see Note 7*) mixed with 200  $\mu\text{L}$  equilibrium buffer. Additionally,



load 200  $\mu\text{L}$  negative cell lysate mixed with 200  $\mu\text{L}$  equilibrium buffer onto the column associated with the bait protein.

22. We found that loading two times the eluted fraction increased its quantity.
23. As negative control, incubate 50  $\mu\text{g}$  bait protein (minus prey) or prey protein alone (minus bait) in 400  $\mu\text{L}$  equilibrium buffer. The minus prey control will ensure that the Ni-NTA agarose resin will correctly capture the His-tagged bait protein alone. The minus bait control will eliminate false positives resulting from an interaction between affinity support and prey protein.
24. A different incubation temperature and time may be required for your specific protein–protein interaction.
25. A prey protein that interacts with the bait protein will be found in the eluted fraction. In contrast, a noninteracting protein will not be retained by the bait protein, will pass through the column, and will be found in the flow-through protein fraction.

## References

1. Costa TRD, Felisberto-Rodrigues C, Meir A, Prevost MS, Redzej A, Trokter M, Waksman G (2015) Secretion systems in Gram-negative bacteria: structural and mechanistic insights. *Nat Rev Microbiol* 13:343–359
2. McBride MJ, Nakane D (2015) *Flavobacterium* gliding motility and the type IX secretion system. *Curr Opin Microbiol* 28:72–77
3. Rodríguez-Negrete E, Bejarano ER, Castillo AG (2014) Using the yeast two-hybrid system to identify protein-protein interactions. *Methods Mol Biol* 1072:241–258
4. Zoued A, Brunet YR, Durand E, Aschtgen M-S, Logger L, Douzi B, Journet L, Cambillau C, Cascales E (2014) Architecture and assembly of the Type VI secretion system. *Biochim Biophys Acta* 1843:1664–1673
5. Boucrot E, Henry T, Borg J-P, Gorvel J-P, Méresse S (2005) The intracellular fate of *Salmonella* depends on the recruitment of kinesin. *Science* 308:1174–1178
6. Laemmli UK (1970) Cleavage of structural proteins during the assembly of the head of bacteriophage T4. *Nature* 227:680–685
7. DiGuan C, Li P, Riggs PD, Inouye H (1988) Vectors that facilitate the expression and purification of foreign peptides in *Escherichia coli* by fusion to maltose-binding protein. *Gene* 67:21–30

## REFERENCES

1. Moreno E, Moriyón I. The Genus *Brucella*. In: Dworkin M, Falkow S, Rosenberg E, Schleifer K-H, Stackebrandt E, editors. *The Prokaryotes: Volume 5: Proteobacteria: Alpha and Beta Subclasses*. New York, NY: Springer New York; 2006. pp. 315–456.
2. D'ANASTASIO R, STANISCIÀ T, MILIA ML, MANZOLI L, CAPASSO L. Origin, evolution and paleoepidemiology of brucellosis. *Epidemiol Infect.* Cambridge University Press; 2010;139: 149–156. doi:10.1017/S095026881000097X
3. Greco E, El-Aguizy O, Ali MF, Foti S, Cunsolo V, Saletti R, et al. Proteomic Analyses on an Ancient Egyptian Cheese and Biomolecular Evidence of Brucellosis. *Anal Chem.* 2018;90: 9673–9676. doi:10.1021/acs.analchem.8b02535
4. Godfroid J, Cloeckaert A, Liautard J-P, Kohler S, Fretin D, Walravens K, et al. From the discovery of the Malta fever's agent to the discovery of a marine mammal reservoir, brucellosis has continuously been a re-emerging zoonosis. *Vet Res. EDP Sciences;* 2005;36: 313–326. doi:10.1051/vetres:2005003
5. Godfroid J, Dahouk AI S, Pappas G, Roth F, Matope G, Muma J, et al. A “One Health” surveillance and control of brucellosis in developing countries: moving away from improvisation. *Comp Immunol Microbiol Infect Dis.* 2013;36: 241–248. doi:10.1016/j.cimid.2012.09.001
6. Pappas G, Papadimitriou P, Akritidis N, Christou L, Tsianos EV. The new global map of human brucellosis. *The Lancet Infectious Diseases.* 2006;6: 91–99. doi:10.1016/S1473-3099(06)70382-6
7. Mailles A, Rautureau S, Le Horgne JM, Poignet-Leroux B, d'Arnoux C, Denetière G, et al. Re-emergence of brucellosis in cattle in France and risk for human health. *Euro Surveill.* 2012;17.
8. Garin-Bastuji B, Hars J, Drapeau A, Cherfa M-A, Game Y, Le Horgne J-M, et al. Reemergence of *Brucella melitensis* in wildlife, France. *Emerg Infect Dis.* 2014;20: 1570–1571. doi:10.3201/eid2009.131517
9. Anses. AVIS et RAPPORT de l'Anses relatif à l'évaluation de la pertinence de la vaccination des bouquetins du Bargy contre la brucellose. 2019;: 1–114.
10. Yanagi M, Yamasato K. Phylogenetic analysis of the family Rhizobiaceae and related bacteria by sequencing of 16S rRNA gene using PCR and DNA sequencer. *FEMS Microbiol Lett.* 1993;107: 115–120. doi:10.1111/j.1574-6968.1993.tb06014.x
11. Olsen SC, Palmer MV. Advancement of Knowledge of *Brucella* Over the Past 50 Years. *Vet Pathol.* 5 ed. 2014;51: 1076–1089. doi:10.1177/0300985814540545
12. Eisenberg T, Hamann H-P, Kaim U, Schlez K, Seeger H, Schauerte N, et al. Isolation of Potentially Novel *Brucella* spp. from Frogs. *Appl Environ Microbiol.* 2012;78: 3753–3755. doi:10.1128/AEM.07509-11
13. Nymo IH, Tryland M, Godfroid J. A review of *Brucella* infection in marine mammals, with special emphasis on *Brucella pinnipedialis* in the hooded seal (*Cystophora cristata*). *Vet Res. BioMed Central Ltd;* 2011;42: 93. doi:10.1186/1297-9716-42-93

14. El-Sayed A, Awad W. International Journal of Veterinary Science and Medicine. International Journal of Veterinary Science and Medicine. Elsevier B.V; 2018;6: S31–S35. doi:10.1016/j.ijvsm.2018.01.008
15. Carmichael LE, Bruner DW. Characteristics of a newly-recognized species of *Brucella* responsible for infectious canine abortions. Cornell Vet. 1968;48: 579–592.
16. BUDDLE MB. Studies on *Brucella ovis* (n.sp.), a cause of genital disease of sheep in New Zealand and Australia. J Hyg (Lond). 1956;54: 351–364. doi:10.1017/s0022172400044612
17. STOENNER HG, LACKMAN DB. A new species of *Brucella* isolated from the desert wood rat, *Neotoma lepida* Thomas. Am J Vet Res. 1957;18: 947–951.
18. Foster G, Osterman BS, Godfroid J, Jacques I, Cloeckaert A. *Brucella ceti* sp. nov. and *Brucella pinnipedialis* sp. nov. for *Brucella* strains with cetaceans and seals as their preferred hosts. International Journal of Systematic and Evolutionary Microbiology. 2007;57: 2688–2693. doi:10.1099/ijls.0.65269-0
19. Audic S, Lescot M, Claverie J-M, Scholz HC. *Brucella microti*: the genome sequence of an emerging pathogen. BMC Genomics. 2009;10: 352–18. doi:10.1186/1471-2164-10-352
20. Scholz HC, Nöckler K, Göllner C, Bahn P, Vergnaud G, Tomaso H, et al. *Brucella inopinata* sp. nov., isolated from a breast implant infection. International Journal of Systematic and Evolutionary Microbiology. 2010;60: 801–808. doi:10.1099/ijls.0.011148-0
21. Whatmore AM, Davison N, Cloeckaert A, Dahouk Al S, Zygmunt MS, Brew SD, et al. *Brucella papionis* sp. nov., isolated from baboons (*Papio* spp.). International Journal of Systematic and Evolutionary Microbiology. 2014;64: 4120–4128. doi:10.1099/ijls.0.065482-0
22. Scholz HC, Revilla-Fernández S, Dahouk SA, Hammerl JA, Zygmunt MS, Cloeckaert A, et al. *Brucella vulpis* sp. nov., isolated from mandibular lymph nodes of red foxes (*Vulpes vulpes*). International Journal of Systematic and Evolutionary Microbiology. 2016;66: 2090–2098. doi:10.1099/ijsem.0.000998
23. Martirosyan A, Moreno E, Gorvel J-P. An evolutionary strategy for a stealthy intracellular *Brucella* pathogen. Immunol Rev. 2011;240: 211–234. doi:10.1111/j.1600-065X.2010.00982.x
24. McDonald WL, Jamaludin R, Mackereth G, Hansen M, Humphrey S, Short P, et al. Characterization of a *Brucella* sp. Strain as a Marine-Mammal Type despite Isolation from a Patient with Spinal Osteomyelitis in New Zealand. Journal of Clinical Microbiology. 2006;44: 4363–4370. doi:10.1128/JCM.00680-06
25. Ollé-Goig JE, Canela-Soler J. An outbreak of *Brucella melitensis* infection by airborne transmission among laboratory workers. Am J Public Health. 1987;77: 335–338. doi:10.2105/ajph.77.3.335
26. Yagupsky P, Baron EJ. Laboratory exposures to brucellae and implications for bioterrorism. Emerg Infect Dis. 2005;11: 1180–1185. doi:10.3201/eid1108.041197
27. Weinstein RA, Singh K. Laboratory-Acquired Infections. CLIN INFECT DIS. 2009;49: 142–147.

28. Doganay GD, Doganay M. Brucella as a potential agent of bioterrorism. *Recent Pat Antiinfect Drug Discov.* 2013;8: 27–33. doi:10.2174/1574891x11308010006
29. Çelebi G, Külah C, Kiliç S, Üstündağ G. Asymptomatic Brucella bacteraemia and isolation of Brucella melitensis biovar 3 from human breast milk. *Scandinavian Journal of Infectious Diseases.* 2009;39: 205–208. doi:10.1080/00365540600978898
30. Tuon FF, Gondolfo RB, Cerchiari N. Human-to-human transmission of Brucella - a systematic review. *Trop Med Int Health.* 2017;22: 539–546. doi:10.1111/tmi.12856
31. Meltzer E, Sidi Y, Smolen G, Banai M, Bardenstein S, Schwartz E. Sexually Transmitted Brucellosis in Humans. *CLIN INFECT DIS.* 2010;51: e12–e15. doi:10.1086/653608
32. Hamdy MER, Amin AS. Detection of Brucella Species in the Milk of Infected Cattle, Sheep, Goats and Camels by PCR. *The Veterinary Journal.* 2002;163: 299–305. doi:10.1053/tvjl.2001.0681
33. Lilenbaum W, de Souza GN, Ristow P, Cortez Moreira M, Fráguas S, da Silva Cardoso V, et al. A serological study on Brucella abortus, caprine arthritis–encephalitis virus and Leptospira in dairy goats in Rio de Janeiro, Brazil. *The Veterinary Journal.* 2007;173: 408–412. doi:10.1016/j.tvjl.2005.12.003
34. de Figueiredo P, Ficht TA, Rice-Ficht A, Rossetti CA, Adams LG. Pathogenesis and Immunobiology of Brucellosis Review of BrucellaeHost Interactions. *The American Journal of Pathology. American Society for Investigative Pathology;* 2015;185: 1505–1517. doi:10.1016/j.ajpath.2015.03.003
35. Kaygusuz TO, Kaygusuz I, Kilic SS, Yalcin S, Felek S. Investigation of hearing loss in patients with acute brucellosis by standard and high-frequency audiometry. *Clinical Microbiology and Infection.* 2005;11: 559–563. doi:10.1111/j.1469-0691.2005.01167.x
36. Young EJ. An overview of human brucellosis. *CLIN INFECT DIS.* 1995;21: 283–9– quiz 290. doi:10.1093/clinids/21.2.283
37. Hull NC, Schumaker BA. Comparisons of brucellosis between human and veterinary medicine. *Infection Ecology & Epidemiology. Taylor & Francis;* 2018;8: 1–13. doi:10.1080/20008686.2018.1500846
38. Franco MP, Mulder M, Gilman RH, Smits HL. Human brucellosis. *The Lancet Infectious Diseases.* 2007;7: 775–786. doi:10.1016/S1473-3099(07)70286-4
39. Ariza J, Bosilkovski M, Cascio A, Colmenero JD, Corbel MJ, Falagas ME, et al. Perspectives for the Treatment of Brucellosis in the 21st Century: The Ioannina Recommendations. *PLoS Med.* 2007;4: e317–7. doi:10.1371/journal.pmed.0040317
40. Hasanjani Roushan MR, Moulana Z, Mohseni Afshar Z, Ebrahimpour S. Risk Factors for Relapse of Human Brucellosis. *GJHS.* 2015;8: 77–6. doi:10.5539/gjhs.v8n7p77
41. Yang X, Skyberg JA, Cao L, Clapp B, Thornburg T, Pascual DW. Progress in Brucella vaccine development. *Front Biol.* 2012;8: 60–77. doi:10.1007/s11515-012-1196-0

42. Schurig GG, Roop RM2, Bagchi T, Boyle S, Buhrman D, Sriranganathan N. Biological properties of RB51; a stable rough strain of *Brucella abortus*. *Vet Microbiol.* 1991;28: 171–188. doi:10.1016/0378-1135(91)90091-s
43. Olsen SC, Hennager SG. Immune Responses and Protection against Experimental *Brucella suis* Biovar 1 Challenge in Nonvaccinated or *B. abortus* Strain RB51-Vaccinated Cattle. *CVI.* 2010;17: 1891–1895. doi:10.1128/CVI.00326-10
44. Blasco JM. A review of the use of *B. melitensis* Rev 1 vaccine in adult sheep and goats. *Prev Vet Med.* 1997;31: 275–283. doi:10.1016/s0167-5877(96)01110-5
45. Blasco JM, Díaz R. *Brucella melitensis* Rev-1 vaccine as a cause of human brucellosis. *Lancet.* 1993;342: 805. doi:10.1016/0140-6736(93)91571-3
46. Maurin M. La brucellose à l’aube du 21e siècle. *Médecine et Maladies Infectieuses.* 2005;35: 6–16. doi:10.1016/j.medmal.2004.08.003
47. Godfroid J. Brucellosis in wildlife. *Rev Sci Tech.* 2002;21: 277–286. doi:10.20506/rst.21.2.1333
48. O'Brien MP, Beja-Pereira A, Anderson N, Ceballos RM, Edwards WH, Harris B, et al. Brucellosis Transmission between Wildlife and Livestock in the Greater Yellowstone Ecosystem: Inferences from DNA Genotyping. *Journal of Wildlife Diseases.* 2017;53: 339–5. doi:10.7589/2015-12-329
49. Mick V, Le Carrou G, Corde Y, Game Y, Jaÿ M, Garin-Bastuji B. *Brucella melitensis* in France: persistence in wildlife and probable spillover from Alpine ibex to domestic animals. *PLoS ONE.* 2014;9: e94168. doi:10.1371/journal.pone.0094168
50. Franc KA, Krecek RC, Häsler BN, Arenas-Gamboa AM. Brucellosis remains a neglected disease in the developing world: a call for interdisciplinary action. *BMC Public Health.* 2018;18: 125. doi:10.1186/s12889-017-5016-y
51. Seleem MN, Boyle SM, Sriranganathan N. Brucellosis: a re-emerging zoonosis. *Vet Microbiol.* 2010;140: 392–398. doi:10.1016/j.vetmic.2009.06.021
52. Gorvel J-P, Moreno E. *Brucella* intracellular life: from invasion to intracellular replication. *Vet Microbiol.* 2002;90: 281–297. doi:10.1016/s0378-1135(02)00214-6
53. Jimenez de Bagues M-P, Dudal S, Dornand J, Gross A. Cellular bioterrorism: how *Brucella* corrupts macrophage physiology to promote invasion and proliferation. *Clin Immunol.* 2005;114: 227–238. doi:10.1016/j.clim.2004.07.010
54. Pizarro-Cerdá J, Méresse S, Parton RG, van der Goot G, Sola-Landa A, Lopez-Goñi I, et al. *Brucella abortus* transits through the autophagic pathway and replicates in the endoplasmic reticulum of nonprofessional phagocytes. *Infect Immun.* 1998;66: 5711–5724. doi:10.1128/IAI.66.12.5711-5724.1998
55. Pizarro-Cerdá J, Moreno E, Sanguedolce V, Mege JL, Gorvel JP. Virulent *Brucella abortus* prevents lysosome fusion and is distributed within autophagosome-like compartments. *Infect Immun.* 1998;66: 2387–2392. doi:10.1128/IAI.66.5.2387-2392.1998

56. Lee JJ, Kim DG, Kim DH, Simborio HL, Min W, Lee HJ, et al. Interplay between clathrin and Rab5 controls the early phagocytic trafficking and intracellular survival of *Brucella abortus* within HeLa cells. *J Biol Chem.* 2013;288: 28049–28057. doi:10.1074/jbc.M113.491555
57. Guzmán-Verri C, Chaves-Olarte E, Eichel-Streiber von C, López-Goñi I, Thelestam M, Arvidson S, et al. GTPases of the Rho Subfamily Are Required for *Brucella abortus* Internalization in Nonprofessional Phagocytes. *J Biol Chem.* 2001;276: 44435–44443. doi:10.1074/jbc.M105606200
58. Sola-Landa A, Pizarro-Cerdá J, Grilló MJ, Moreno E, Moriyón I, Blasco JM, et al. A two-component regulatory system playing a critical role in plant pathogens and endosymbionts is present in *Brucella abortus* and controls cell invasion and virulence. *Mol Microbiol.* 1998;29: 125–138. doi:10.1046/j.1365-2958.1998.00913.x
59. Lopez-Goñi I, Guzmán-Verri C, Manterola L, Sola-Landa A, Moriyón I, Moreno E. Regulation of *Brucella* virulence by the two-component system BvrR/BvrS. *Vet Microbiol.* 2002;90: 329–339. doi:10.1016/s0378-1135(02)00218-3
60. Watarai M, Makino SI, Michikawa M, Yanagisawa K, Murakami S, Shirahata T. Macrophage Plasma Membrane Cholesterol Contributes to *Brucella abortus* Infection of Mice. *Infect Immun.* 2002;70: 4818–4825. doi:10.1128/IAI.70.9.4818-4825.2002
61. Naroeni A. Role of Cholesterol and the Ganglioside GM1 in Entry and Short-Term Survival of *Brucella suis* in Murine Macrophages. *Infect Immun.* 2002;70: 1640–1644. doi:10.1128/IAI.70.3.1640-1644.2002
62. Porte F, Naroeni A, Ouahrani-Bettache S, Liautard JP. Role of the *Brucella suis* Lipopolysaccharide O Antigen in Phagosomal Genesis and in Inhibition of Phagosome-Lysosome Fusion in Murine Macrophages. *Infect Immun.* 2003;71: 1481–1490. doi:10.1128/IAI.71.3.1481-1490.2003
63. Pei J, Turse JE, Ficht TA. Evidence of *Brucella abortus* OPS dictating uptake and restricting NF- $\kappa$ B activation in murine macrophages. *Microbes and Infection.* 2008;10: 582–590. doi:10.1016/j.micinf.2008.01.005
64. Oliveira SC, de Oliveira FS, Macedo GC, de Almeida LA, Carvalho NB. The role of innate immune receptors in the control of *Brucella abortus* infection: toll-like receptors and beyond. *Microbes and Infection.* 2008;10: 1005–1009. doi:10.1016/j.micinf.2008.07.005
65. Lee JJ, Kim DH, Kim DG, Lee HJ, Min W, Rhee MH, et al. Toll-Like Receptor 4-Linked Janus Kinase 2 Signaling Contributes to Internalization of *Brucella abortus* by Macrophages. Blanke SR, editor. *Infect Immun.* 2013;81: 2448–2458. doi:10.1128/IAI.00403-13
66. Kim S, Watarai M, Suzuki H, Makino S-I, Kodama T, Shirahata T. Lipid raft microdomains mediate class A scavenger receptor-dependent infection of *Brucella abortus*. *Microbial Pathogenesis.* 2004;37: 11–19. doi:10.1016/j.micpath.2004.04.002
67. Watarai M, Kim S, Erdenebaatar J, Makino S-I, Horiuchi M, Shirahata T, et al. Cellular Prion Protein Promotes *Brucella* Infection into Macrophages. *The Journal of Experimental Medicine.* 2003;198: 5–17. doi:10.1084/jem.20021980



68. Nakato G, Hase K, Suzuki M, Kimura M, Ato M, Hanazato M, et al. Cutting Edge: *Brucella abortus* exploits a cellular prion protein on intestinal M cells as an invasive receptor. *The Journal of Immunology*. 2012;189: 1540–1544. doi:10.4049/jimmunol.1103332
69. Fontes P, Alvarez-Martinez M-T, Gross A, Carnaud C, Kohler S, Liautard J-P. Absence of evidence for the participation of the macrophage cellular prion protein in infection with *Brucella suis*. *Infect Immun*. 2005;73: 6229–6236. doi:10.1128/IAI.73.10.6229-6236.2005
70. Castaneda-Roldan EI, Avelino-Flores F, Dall'Agnol M, Freer E, Cedillo L, Dornand J, et al. Adherence of *Brucella* to human epithelial cells and macrophages is mediated by sialic acid residues. *Cellular Microbiology*. 3rd ed. John Wiley & Sons, Ltd; 2004;6: 435–445. doi:10.1111/j.1462-5822.2004.00372.x
71. Castañeda-Roldán EI, Ouahrani-Bettache S, Saldaña Z, Avelino F, Rendón MA, Dornand J, et al. Characterization of SP41, a surface protein of *Brucella* associated with adherence and invasion of host epithelial cells. *Cellular Microbiology*. 2006;8: 1877–1887. doi:10.1111/j.1462-5822.2006.00754.x
72. Czibener C, Merwaiss F, Guaimas F, Del Giudice MG, Serantes DAR, Spera JM, et al. BigA is a novel adhesin of *Brucella* that mediates adhesion to epithelial cells. *Cellular Microbiology*. 2015;18: 500–513. doi:10.1111/cmi.12526
73. Ruiz-Ranwez V, Posadas DM, Van der Henst C, Estein SM, Arocena GM, Abdian PL, et al. BtaE, an Adhesin That Belongs to the Trimeric Autotransporter Family, Is Required for Full Virulence and Defines a Specific Adhesive Pole of *Brucella suis*. Payne SM, editor. *Infect Immun*. 3rd ed. 2013;81: 996–1007. doi:10.1128/IAI.01241-12
74. Starr T, Ng TW, Wehrly TD, Knodler LA, Celli J. *Brucella* Intracellular Replication Requires Trafficking Through the Late Endosomal/Lysosomal Compartment. *Traffic*. 2008;9: 678–694. doi:10.1111/j.1600-0854.2008.00718.x
75. Porte F, Liautard JP, Köhler S. Early acidification of phagosomes containing *Brucella suis* is essential for intracellular survival in murine macrophages. *Infect Immun*. 1999;67: 4041–4047. doi:10.1128/IAI.67.8.4041-4047.1999
76. Lacerda TLS, Salcedo SP, Gorvel J-P. *Brucella* T4SS: the VIP pass inside host cells. *Curr Opin Microbiol*. 2013;16: 45–51. doi:10.1016/j.mib.2012.11.005
77. Arellano-Reynoso B, Lapaque N, Salcedo S, Briones G, Ciocchini AE, Ugalde R, et al. Cyclic  $\beta$ -1,2-glucan is a *brucella* virulence factor required for intracellular survival. *Nat Immunol*. 2005;6: 618–625. doi:10.1038/ni1202
78. Celli J, de Chastellier C, Franchini D-M, Pizarro-Cerdá J, Moreno E, Gorvel J-P. *Brucella* evades macrophage killing via VirB-dependent sustained interactions with the endoplasmic reticulum. *The Journal of Experimental Medicine*. 2003;198: 545–556. doi:10.1084/jem.20030088
79. Celli J, Salcedo SP, Gorvel J-P. *Brucella* coopts the small GTPase Sar1 for intracellular replication. *PNAS*. 2005;102: 1673–1678. doi:10.1073/pnas.0406873102
80. Fugier E, Salcedo SP, de Chastellier C, Pophillat M, Muller A, Arce-Gorvel V, et al. The glyceraldehyde-3-phosphate dehydrogenase and the small GTPase Rab 2 are crucial for *Brucella* replication. *PLOS Pathog*. 2009;5: e1000487. doi:10.1371/journal.ppat.1000487

81. Comerci DJ, Martínez-Lorenzo MJ, Sieira R, Gorvel JP, Ugalde RA. Essential role of the VirB machinery in the maturation of the *Brucella abortus*-containing vacuole. *Cellular Microbiology*. 2001;3: 159–168. doi:10.1046/j.1462-5822.2001.00102.x
82. Sieira R, Comerci DJ, Sánchez DO, Ugalde RA. A homologue of an operon required for DNA transfer in *Agrobacterium* is required in *Brucella abortus* for virulence and intracellular multiplication. *JB*. 2000;182: 4849–4855. doi:10.1128/jb.182.17.4849-4855.2000
83. Myeni S, Child R, Ng TW, Kupko JJ, Wehrly TD, Porcella SF, et al. *Brucella* Modulates Secretory Trafficking via Multiple Type IV Secretion Effector Proteins. Valdivia RH, editor. *PLOS Pathog*. 2013;9: e1003556–18. doi:10.1371/journal.ppat.1003556
84. de Barsy M, Jamet A, Filopon D, Nicolas C, Laloux G, Rual J-F, et al. Identification of a *Brucella* spp. secreted effector specifically interacting with human small GTPase Rab2. *Cellular Microbiology*. 2011;13: 1044–1058. doi:10.1111/j.1462-5822.2011.01601.x
85. Miller CN, Smith EP, Cundiff JA, Knodler LA, Blackburn JB, Lupashin V, et al. A *Brucella* Type IV Effector Targets the COG Tethering Complex to Remodel Host Secretory Traffic and Promote Intracellular Replication. *Cell Host and Microbe*. Elsevier Inc; 2017;;: 1–21. doi:10.1016/j.chom.2017.07.017
86. Deghelt M, Letesson J-J, De Bolle X. On the link between cell cycle and infection of the Alphaproteobacterium *Brucella abortus*. *Microb Cell*. 2014;1: 346–348. doi:10.15698/mic2014.10.171
87. De Bolle X, Crosson S, Matroule J-Y, Letesson J-J. *Brucella abortus* Cell Cycle and Infection Are Coordinated. *Trends in Microbiology*. 2015;23: 812–821. doi:10.1016/j.tim.2015.09.007
88. Barquero-Calvo E, Chaves-Olarte E, Weiss DS, Guzmán-Verri C, Chacón-Díaz C, Rucavado A, et al. *Brucella abortus* Uses a Stealthy Strategy to Avoid Activation of the Innate Immune System during the Onset of Infection. Ojcius D, editor. *PLoS ONE*. 2007;2: e631–14. doi:10.1371/journal.pone.0000631
89. Gross A, Terraza A, Ouahrani-Bettache S, Liautard JP, Dornand J. In vitro *Brucella suis* infection prevents the programmed cell death of human monocytic cells. *Infect Immun*. 2000;68: 342–351. doi:10.1128/iai.68.1.342-351.2000
90. Starr T, Child R, Wehrly TD, Hansen B, Hwang S, López-Otin C, et al. Selective subversion of autophagy complexes facilitates completion of the *Brucella* intracellular cycle. *Cell Host and Microbe*. 2012;11: 33–45. doi:10.1016/j.chom.2011.12.002
91. Huang J, Brumell JH. Bacteria-autophagy interplay: a battle for survival. *Nat Rev Microbiol*. 2014;12: 101–114. doi:10.1038/nrmicro3160
92. Celli J. The Intracellular Life Cycle of *Brucella* spp. *Microbiology Spectrum*. 2019;7: 1–17. doi:10.1128/microbiolspec.BAI-0006-2019
93. O'Callaghan D, Cazevieille C, Allardet-Servent A, Boschirolu ML, Bourg G, Foulongne V, et al. A homologue of the *Agrobacterium tumefaciens* VirB and *Bordetella pertussis* Ptl type IV secretion systems is essential for intracellular survival of *Brucella suis*. *Mol Microbiol*. 1999;33: 1210–1220. doi:10.1046/j.1365-2958.1999.01569.x

94. Juhas M, Crook DW, Hood DW. Type IV secretion systems: tools of bacterial horizontal gene transfer and virulence. *Cellular Microbiology*. 2008;10: 2377–2386. doi:10.1111/j.1462-5822.2008.01187.x
95. Lavigne JP, Botella E, O'Callaghan D. [Type IV secretion system and their effectors: an update]. *Pathol Biol (Paris)*. 2006;54: 296–303. doi:10.1016/j.patbio.2005.04.006
96. Christie PJ. Type IV secretion: the *Agrobacterium* VirB/D4 and related conjugation systems. *Biochim Biophys Acta*. 2004;1694: 219–234. doi:10.1016/j.bbamcr.2004.02.013
97. Sexton JA, Vogel JP. Type IV secretion by intracellular pathogens. *Traffic*. 2002;3: 178–185. doi:10.1034/j.1600-0854.2002.030303.x
98. Kaplan-Türköz B, Jiménez-Soto LF, Dian C, Ertl C, Remaut H, Louche A, et al. Structural insights into *Helicobacter pylori* oncoprotein CagA interaction with  $\beta$ 1 integrin. *PNAS*. 2012;109: 14640–14645. doi:10.1073/pnas.1206098109
99. Kaplan-Türköz B, Terradot L. [Structure and mode of injection of the oncoprotein CagA of *Helicobacter pylori*]. *Med Sci (Paris)*. 2013;29: 33–36. doi:10.1051/medsci/2013291011
100. Terradot L, Waksman G. Architecture of the *Helicobacter pylori* Cag-type IV secretion system. *FEBS J*. 2011;278: 1213–1222. doi:10.1111/j.1742-4658.2011.08037.x
101. Boschiroli ML, Ouahrani-Bettache S, Foulongne V, Michaux-Charachon S, Bourg G, Allardet-Servent A, et al. The *Brucella suis* virB operon is induced intracellularly in macrophages. *PNAS*. 2002;99: 1544–1549. doi:10.1073/pnas.032514299
102. Vogel JP, Andrews HL, Wong SK, Isberg RR. Conjugative transfer by the virulence system of *Legionella pneumophila*. *Science*. 1998;279: 873–876. doi:10.1126/science.279.5352.873
103. Gomez-Valero L, Rusniok C, Carson D, Mondino S, Pérez-Cobas AE, Rolando M, et al. More than 18,000 effectors in the *Legionella* genus genome provide multiple, independent combinations for replication in human cells. *PNAS*. 2019;116: 2265–2273. doi:10.1073/pnas.1808016116
104. Marchesini MI, Herrmann CK, Salcedo SP, Gorvel J-P, Comerci DJ. In search of *Brucella abortus* type IV secretion substrates: screening and identification of four proteins translocated into host cells through VirB system. *Cellular Microbiology*. 2011;13: 1261–1274. doi:10.1111/j.1462-5822.2011.01618.x
105. Döhmer PH, Valguarnera E, Czibener C, Ugalde JE. Identification of a type IV secretion substrate of *Brucella abortus* that participates in the early stages of intracellular survival. *Cellular Microbiology*. 2013;16: 396–410. doi:10.1111/cmi.12224
106. de Jong MF, Sun Y-H, Hartigh den AB, van Dijl JM, Tsolis RM. Identification of VceA and VceC, two members of the VjbR regulon that are translocated into macrophages by the *Brucella* type IV secretion system. *Mol Microbiol*. 2008;70: 1378–1396. doi:10.1111/j.1365-2958.2008.06487.x
107. Spera JM, Guaimas F, Corvi MM, Ugalde JE. *Brucella* Hijacks Host-Mediated Palmitoylation To Stabilize and Localize PrpA to the Plasma Membrane. Roy CR, editor. *Infect Immun*. 2018;86: 213–25. doi:10.1128/IAI.00402-18

108. de Jong MF, Starr T, Winter MG, Hartigh den AB, Child R, Knodler LA, et al. Sensing of bacterial type IV secretion via the unfolded protein response. *mBio*. 2013;4: e00418–12. doi:10.1128/mBio.00418-12
109. Byndloss MX, Tsai AY, Walker GT, Miller CN, Young BM, English BC, et al. Brucella abortus Infection of Placental Trophoblasts Triggers Endoplasmic Reticulum Stress-Mediated Cell Death and Fetal Loss via Type IV Secretion System-Dependent Activation of CHOP. *mBio*. 2019;10. doi:10.1128/mBio.01538-19
110. Zhi F, Zhou D, Bai F, Li J, Xiang C, Zhang G, et al. VceC Mediated IRE1 Pathway and Inhibited CHOP-induced Apoptosis to Support Brucella Replication in Goat Trophoblast Cells. *Int J Mol Sci*. 2019;20. doi:10.3390/ijms20174104
111. Zhang J, Li M, Li Z, Shi J, Zhang Y, Deng X, et al. Deletion of the Type IV Secretion System Effector VceA Promotes Autophagy and Inhibits Apoptosis in Brucella-Infected Human Trophoblast Cells. *Curr Microbiol*. 2019;76: 510–519. doi:10.1007/s00284-019-01651-6
112. Marchesini MI, Morrone Seijo SM, Guaimas FF, Comerci DJ. A T4SS Effector Targets Host Cell Alpha-Enolase Contributing to Brucella abortus Intracellular Lifestyle. *Front Cell Infect Microbiol*. 2016;6: 553–14. doi:10.3389/fcimb.2016.00153
113. Arriola Benitez PC, Rey Serantes D, Herrmann CK, Pesce Viglietti AI, Vanzulli S, Giambartolomei GH, et al. The Effector Protein BPE005 from Brucella abortus Induces Collagen Deposition and Matrix Metalloproteinase 9 Downmodulation via Transforming Growth Factor  $\beta$ 1 in Hepatic Stellate Cells. *Infect Immun*. 2016;84: 598–606. doi:10.1128/IAI.01227-15
114. Tisdale EJ, Balch WE. Rab2 is essential for the maturation of pre-Golgi intermediates. *J Biol Chem*. 1996;271: 29372–29379. doi:10.1074/jbc.271.46.29372
115. Miller CN, Smith EP, Cundiff JA, Knodler LA, Blackburn JB, Lupashin V, et al. A Brucella Type IV Effector Targets the COG Tethering Complex to Remodel Host Secretory Traffic and Promote Intracellular Replication. *Cell Host and Microbe*. Elsevier Inc; 2017;22: 317–329.e7. doi:10.1016/j.chom.2017.07.017
116. Smith EP, Cotto-Rosario A, Borghesan E, Held K, Miller CN, Celli J. Epistatic Interplay between Type IV Secretion Effectors Engages the Small GTPase Rab2 in the Brucella Intracellular Cycle. *mBio*. 2020;11. doi:10.1128/mBio.03350-19
117. Salcedo SP, Marchesini MI, Degos C, Terwagne M, Bargen von K, Lepidi H, et al. BtpB, a novel Brucella TIR-containing effector protein with immune modulatory functions. *Front Cell Infect Microbiol*. *Frontiers*; 2013;3: 28. doi:10.3389/fcimb.2013.00028
118. CirI C, Wieser A, Yadav M, Duerr S, Schubert S, Fischer H, et al. Subversion of Toll-like receptor signaling by a unique family of bacterial Toll/interleukin-1 receptor domain [ndash]containing proteins. *Nature Medicine*. Nature Publishing Group; 2008;14: 399–406. doi:10.1038/nm1734
119. Salcedo SP, Marchesini MI, Lelouard H, Fugier E, Jolly G, Balor S, et al. Brucella Control of Dendritic Cell Maturation Is Dependent on the TIR-Containing Protein Btp1. *PLOS Pathog*. Public Library of Science; 2008;4: e21. doi:10.1371/journal.ppat.0040021

120. Radhakrishnan GK, Yu Q, Harms JS, Splitter GA. Brucella TIR Domain-containing Protein Mimics Properties of the Toll-like Receptor Adaptor Protein TIRAP. *J Biol Chem. American Society for Biochemistry and Molecular Biology*; 2009;284: 9892–9898. doi:10.1074/jbc.M805458200
121. Sengupta D, Koblansky A, Gaines J, Brown T, West AP, Zhang D, et al. Subversion of innate immune responses by Brucella through the targeted degradation of the TLR signaling adapter, MAL. *J Immunol. American Association of Immunologists*; 2010;184: 956–964. doi:10.4049/jimmunol.0902008
122. Durward M, Radhakrishnan G, Harms J, Bareiss C, Magnani D, Splitter GA. Active evasion of CTL mediated killing and low quality responding CD8+ T cells contribute to persistence of brucellosis. *PLoS ONE*. 2012;7: e34925. doi:10.1371/journal.pone.0034925
123. Döhmer PH, Valguarnera E, Czibener C, Ugalde JE. Identification of a type IV secretion substrate of Brucella abortus that participates in the early stages of intracellular survival. *Cellular Microbiology*. 2014;16: 396–410. doi:10.1111/cmi.12224
124. Medzhitov R, Janeway CAJ. Innate immune induction of the adaptive immune response. *Cold Spring Harb Symp Quant Biol*. 1999;64: 429–435. doi:10.1101/sqb.1999.64.429
125. Pulendran B, Ahmed R. Translating innate immunity into immunological memory: implications for vaccine development. *Cell*. 2006;124: 849–863. doi:10.1016/j.cell.2006.02.019
126. Akira S, Uematsu S, Takeuchi O. Pathogen recognition and innate immunity. *Cell*. 2006;124: 783–801. doi:10.1016/j.cell.2006.02.015
127. Hoffmann JA, Kafatos FC, Janeway CA, Ezekowitz RA. Phylogenetic perspectives in innate immunity. *Science*. 1999;284: 1313–1318. doi:10.1126/science.284.5418.1313
128. Medzhitov R. Recognition of microorganisms and activation of the immune response. *Nature*. 2007;449: 819–826. doi:10.1038/nature06246
129. Takeuchi O, Akira S. Pattern Recognition Receptors and Inflammation. *Cell*. Elsevier Inc; 2010;140: 805–820. doi:10.1016/j.cell.2010.01.022
130. Krieger M. The other side of scavenger receptors: pattern recognition for host defense. *Curr Opin Lipidol*. 1997;8: 275–280. doi:10.1097/00041433-199710000-00006
131. Hashimoto C, Hudson KL, Anderson KV. The Toll gene of Drosophila, required for dorsal-ventral embryonic polarity, appears to encode a transmembrane protein. *Cell*. 1988;52: 269–279. doi:10.1016/0092-8674(88)90516-8
132. Stein D, Roth S, Vogelsang E, Nüsslein-Volhard C. The polarity of the dorsoventral axis in the Drosophila embryo is defined by an extracellular signal. *Cell*. 1991;65: 725–735. doi:10.1016/0092-8674(91)90381-8
133. Lemaitre B, Nicolas E, Michaut L, Reichhart JM, Hoffmann JA. The dorsoventral regulatory gene cassette spätzle/Toll/cactus controls the potent antifungal response in Drosophila adults. *Cell*. 1996;86: 973–983. doi:10.1016/s0092-8674(00)80172-5

134. Tenor JL, Aballay A. A conserved Toll-like receptor is required for *Caenorhabditis elegans* innate immunity. *EMBO Rep.* 2008;9: 103–109. doi:10.1038/sj.embor.7401104
135. Akira S, Hemmi H. Recognition of pathogen-associated molecular patterns by TLR family. *Immunol Lett.* 2003;85: 85–95. doi:10.1016/s0165-2478(02)00228-6
136. Bell JK, Mullen GED, Leifer CA, Mazzoni A, Davies DR, Segal DM. Leucine-rich repeats and pathogen recognition in Toll-like receptors. *Trends Immunol.* 2003;24: 528–533. doi:10.1016/s1471-4906(03)00242-4
137. Choe J, Kelker MS, Wilson IA. Crystal structure of human toll-like receptor 3 (TLR3) ectodomain. *Science.* 2005;309: 581–585. doi:10.1126/science.1115253
138. Imler JL, Hoffmann JA. Toll receptors in innate immunity. *Trends Cell Biol.* 2001;11: 304–311. doi:10.1016/s0962-8924(01)02004-9
139. Luo C, Zheng L. Independent evolution of Toll and related genes in insects and mammals. *Immunogenetics.* 2000;51: 92–98. doi:10.1007/s002510050017
140. Xu Y, Tao X, Shen B, Horng T, Medzhitov R, Manley JL, et al. Structural basis for signal transduction by the Toll/interleukin-1 receptor domains. *Nature.* 2000;408: 111–115. doi:10.1038/35040600
141. Li C, Zienkiewicz J, Hawiger J. Interactive sites in the MyD88 Toll/interleukin (IL) 1 receptor domain responsible for coupling to the IL1beta signaling pathway. *J Biol Chem.* 2005;280: 26152–26159. doi:10.1074/jbc.M503262200
142. Slack JL, Schooley K, Bonnert TP, Mitcham JL, Qwarnstrom EE, Sims JE, et al. Identification of two major sites in the type I interleukin-1 receptor cytoplasmic region responsible for coupling to pro-inflammatory signaling pathways. *J Biol Chem.* 2000;275: 4670–4678. doi:10.1074/jbc.275.7.4670
143. O'Neill LAJ, Bowie AG. The family of five: TIR-domain-containing adaptors in Toll-like receptor signalling. *Nat Rev Immunol.* 2007;7: 353–364. doi:10.1038/nri2079
144. Takeda K, Akira S. Toll-like receptors. *Curr Protoc Immunol.* 2015;109: 14.12.1–14.12.10. doi:10.1002/0471142735.im1412s109
145. Cervantes JL, Weinerman B, Basole C, Salazar JC. TLR8: the forgotten relative revindicated. *Cell Mol Immunol.* 2012;9: 434–438. doi:10.1038/cmi.2012.38
146. Beutler BA. TLRs and innate immunity. *Blood.* 2009;113: 1399–1407. doi:10.1182/blood-2008-07-019307
147. Kumar H, Kawai T, Akira S. Pathogen recognition by the innate immune system. *Int Rev Immunol.* 2011;30: 16–34. doi:10.3109/08830185.2010.529976
148. Zhao B, Shu C, Gao X, Sankaran B, Du F, Shelton CL, et al. Structural basis for concerted recruitment and activation of IRF-3 by innate immune adaptor proteins. *PNAS.* 2016;113: E3403–12. doi:10.1073/pnas.1603269113
149. Gay NJ, Symmons MF, Gangloff M, Bryant CE. Assembly and localization of Toll-like receptor signalling complexes. *Nat Rev Immunol.* 2014;14: 546–558. doi:10.1038/nri3713

150. Moresco EMY, LaVine D, Beutler B. Toll-like receptors. *Current Biology*. 2011;21: R488–93. doi:10.1016/j.cub.2011.05.039
151. Carty M, Goodbody R, Schröder M, Stack J, Moynagh PN, Bowie AG. The human adaptor SARM negatively regulates adaptor protein TRIF-dependent Toll-like receptor signaling. *Nat Immunol*. 2006;7: 1074–1081. doi:10.1038/ni1382
152. Lord KA, Abdollahi A, Hoffman-Liebermann B, Liebermann DA. Dissection of the immediate early response of myeloid leukemia cells to terminal differentiation and growth inhibitory stimuli. *Cell Growth Differ*. 1990;1: 637–645.
153. Chang ZL. Important aspects of Toll-like receptors, ligands and their signaling pathways. *Inflamm Res*. 2010;59: 791–808. doi:10.1007/s00011-010-0208-2
154. Kawai T, Akira S. The role of pattern-recognition receptors in innate immunity: update on Toll-like receptors. *Nat Immunol*. 2010;11: 373–384. doi:10.1038/ni.1863
155. Yamamoto M, Sato S, Mori K, Hoshino K, Takeuchi O, Takeda K, et al. Cutting edge: a novel Toll/IL-1 receptor domain-containing adapter that preferentially activates the IFN-beta promoter in the Toll-like receptor signaling. *The Journal of Immunology*. 2002;169: 6668–6672. doi:10.4049/jimmunol.169.12.6668
156. Ullah MO, Sweet MJ, Mansell A, Kellie S, Kobe B. TRIF-dependent TLR signaling, its functions in host defense and inflammation, and its potential as a therapeutic target. *J Leukoc Biol*. 2016;100: 27–45. doi:10.1189/jlb.2RI1115-531R
157. Underhill DM. Toll-like receptors and microbes take aim at each other. *Current Opinion in Immunology*. 2004;16: 483–487. doi:10.1016/j.coi.2004.05.012
158. Kawahara K, Tsukano H, Watanabe H, Lindner B, Matsuura M. Modification of the structure and activity of lipid A in *Yersinia pestis* lipopolysaccharide by growth temperature. *Infect Immun*. 2002;70: 4092–4098. doi:10.1128/iai.70.8.4092-4098.2002
159. Matsuura M, Takahashi H, Watanabe H, Saito S, Kawahara K. Immunomodulatory effects of *Yersinia pestis* lipopolysaccharides on human macrophages. *Clin Vaccine Immunol*. 2010;17: 49–55. doi:10.1128/CVI.00336-09
160. Andersen-Nissen E, Smith KD, Strobe KL, Barrett SLR, Cookson BT, Logan SM, et al. Evasion of Toll-like receptor 5 by flagellated bacteria. *PNAS*. 2005;102: 9247–9252. doi:10.1073/pnas.0502040102
161. Fretin D, Fauconnier A, Köhler S, Halling S, Léonard S, Nijskens C, et al. The sheathed flagellum of *Brucella melitensis* is involved in persistence in a murine model of infection. *Cellular Microbiology*. 2005;7: 687–698. doi:10.1111/j.1462-5822.2005.00502.x
162. Terwagne M, Ferooz J, Rolán HG, Sun Y-H, Atluri V, Xavier MN, et al. Innate immune recognition of flagellin limits systemic persistence of *Brucella*. *Cellular Microbiology*. 2013;15: 942–960. doi:10.1111/cmi.12088
163. Lapaque N, Moriyón I, Moreno E, Gorvel J-P. *Brucella* lipopolysaccharide acts as a virulence factor. *Curr Opin Microbiol*. 2005;8: 60–66. doi:10.1016/j.mib.2004.12.003

164. Nigou J, Zelle-Rieser C, Gilleron M, Thurnher M, Puzo G. Mannosylated lipoarabinomannans inhibit IL-12 production by human dendritic cells: evidence for a negative signal delivered through the mannose receptor. *The Journal of Immunology*. 2001;166: 7477–7485. doi:10.4049/jimmunol.166.12.7477
165. Vergne I, Gilleron M, Nigou J. Manipulation of the endocytic pathway and phagocyte functions by *Mycobacterium tuberculosis* lipoarabinomannan. *Front Cell Infect Microbiol*. 2014;4: 187. doi:10.3389/fcimb.2014.00187
166. Rana RR, Zhang M, Spear AM, Atkins HS, Byrne B. Bacterial TIR-containing proteins and host innate immune system evasion. *Med Microbiol Immunol*. 2012;202: 1–10. doi:10.1007/s00430-012-0253-2
167. Newman RM, Salunkhe P, Godzik A, Reed JC. Identification and characterization of a novel bacterial virulence factor that shares homology with mammalian Toll/interleukin-1 receptor family proteins. *Infect Immun. American Society for Microbiology*; 2006;74: 594–601. doi:10.1128/IAI.74.1.594-601.2006
168. Yadav M, Zhang J, Fischer H, Huang W, Lutay N, Cirl C, et al. Inhibition of TIR domain signaling by TcpC: MyD88-dependent and independent effects on *Escherichia coli* virulence. *PLOS Pathog*. 2010;6: e1001120. doi:10.1371/journal.ppat.1001120
169. Chaudhary A, Ganguly K, Cabantous S, Waldo GS, Micheva-Viteva SN, Nag K, et al. The *Brucella* TIR-like protein TcpB interacts with the death domain of MyD88. *Biochemical and Biophysical Research Communications*. Elsevier Inc; 2011;: 1–6. doi:10.1016/j.bbrc.2011.11.104
170. Mol JPS, Costa EA, Carvalho AF, Sun Y-H, Tsolis RM, Paixão TA, et al. Early transcriptional responses of bovine chorioallantoic membrane explants to wild type,  $\Delta$ virB2 or  $\Delta$ btpB *Brucella abortus* infection. *PLoS ONE*. 2014;9: e108606. doi:10.1371/journal.pone.0108606
171. Alaidarous M, Ve T, Casey LW, Valkov E, Ericsson DJ, Ullah MO, et al. Mechanism of bacterial interference with TLR4 signaling by *Brucella* Toll/interleukin-1 receptor domain-containing protein TcpB. *J Biol Chem*. 2014;289: 654–668. doi:10.1074/jbc.M113.523274
172. Snyder GA, Lai W, Brown L, Blanco J, Beadenkopf R, wang Y, et al. Therapeutic targeting of intracellular Toll-like and interleukin-1/18 receptor (TIR) resistance domain containing proteins for protection against infection, inflammation and disease. *J Immunol*. 2020;204: 226.7.
173. Xiong D, Song L, Geng S, Jiao Y, Zhou X, Song H, et al. *Salmonella* Coiled-Coil- and TIR-Containing TcpS Evades the Innate Immune System and Subdues Inflammation. *Cell Rep*. 2019;28: 804–818.e7. doi:10.1016/j.celrep.2019.06.048
174. Felix C, Kaplan-Türköz B, Ranaldi S, Koelblen T, Terradot L, O'Callaghan D, et al. The *Brucella* TIR domain containing proteins BtpA and BtpB have a structural WxxxE motif important for protection against microtubule depolymerisation. *Cell Commun Signal*. 2014;12: 53. doi:10.1186/s12964-014-0053-y
175. Kaplan-Türköz B, Koelblen T, Felix C, Candusso M-P, O'Callaghan D, Vergunst AC, et al. Structure of the Toll/interleukin 1 receptor (TIR) domain of the immunosuppressive *Brucella* effector BtpA/Btp1/TcpB. *FEBS Letters. Federation of European Biochemical Societies*; 2013;587: 3412–3416. doi:10.1016/j.febslet.2013.09.007



176. Radhakrishnan GK, Harms JS, Splitter GA. Modulation of microtubule dynamics by a TIR domain protein from the intracellular pathogen *Brucella melitensis*. *Biochem J.* 2011;439: 79–83. doi:10.1042/BJ20110577
177. Smith JA, Khan M, Magnani DD, Harms JS, Durward M, Radhakrishnan GK, et al. *Brucella* induces an unfolded protein response via TcpB that supports intracellular replication in macrophages. *PLOS Pathog.* 2013;9: e1003785. doi:10.1371/journal.ppat.1003785
178. Snyder GA, Deredge D, Waldhuber A, Fresquez T, Wilkins DZ, Smith PT, et al. Crystal structures of the Toll/Interleukin-1 receptor (TIR) domains from the *Brucella* protein TcpB and host adaptor TIRAP reveal mechanisms of molecular mimicry. *J Biol Chem.* 2014;289: 669–679. doi:10.1074/jbc.M113.523407
179. Askarian F, van Sorge NM, Sangvik M, Beasley FC, Henriksen JR, Sollid JUE, et al. A *Staphylococcus aureus* TIR domain protein virulence factor blocks TLR2-mediated NF- $\kappa$ B signaling. *J Innate Immun.* 2014;6: 485–498. doi:10.1159/000357618
180. Patot S, Imbert P, Baude J, Martins Simões P, Campergue J-B, Louche A, et al. The TIR Homologue Lies near Resistance Genes in *Staphylococcus aureus*, Coupling Modulation of Virulence and Antimicrobial Susceptibility. *PLOS Pathog.* 2017;13: e1006092. doi:10.1371/journal.ppat.1006092
181. Rana RR, Simpson P, Zhang M, Jennions M, Ukegbu C, Spear AM, et al. *Yersinia pestis* TIR-domain protein forms dimers that interact with the human adaptor protein MyD88. *Microbial Pathogenesis.* Elsevier Ltd; 2011;51: 89–95. doi:10.1016/j.micpath.2011.05.004
182. Low LY, Mukasa T, Reed JC, Pascual J. Characterization of a TIR-like protein from *Paracoccus denitrificans*. *Biochemical and Biophysical Research Communications.* 2007;356: 481–486. doi:10.1016/j.bbrc.2007.03.003
183. Waldhuber A, Snyder GA, Römmler F, Cirl C, Müller T, Xiao TS, et al. A Comparative Analysis of the Mechanism of Toll-Like Receptor-Disruption by TIR-Containing Protein C from Uropathogenic *Escherichia coli*. *Pathogens.* 2016;5. doi:10.3390/pathogens5010025
184. Snyder GA, Cirl C, Jiang J, Chen K, Waldhuber A, Smith P, et al. Molecular mechanisms for the subversion of MyD88 signaling by TcpC from virulent uropathogenic *Escherichia coli*. *Proc Natl Acad Sci USA.* 2013;110: 6985.
185. Imbert PR, Louche A, Luizet J-B, Grandjean T, Bigot S, Wood TE, et al. A *Pseudomonas aeruginosa* TIR effector mediates immune evasion by targeting UBAP1 and TLR adaptors. *The EMBO Journal.* 2017;36: 1869–1887. doi:10.15252/embj.201695343
186. Waldhuber A, Puthia M, Wieser A, Cirl C, Dürr S, Neumann-Pfeifer S, et al. Uropathogenic *Escherichia coli* strain CFT073 disrupts NLRP3 inflammasome activation. *J Clin Invest.* 2016;126: 2425–2436. doi:10.1172/JCI81916
187. Essuman K, Summers DW, Sasaki Y, Mao X, DiAntonio A, Milbrandt J. The SARM1 Toll/Interleukin-1 Receptor Domain Possesses Intrinsic NAD(+) Cleavage Activity that Promotes Pathological Axonal Degeneration. *Neuron.* 2017;93: 1334–1343.e5. doi:10.1016/j.neuron.2017.02.022

188. Essuman K, Summers DW, Sasaki Y, Mao X, Yim AKY, DiAntonio A, et al. TIR Domain Proteins Are an Ancient Family of NAD<sup>+</sup>-Consuming Enzymes. *Current Biology*. Elsevier Ltd; 2018;28: 421–430.e4. doi:10.1016/j.cub.2017.12.024
189. Horsefield S, Burdett H, Zhang X, Manik MK, Shi Y, Chen J, et al. NAD(+) cleavage activity by animal and plant TIR domains in cell death pathways. *Science*. 2019;365: 793–799. doi:10.1126/science.aax1911
190. Wan L, Essuman K, Anderson RG, Sasaki Y, Monteiro F, Chung E-H, et al. TIR domains of plant immune receptors are NAD(+)-cleaving enzymes that promote cell death. *Science*. 2019;365: 799–803. doi:10.1126/science.aax1771
191. Cremer T, Cremer M. Chromosome territories. *Cold Spring Harbor Perspectives in Biology*. 2010;2: a003889. doi:10.1101/cshperspect.a003889
192. Lamond AI, Earnshaw WC. Structure and function in the nucleus. *Science*. American Association for the Advancement of Science; 1998;280: 547–553. doi:10.1126/science.280.5363.547
193. Matera AG. Nuclear bodies: multifaceted subdomains of the interchromatin space. *Trends Cell Biol*. 1999;9: 302–309. doi:10.1016/s0962-8924(99)01606-2
194. Carmo-Fonseca M, Rino J. RNA seeds nuclear bodies. *Nat Cell Biol*. 2011;13: 110–112. doi:10.1038/ncb0211-110
195. Nunes VS, Moretti NS. Nuclear subcompartments: an overview. *Cell Biol Int*. 2016;41: 2–7. doi:10.1002/cbin.10703
196. Boulon S, Westman BJ, Hutten S, Boisvert F-M, Lamond AI. The nucleolus under stress. *Mol Cell*. 2010;40: 216–227. doi:10.1016/j.molcel.2010.09.024
197. Derenzini M, Trerè D, Pession A, Montanaro L, Sirri V, Ochs RL. Nucleolar function and size in cancer cells. *The American Journal of Pathology*. 1998;152: 1291–1297.
198. Tiku V, Antebi A. Nucleolar Function in Lifespan Regulation. *Trends Cell Biol*. 2018;28: 662–672. doi:10.1016/j.tcb.2018.03.007
199. Ahmad Y, Boisvert F-M, Gregor P, Cobley A, Lamond AI. NOPdb: Nucleolar Proteome Database--2008 update. *Nucleic Acids Res*. 2009;37: D181–4. doi:10.1093/nar/gkn804
200. Pederson T. The plurifunctional nucleolus. *Nucleic Acids Res*. 1998;26: 3871–3876. doi:10.1093/nar/26.17.3871
201. Boisvert F-M, van Koningsbruggen S, Navascués J, Lamond AI. The multifunctional nucleolus. *Nat Rev Mol Cell Biol*. 2007;8: 574–585. doi:10.1038/nrm2184
202. Lempiäinen H, Shore D. Growth control and ribosome biogenesis. *Current Opinion in Cell Biology*. 2009;21: 855–863. doi:10.1016/j.ceb.2009.09.002
203. Henras AK, Soudet J, Gêrus M, Lebaron S, Caizergues-Ferrer M, Mougin A, et al. The post-transcriptional steps of eukaryotic ribosome biogenesis. *Cell Mol Life Sci*. 2008;65: 2334–2359. doi:10.1007/s00018-008-8027-0

204. Kusnadi EP, Hannan KM, Hicks RJ, Hannan RD, Pearson RB, Kang J. Regulation of rDNA transcription in response to growth factors, nutrients and energy. *Gene*. 2015;556: 27–34. doi:10.1016/j.gene.2014.11.010
205. Kressler D, Hurt E, Bassler J. Driving ribosome assembly. *Biochim Biophys Acta*. 2010;1803: 673–683. doi:10.1016/j.bbamcr.2009.10.009
206. Panse VG, Johnson AW. Maturation of eukaryotic ribosomes: acquisition of functionality. *Trends Biochem Sci*. 2010;35: 260–266. doi:10.1016/j.tibs.2010.01.001
207. Finkbeiner E, Haindl M, Muller S. The SUMO system controls nucleolar partitioning of a novel mammalian ribosome biogenesis complex. *The EMBO Journal*. Nature Publishing Group; 2011;30: 1067–1078. doi:10.1038/emboj.2011.33
208. Lallemand-Breitenbach V, Zhu J, Puvion F, Koken M, Honoré N, Doubeikovsky A, et al. Role of promyelocytic leukemia (PML) sumolation in nuclear body formation, 11S proteasome recruitment, and As2O3-induced PML or PML/retinoic acid receptor alpha degradation. *The Journal of Experimental Medicine*. 2001;193: 1361–1371. doi:10.1084/jem.193.12.1361
209. Lallemand-Breitenbach V, de Thé H. PML nuclear bodies: from architecture to function. *Current Opinion in Cell Biology*. 2018;52: 154–161. doi:10.1016/j.ceb.2018.03.011
210. Negorev D, Maul GG. Cellular proteins localized at and interacting within ND10/PML nuclear bodies/PODs suggest functions of a nuclear depot. *Oncogene*. 2001;20: 7234–7242. doi:10.1038/sj.onc.1204764
211. Zhong S, Salomoni P, Pandolfi PP. The transcriptional role of PML and the nuclear body. *Nat Cell Biol*. 2000;2: E85–90. doi:10.1038/35010583
212. Torok D, Ching RW, Bazett-Jones DP. PML nuclear bodies as sites of epigenetic regulation. *Front Biosci (Landmark Ed)*. 2009;14: 1325–1336. doi:10.2741/3311
213. Wang ZG, Ruggero D, Ronchetti S, Zhong S, Gaboli M, Rivi R, et al. PML is essential for multiple apoptotic pathways. *Nat Genet*. 1998;20: 266–272. doi:10.1038/3073
214. Dellaire G, Bazett-Jones DP. PML nuclear bodies: dynamic sensors of DNA damage and cellular stress. *Bioessays*. 2004;26: 963–977. doi:10.1002/bies.20089
215. Beech SJ, Lethbridge KJ, Killick N, McGlincy N, Leppard KN. Isoforms of the promyelocytic leukemia protein differ in their effects on ND10 organization. *Exp Cell Res*. 2005;307: 109–117. doi:10.1016/j.yexcr.2005.03.012
216. Salomoni P, Ferguson BJ, Wyllie AH, Rich T. New insights into the role of PML in tumour suppression. *Cell Res*. 2008;18: 622–640. doi:10.1038/cr.2008.58
217. Sidik SM, Salsman J, Dellaire G, Rohde JR. Shigella infection interferes with SUMOylation and increases PML-NB number. *PLoS ONE*. 2015;10: e0122585. doi:10.1371/journal.pone.0122585
218. Ribet D, Lallemand-Breitenbach V, Ferhi O, Nahori M-A, Varet H, de Thé H, et al. Promyelocytic Leukemia Protein (PML) Controls *Listeria monocytogenes* Infection. Casadevall A, editor. *mBio*. American Society for Microbiology; 2017;8: e02179–16–16. doi:10.1128/mBio.02179-16

219. Meluh PB, Koshland D. Evidence that the MIF2 gene of *Saccharomyces cerevisiae* encodes a centromere protein with homology to the mammalian centromere protein CENP-C. *Mol Biol Cell*. 1995;6: 793–807. doi:10.1091/mbc.6.7.793
220. Boddy MN, Howe K, Etkin LD, Solomon E, Freemont PS. PIC 1, a novel ubiquitin-like protein which interacts with the PML component of a multiprotein complex that is disrupted in acute promyelocytic leukaemia. *Oncogene*. 1996;13: 971–982.
221. Shen Z, Pardington-Purtymun PE, Comeaux JC, Moyzis RK, Chen DJ. Associations of UBE2I with RAD52, UBL1, p53, and RAD51 proteins in a yeast two-hybrid system. *Genomics*. 1996;37: 183–186. doi:10.1006/geno.1996.0540
222. Okura T, Gong L, Kamitani T, Wada T, Okura I, Wei CF, et al. Protection against Fas/APO-1- and tumor necrosis factor-mediated cell death by a novel protein, sentrin. *The Journal of Immunology*. 1996;157: 4277–4281.
223. Hay RT. SUMO: a history of modification. *Mol Cell*. 2005;18: 1–12. doi:10.1016/j.molcel.2005.03.012
224. Geiss-Friedlander R, Melchior F. Concepts in sumoylation: a decade on. *Nat Rev Mol Cell Biol*. 2007;8: 947–956. doi:10.1038/nrm2293
225. Muller S, Ledl A, Schmidt D. SUMO: a regulator of gene expression and genome integrity. *Oncogene*. 2004;23: 1998–2008. doi:10.1038/sj.onc.1207415
226. Wasik U, Filipek A. Non-nuclear function of sumoylated proteins. *BBA - Molecular Cell Research*. Elsevier B.V; 2014;1843: 2878–2885. doi:10.1016/j.bbamcr.2014.07.018
227. Guo D, Li M, Zhang Y, Yang P, Eckenrode S, Hopkins D, et al. A functional variant of SUMO4, a new I kappa B alpha modifier, is associated with type 1 diabetes. *Nat Genet*. 2004;36: 837–841. doi:10.1038/ng1391
228. Bohren KM, Nadkarni V, Song JH, Gabbay KH, Owerbach D. A M55V polymorphism in a novel SUMO gene (SUMO-4) differentially activates heat shock transcription factors and is associated with susceptibility to type I diabetes mellitus. *J Biol Chem*. 2004;279: 27233–27238. doi:10.1074/jbc.M402273200
229. Hendriks IA, Vertegaal ACO. A comprehensive compilation of SUMO proteomics. *Nat Rev Mol Cell Biol*. 2016;17: 581–595. doi:10.1038/nrm.2016.81
230. Liang Y-C, Lee C-C, Yao Y-L, Lai C-C, Schmitz ML, Yang W-M. SUMO5, a Novel Poly-SUMO Isoform, Regulates PML Nuclear Bodies. *Sci Rep*. 2016;6: 26509. doi:10.1038/srep26509
231. Hickey CM, Wilson NR, Hochstrasser M. Function and regulation of SUMO proteases. *Nat Rev Mol Cell Biol*. 2012;13: 755–766. doi:10.1038/nrm3478
232. Lois LM, Lima CD. Structures of the SUMO E1 provide mechanistic insights into SUMO activation and E2 recruitment to E1. *The EMBO Journal*. 2005;24: 439–451. doi:10.1038/sj.emboj.7600552
233. Yasugi T, Howley PM. Identification of the structural and functional human homolog of the yeast ubiquitin conjugating enzyme UBC9. *Nucleic Acids Res*. 1996;24: 2005–2010. doi:10.1093/nar/24.11.2005

234. Reverter D, Lima CD. Insights into E3 ligase activity revealed by a SUMO-RanGAP1-Ubc9-Nup358 complex. *Nature*. 2005;435: 687–692. doi:10.1038/nature03588
235. Shin EJ, Shin HM, Nam E, Kim WS, Kim J-H, Oh B-H, et al. DeSUMOylating isopeptidase: a second class of SUMO protease. *EMBO Rep*. 2012;13: 339–346. doi:10.1038/embor.2012.3
236. Schulz S, Chachami G, Kozackiewicz L, Winter U, Stankovic-Valentin N, Haas P, et al. Ubiquitin-specific protease-like 1 (USPL1) is a SUMO isopeptidase with essential, non-catalytic functions. *EMBO Rep*. 2012;13: 930–938. doi:10.1038/embor.2012.125
237. Gong L, Millas S, Maul GG, Yeh ET. Differential regulation of sentrinized proteins by a novel sentrin-specific protease. *J Biol Chem*. 2000;275: 3355–3359. doi:10.1074/jbc.275.5.3355
238. Song J, Durrin LK, Wilkinson TA, Krontiris TG, Chen Y. Identification of a SUMO-binding motif that recognizes SUMO-modified proteins. *PNAS*. 2004;101: 14373–14378. doi:10.1073/pnas.0403498101
239. Kerscher O. SUMO junction-what's your function? New insights through SUMO-interacting motifs. *EMBO Rep*. 2007;8: 550–555. doi:10.1038/sj.embor.7400980
240. Li C, Peng Q, Wan X, Sun H, Tang J. C-terminal motifs in promyelocytic leukemia protein isoforms critically regulate PML nuclear body formation. *J Cell Sci*. 2017;130: 3496–3506. doi:10.1242/jcs.202879
241. Chymkowitch P, Nguéa P A, Enserink JM. SUMO-regulated transcription: challenging the dogma. *Bioessays*. 2015;37: 1095–1105. doi:10.1002/bies.201500065
242. Ribet D, Hamon M, Gouin E, Nahori M-A, Impens F, Neyret-Kahn H, et al. *Listeria monocytogenes* impairs SUMOylation for efficient infection. *Nature*. 2010;464: 1192–1195. doi:10.1038/nature08963
243. Everett RD, Boutell C, Hale BG. Interplay between viruses and host sumoylation pathways. *Nat Rev Microbiol*. 2013;11: 400–411. doi:10.1038/nrmicro3015
244. Lapaquette P, Fritah S, Lhocine N, Andrieux A, Nigro G, Mounier J, et al. *Shigella* entry unveils a calcium/calpain-dependent mechanism for inhibiting sumoylation. *Elife*. 2017;6. doi:10.7554/eLife.27444
245. Wu F, Zhu S, Ding Y, Beck WT, Mo Y-Y. MicroRNA-mediated regulation of Ubc9 expression in cancer cells. *Clin Cancer Res*. 2009;15: 1550–1557. doi:10.1158/1078-0432.CCR-08-0820
246. Verma S, Mohapatra G, Ahmad SM, Rana S, Jain S, Khalsa JK, et al. *Salmonella* Engages Host MicroRNAs To Modulate SUMOylation: a New Arsenal for Intracellular Survival. *Molecular and Cellular Biology*. 2015;35: 2932–2946. doi:10.1128/MCB.00397-15
247. Sá-Pessoa J, Przybyszewska K, Vasconcelos FN, Dumigan A, Frank CG, Hopley L, et al. *Klebsiella pneumoniae* Reduces SUMOylation To Limit Host Defense Responses. *mBio*. 2020;11. doi:10.1128/mBio.01733-20
248. Dunphy PS, Luo T, McBride JW. *Ehrlichia chaffeensis* exploits host SUMOylation pathways to mediate effector-host interactions and promote intracellular survival. *Infect Immun*. 2014;82: 4154–4168. doi:10.1128/IAI.01984-14

249. Jo K, Kim EJ, Yu HJ, Yun C-H, Kim DW. Host Cell Nuclear Localization of *Shigella flexneri* Effector OspF Is Facilitated by SUMOylation. *J Microbiol Biotechnol*. 2017;27: 610–615. doi:10.4014/jmb.1611.11066
250. Nayak A, Müller SM. SUMO-specific proteases/isopeptidases: SENPs and beyond. 2014;: 1–7. doi:10.1186/s13059-014-0422-2
251. Zunino R, Braschi E, Xu L, McBride HM. Translocation of SenP5 from the nucleoli to the mitochondria modulates DRP1-dependent fission during mitosis. *J Biol Chem*. 2009;284: 17783–17795. doi:10.1074/jbc.M901902200
252. Huang W, Ghisletti S, Saijo K, Gandhi M, Aouadi M, Tesz GJ, et al. Coronin 2A mediates actin-dependent de-repression of inflammatory response genes. *Nature*. 2011;470: 414–418. doi:10.1038/nature09703
253. Nayak A, Viale-Bouroncle S, Morscheck C, Muller S. The SUMO-specific isopeptidase SENP3 regulates MLL1/MLL2 methyltransferase complexes and controls osteogenic differentiation. *Mol Cell*. 2014;55: 47–58. doi:10.1016/j.molcel.2014.05.011
254. Raman N, Weir E, Muller S. The AAA ATPase MDN1 Acts as a SUMO-Targeted Regulator in Mammalian Pre-ribosome Remodeling. *Mol Cell*. 2016;64: 607–615. doi:10.1016/j.molcel.2016.09.039
255. Mikolajczyk J, Drag M, Békés M, Cao JT, Ronai Z, Salvesen GS. Small Ubiquitin-related Modifier (SUMO)-specific Proteases. *J Biol Chem*. 2007;282: 26217–26224. doi:10.1074/jbc.M702444200
256. Xu Z, Lam LSM, Lam LH, Chau SF, Ng TB, Au SWN. Molecular basis of the redox regulation of SUMO proteases: a protective mechanism of intermolecular disulfide linkage against irreversible sulfhydryl oxidation. *FASEB J*. 2008;22: 127–137. doi:10.1096/fj.06-7871com
257. Huang C, Han Y, Wang Y, Sun X, Yan S, Yeh ETH, et al. SENP3 is responsible for HIF-1 transactivation under mild oxidative stress via p300 de-SUMOylation. *The EMBO Journal*. 2009;28: 2748–2762. doi:10.1038/emboj.2009.210
258. Han Y, Huang C, Sun X, Xiang B, Wang M, Yeh ETH, et al. SENP3-mediated de-conjugation of SUMO2/3 from promyelocytic leukemia is correlated with accelerated cell proliferation under mild oxidative stress. *J Biol Chem*. 2010;285: 12906–12915. doi:10.1074/jbc.M109.071431
259. Wang Y, Yang J, Yang K, Cang H, Huang X-Z, Li H, et al. The biphasic redox sensing of SENP3 accounts for the HIF-1 transcriptional activity shift by oxidative stress. *Acta Pharmacol Sin*. 2012;33: 953–963. doi:10.1038/aps.2012.40
260. Kunz K, Piller T, Muller S. SUMO-specific proteases and isopeptidases of the SENP family at a glance. *J Cell Sci*. 2018;131: jcs211904–8. doi:10.1242/jcs.211904
261. Zhang Y, Yang K, Yang J, Lao Y, Deng L, Deng G, et al. SENP3 Suppresses Osteoclastogenesis by De-conjugating SUMO2/3 from IRF8 in Bone Marrow-Derived Monocytes. *Cell Rep*. 2020;30: 1951–1963.e4. doi:10.1016/j.celrep.2020.01.036

262. Wei B, Huang C, Liu B, Wang Y, Xia N, Fan Q, et al. Mitotic Phosphorylation of SENP3 Regulates DeSUMOylation of Chromosome-Associated Proteins and Chromosome Stability. *Cancer Res.* 2018;78: 2171–2178. doi:10.1158/0008-5472.CAN-17-2288
263. Lao Y, Yang K, Wang Z, Sun X, Zou Q, Yu X, et al. DeSUMOylation of MKK7 kinase by the SUMO2/3 protease SENP3 potentiates lipopolysaccharide-induced inflammatory signaling in macrophages. *J Biol Chem.* 2018;293: 3965–3980. doi:10.1074/jbc.M117.816769
264. Barry R, John SW, Liccardi G, Tenev T, Jaco I, Chen C-H, et al. SUMO-mediated regulation of NLRP3 modulates inflammasome activity. *Nature Communications.* 2018;9: 3001. doi:10.1038/s41467-018-05321-2
265. Shao L, Liu Y, Wang W, Li A, Wan P, Liu W, et al. SUMO1 SUMOylates and SENP3 deSUMOylates NLRP3 to orchestrate the inflammasome activation. *FASEB J.* 2020;34: 1497–1515. doi:10.1096/fj.201901653R
266. Jewell JL, Guan K-L. Nutrient signaling to mTOR and cell growth. *Trends Biochem Sci.* 2013;38: 233–242. doi:10.1016/j.tibs.2013.01.004
267. Yun C, Wang Y, Mukhopadhyay D, Backlund P, Kolli N, Yergey A, et al. Nucleolar protein B23/nucleophosmin regulates the vertebrate SUMO pathway through SENP3 and SENP5 proteases. *J Cell Biol.* 2008;183: 589–595. doi:10.1083/jcb.200807185
268. Raman N, Nayak A, Muller S. mTOR signaling regulates nucleolar targeting of the SUMO-specific isopeptidase SENP3. *Molecular and Cellular Biology. American Society for Microbiology;* 2014;34: 4474–4484. doi:10.1128/MCB.00801-14
269. Haindl M, Harasim T, Eick D, Muller S. The nucleolar SUMO-specific protease SENP3 reverses SUMO modification of nucleophosmin and is required for rRNA processing. *EMBO Rep.* 2008;9: 273–279. doi:10.1038/embor.2008.3
270. Castle CD, Cassimere EK, Denicourt C. LAS1L interacts with the mammalian Rix1 complex to regulate ribosome biogenesis. *Mol Biol Cell.* 2012;23: 716–728. doi:10.1091/mbc.E11-06-0530
271. Finkbeiner E, Haindl M, Muller S. The SUMO system controls nucleolar partitioning of a novel mammalian ribosome biogenesis complex. *The EMBO Journal. Nature Publishing Group;* 2011;30: 1067–1078. doi:10.1038/emboj.2011.33
272. Finkbeiner E, Haindl M, Raman N, Muller S. SUMO routes ribosome maturation. *Nucleus.* 2011;2: 527–532. doi:10.4161/nucl.2.6.17604
273. Yun C, Wang Y, Mukhopadhyay D, Backlund P, Kolli N, Yergey A, et al. Nucleolar protein B23/nucleophosmin regulates the vertebrate SUMO pathway through SENP3 and SENP5 proteases. *J Cell Biol.* 2008;183: 589–595. doi:10.1083/jcb.200807185
274. Germain-Lee EL, Obie C, Valle D. NVL: a new member of the AAA family of ATPases localized to the nucleus. *Genomics.* 1997;44: 22–34. doi:10.1006/geno.1997.4856
275. Nagahama M, Hara Y, Seki A, Yamazoe T, Kawate Y, Shinohara T, et al. NVL2 is a nucleolar AAA-ATPase that interacts with ribosomal protein L5 through its nucleolar localization sequence. *Mol Biol Cell.* 2004;15: 5712–5723. doi:10.1091/mbc.e04-08-0692

276. Nagahama M, Yamazoe T, Hara Y, Tani K, Tsuji A, Tagaya M. The AAA-ATPase NVL2 is a component of pre-ribosomal particles that interacts with the DExD/H-box RNA helicase DOB1. *Biochemical and Biophysical Research Communications*. 2006;346: 1075–1082. doi:10.1016/j.bbrc.2006.06.017
277. Price CTD, Jones SC, Amundson KE, Kwai YA. Host-mediated post-translational prenylation of novel dot/icm-translocated effectors of legionella pneumophila. *Front Microbiol*. 2010;1: 131. doi:10.3389/fmicb.2010.00131
278. Reinicke AT, Hutchinson JL, Magee AI, Mastroeni P, Trowsdale J, Kelly AP. A *Salmonella typhimurium* effector protein SifA is modified by host cell prenylation and S-acylation machinery. *J Biol Chem*. 2005;280: 14620–14627. doi:10.1074/jbc.M500076200
279. Boucrot E, Beuzón CR, Holden DW, Gorvel J-P, Méresse S. *Salmonella typhimurium* SifA effector protein requires its membrane-anchoring C-terminal hexapeptide for its biological function. *J Biol Chem*. 2003;278: 14196–14202. doi:10.1074/jbc.M207901200
280. Ivanov SS, Charron G, Hang HC, Roy CR. Lipidation by the host prenyltransferase machinery facilitates membrane localization of *Legionella pneumophila* effector proteins. *J Biol Chem*. 2010;285: 34686–34698. doi:10.1074/jbc.M110.170746
281. Luizet J-B, Raymond J, Lacerda TLS, Bonici M, Lembo F, Willemart K, et al. *Brucella* effector hijacks endoplasmic reticulum quality control machinery to prevent premature egress. *bioRxiv*. 2019;: 699330.
282. Yoshikatsu Y, Ishida Y-I, Sudo H, Yuasa K, Tsuji A, Nagahama M. NVL2, a nucleolar AAA-ATPase, is associated with the nuclear exosome and is involved in pre-rRNA processing. *Biochemical and Biophysical Research Communications*. 2015;464: 780–786. doi:10.1016/j.bbrc.2015.07.032
283. Treacy-Abarca S, Mukherjee S. *Legionella* suppresses the host unfolded protein response via multiple mechanisms. *Nature Communications*. 2015;6: 7887. doi:10.1038/ncomms8887
284. Vonaesch P, Campbell-Valois F-X, Dufour A, Sansonetti PJ, Schnupf P. *Shigella flexneri* modulates stress granule composition and inhibits stress granule aggregation. *Cellular Microbiology*. 2016;18: 1892. doi:10.1111/cmi.12675
285. Eulalio A, Fröhlich KS, Mano M, Giacca M, Vogel J. A candidate approach implicates the secreted *Salmonella* effector protein SpvB in P-body disassembly. *PLoS ONE*. 2011;6: e17296. doi:10.1371/journal.pone.0017296
286. Tsalikis J, Tattoli I, Ling A, Sorbara MT, Croitoru DO, Philpott DJ, et al. Intracellular Bacterial Pathogens Trigger the Formation of U Small Nuclear RNA Bodies (U Bodies) through Metabolic Stress Induction. *J Biol Chem*. 2015;290: 20904–20918. doi:10.1074/jbc.M115.659466
287. Wyant GA, Abu-Remaileh M, Frenkel EM, Laqtom NN, Dharamdasani V, Lewis CA, et al. NUFIP1 is a ribosome receptor for starvation-induced ribophagy. *Science*. 2018;360: 751–758. doi:10.1126/science.aar2663
288. Denton D, Kumar S. Ribophagy: new receptor discovered. *Cell Res*. 2018;28: 699–700. doi:10.1038/s41422-018-0054-2



289. Blasi E, Mathieson BJ, Varesio L, Cleveland JL, Borchert PA, Rapp UR. Selective immortalization of murine macrophages from fresh bone marrow by a raf/myc recombinant murine retrovirus. *Nature*. 1985;318: 667–670. doi:10.1038/318667a0
290. Raffatellu M, Sun Y-H, Wilson RP, Tran QT, Chessa D, Andrews-Polymenis HL, et al. Host restriction of *Salmonella enterica* serotype Typhi is not caused by functional alteration of SipA, SopB, or SopD. *Infect Immun*. 2005;73: 7817–7826. doi:10.1128/IAI.73.12.7817-7826.2005
291. Rolando M, Sanulli S, Rusniok C, Gomez-Valero L, Bertholet C, Sahr T, et al. Legionella pneumophila Effector RomA Uniquely Modifies Host Chromatin to Repress Gene Expression and Promote Intracellular Bacterial Replication. *Cell Host and Microbe*. Elsevier Inc; 2013;13: 395–405. doi:10.1016/j.chom.2013.03.004
292. Kabsch W. Automatic processing of rotation diffraction data from crystals of initially unknown symmetry and cell constants. *Journal of Applied Crystallography*. 1993;26: 795–800. doi:10.1107/S0021889893005588
293. Dodson EJ, Winn M, Ralph A. Collaborative Computational Project, number 4: providing programs for protein crystallography. *Methods Enzymol*. 1997;277: 620–633. doi:10.1016/s0076-6879(97)77034-4
294. Zwart PH, Grosse-Kunstleve RW, Lebedev AA, Murshudov GN, Adams PD. Surprises and pitfalls arising from (pseudo)symmetry. *Acta Crystallogr D Biol Crystallogr*. 2008;64: 99–107. doi:10.1107/S090744490705531X
295. Adams PD, Grosse-Kunstleve RW, Hung LW, Ioerger TR, McCoy AJ, Moriarty NW, et al. PHENIX: building new software for automated crystallographic structure determination. *Acta Crystallogr D Biol Crystallogr*. 2002;58: 1948–1954. doi:10.1107/s0907444902016657
296. Petoukhov MV, Franke D, Shkumatov AV, Tria G, Kikhney AG, Gajda M, et al. New developments in the ATSAS program package for small-angle scattering data analysis. *Journal of Applied Crystallography*. 2012;45: 342–350. doi:10.1107/S0021889812007662
297. Schneidman-Duhovny D, Hammel M, Tainer JA, Sali A. Accurate SAXS profile computation and its assessment by contrast variation experiments. *Biophys J*. 2013;105: 962–974. doi:10.1016/j.bpj.2013.07.020
298. Svergun DI, Petoukhov MV, Koch MH. Determination of domain structure of proteins from X-ray solution scattering. *Biophys J*. 2001;80: 2946–2953. doi:10.1016/S0006-3495(01)76260-1
299. Yan L, Liu W, Zhang H, Liu C, Shang Y, Ye Y, et al. Ube2g2–gp78-mediated HERP polyubiquitylation is involved in ER stress recovery. *J Cell Sci*. 2014;127: 1417.
300. Thalappilly S, Suliman M, Gayet O, Soubeyran P, Hermant A, Lecine P, et al. Identification of multi-SH3 domain-containing protein interactome in pancreatic cancer: a yeast two-hybrid approach. *Proteomics*. 2008;8: 3071–3081. doi:10.1002/pmic.200701157
301. Walhout AJ, Vidal M. High-throughput yeast two-hybrid assays for large-scale protein interaction mapping. *Methods*. 2001;24: 297–306. doi:10.1006/meth.2001.1190

302. Orr-Weaver TL, Szostak JW. Yeast recombination: the association between double-strand gap repair and crossing-over. *Proc Natl Acad Sci U S A*. 1983;80: 4417–4421. doi:10.1073/pnas.80.14.4417
  303. Dolezal P, Aili M, Tong J, Jiang J-H, Marobbio CMT, Lee SF, et al. Legionella pneumophila secretes a mitochondrial carrier protein during infection. *PLOS Pathog*. 2012;8: e1002459. doi:10.1371/journal.ppat.1002459
  304. Burette M, Allombert J, Lambou K, Maarifi G, Nisole S, Di Russo Case E, et al. Modulation of innate immune signaling by a Coxiella burnetii eukaryotic-like effector protein. *PNAS*. 2020;117: 13708–13718. doi:10.1073/pnas.1914892117
  305. Urae S, Harita Y, Udagawa T, Ode KL, Nagahama M, Kajiho Y, et al. A cellular model of albumin endocytosis uncovers a link between membrane and nuclear proteins. *J Cell Sci*. 2020;133. doi:10.1242/jcs.242859
  306. Hansen M, Rubinsztein DC, Walker DW. Autophagy as a promoter of longevity: insights from model organisms. *Nat Rev Mol Cell Biol*. 2018;19: 579–593. doi:10.1038/s41580-018-0033-y
  307. Taguchi Y, Imaoka K, Kataoka M, Uda A, Nakatsu D, Horii-Okazaki S, et al. Yip1A, a novel host factor for the activation of the IRE1 pathway of the unfolded protein response during Brucella infection. *PLOS Pathog*. 2015;11: e1004747. doi:10.1371/journal.ppat.1004747
  308. Beese CJ, Brynjólfssdóttir SH, Frankel LB. Selective Autophagy of the Protein Homeostasis Machinery: Ribophagy, Proteaphagy and ER-Phagy. *Front Cell Dev Biol*. 2019;7: 373. doi:10.3389/fcell.2019.00373
  309. An H, Harper JW. Systematic analysis of ribophagy in human cells reveals bystander flux during selective autophagy. *Nat Cell Biol*. 2018;20: 135–143. doi:10.1038/s41556-017-0007-x
  310. Liu K, Guo C, Lao Y, Yang J, Chen F, Zhao Y, et al. A fine-tuning mechanism underlying self-control for autophagy: deSUMOylation of BECN1 by SENP3. *Autophagy*. 2020;16: 975–990. doi:10.1080/15548627.2019.1647944
-